Design and Membrane Selection for Gas to Gas Humidifiers for Fuel Cell Applications

By

Ryan Huizing

A thesis
presented to the University of Waterloo
in the fulfillment of the
thesis requirement for the degree of
Master of Applied Science
in
Chemical Engineering

Waterloo, Ontario, Canada, 2007

I hereby declare that I am the sole author of this thesis. This is a true copy of the thesis, including any required final revisions, as accepted by my examiners.

I understand that my thesis may be made electronically available to the public.

Ryan Huizing

Abstract

In its present form, polymer electrolyte membrane fuel cell (PEMFC) technology requires some method of humidification to ensure that high performance and long life of the fuel cell membrane is maintained. External humidification utilizing 'gas to gas' membrane based planar humidifiers is one method of humidifying fuel cell reactant gases. This type of humidification offers the benefit of recycling heat and moisture from the fuel cell exhaust, and returning it to the reactants entering the fuel cell.

In designing a planar membrane based fuel cell humidifier the two important areas to be considered are:

- humidifier channel and plate design; and
- humidifier membrane selection.

In this work a humidifier design procedure was developed based on prototype humidifier testing. This design procedure involves selection of design parameters based on a dimensionless parameter which describes the ratio of gas residence time, and water diffusion time from the membrane surface. Humidifiers of different flow channel geometries were created with a rapid prototyping technique. These humidifier units were tested at different operating conditions in an attempt to validate the design equations involving a design parameter which is the ratio between the residence times of gas in the humidifier over the diffusion time of water from the surface of the membrane into the channel. This parameter offers a good starting point for humidifier design, the target value of this parameter was found to be between 2.0 and 4.0, with a desired value of 3.0. A fuel cell stack humidifier design procedure and suggestions are presented based this parameter. The design also considers designing a humidifier on limited volume constraints in which the humidifier would have to fit into the fuel cell system.

A membrane selection procedure was developed based on design criteria requirements developed during this work for the fuel cell humidifier. This criterion includes high water permeation, low air permeation, good mechanical strength, robust handling, and long lifetime under various operating conditions. . Specific values for membrane selection included a water flux of greater than 14 kg m^{-2} h^{-1} in a water permeation test, less than 3

cm^3 min^{-1} cm^{-2} kPa^{-1} air permeation when the membrane was dry, and a lifetime of at least 1500 hours of operation without performance degradation. Sixty membranes from various sources were screened for candidacy for use in the humidifier application. Membranes which passed the initial screenings were tested for durability at high and moderate temperature conditions. These membranes were operated until failure, at which time analysis was completed to determine the failure modes of the membrane. Mitigation strategies were proposed when applicable. Recommendations were made for membrane materials for the proposed operating requirements. Suggested membranes materials included those based on UHMWPE and inorganic additives, as well as homogenous membranes based on Nylon 6,6, PEEK, and PFSA.

Acknowledgements

I would like to acknowledge the Natural Sciences and Engineering Research Council (NSERC) for their financial support, as well as DPoint Technologies for their financial contributions and assistance.

I would also like to thank Dr. Leonardo Simon for his assistance and the usage of the Minimat materials testing equipment in his laboratory. As well thank you to Dr. Marios Ionnidis for allowing me access to his ASDA equipment, and Jeff Gostick for his help in using this equipment. I would like to thank Sumit Kundu for training me to use the scanning electron microscope, and his assistance with various equipment in Dr. Fowler's laboratory. I would like to acknowledge the work of Kevin Nold and Stewart Hinze, both undergraduate students who assisted in completing some of the experimental work presented here.

I would like to thank Dr. Fowler for this opportunity, his support, and input. Thank you also to Dr. Walter Merida at the University of British Columbia for usage of his laboratory equipment and his guidance.

I would like to thank Pat Anderson for her patience in dealing with my apparent inability to grasp anything bureaucratic. Grace the custodian for cleaning my messes, and providing me with interesting stories and smiles late at night in the lab. My appreciation goes out to Dr. Simon and Dr. Ali Elkamel for taking the time to act as readers for this thesis.

Finally I would like to thank James Dean, Chad Comeault, and the rest of the team at DPoint Technologies not only for this opportunity, but for their hospitality when I worked in Vancouver, and their guidance and teachings along the way.

Dedication

To begin I would like to dedicate this thesis to Oskar, through all the late nights and early mornings, the good and the bad, you were a constant. Constantly pawing at my door, meowing, begging for food, you have a serious eating disorder, but I still love you, you fuzzy butterball.

I would also like thank Dr. Fowler again for his gentle guidance, encouragement, and for being a voice of experience I could count on. The same to James and Chad at DPoint, you were all I could have hoped for and more in an industrial sponsor.

I want to thank my wonderful lab-mates Charles, Erik, Jeff, Matt, and Sumit for their help and making this experience fun. A special thank you goes out to Erik for providing me with the extra incentive to finish this thesis, enjoy your special run down King St! It'll be legendary.

Extra thanks to all my amazing friends, some who I've met along the way, others who have been there all along. Who would have thought this graduate school thing could be so much fun? Namely I would like to thank Aaron, Andrew, Andy, Ariella, Brian, Carly, Cyndie, Derek, Emily, Erik, Heather, Jake, Jeff, Joel, Jordan, Layal, Loughlin, Matt, Megan, Natalie, Nick, and Stacy. Without friends like these I wouldn't be half the person I am today and I certainly wouldn't have made it through these past two years. A special thank you goes to Layal not only for helping edit this thesis, but for being there for me through everything; I am truly blessed to have you as a friend.

Finally I would like to dedicate this thesis to my family, my grandparents Ollie and Eva, and especially my parents Nancy and Nick, you raised me well, you instilled a sense inquiry in me, and have supported me through all of this. Thank you; you will never really know how grateful I am.

And now onwards to new things, "forward, not backward, upward not forward, and always twirling, twirling, twirling towards freedom"…

Table of Contents

1.0 Introduction and Background 1
1.1 General Background 1
1.2 Fuel Cell Components 1
1.2.1 Electrolyte 2
1.2.2 Catalyst Layer or Electrodes 2
1.2.3 Gas Diffusion Layer 2
1.2.4 Bi-Polar Flow Field Plates 2
1.2.5 The Stack 3
1.3 Fuel Cell Voltage Losses 3
1.3.1 Activation Losses 4
1.3.2 Ohmic Losses 5
1.3.3 Mass Transport Losses 5
1.3.4 Overall Fuel Cell Equation 6
1.4 The Importance of Fuel Cell Humidification 6
1.4.1 Nafion™ Structure 7
1.4.2 PFSA Reactions with Water 8
1.4.3 Dehydration of the Membrane 9
1.4.4 Flooding 10
1.5 Water and Heat Balances in PEMFC's 11
1.5.1 Water Balance 11
1.5.1.1 Electro-Osmotic Drag 11
1.5.1.2 Water Production 12
1.5.1.3 Back Diffusion 12
1.5.1.4 Humidification of Gases 13
1.5.1.5 Overall Balance 16
1.6 Humidification Methods 17
1.6.1 Internal Humidification 19
1.6.1.1 Special Stack Designs 19
1.6.1.2 Direct Liquid or Steam Injection 20
1.6.1.3 Membrane Additives 20
1.6.1.4 Wicks, Sponges and Porous Plates 21
1.6.2 External Humidification 21
1.6.2.1 Bubbler Humidifier 21
1.6.2.2 Enthalpy Wheel Humidifier 22
1.6.2.3 Membrane Based Humidifiers 23
1.6.2.3.1 Shell and Tube Membrane Based Humidifiers 23
1.6.2.3.2 Plate and Frame Membrane Based Humidifiers 24
1.6.2.3.3 Pleated Designs 25
1.6.2.4 Comparison of Humidification Methods 25
1.7 Planar Membrane Based Gas to Gas Humidifier Specifics 27
1.8 Project Goals 28
2.0 Experimental Methods 29
2.1 Water Permeation Testing 29
2.1.1 Static Water Vapour Permeation Test 29
2.1.2 Dynamic Water Permeation Test 30
2.2 Air Permeation Testing 36
2.3 Mechanical Strength Testing 37
2.4 Scanning Electron Microscopy and Energy Dispersive X-ray Spectroscopy 39

2.5 Accelerated Aging 41
2.6 Axisymmetric Drop Shape Analysis 42
2.7 Durability Testing 44
2.7.1 Low Temperature Durability Station 45
2.7.2 High Temperature Durability Station 47
3.0 Membranes for Gas to Gas Humidifiers 49
3.1 General Membrane Selection Procedure 49
3.2 Defining Operating Conditions 50
3.3 Membrane Selection Criteria 50
3.3.1 Water Permeation 51
3.3.2 Air Permeation 51
3.3.3 Mechanical Strength 52
3.3.4 Handling and Dimensional Stability 55
3.3.5 Lifetime 55
3.3.6 Overall Testing Procedure 56
3.4 Membranes Materials 57
3.4.1 Industries 57
3.4.1.1 Reverse Osmosis 57
3.4.1.2 Nanofiltration 57
3.4.1.3 Ultrafiltration 58
3.4.1.4 Microfiltration 58
3.4.1.5 Gas Separations 58
3.4.1.6 Pervaporation 59
3.4.1.7 Electrodialysis and Fuel Cells 60
3.4.1.8 Battery Separator Applications 60
3.4.2 Membrane Classification 60
3.4.2.1 Porous Membranes 60
3.4.2.2 Dense Membranes 61
3.4.2.3 Isotropic and Anisotropic Membranes 63
3.5 Summary of Membranes Materials Acquired and Tested 64
3.5.1 Membrane-01 64
3.5.2 Membrane-02 64
3.5.3 Membrane-03 64
3.5.4 Membrane-04 64
3.5.5 Membrane-05 64
3.5.6 Membrane-06 65
3.5.7 Membrane-07 65
3.5.8 Membrane-08 65
3.5.9 Membrane-09 65
3.5.10 Membrane-10 65
3.5.11 Membrane-11 65
3.5.12 Membrane-12 66
3.5.13 Membrane-13 66
3.5.14 Membrane-14 66
3.5.15 Membrane-15 66
3.5.16 Membrane-16 66
3.5.17 Membrane-17 66
3.5.18 Membrane-18 66
3.5.19 Membrane-19 67
3.5.20 Membrane-20 67

3.5.21 Membrane-21 67
3.5.22 Membrane-22 67
3.5.23 Membrane-23 67
3.5.24 Membrane-24 67
3.5.25 Membrane-25 67
3.5.26 Membrane-26 68
3.5.27 Membrane-27 68
3.5.28 Membrane-28 68
3.5.29 Membrane-29 68
3.5.30 Membrane-30 68
3.5.31 Membrane-31 68
3.5.32 Membrane-32 68
3.5.33 Membrane-33 68
3.5.34 Membrane-34 69
3.5.35 Membrane-35 69
3.5.36 Membrane-36 69
3.5.37 Membrane-37 69
3.5.38 Membrane-38 69
3.5.39 Membrane-39 69
3.5.40 Membrane-40 69
3.5.41 Membrane-41 70
3.5.42 Membrane-42 70
3.5.43 Membrane-43 70
3.5.44 Membrane-44 70
3.5.45 Membrane-45 70
3.5.46 Membrane-46 70
3.5.47 Membrane-47 70
3.5.48 Membrane-48 71
3.5.49 Membrane-49 71
3.5.50 Membrane-50 71
3.5.51 Membrane-51 71
3.5.52 Membrane-52 71
3.5.53 Membrane-53 71
3.5.54 Membrane-54 71
3.5.55 Membrane-55 71
3.5.56 Membrane-56 72
3.5.57 Membrane-57 72
3.5.58 Membrane-58 72
3.5.59 Membrane-59 72
3.5.60 Membrane-60 72
3.5.61 Membrane-61 72
4.0 Design Methodology for Plate and Frame Humidifiers 73
4.1 Gas to Gas Planar Humidifiers 73
4.2 Background for Design Process 75
4.2.1 General Considerations 75
4.2.2 Development of the Dimensionless Parameter 76
4.2.2.1 Residence Time 77
4.2.2.2 The Diffusion Time 77
4.2.2.3 The ‘R-Value’ 79
4.3 Experimental 79

4.3.1 Prototype Humidifiers 79
4.3.2 Humidifier Testing Procedures 80
4.4 Results and Discussion 81
4.4.1 Residence Time 81
4.4.2 Diffusion Time 82
4.4.3 The 'R-Value' Parameter 84
4.5 Gas to Gas Membrane Plate and Frame Humidifier Design Procedure 86
4.5.1 Background for the Design Procedure 86
4.5.2 Using the Design Procedure, an Example 90
4.6 Conclusions 94
5.0 Membrane Evaluation Results and Discussion 95
5.1 Water Permeation Testing 95
5.1.1 Static Water Vapour Permeation Testing 95
5.1.1.1 Results 95
5.1.1.2 Discussion 98
5.1.2 Dynamic Water Permeation Testing 98
5.2 Air Permeation Testing 102
5.3 Mechanical Strength Testing 104
5.3.1 Statistical Methods 104
5.3.2 Membranes 16 and 19 106
5.3.3 Membranes 8 and 16 108
5.3.4 Temperature and Humidity Effect on Membrane 16 109
5.4 Axisymmetric Drop Shape Analysis 110
5.4.1 Background 110
5.4.2 Time-Dependant Contact Angles, Drop Volumes, and Drop Radii Results 110
5.4.3 Effectiveness of Using ADSA for Membrane Qualification 111
5.4.4 Membrane Specific ADSA Considerations 112
5.4.4.1 Membrane 16 113
5.4.4.2 Membrane 48 114
5.4.4.3 Membrane 4 115
5.4.4.4 Membrane 58 116
5.4.4.5 Membrane 46 117
5.4.5 Conclusions for ADSA Testing 117
5.5 Accelerated Aging 118
5.5.1 Oxidation of Polyethylene 118
5.5.1.1 Effects of Process Conditions on Polyethylene 118
5.5.1.2 Mechanism of Oxidation 119
5.5.1.2.1 Initiation, Reaction 1 119
5.5.1.2.2 Propagation, Reactions 2 through 5 119
5.5.1.2.3 Termination, Reactions 6, 7, and 8 120
5.5.1.3 Preventative Measures 120
5.5.2 PEROX Accelerated Oxidation Test 120
5.6 Analysis of Silica Content of s-PEEK Membranes 123
5.7 Summary of Results 125
6.0 Membrane Durability Testing and Failure Analysis 127
6.1 Membrane 2 127
6.1.1 Low Temperature Durability Testing 127
6.1.1.1 Failure Analysis 128
6.1.2 High Temperature Durability Testing 129
6.1.2.1 Failure Analysis 129

6.2 Membranes 3 and 4 130
6.2.1 Low Temperature Durability Testing 130
6.2.1.1 Failure Analysis 131
6.3 Membrane 5 131
6.3.1 High Temperature Durability Testing 132
6.3.1.1 Failure Analysis 132
6.4 Membrane 8 132
6.4.1 Low Temperature Durability Testing 132
6.4.1.1 Failure Analysis 134
6.5 Membrane 10 134
6.5.1 Low Temperature Durability Testing 134
6.5.1.1 Failure Analysis 135
6.6 Membrane 12 135
6.6.1 Low Temperature Durability Testing 135
6.6.1.1 Failure Analysis 136
6.6.2 High Temperature Durability Testing 136
6.6.2.1 Failure Analysis 136
6.7 Membrane 15 140
6.7.1 Low Temperature Durability Testing 140
6.7.1.1 Failure Analysis 140
6.8 Membrane 16 142
6.8.1 Low Temperature Durability Testing 143
6.8.1.1 Failure Analysis 144
6.8.2 High Temperature Durability Testing 151
6.8.2.1 Failure Analysis 151
6.9 Membrane 20 152
6.9.1 Low Temperature Durability Testing 152
6.9.1.1 Failure Analysis 153
6.10 Membranes 21 to 24 157
6.10.1 Low Temperature Durability Testing 158
6.11 Membrane 32 161
6.11.1 Low Temperature Durability Testing 161
6.11.1.1 Failure Analysis 161
6.12 Membrane 40 162
6.12.1 Low Temperature Durability Testing 162
6.12.1.1 Failure Analysis 162
6.13 Membrane 43 164
6.13.1 Low Temperature Durability Testing 164
6.13.1.1 Failure Analysis 165
6.14 Membrane 45 165
6.14.1 High Temperature Durability Testing 165
6.14.1.1 Failure Analysis 166
6.15 Membrane 46 166
6.15.1 Low Temperature Durability Testing 166
6.16 Membranes 50 through 54 168
6.16.1 Low Temperature Durability Testing 168
6.16.1.1 Failure Analysis 169
6.17 Membrane 55 170
6.17.1 High Temperature Durability Testing 170
6.18 Summary of Durability Results 171

7.0 Conclusions and Recommendations 175
7.1.1 Humidifier Channel and Plate Design 175
7.1.2 Humidifier Membrane Selection 175
7.1.3 Recommendations for Future Studies 178
7.1.4 Final Recommendations 179
8.0 References 180
A.0 Calculation of Absorptive Flux for ADSA 186
B.0 Calculated Membrane Parameters 188
B.1 Membrane Water Flux and Air Permeation Values 188
C.0 Sample Calculations 190
C.1 Water Flux Calculations 190
C.2 Air Permeation Calculations 192
D.0 Humidifier Phenomena 194
D.1 Orientation Effects 194
D.2 Flow Arrangement 195
D.3 Temperature and Flow Effects 196
D.4 Relative Humidity Effect 197
D.5 Membrane Thickness 198

List of Tables

Table 1-1: Constants for the Wagner equation for an air-water system 14
Table 1-2: Summary of advantages and disadvantages of humidification methods. 26
Table 2-1: Operating conditions for low and high temperature durability stations. 44
Table 3-1: Conditions of high and low temperature operational regimes. 50
Table 4-1: Geometries for various humidifiers tested. 80
Table 4-2: Parameters used in the sample humidifier design presented. 91
Table 5-1: Static water permeation test results from various membrane tests. 97
Table 5-2: Comparison of results for flat and ribbed silica/UHMWPE materials. 107
Table 5-3: Statistical analysis comparing the means for yield and modulus of flat and ribbed membranes. 107
Table 5-4: Comparison of results for two similar flat sheet silica/UHMWPE materials. 108
Table 5-5: Statistical analysis comparing the means for yield and modulus similar flat silica/PE materials. 108
Table 5-6: Comparison of mechanical tests on membrane 16 in dry and wet state, at room temperature and 75^{o}C. 109
Table 5-7: Membranes studied using ADSA. 110
Table 5-8: Summary of ADSA Testing Results. 111
Table 5-9: Average Evaporation Corrected Absorptive Fluxes and Net Absorption for the Five Membranes 111
Table 5-10: Summary of s-PEEK/silica membranes tested. 124
Table 6-1: EDS results for Membrane 16 at BOL and EOL 147
Table 6-2: Performance decrease in membranes with different plasticizer oil types over 15 hours of LTDS. 160
Table 6-3: Summary of membranes tested on the LTDS with failures, failure mechanisms and recommendations. 171
Table 6-4: Summary of membranes tested on the HTDS with failures, failure mechanisms and recommendations 173
Table 7-1: Summary of criteria for membrane materials. 176
Table 7-2: Summary of experimental procedures used to screen membrane materials for fuel cell humidifiers. 176
Table B-1: Summary of water flux and dry air permeation values for all membranes. ... 188
Table C-1: Averaged data for results shown in Figure C-1. 191
Table C-2: Specific humidity and water flux for sample data at different flow rates. 192

List of Figures

Figure 1-1: Standard Fuel Cell Components. 3
Figure 1-2: Polarization curve for a fuel cell. 4
Figure 1-3: Example of the structure of perfluorosulphonic acid PTFE copolymer (PFSA) Nafion™. 7
Figure 1-4: Microstructure of Nafion in the presence of water. 8
Figure 1-5: Comparison of fuel cell performance with and without external humidification 10
Figure 1-6: Performance of fuel cell under saturated and flooding conditions. 11
Figure 1-7: Water content in the fuel cell as a function of temperature, stoichiometry, and pressure 17
Figure 1-8: Water balance in the fuel cell. 18
Figure 1-9: A double path flow field design 20
Figure 1-10: Emprise enthalpy wheel humidifier. 23
Figure 1-11: Shell and tube based hollow fiber membrane humidifier 24
Figure 1-12: Planar membrane based humidifier. 24
Figure 1-13: Pleated humidifier, pleat-pack is folded membrane within a clam-shell housing. 25
Figure 1-14: Planar membrane based gas to gas humidifier for 1.5kW fuel cell. 27
Figure 2-1: Cup test equipment for static water permeation test. 30
Figure 2-2: Cup test equipment for static water permeation test. 30
Figure 2-3: Greenlight Power Technologies, G-50 Fuel Cell Test Station 31
Figure 2-4: CAD drawing of a plate for the dynamic water permeation test. 32
Figure 2-5: Assembly of a test module for dynamic water permeation test. 32
Figure 2-6: Surface mesh of solid model of flow channels for the water permeation test module in ANSYS Workbench™ 9.0. 33
Figure 2-7: Pressure contour for water permeation module for air at 25^{o}C at 4 SLPM. 34
Figure 2-8: Velocity profile for water permeation module for air at 25^{o}C at 4 SLPM. 34
Figure 2-9: Conditions for standard dynamic water permeation test. 35
Figure 2-10: Air permeation testing apparatus. 36
Figure 2-11: Stress-strain test on membrane material. 38
Figure 2-12: Stress-strain curve for a polymer membrane demonstrating Young's Modulus and Yield Strength. 39
Figure 2-13: Samples mounted on stubs prepared for SEM analysis. 41
Figure 2-14: Sessile drop on membrane surface. 42
Figure 2-15: Process flow diagram of the low temperature durability station (LTDS). .....

Figure 2-16: Photograph of the LTDS. 47
Figure 2-17: Process flow diagram of the high temperature durability station (HTDS). 48
Figure 2-18: Photograph of the HTDS. 48
Figure 3-1: Membrane selection procedure. 49
Figure 3-2: Cross-section of humidifier channel showing membrane creep under pressure. 53
Figure 3-3: COSMOSXpress simulation of membrane deflection into the humidifier channel under 50 kPa of pressure, membrane elastic modulus of 75 MPa, deformation is exaggerated by a factor of 11.3. 54
Figure 3-4: Membrane deflection at 50 kPa, as a function of elastic modulus, as simulated by COSMOSXpress. 54
Figure 3-5: Membrane testing procedure 56
Figure 3-6: Comparison of transport in porous and dense membranes. 59
Figure 3-7: Comparison of transport in porous and solution-diffusion type membranes 62
Figure 3-8: Cross-sectional profile of solution-diffusion process. 62
Figure 3-9: Comparison of isotropic and anisotropic membranes. 63
Figure 4-1: Single humidifier plate. 73
Figure 4-2: Schematic of transport in the channel of the heat and moisture exchanger. 74
Figure 4-3: General schematic for operation of humidifier. 74
Figure 4-4: Humidifier performance as a function of residence time, values for three plate sets with different channel depths (1.0, 1.4, and 2.0 mm), at stream 3 temperature and dew point of 75°C, flow rates from 10 to 60 SLPM. 81
Figure 4-5: : Humidifier performance as a function of diffusion time, values for three plate sets of differing channel depths (1.0, 1.4, and 2.0 mm) at residence times of 0.1 and 0.2s, at stream 3 temperature and dew point of 75°C. 83
Figure 4-6: Response surface for tests completed at 65°C, showing the combined effects of velocity (m/s) and channel depth (mm) on WRR (%). 84
Figure 4-7: Stream 2, dry outlet humidity ratios for experiments at different R-values with three plate sets (1.0, 1.4, and 2.0 mm) at three wet inlet stream 3 dew point temperatures (55, 65, and 75°C) and various flow rates (10 to 60 SLPM). 85
Figure 4-8: Water recovery ratios for various humidifiers (see Table 4-1) as a function of the R-value at stream 3 dew point temperature of 65°C. 86
Figure 4-9: External humidifier geometry. 87
Figure 4-10: Flowchart for humidifier design procedure. 92
Figure 5-1: Static water permeation tests for four membranes at 80°C 95
Figure 5-2: Static water permeation tests for four membranes at 22°C 96
Figure 5-3: Dynamic water permeation tests for three membranes, Stream 3 inlet: 80°C and 100% RH, Stream 1 inlet: 22°C, 0% RH. 97
Figure 5-4: Water permeation test for Membrane 16 at S1: 23°C, 0% RH; and S3: 75°C,

100% RH, membrane area = 33.24 cm^2 99

Figure 5-5: Velocity normalized flux of water through membrane 16, in the water permeation test module S1: 23°C, 0% RH; and S3: 75°C, 100% RH, membrane area = 33.24 cm^2 100

Figure 5-6: Comparison of three membranes, demonstrating the increase in resolution at higher flow rates in water permeation module, at conditions S1: 23°C, 0% RH; and S3: 75°C, 100% RH, membrane area = 33.24 cm^2. 101

Figure 5-7: Membrane water flux values at 6 SLPM in water permeation module at conditions S1: 23°C, 0% RH; and S3: 75°C, 100% RH, membrane area = 33.24 cm^2. 101

Figure 5-8: Air permeation plots for three membranes. 102

Figure 5-9: Wet and dry air permeation for two membranes. 103

Figure 5-10: Dry air permeation for membranes at 21 kPa, module area = 5 cm^2. 104

Figure 5-11: Ribbed membrane orientation in experiments. 106

Figure 5-12: Cross sections flat and ribbed membranes, ribs are not to scale, number of rib is not to scale. 107

Figure 5-13: In humidifier performance for membranes tested. 112

Figure 5-14: Absorptive flux in membrane 16 over time. 113

Figure 5-15: Change in surface tensions at the membrane – water interface over time... 114

Figure 5-16: Change of membrane 48 shape over time, shown to alter the ability of the camera to gain time dependent information. 115

Figure 5-17: Absorptive flux in membrane 4 over time. 116

Figure 5-18: Sessile drops on membrane 46 with time. 117

Figure 5-19: Rate of polyethylene oxidation with temperature (Wilson, 1955). 118

Figure 5-20: Percent weight loss in polyethylene and silica membranes with (20) and without antioxidant (16) in PEROX test. 121

Figure 5-21: Rate of weight loss in polyethylene and silica membranes with (20) and without antioxidant (16) in PEROX test. 122

Figure 5-22: Average elastic modulus of membranes with and without antioxidant coating before and after PEROX test. 123

Figure 5-23: Water transport performance of s-PEEK/silica membranes with different silica content. 124

Figure 5-24: Surface contour plot of the effects of silica % and flow on the water flux of the s-PEEK/silica membranes. 125

Figure 5-25: Membrane testing results chart. 126

Figure 6-1: Water transport tests results for Membrane 2 on LTDS at BOL and after 730 hours of operation. 128

Figure 6-2: Water transport performance decrease at 4 and 6 SLPM in membrane 2 on HTDS over time. 129

Figure 6-3: Membrane 2 after 700 hours on the HTDS, cracking in material. 130
Figure 6-4: Water transport tests results for Membrane 4 on LTDS at BOL and up to 550 hours of operation. 131
Figure 6-5: Water transport performance decrease at 4 and 6 SLPM in membrane 8 on LTDS over time. 133
Figure 6-6: Dry air crossover in test module for membrane 8 over time while under operation on the LTDS. 133
Figure 6-7: Deformation of membrane 10 after 558 hours of testing on LTDS. 134
Figure 6-8: Water transport performance decrease at 4 and 6 SLPM in membrane 12 on LTDS over time. 135
Figure 6-9: Water transport performance decrease at 4 and 6 SLPM in membrane 12 on HTDS over time. 136
Figure 6-10: Membrane 12, new at 1000x magnification under SEM. 138
Figure 6-11: Membrane 12 at 1000x magnification after 1146 hours of operation on HTDS under SEM 138
Figure 6-12: Membrane 12, new at 20000x magnification under SEM. 139
Figure 6-13: Membrane 12 at 20000x magnification after 1146 hours of operation on HTDS under SEM 139
Figure 6-14: Membrane 15 water transport performance at 4 SLPM, from BOL to 20 hours, operating at stream 1 temperature of 23°C and 0% RH and stream 3 temperature of 75°C and 100% RH. 140
Figure 6-15: Membrane 15, new under SEM at 10000x magnification. 141
Figure 6-16: Membrane 15 after 20 hours of operation, under SEM at 10000x magnification, on the dry side of the membrane. 141
Figure 6-17: Membrane 15 at BOL, 20 hours of operation, and then after being washed with hexane, operating at stream 1 temperature of 23°C and 0% RH, and stream 3 temperature of 75°C and 100% RH. 142
Figure 6-18: Water transport performance for two samples of membrane 16 over time during operation on the LTDS. 143
Figure 6-19: Air crossover at 21 kPa for membrane 16 over time during operation on LTDS 144
Figure 6-20: Membrane 16 at BOL under SEM at 30000x magnification. 145
Figure 6-21: Dry side of membrane 16 at EOL under SEM at 30000x magnification. ... 145
Figure 6-22: Wet side of membrane 16 at EOL under SEM at 30000x magnification. ... 146
Figure 6-23: Cross-section of membrane 16 at EOL at 250x magnification. 147
Figure 6-24: Cross-section of membrane 16 at EOL, at 1000x magnification, the boxes indicate the location of EDS scans. 148
Figure 6-25: Atomic percentages of carbon and silicon through a cross-section of membrane 16 at the EOL. 148
Figure 6-26: Ratio of silicon to carbon through a cross-section of membrane 16 at EOL.

..... 149
Figure 6-27: Movement of polyethylene in the membrane 16 under operation leading to loss of silica on the wet side of the membrane. 150
Figure 6-28: Cracking of membrane 16 after 300 hours of operation on HTDS. 151
Figure 6-29: Membrane 16 tensile testing for BOL and EOL material from the HTDS.. 152
Figure 6-30: Stream 2 wet and dry bulb temperature for membrane 20 from BOL to 11 hours of operation. 153
Figure 6-31: Membrane 20 under SEM at 5000x magnification at BOL. 154
Figure 6-32: Dry side of membrane 20 after 20 hours of operation, under SEM at 5000x magnification. 154
Figure 6-33: Wet side of membrane 20 after 20 hours of operation, under SEM at 5000x magnification. 155
Figure 6-34: Membrane 20 after 20 hours of operation, at 100x magnification, surface is largely coated, with some areas of exposed silica. 156
Figure 6-35: Membrane 20 after 20 hours of operation, at 1000x magnification showing interface between the silica and the fouling covering the membrane. 156
Figure 6-36: Membrane 20 after 20 hours of operation, at 5000x magnification showing interface between the silica and the fouling covering the membrane. 157
Figure 6-37: Water transfer performance of membrane 21, containing 'Oil A' at BOL and after 15 hours of operation. 158
Figure 6-38: Water transfer performance of membrane 22, containing 'Oil B' at BOL and after 15 hours of operation. 159
Figure 6-39: Water transfer performance of membrane 23, containing 'Oil C' at BOL and after 15 hours of operation. 159
Figure 6-40: Water transfer performance of membrane 24, containing 'Oil D' at BOL and after 15 hours of operation. 160
Figure 6-41: Delaminating of s-PEEK from porous substrate in membrane 31, after 1 hour of operation at stream 3 temperature of 75^{o}C, 100% RH. 161
Figure 6-42: Degradation in water transport performance for membrane 40 over time on the LTDS. 162
Figure 6-43: Membrane 40 at BOL, under SEM at 1000x magnification. 163
Figure 6-44: Membrane 40 after 1000 hours of operation (EOL) under SEM at 1000x magnification. 164
Figure 6-45: Water transport performance of membrane 43 over time on the LTDS..... 165
Figure 6-46: Failure due to cracking of membrane 45 on HTDS (sample is 28cm long). 166
Figure 6-47: Results for membrane 46 on LTDS over 2000 hours. 167
Figure 6-48: Surface of membrane 46 after 2000 hours of operation on the LTDS, flaking of surface can be observed. 167
Figure 6-49: Water transport performance for membrane 50 at BOL and 300 hours of operation on the LTDS. 168

Figure 6-50: Membrane 50 after 500 hours of operation on the LTDS. 169

Figure 6-51: Performance of Membrane 55 after 1100 hours of operation on HTDS. 170

Figure C-1: Data for stream 2 wet and dry temperatures recorded for testing a membrane at different flow rates, with stream 3 at 75^{o}C and 100% relative humidity and stream at 25^{o}C and 0% relative humidity. 190

Figure D-1: Test module arrangements for orientation tests, 1)Vertical – Wet on Top; 2) Vertical – Dry on Top; 3) Horizontal – Wet on Top; 4) Horizontal – Dry on Top; 5) Horizontal – Membrane Vertical. 194

Figure D-2: Results for humidifier orientation tests. 195

Figure D-3: Comparison of performance under co-flow and counter-flow arrangements. 196

Figure D-4: Temperature and flow effects of humidifier test module. 197

Figure D-5: Effect of relative humidity of stream 3 on water flux, stream 3 conditions: 75^{o}C, 0 to 100% RH; stream 1: 75^{o}C, 0% RH. 198

Figure D-6: Results for test with a single membrane and two membranes stacked together at stream 3 conditions: 75o, 100% RH; stream 1: 25oC, 0% RH. 199

Chapter 1

1.0 Introduction and Background

1.1 General Background

Polymer electrolyte membrane fuel cells (PEMFC's) act as energy conversion devices that change the chemical energy of hydrogen into electrical energy. This is accomplished through the use of a proton exchanging polymer membrane that has catalyst layers attached on either side acting as the electrodes; this is generally referred to as a membrane electrode assembly (MEA). This membrane must remain fully saturated with water to maintain conductivity, and so reactant streams must be maintained at high relativity humidity. Thus, PEMFC's require the use of reactant humidifiers, and this project addresses the design and selection of membranes for such a humidifier.

On the anode side of the MEA the catalyst layer helps split hydrogen gas into protons and electrons. The membrane then allows the transference of protons while acting as an insulating barrier to the passage of electrons and gases. The anode and cathode sides of the membrane can then be electrically connected to form a circuit through which work can be done. At the cathode, another catalyst layer helps combine oxygen gas with the transferred protons and electrons to produce water. These membranes are a based on sulphonated fluoropolymers, also known as perfluoronated sulphonic acid (PFSA), the most common of which are manufactured under the trade name Nafion™. The anode, cathode, and overall reactions are listed below (Larminie and Dicks, 2003).

Anode:	$H_2 \rightarrow 2H^+ + 2e^-$	[1-1]
Cathode:	$1/2\ O_2 + 2e^- + 2H^+ \rightarrow H_2O$	[1-2]
Overall:	$H_2 + 1/2\ O_2 \rightarrow H_2O$	[1-3]
In full:	$H_2 + 1/2\ O_2 \rightarrow H_2O$ + electrical power + waster heat	[1-4]

1.2 Fuel Cell Components

Fuels cells consist of various components that are stacked together to function as a complete unit. The components are detailed below and a single cell and stack can be

visualized below in Figure 1-1.

1.2.1 Electrolyte

The electrolyte in PEMFC's has traditionally consisted of PFSA polymer. The polymer acts as a medium through which proton exchange may occur. PFSA allows the passage of protons (H^+) from the anode, where hydrogen gas is supplied; to the cathode where oxygen gas is supplied. The electrolyte also acts as an electronic insulator and a barrier to gas crossover.

1.2.2 Catalyst Layer or Electrodes

The catalyst layer is typically based on a platinum catalyst which is supported on carbon particles. These structures are then deposited and fixed onto the electrolyte surface. This creates a three phase boundary layer where the reactant gases, electrons, and protons simultaneously interact with the supported catalyst and the electrolyte (Larminie and Dicks, 2003).

1.2.3 Gas Diffusion Layer

The gas diffusion layer (GDL) is a carbon based paper or cloth material which is compressed between the flow field plates and the catalyst coated membrane. The GDL is porous and provides consistent and well distributed electrical contact between the fuel cell plate and the catalyst layer; as well it acts to equally distribute the reactant gases to the catalyst sites where the fuel cell reaction occurs. The GDL must also be able to remove water away from the electrolyte surface as to prevent fuel cell flooding.

1.2.4 Bi-Polar Flow Field Plates

Finally the flow field plates provide the structural support necessary to keep the fuel cell assembly together. These plates have flow fields in their surfaces through which the reactants can be supplied to the fuel cell, and the products of the fuel cell reactants can be removed. They also act as a connection through which electrons can travel from one reaction site to the next. These plates are most often bi-polar in nature, in that they provide reactants to the anode on one side and to the cathode on the other side. This way the electrons produced in the anode reaction on one side of the plate can travel easily through

the plate to the cathode side of the next cell where they can be used in the cathode reaction.

1.2.5 The Stack

Single fuel cells can be created with a catalyst coated membrane flanked by gas diffusion layers and held together by bi-polar flow field plates. These single cells can produce a current at a certain voltage depending on the active area of the catalyst on the electrolyte and the reactants provided to the cell. By stacking these cells together in series increased voltages and power at a given current density can be created. Thus the fuel cell stack is created.

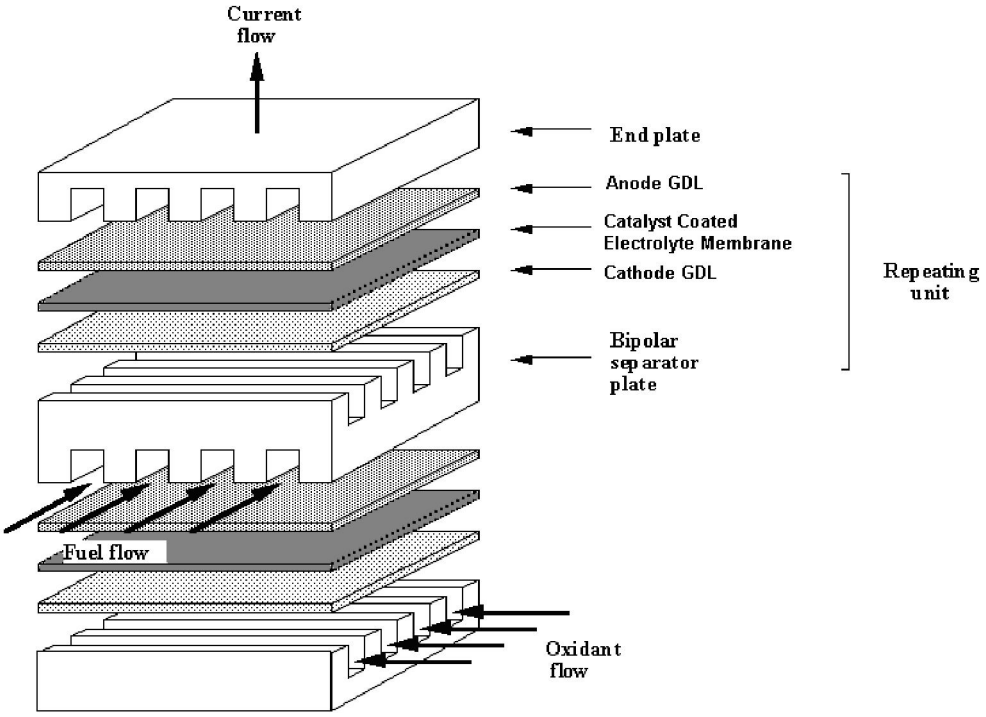

Figure 1-1: Standard Fuel Cell Components (Kinoshita, 2001).

1.3 Fuel Cell Voltage Losses

The electrical performance of a fuel cell can be understood by drawing a current from the fuel cell and recording the operating voltage at that current. For consistency in reporting data, currents are often expressed as current densities (mA/cm^2). Plotting the operating voltage against current density gives what is called a polarization curve, as seen in Figure

1-2. There are three distinct parts of this curve which result from three distinct types of loses in the fuel cell. To optimize fuel cell performance, these losses should be minimized so as to maximize operating voltage at a given current, in order to maximize power.

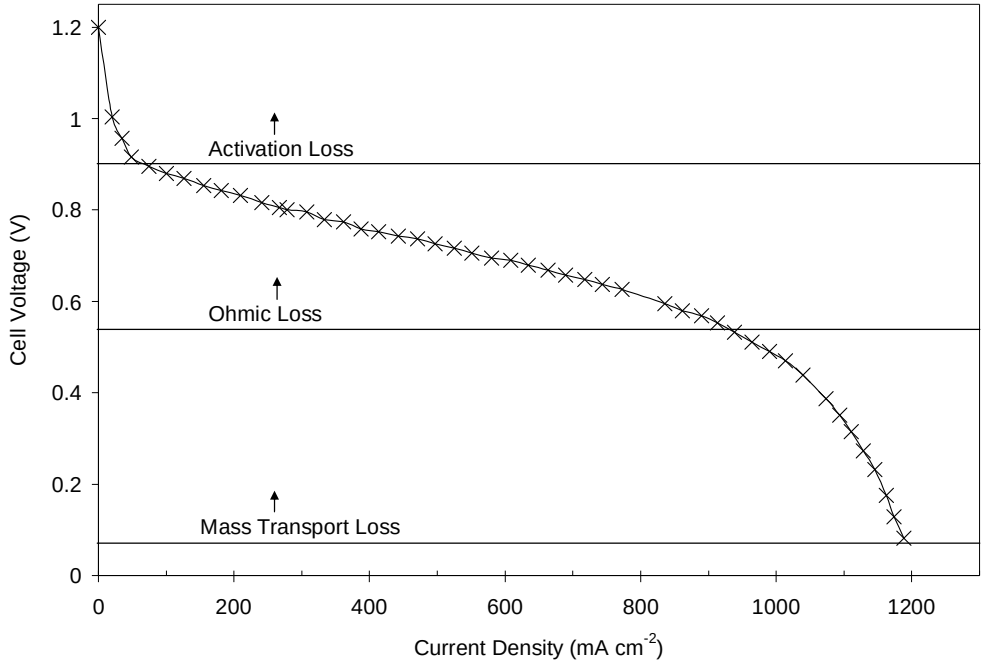

Figure 1-2: Polarization curve for a fuel cell.

1.3.1 Activation Losses

In a fuel cell electrochemical reactions occur at the fuel cell electrodes in the catalyst layers. These reactions result in the movement of electrons to the cathode electrode from the anode electrode. A voltage loss, activation overpotential is associated with these reactions, this can be described by the Tafel or Bulter-Volmer equations can be used to describe this voltage loss (Bernardi and Verbrugge, 1992).

$$i = i_0 \left\{ \exp\left(-\alpha \frac{zF}{RT} \Delta\eta_{act} \right) - \exp\left((1-\alpha) \frac{zF}{RT} \Delta\eta_{act} \right) \right\} \qquad [1\text{-}5]$$

In this equation, i is current density in A m^{-2}, i_o is an exchange current density, α is a charge transfer coefficient, z is the number of electrons transported for the reaction, F is the Faraday's constant, R is the universal gas constant, T is the temperature, and η_{act} is the activation overpotential. For positive voltage the left exponential becomes

negligible and the equation can be arranged to describe the activation overpotential:

$$\Delta\eta_{act} = \beta \ln\left(\frac{i}{i_0}\right) \quad [1\text{-}6]$$

In which β is a constant for the reaction. This describes the voltage loss due to activation, which will decrease with increased temperature, increased effective catalyst area, increased reactant concentrations, and increased pressure (Larminie and Dicks, 2003). These losses cause the voltage drop in the polarization curve in Figure 1-2 at low current density (<100mA/cm^2).

1.3.2 Ohmic Losses

In the electrolyte there will be resistance to the flow of the ions (protons) generated which will cause another potential loss in the fuel cell. Also the electrons generated must travel through the electrodes, the diffusion layers, the plates, and the cell interconnects; so there will be contact and electrical resistances impeding electron flow as well. The resistance to electron and ion flow can be described by Ohm's Law. The Ohmic loss will be represented by:

$$\Delta\eta_{ohmic} = IR \quad [1\text{-}7]$$

In this equation, η_{ohmic} is ohmic overpotential, I is current, and R is resistance. The value of R is the sum of all resistances present in the fuel cell:

$$R = r_{ionic} + r_{electrical} + r_{contact} \quad [1\text{-}8]$$

In this equation, r represent resistances in the fuel cell, generally the ionic resistance will be the dominant resistance. The linear voltage drop in the polarization curve in Figure 1-2 at intermediate current densities (~100 mA cm^{-2} – 1000 mA cm^{-2}) is caused by Ohmic loses.

1.3.3 Mass Transport Losses

As the current drawn from the fuel cell is increased the rate at which reactants (O_2) and products (H_2O) at the cathode must travel to and from the reaction sites increases. Eventually, the reaction becomes limited in by the mass transport of oxygen to the catalyst sites. At this point voltage loses are observed due to this mass transport limitation. These losses are predominant as the limiting current density is approached, which is usually at current densities greater than 1000 mA/cm^2 as seen in Figure 1-2. The losses can be represented by the following empirical equation (Chamberlin et al., 1994):

$$\Delta\eta_{trans} = m \cdot \exp(n \cdot i) \qquad [1\text{-}9]$$

In this equation, η_{trans} is the mass transport overpotential, m and n and fitting coefficients, and i is current density.

1.3.4 Overall Fuel Cell Equation

In order to create an overall equation for the fuel cell voltage performance at a given current the three voltage loss equations are added together to generate the overall fuel cell equation, giving the output voltage of the fuel cell, V_{cell} (Kim et al., 1995; Laurencelle et al., 2001):

$$V_{cell} = E_0 - \eta_{act} - \eta_{ohmic} - \eta_{trans} \qquad [1\text{-}10]$$

$$V_{cell} = E_0 - iR - A\ln(i) - m\exp(ni) \qquad [1\text{-}11]$$

E_0 represents the open cell voltage of the fuel cell. This can be described in terms of the potential of the fuel cell reaction. Since the oxygen reduction reaction is slower than the hydrogen oxidation reaction, the voltage loss from the oxygen reaction dominates and (Srinivasan et al., 1988):

$$E_0 = E_r + 2.303\frac{RT}{\alpha F}\log(i_0) \qquad [1\text{-}12]$$

Equation 1-11 can be fit to polarization curves for a fuel cell such as the voltage-current curve in Figure 1-2, using E_0, A, R, m, and n as parameters.

1.4 The Importance of Fuel Cell Humidification

1.4.1 Nafion™ Structure

As stated previously Nafion™ is a sulphonated fluoropolymer, generally used as the ion exchange medium driving the fuel cell reaction. Similar ionomers used in fuel cells are based of PFSA as well. PFSA is produced by first perfluorinating a polyethylene chain. In this process hydrogen atoms on the polyethylene chain are substituted with fluorine atoms. This produces polytetrafluoroethylene (PTFE) better known as Teflon™. Next, fluorinated monomers ending in sulphonic acid (HSO_3) groups are added to the PTFE chain (Grot, 1972). This sulphonation step creates a perfluorosulphonic acid PTFE copolymer (PFSA), the most common family of which is called Nafion™, an example structure is shown in Figure 1-3.

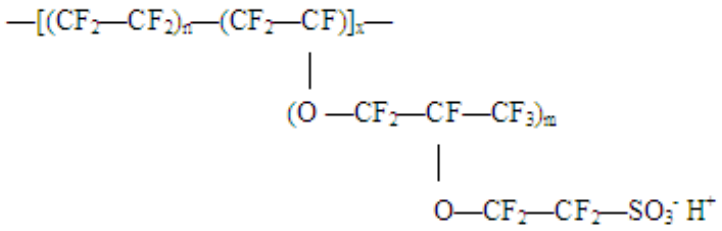

Figure 1-3: Example of the structure of perfluorosulphonic acid PTFE copolymer (PFSA) Nafion™.

There are two important parts of this polymer that are seen in Figure 1-3, (i) the perfluoronated backbone and (ii) the ionic bonded sulphonic acid functional group. The perfluoronated backbone is by nature highly hydrophobic, while the sulphonic acid group is highly hydrophilic. In the presence of water this leads to hydrophilic/hydrophobic nano-separation in the membrane polymer matrix. The sulphonic acid groups form clusters supported by the hydrophobic domain (Kreuer, 2001). This is seen in Figure 1-4 below.

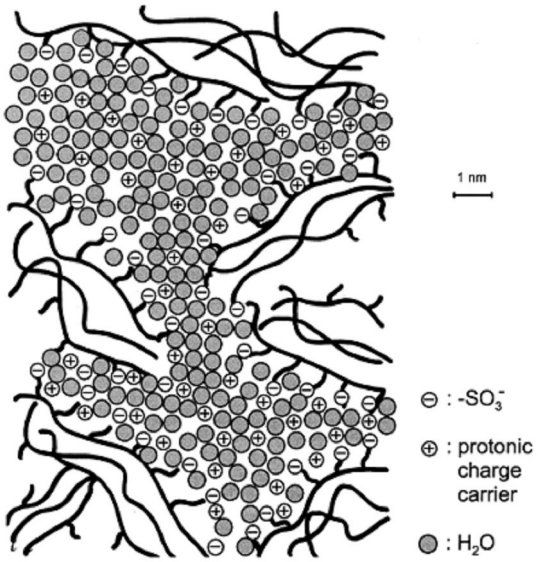

Figure 1-4: Microstructure of Nafion in the presence of water (Kreuer et al., 2004).

In the dry state the average cluster contains 26 SO_3^- groups; while in the presence of water the cluster expands containing about 70 SO_3^- groups (Gierke and Hsu, 1982). In this hydrated structure water and protons can move with relative ease through the membrane.

1.4.2 PFSA Reactions with Water

The environment created by clustering of the hydrophilic sulphonic groups creates an amorphous acidic environment in which protons will travel from the anode to the cathode during fuel cell operation. Evidently the presence of water is important for the proper functioning of PFSA, and on a larger scale the fuel cell system, since protons are carried through the membrane attached to water in a solvated form. It has been shown that increasing the number of water molecules in relation to the number of SO_3^- groups in the membrane will increase the ionic conductivity of the PFSA membrane (Gavach et al., 1989). An average of six water molecules per SO_3^- group represents the minimum threshold for hydration and in a well hydrated membrane the ratio of water molecules to SO_3^- groups will approach 20 (Escoubes and Pineri, 1982; Larminie and Dicks, 2003). An increase in ionic conductivity will lower the Ohmic resistance described in Section 1.3.2, which will lead to an increase in the fuel cell voltage at a given current, thereby increasing the overall fuel cell power output.

The presence of water also causes swelling of PFSA membranes in the order of 10 to 20%.

In the case of Nafion 117™ it has been described by (Motupally et al., 2000):

$$\delta_M = \delta_{M0}(1 + 0.11121\lambda_{avg}) \quad [1\text{-}13]$$

In this equation, δ_M is the thickness of membrane, δ_{M0} is the dry thickness of the membrane, and λ_{avg} is the average water content in the membrane. The water content in this type of membrane has been fit to an empirical equation (Zawodzinski et al., 1993):

$$\lambda = 0.043 + 17.81a_W - 39.85a_W^2 + 36.0a_W^3 \quad [1\text{-}14]$$

Where a_w is the activity of water in the vapour phase around the membrane surface;

$$a_W = \frac{P_W}{P_{sat}(T)} \quad [1\text{-}15]$$

In this equation, P_W is the partial pressure of water in the gas stream, and P_{sat} is the saturation vapour pressure at the given temperature. Continuous drying and wetting of PFSA membranes will cause swelling and contraction of the polymer. This will lead to mechanical stresses in the membrane, which may lead to failure.

1.4.3 Dehydration of the Membrane

The kinetics of the fuel cell reaction described in Section 1.3 state that to maximize efficiency, the fuel cell should be operated at elevated temperatures and at gas flow rates greater than the stoichiometry of the reaction. The accelerated flow of gases through the fuel cell at elevated temperatures will lead to the evaporation of any excess water collected in the membrane or water produced by the fuel cell reaction.

As water is removed from the fuel cell, the membrane begins to dry out. This leads to the dissociation of the SO_3^- - H_2O clusters described previously. This in turn limits the rate at which protons can be transported through the electrolyte, which leads to increased ionic or electrolyte resistance as described in Section 1.3.2. Increased resistance causes more rapid voltage drops with increased current, which may lead to fuel cell failure or decreased performance (Watanabe et al., 1993; Zawodzinski et al., 1993). To maintain performance the fuel cell reactant gases must be humidified, so that excessive evaporation of water will

be minimized. The effect of external humidification on the fuel cell performance is shown in Figure 1-5.

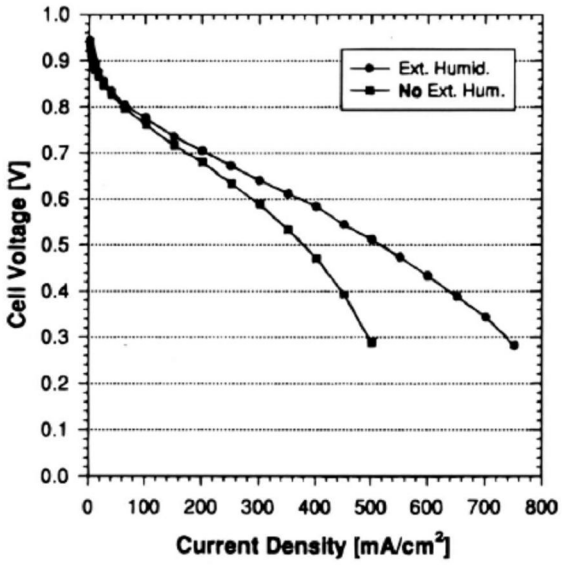

Figure 1-5: Comparison of fuel cell performance with and without external humidification (Buchi and Srinivasan, 1997).

Localized drying of the membrane can lead to areas of high and low ionic resistance within the membrane. This will cause current gradients throughout the membrane. Areas of low resistance and high current will see increased transport, leading to accelerated failure at that location (Hakenjos et al., 2004). This causes temperature gradients across the plane of the membrane, compounding the problem. Localized drying may also cause mechanical stresses in the electrolyte due to the variations in membrane expansion in the presence of water as described in Section 1.4.2. This may also lead to premature membrane failure.

1.4.4 Flooding

Excess water accumulation in the fuel cell will lead to an increase in water condensation and flooding in the fuel cell. This becomes a problem as water clogs pores in the GDL and blocks channels in the flow field plates. The excess water will act as a barrier to oxygen mass transport to the cathode catalyst sites (Lee et al., 2003). This leads to a decreased effective catalyst active area, and thus an increase in activation losses. Also increased are mass transport voltage losses indicated in Section 1.3.3, leading to further power loss. The

performance of a fuel cell under saturated and flooding conditions can be seen in Figure 1-6.

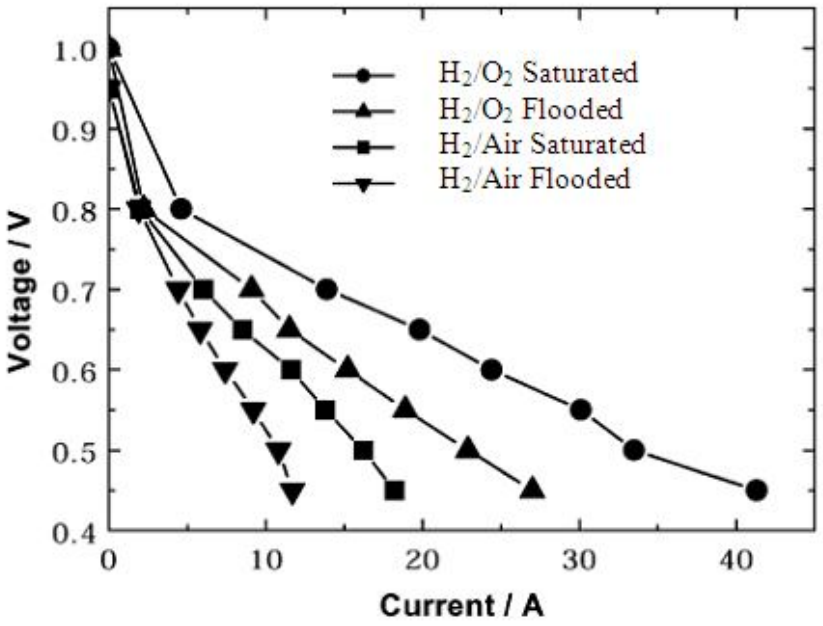

Figure 1-6: Performance of fuel cell under saturated and flooding conditions (Yoon et al., 2003).

1.5 Water and Heat Balances in PEMFC's

1.5.1 Water Balance

Water content in PFSA membranes is affected by four phenomenon; electro-osmotic drag, water production, back diffusion, and reactant stream humidification. These processes are summarized in the following sections.

1.5.1.1 Electro-Osmotic Drag

Electro-osmotic drag refers to the water molecules that are brought from the anode to the cathode by the motion of protons in the electrolyte due to the potential gradient (Choi et al., 2000). Thus water in the anode stream condenses and moves across the membrane with the protons. An electro-osmotic drag coefficient is defined as a parameter which describes the number of water molecules that are transported to the cathode per proton. For Nafion 117 membrane materials in contact with water vapour this value has been

shown to be between 1 and 1.4 which corresponds to λ the water content of the membrane (H_2O/SO_3^- ratio) of 11(Fuller and Newman, 1992). For membranes saturated in liquid water this value has been reported as approximately 2.5 corresponding to a λ of 22 (Zawodzinski et al., 1993). Evidently this value varies depending on the water content of the membrane which can be calculated from Equation 1-14. If it is assumed that the osmotic drag coefficient, n_{drag} is linearily proportional to the water content then (Springer et al., 1991):

$$n_{drag} = \frac{2.5}{22}\lambda \qquad [1\text{-}16]$$

And,

$$N_{W,drag} = n_{drag} \cdot \left(\frac{2I}{F}\right) \qquad [1\text{-}17]$$

In this equation, $N_{w,drag}$ refers to the moles of water transported per second by electro-osmotic drag.

1.5.1.2 Water Production

Water production occurs due to the fuel cell reaction at the cathode according to Equation 1-3. In molar terms, by a simple Faraday's relationship, water production occurs at a rate of (Larminie and Dicks, 2003):

$$N_{W,prod} = \frac{I}{2F} \qquad [1\text{-}18]$$

In this equation, $N_{w,prod}$ refers to the moles of water produced by the fuel cell reaction per second.

1.5.1.3 Back Diffusion

Due to the excess water that is collected at the cathode due to electro-osmotic drag and water production, a concentration gradient is created from the cathode to the anode. This leads to back diffusion of water through the membrane to the anode, following Fick's Law (Nguyen and White, 1993):

$$N_{W,diff} = D_W \frac{dc_W}{dy} \quad [1\text{-}19]$$

In this equation $N_{w,diff}$ is the moles of water transported by diffusion per second, D_w is the diffusion coefficient of water in the membrane, c_w is the concentration of water, and y is the position axially through the membrane from surface to surface. When approximated by a single-step linear difference between the concentration at the anode and the cathode surfaces this equation changes to the following (Nguyen and White, 1993):

$$N_{W,diff} = D_W \frac{c_{W,C} - c_{W,A}}{\delta_M} \quad [1\text{-}20]$$

Where $c_{w,c}$ and $c_{w,a}$ refer to the water concentration at the cathode and anode surfaces respectively, and δ_M is the thickness of the membrane. The diffusion coefficient can be approximated by the following equations (Nguyen and White, 1993):

When the activity of water at the anode, a_a is less than or equal to 1, meaning that the water is in the vapour form;

$$D_w = \left(0.0049 + 2.02a_a - 4.53a_a^2 + 4.09a_a^3\right) D^o \exp\left[2416\left[\frac{1}{303} - \frac{1}{273+T_s}\right]\right] \quad [1\text{-}21]$$

When a_a is greater than 1, meaning that there is liquid water at the surface;

$$D_w = \left(1.59 + 0.159\left(a_a - 1\right)\right) D^o \exp\left[2416\left[\frac{1}{303} - \frac{1}{273+T_s}\right]\right] \quad [1\text{-}22]$$

In the above equations, D_w refers to the effective diffusion coefficient of water in the membrane, D^o is the self diffusion coefficient of water in the membrane, and T_s is the temperature of the membrane.

1.5.1.4 Humidification of Gases

As stated in Section 1.4.3 it is essential to humidify the reactant gases in order to prevent the rapid dehydration of the membrane, which would lead to fuel cell performance degradation. In order to properly humidify the reactant streams an understanding of the psychrometrics of air and water vapour is required. The amount of water that must be

added to saturate a reactant stream is directly related to the saturation vapour pressure of the stream. The cathode reactant stream equations are shown below, and similar equations are used for the anode stream. The saturation vapour pressure (p_{ws}) of a given stream of air at a given temperature (T) can be calculated according to the vapour-liquid equilibrium from equations of state, such as the empirical Wagner equation (Smith et al., 2001):

$$\ln P_{vpr} = \frac{A(1-T_r)+B(1-T_r)^{1.5}+C(1-T_r)^3+D(1-T_r)^6}{T_r} \quad [1\text{-}23]$$

Where, T_r is the reduced temperature:

$$T_r = \frac{T}{T_c} \quad [1\text{-}24]$$

And P_{vpr}, is the reduced vapour pressure:

$$P_{vpr} = \frac{P_{sat}}{P_c} \quad [1\text{-}25]$$

Table 1-1: Constants for the Wagner equation for an air-water system (Reid et al., 1987).

Constant	Value
A	-7.775
B	1.466
C	-2.771
D	-1.317
T_c	647.31
$\ln P_c$	10.003

The vapour pressure (P_w) in the stream is related to the relative humidity by the following equation:

$$RH = \frac{P_w}{P_{sat}} \times 100 \quad [1\text{-}26]$$

The specific humidity or humidity ratio refers to the ratio of water to the other gases in the air and is described by the following equation:

$$\omega = \frac{m_w}{m_a} \qquad [1\text{-}27]$$

In which m_w is the mass of water per unit volume and m_a is the mass of air per unit volume. The mass of a species in a gas mixture can be calculated from an equation of state such as the ideal gas equation.

The partial pressure of air (P_a) is unknown, but the overall pressure (atmospheric) and the vapour pressure (P_w) are known. So:

$$P_a = P - P_w \qquad [1\text{-}28]$$

And,

$$\omega = \frac{m_w}{m_a} = \frac{P_w \cdot M_w}{P_a \cdot M_a} = \frac{P_w}{P - P_w} \cdot \frac{M_w}{M_a} \qquad [1\text{-}29]$$

In which the molecular weights of water and air are given as 18.02 g/mol and 28.97 g/mol respectively. The atmospheric pressure (P) is taken as 101325 Pa.

This equation defines the amount of water that must be added to a given stream at a given vapour pressure, P_w. If the fuel cell temperature is greater than the temperature of the reactant stream then the relative humidity of the stream will decrease as it enters the fuel cell and is heated. This will cause evaporation of water from the fuel cell proportional to the relative humidity. Once the stream is fully saturated at the fuel cell temperature, no further evaporation will occur.

The required oxygen molar flow, N_{O2} for the fuel cell reaction can be determined from the desired current to be drawn from the fuel cell;

$$N_{O2} = \frac{I\chi}{4F} \qquad [1\text{-}30]$$

Where χ is the number of cells in the fuel cell stack. From this equation a value for molar flow of air to the fuel cell can be determined.

$$N_{Air} = \psi \frac{N_{O2}}{0.21} \qquad [1\text{-}31]$$

In which ψ is the desired stoichometric coefficient, this is the excess flow of reactant supplied to the fuel above that required for the fuel cell reaction. Since the flow of air to the fuel cell is known from the above equation, and the ratio of water to air is known from Equation 1-29, the required amount of water to be added to the reactant streams can easily be calculated.

1.5.1.5 Overall Balance

From the above equations and knowledge of the process conditions for the fuel cell, the molar flows of water to and from the anode and cathode of the fuel can be calculated. When all the flows are added together an overall expected molar water balance on the fuel cell can be determined. Depending on the current, excess or insufficient water may be present at the anode or at the cathode. This balance should ideally be maintained by controlling the water added by humidification to the reactant streams.

Similar calculations where reviewed by Merida; the results are shown in Figure 1-7, where ζ represents the water content in the fuel cell (Merida, 2002). In practical systems it is desirable to operate the fuel cell at increased temperatures and increased cathode stoichiometry to minimize activation and concentration losses. However, Figure 1-7 illustrates that unless the reactants are humidified, drying conditions will prevail for any practical stoichiometry above 60^{o}C at low pressures. Under these conditions, the fuel cell membrane will lose water content and thus lose its proton conductivity rapidly, leading to fuel cell performance losses or fuel cell failure.

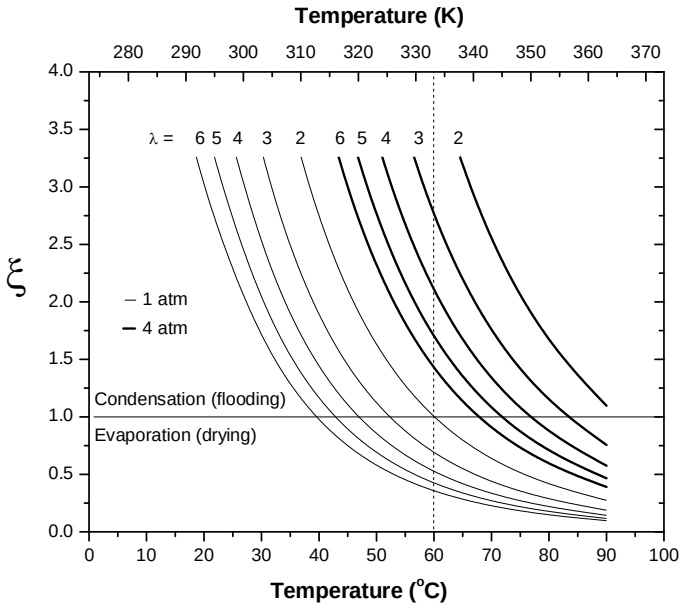

Figure 1-7: Water content in the fuel cell as a function of temperature, stoichiometry, and pressure (Merida, 2002).

1.6 Humidification Methods

The importance of fuel cell humidification has been demonstrated in the preceding sections. It is imperative that water be provided to the fuel cell in appropriate proportions in order to minimize power losses. There are many methods through which the water may be provided to the fuel cell. These methods are described below.

Fuel cells may be humidified by internal and external methods. Internal humidification refers to the addition of water directly into the fuel cell, or a method of keeping the water produced by the reaction in Equation 1-4 within the fuel cell. External humidification involves the use of a humidification unit to provide the fuel cell with humidified gas prior to the gases entering the stack itself. External humidification may bring added complexity to the fuel cell system.

As demonstrated in Figure 1-8, when external humidification is present and the fuel cell membrane is saturated at steady state conditions, the inlet stream, along with the excess water produced by the fuel cell reaction, will allow the fuel cell cathode exhaust to contain enough excess water to fully humidify the incoming cathode stream (there will also be excess water). Since the fuel cell exhaust stream exits the fuel cell fully humidified and heated to the stack operating temperature, it makes sense from an efficiency stand point

to harness this exhaust to heat and humidify the inlet streams. This will reduce the requirement to carry an external water supply.

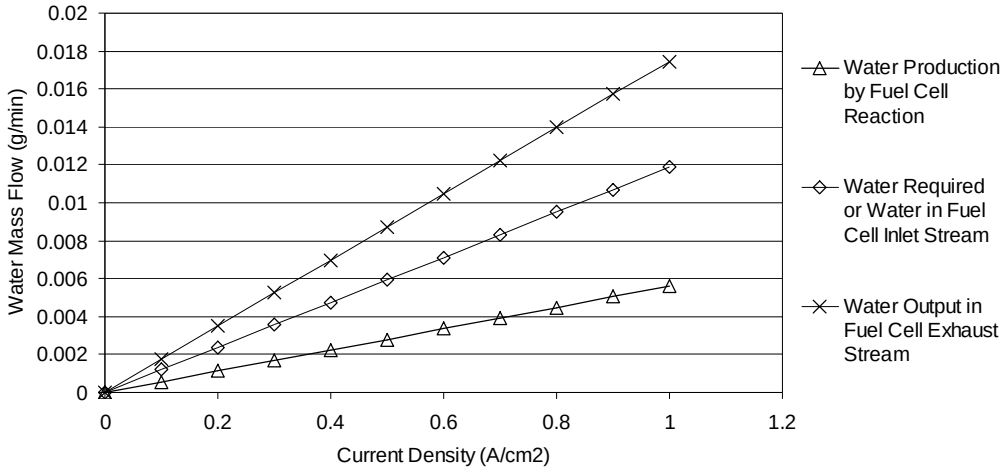

Figure 1-8: Water balance in the fuel cell.

It should be noted that under limited operating conditions, fuel cells may be run without any humidification, relying on the product water to maintain membrane saturation. This involves a careful balance of the reactant flow rates and temperatures so that electro-osmotic drag and back diffusion in the membrane can be equilibrated (Buchi and Srinivasan, 1997). However this limits fuel cell operation to a narrow range of operating temperatures and flow conditions, which is undesirable. Also, extended use of cathode exhaust water may allow for accumulation of contamination, so regular purging is required.

Operation of the fuel cell with no cathode humidification, but full anode saturation, has been shown to decrease overall performance only by 6% at 400 mA/cm^2 (Williams et al., 2004). However the decrease in performance is amplified at increased current densities and the long term performance under these conditions has not been specified.

Fully saturating the cathode stream has been shown to lead to performance losses at greater current densities, likely due to flooding of the gas diffusion electrodes and flow channels (Williams et al., 2004). It is desired to be able to provide reactant air at the cathode at a relative humidity which is slightly below saturation (75-90% RH) so that excess water at the cathode can be effectively removed from the fuel cell.

1.6.1 Internal Humidification

1.6.1.1 Special Stack Designs

Many methods of internal humidification have been proposed. Membrane type humidification chambers in series with the fuel cell stack were created in one example (Choi et al., 1998). In this design, a membrane gas to gas humidifier was part of the fuel cell unit, and the cooling water for the stack was passed on one side of these membranes while the dry inlet gases were passed along the other side of the membranes. This method was effective given the use of the correct type of membrane; however, it involved added complexity in the design of the fuel cell stack and flow channels. Also, the cooling water for the stack would be depleted over time, adding to the system's complexity.

A similar method involves extending the fuel cell membrane to include a humidification section of membrane without a catalyst layer within the cell(Santis et al., 2004). Each individual cell has a humidification section in which entering air is humidified by the exhaust gases before entering the active area of the fuel cell. This method sufficiently humidifies the air, but suffers from the complexity it adds to the fuel cell design. This design also involves using extra fuel cell membrane material, which is generally a PFSA based polymer. These polymers are expensive and will mean that the cost of humidification will be high.

It has also been proposed that humidification problems in the fuel cell can be alleviated by specially designed flow field pathways (Kaufman and Terry, 1998; Qi and Kaufman, 2002). By using a 'double path' design, as shown in Figure 1-9, where two flow fields pass along side each other, and one flow field inlet is located at the other flow field outlet. In this way, the two flow fields distribute water more evenly over the membranes and water concentration in the flow field channel remains relatively constant; unlike in single path designs, where the concentration of water in the channel increases from inlet to outlet. Although this method works better than no humidification and provides even humidification distribution, it has been shown that further performance improvements could be made by humidifying the reactant air before it enters the fuel cell.

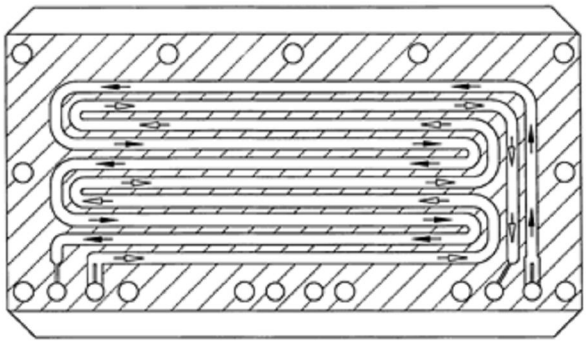

Figure 1-9: A double path flow field design (Qi and Kaufman, 2002).

1.6.1.2 Direct Liquid or Steam Injection

Another method of internal humidification involves direct liquid injection into the fuel cell stack (Wood et al., 1998). In this design, liquid water is preheated to fuel cell temperature and then pumped directly into the fuel cell reactant streams. This method provides significant fuel cell performance increases in comparison to not humidifying the reactant streams. If a compressor is used and after-cooling is required, the evaporative cooling effect may be beneficial. However, this method adds complexity to the fuel cell system and requires undesirable parasitic losses. Similar systems can be created using a steam generator to provide hot saturated air for the fuel cell, though without a significant heat source significant power losses would be expected in the production of steam.

1.6.1.3 Membrane Additives

Membranes with additives of platinum nano-crystals and metal oxides such as TiO_2 and SiO_2, have been produced and are reported to aid in the self-humidification of fuel cells (Watanabe et al., 1996; Watanabe et al., 1998; Kwak et al., 2003; Liu et al., 2003; Uchida et al., 2003). Embedded platinum acts to react with diffusing H_2 and O_2 gases to produce water in the membrane, demonstrating reduced ionic resistance and gas crossover in the membrane. Metal oxides are added to retain water within the membrane. This leads to reduced water migration within the fuel cell and more uniform water distribution in the membrane. These additives are also reported to assist fuel cells in cold-start conditions. Fuel cells with these types of membranes have demonstrated increased performance over a non-humidified fuel cell, but still benefit from additional fuel cell humidification. Furthermore, a careful balance of metal oxides and platinum is required to ensure that

short-circuiting of the fuel cell does not occur by the platinum additives, and that flooding does not occur as a result of metal oxide additives. In addition, the effects of these additives on membrane lifetime and durability are not clear. Despite these limitations, these specialized membranes have been reported to assist fuel cells in cold-start conditions.

1.6.1.4 Wicks, Sponges and Porous Plates

A method embedding hydrophilic wicks into the membrane has been reported (Watanabe et al., 1993). The wicks draw water directly to the membrane from a reservoir. The advantage of this method is that it continuously supplies water on demand to where the water is needed. Problematically, the wicking system requires complicated seals to prevent external leaks in the fuel cell, adds significant complexity to the fuel cell assembly, and the water supply must be periodically replenished.

In another internal humidification scheme, water absorbing sponges were placed strategically along the flow fields in the bipolar plates (Ge et al., 2005). These sponges acted to retain water produced in the fuel cell cathode exhaust and redistribute it to the fuel cell inlet region, where humidification is required. It was found that the presence of the sponges showed increased fuel cell performance under dry inlet reactant gas conditions. However, the sponges were shown to be ineffective at increased current densities and temperatures. Also the sponges required a special flow field plate design to ensure that cell compression and sealing were not a problem.

A final internal humidification scheme has been to utilize porous bi-polar plates (Besmann et al., 2000; He et al., 2000). These plates are highly porous in the flow-field regions, allowing them to absorb product water and keep it in the fuel cell environment, capillary action allow water collected at one location within the fuel cell to move to other locations. This scheme has the added benefit of self-regulating water distribution within the fuel cell.

1.6.2 External Humidification

1.6.2.1 Bubbler Humidifier

A bubbler is a common external humidification system. In a bubble type humidifier, the reactant stream is passed through a sparger into a heated column of water where the air

bubbles in contact with water are humidified. The amount of water transferred to the gas stream is a function of the heat of the water, the contact air of the water-air interface, and the contact time the air bubbles have with the water (Rajalakshmi et al., 2002). Thus the decreasing bubble size (effectively increasing the air-water interface) and increasing column length and temperature will increase the level of humidification achieved (Thorat et al., 1998).

Bubbler humidifiers, when properly designed can provide humidified gases reliably at various flow rates and temperatures. Unfortunately the flow rate of the gas provided becomes limited by the length of the column and the size of the sparger holes to produce smaller bubbles. Size constraints on the height of the column and pressure drops due to smaller sparger holes become an issue when designing for high flow rate bubble type humidifiers. Another issue from a fuel cell system perspective is that these types of humidifiers create significant parasitic power losses, as power from the fuel cell must be used to heat the bubble column (Glises et al., 2005). As well, bubblers must be refilled with water intermittently. These limitations make this method of humidification impractical beyond the laboratory scale.

1.6.2.2 Enthalpy Wheel Humidifier

Emprise produces the Humidicore enthalpy wheel humidifier, which is based around a ceramic honeycomb material named Cordierite (EmpriseCorporation, 2007). This material absorbs water from the fuel cell exhaust stream. The Cordierite core is constantly rotating bringing the moist material into contact with the dry inlet reactant stream. The functioning of the humidifier can be seen below in Figure 1-10. This humidifier does produce a small parasitic loss, and may add to system complexity under transient operation, as well the unit is costly.

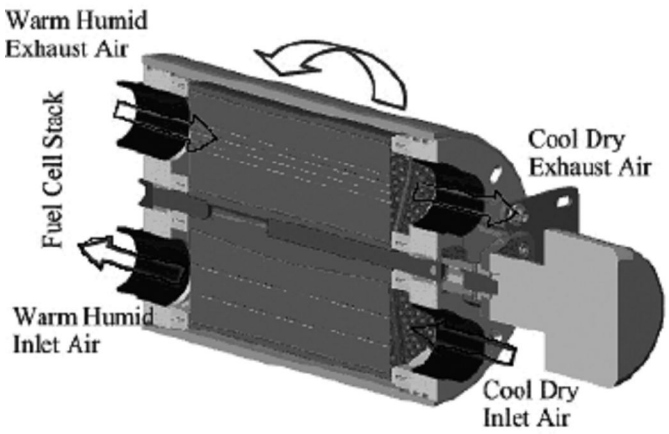

Figure 1-10: Emprise enthalpy wheel humidifier (EmpriseCorporation, 2007).

1.6.2.3 Membrane Based Humidifiers

Membrane humidifiers fall into two basic categories: planar and tubular. These devices are similar to plate-and-frame and shell-and-tube heat exchangers, respectively. The membranes in these humidifiers are usually hydrophilic polymers that act as the media for transporting moisture and heat from the fuel cell exhaust streams to the inlet reactant streams prior to entering the fuel cell.

1.6.2.3.1 Shell and Tube Membrane Based Humidifiers

Gas-to-gas and liquid-to-gas membrane humidifiers are commercially available in a shell and tube arrangement. In these humidifiers the hot and wet exhaust gas from the fuel cell is passed through hollow fibre membrane tubes. Meanwhile, on the shell side, the cool dry inlet gas is passed over the outer surface of the membrane tubes. A concentration and thermal gradient between the two sides of the membrane drives water and heat transfer to the incoming gas stream, causing it to be heated and humidified prior to entering the fuel cell. The general architecture of this type of humidifier is demonstrated in Figure 1-11. One embodiment of this design is produced by PermaPure, in which the membrane tubes are made of the hydrophilic polymer Nafion™ (PermapureInc., 2007). Nafion™ tubes allow for efficient transport of heat and humidity while providing a barrier to gas transport. Similar shell and tube humidifiers have been reported using various other membrane materials (Takahiro, 2004; Hiroshi et al., 2005; Masaharu et al., 2005; Tanaka, 2005).

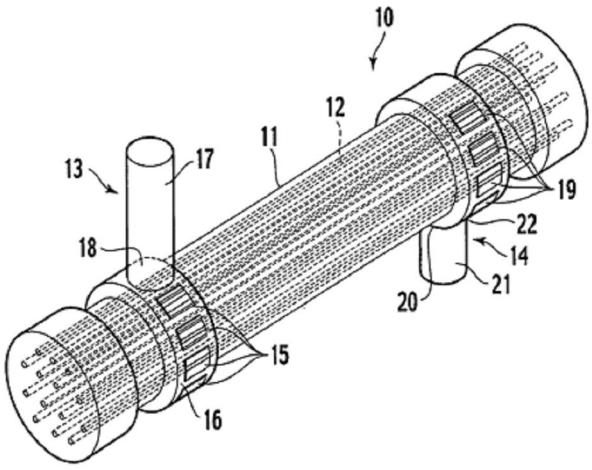

Figure 1-11: Shell and tube based hollow fiber membrane humidifier (Tanaka and Inamura, 2005).

1.6.2.3.2 Plate and Frame Membrane Based Humidifiers

The planar gas to gas or water to gas humidifier operates similarly to a plate and frame heat exchanger. Hot humidified air exiting the fuel cell flows along one side of the membrane, and cool dry air on its way into the fuel cell flows along the other side of the membrane. The membrane is permeable to water, either through pores, hydrophilic additives, or an inherent hydrophilicity. Water and heat are thus transferred through the membrane from the hot wet stream to the cool dry stream, providing humidity to the fuel cell; this is shown in Figure 1-12. Numerous patents describe this type of humidifier, namely those coming from Ballard Power Systems (Barton et al., 2001; Voss et al., 2002; Mossman, 2005).

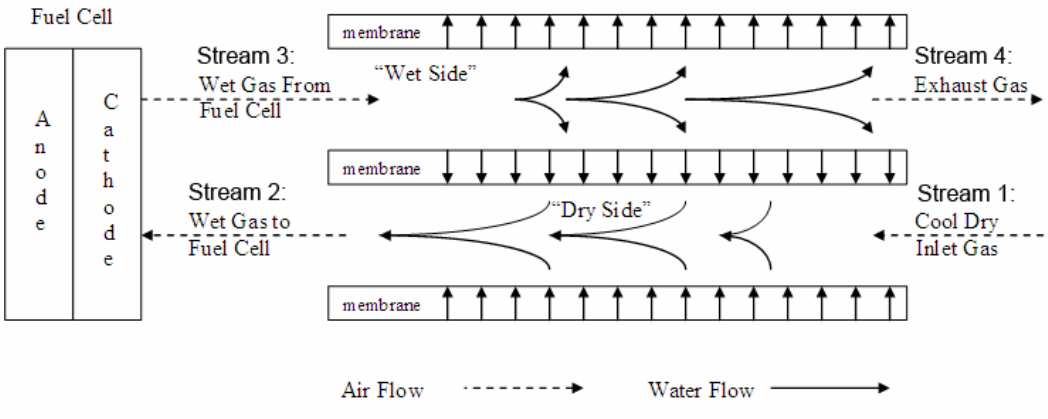

Figure 1-12: Planar membrane based humidifier.

1.6.2.3.3 Pleated Designs

The concept of a pleated humidifier design has been reported in the patent literature (Hasegawa et al., 2007). The state of the art involves pleating a hydrophilic membrane material with inserts or mesh in order to create channels through which the gas streams can flow. Pleating the membrane material and inserting it into a frame with well designed manifolds creates an architecture by which hot, wet gas may flow on one side of the membrane, while cold, dry gas may flow on the other side of the membrane. This is demonstrated in Figure 1-13. The pleated humidifier has a significant volume per membrane area advantage over other membrane humidifiers. Additionally, the assembly of this type of humidifier involves very few steps in contrast to the plate and frame architecture.

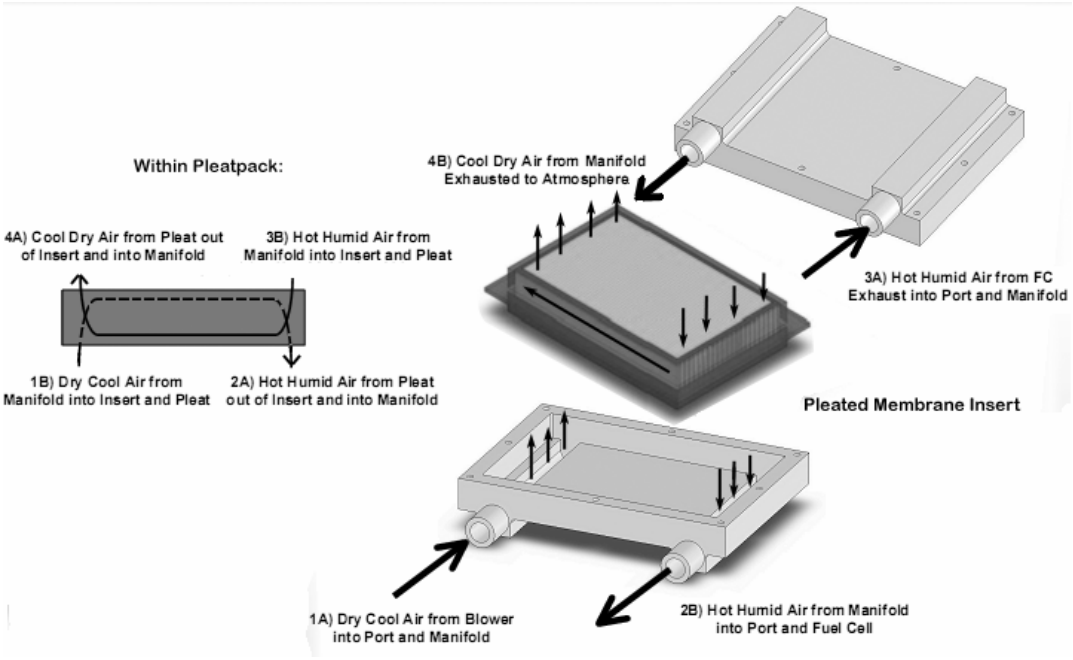

Figure 1-13: Pleated humidifier, pleat-pack is folded membrane within a clam-shell housing.

1.6.2.4 Comparison of Humidification Methods

The advantages and disadvantages of the various humidification schemes that were presented are summarized in Table 1-2.

Table 1-2: Summary of advantages and disadvantages of humidification methods.

Humidification Strategy	Advantages	Disadvantages
No Humidification	- No extra components	- Very limited fuel cell operating regime - Increased likelihood of fuel cell membrane failure
Internal Humidification	- No additional external components - Humidification may be self limiting	- Complication of fuel cell design - Possible durability problems - May have limited operating regimes
Bubble Column	- Accurate and well controlled humidification - Highly durable	- Large parasitic power losses due to heating of water column - More complicated control requirements - Increased flows require larger columns, and greater pressures - Realistically limited to lab scale - Requires onboard water
Liquid or Steam Injection	- Very precise control of humidification level - Highly durable	- Complicated control requirement - Onboard water required - Parasitic power losses due to heating and vaporizing water - Possible mechanical part failure
Enthalpy Wheel	- Recycles exhaust heat and moisture - Passive control	- Small parasitic power losses - Possible mechanical part and seal failure
Shell and Tube	- Recycles exhaust heat and moisture - Passive control	- Limited hollow fiber materials, which are expensive - Awkward to incorporate into system
Plate and Frame	- Recycles exhaust heat and moisture - Passive control	- Large number of parts to assemble
Pleated Design	- Recycles exhaust heat and moisture - Passive control - Increased volume to membrane ratio	- Difficult to predict flow distribution - Increased pressure drops

1.7 Planar Membrane Based Gas to Gas Humidifier Specifics

This project deals specifically with planar gas to gas membrane based humidifiers. The planar membrane based humidifier is an external humidification device that acts to recycle heat and humidity in the fuel cell system. This device is a standard part in many state of the art PEM fuel cell systems. A commercial planar membrane based humidifier with its gas stream ports labeled is shown in Figure 1-14.

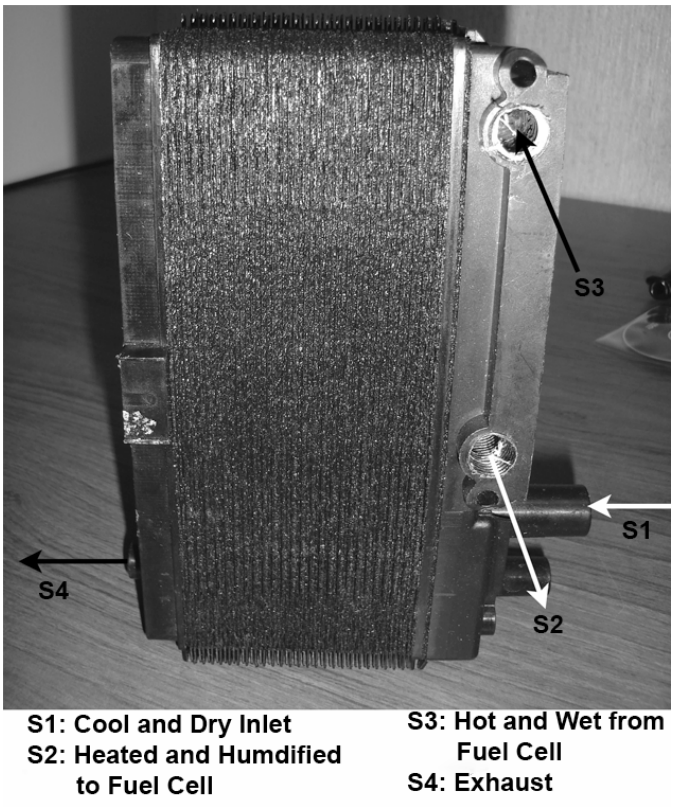

Figure 1-14: Planar membrane based gas to gas humidifier for 1.5kW fuel cell.

The design of the humidifier means it is coupled to the inlet and outlet air streams of the fuel cell, and operates as shown in Figure 1-12. Gas entering the humidifier (stream 1) gains heat and humidity through the fuel cell system before entering the fuel cell (stream 2). In the fuel cell environment, the gas stream has decrease in oxygen content as the fuel cell reaction occurs; as well the stream is likely to increase in water and heat content before exiting the fuel cell as exhaust (stream 3). This hot and wet exhaust stream now enters the humidifier where the heat and humidity in the stream will be transported back to the inlet stream, before exiting the system at stream 4.

1.8 Project Goals

This project had three major goals:

- Developing a method by which to design planar gas to gas humidifiers.
- Developing a methodology for screening and identifying membranes for gas to gas fuel cell humidifiers.
- Testing the lifetime and durability of candidate membranes at fuel cell system operating conditions, and understanding the failure mechanisms of these membranes.

Chapter 2

2.0 Experimental Methods

2.1 Water Permeation Testing

Membrane materials with high water permeation are desirable for use in the fuel cell humidifier. This is explained in greater detail in Section 3.3.1. As such, a method for testing the water permeation of various membranes was developed in order to compare different membranes. Two methods were used in order to quantify the rate of water transport through the membranes, a static water vapour permeation test, and a dynamic water permeation test.

2.1.1 Static Water Vapour Permeation Test

The static method testing was based on ASTM E-96 in order to evaluate water vapour transmission through the membrane material (ASTM-E96, 2005). In this test a cup is filled with de-ionized water and a membrane positioned over the cup, hence the name 'cup test'. A gap of 1.5 cm is left between the water surface and the membrane. The gasket seal between the membrane and the cup ensures that water can only be transported through the membrane material. The test apparatus is shown in Figure 2-1 and Figure 2-2. The total weight of the apparatus is measured at time zero, and the cup is left undisturbed at a set temperature and relative humidity. The weight of the apparatus is measured periodically. At this time the room temperature and relative humidity are recorded as well. Plotting the loss in mass against time generally produces a linear graph. The slope of this graph represents the water vapour transmission rate in units of mass per time, while the intercept represents the initial weight. This rate can be divided by the membrane active area to express the water vapour flux in units of mass per time per area. The flux can be divided by the vapour pressure difference between the inside and outside of the membrane surfaces will give the vapour pressure difference normalized flux in units of mass per time per area per unit vapour pressure differential.

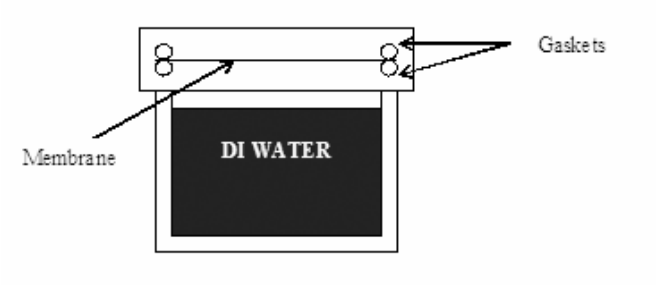

Figure 2-1: Cup test equipment for static water permeation test.

Figure 2-2: Cup test equipment for static water permeation test.

2.1.2 Dynamic Water Permeation Test

The differences between the conditions under which static water permeation tests were completed and the environment in which the membrane is used in the actual humidifier prompted the consideration of a new method by which to test the water permeation of the membrane materials. A dynamic test in which the humidifier conditions could be simulated was desired. This would allow flux measurement to be taken in the actual operating regime of the humidifier. In order to do so equipment which could provide air streams at various temperature, relative humidity, flow, and pressure conditions was required. A Greenlight Power Technologies FCATS™ G-50 Fuel Cell Test Station as shown in Figure 2-3 was used for these experiments.

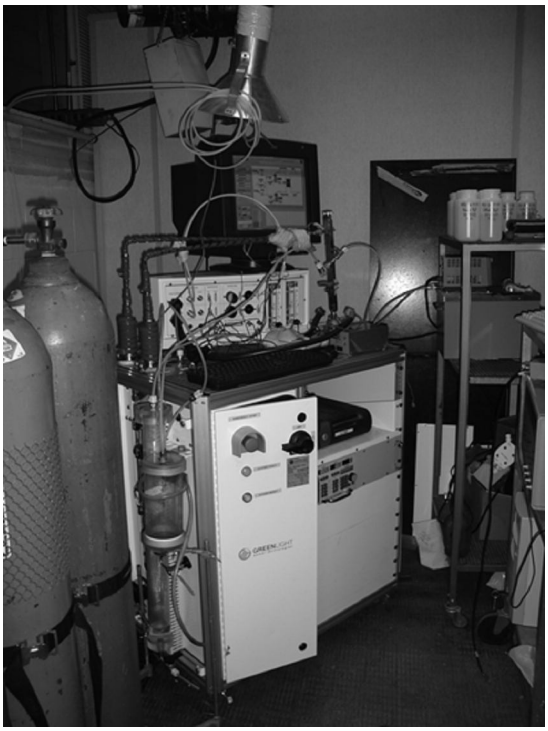

Figure 2-3: Greenlight Power Technologies, G-50 Fuel Cell Test Station

The test station supplies air at temperatures ranging from 20 to 95^{o}C at relative humidity from 0 to 100%. As well the air flow rates from 0 to 10 SLPM at pressures from 0 to 400 kPag are achievable with the station. The station runs from a National Instruments Labview™ based platform that allows completely automated system control and data logging capabilities.

In order to test the membrane materials a special test module was designed and created in which the membrane could be housed while testing. This module consisted of two plates with a flow field machined into their surface as shown in Figure 2-4. Two of these plates could be bolted together with a membrane and gaskets between them as outlined in Figure 2-5. This allowed air streams to be provided on either side of the membrane as various flow, pressure, temperature, and relative humidity conditions. Membrane materials were cut into 4.5 cm by 18 cm pieces for use in these modules.

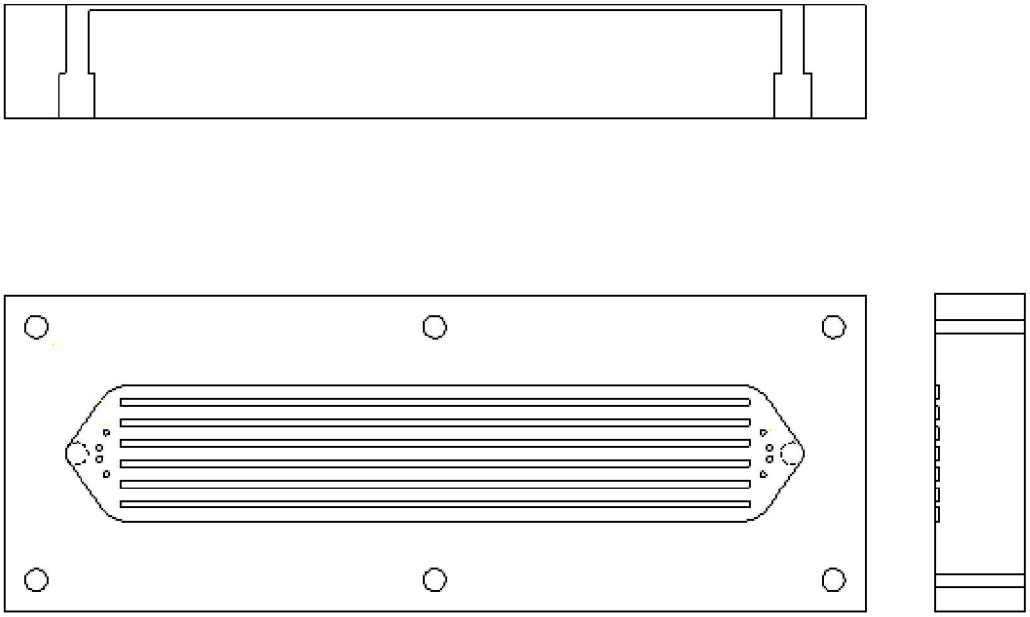

Figure 2-4: CAD drawing of a plate for the dynamic water permeation test.

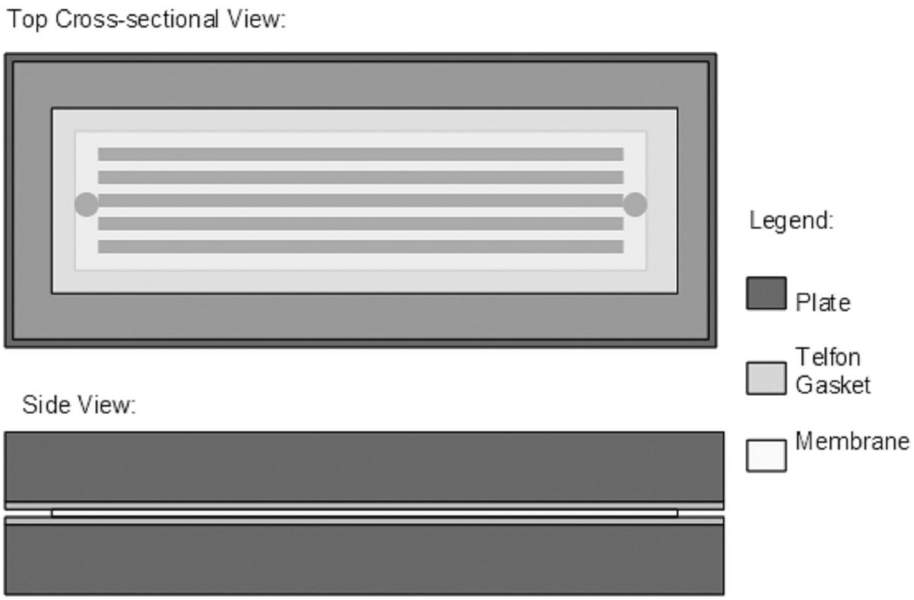

Figure 2-5: Assembly of a test module for dynamic water permeation test.

In the design of this test module, it was imperative to ensure that relatively equal flow distribution occurred through all the channels. This would insure that the full membrane area, 33.24 cm^2 was being utilized in the experiments. The flow distribution was confirmed for a regime; based on 4 SLPM using computational fluid dynamics (CFD) software. A three dimensional solid model of the water permeation test module flow plate

was created in SolidWorks 2005, and then imported into ANSYS Workbench™ 9.0 for meshing, a detail of the meshing of the plate is shown in Figure 2-6. A volume mesh was created, and imported into ANSYS CFX 10.0™ to simulate the flow of air through the module. A flow rate of 4 SLPM was chosen, and the fluid was air at 25^{o}C. The simulation reached convergence and the results were analyzed. The pressure contour for the module is shown in Figure 2-7. The velocity vector profile is shown in Figure 2-8. From Figure 2-7 it can be seen that there is a relatively little pressure difference between the channels, never greater than 20 Pa. From Figure 2-8 it can seen there is fairly equal velocities between the channels, the range is between 3.5 and 3.75 m/s.

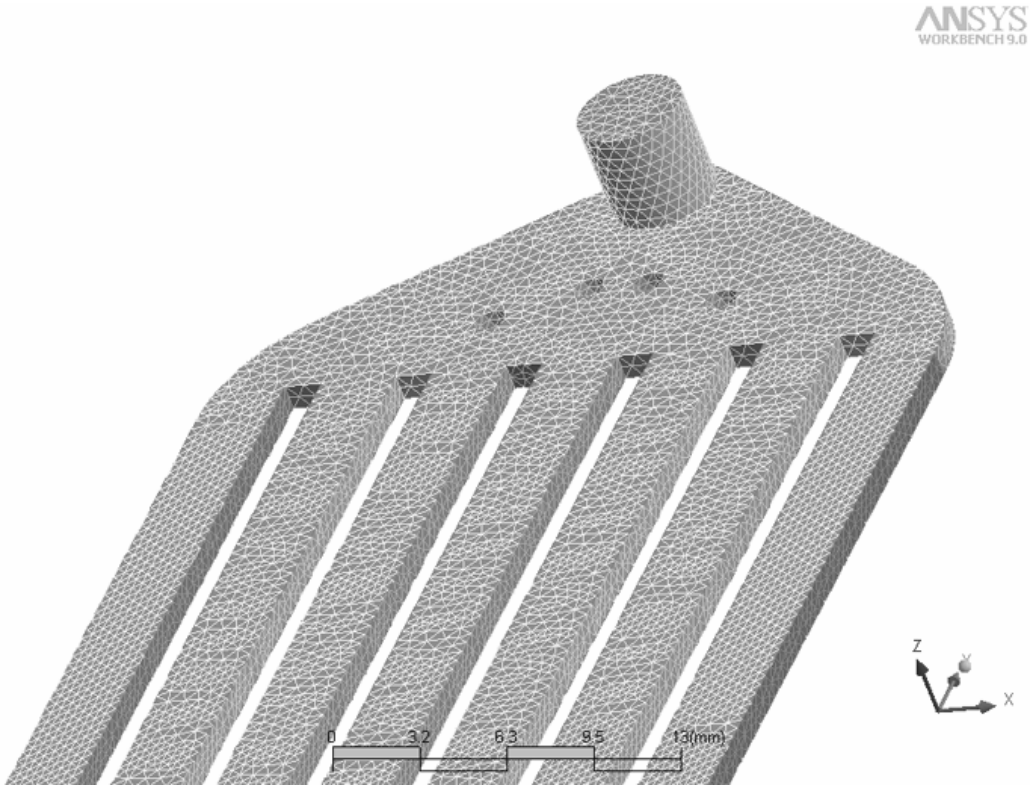

Figure 2-6: Surface mesh of solid model of flow channels for the water permeation test module in ANSYS Workbench™ 9.0.

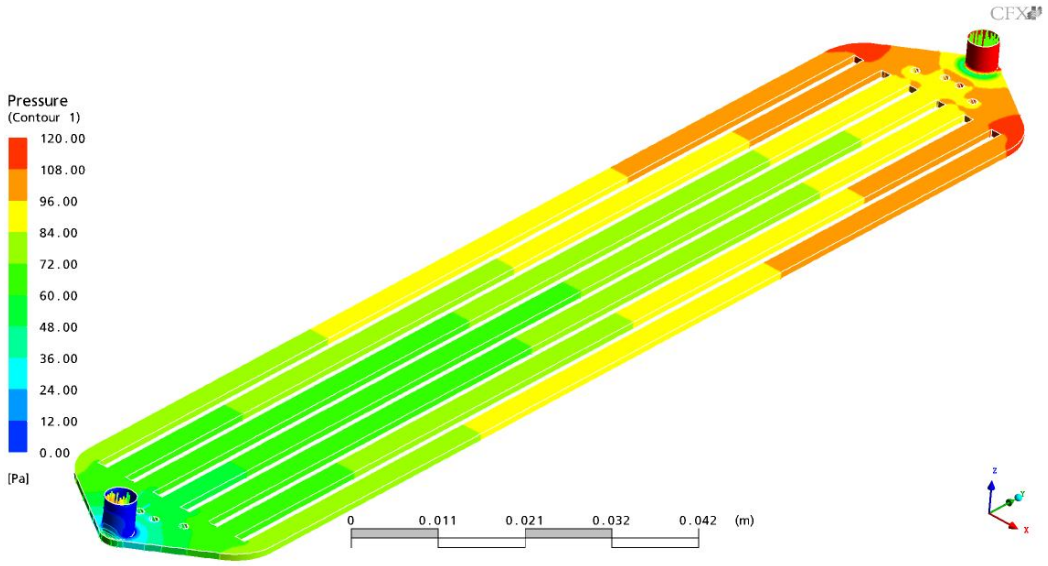

Figure 2-7: Pressure contour for water permeation module for air at 25^{o}C at 4 SLPM.

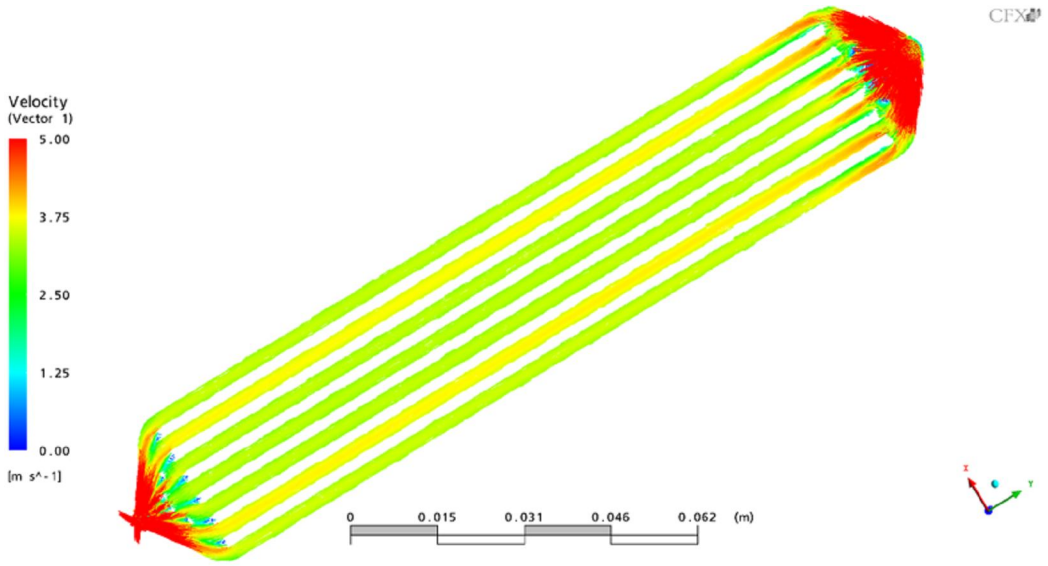

Figure 2-8: Velocity profile for water permeation module for air at 25^{o}C at 4 SLPM.

In order to compare different type of membranes in this test, appropriate operating conditions were selected; the general conditions for the water permeation test are summarized in Figure 2-9. In the dynamic water permeation test, the flows at S1 and S3 are maintained at equal flow rates at each flow set point from one to six SLPM. At each flow rate the experiment was ran until steady state operation was achieved, at which point data was recorded in 10 second intervals for 15 minutes.

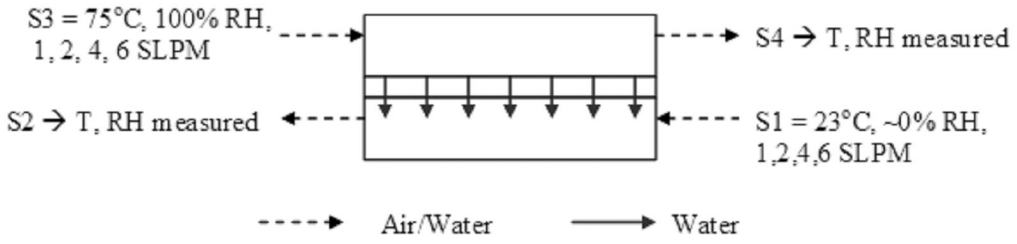

Figure 2-9: Conditions for standard dynamic water permeation test.

In order to determine the water transport through the membrane, two methods were used. One method involved using a condenser on ice, with anhydrous calcium carbonate was used on the S2 and S4 outlets to collect water under steady state at each flow rate. For increased flows it the second method used sensors. It was found that the water balance could be completed by measuring the wet-bulb and dry-bulb temperature on the S2 and S4 outlets. This was completed using a standard K-type thermocouple to measure the dry-bulb temperature; this was followed inline with a K-type thermocouple with a cotton wick attached to a water reservoir in order to measure the wet-bulb temperature. This works on the principle of evaporative cooling, due water evaporating from the wick into the less than saturated gas stream (Bird et al., 2007). From the values of the wet-bulb temperature (T_{wb}) and dry-bulb temperature (T_{db}) in ^{o}C, the humidity ratio of the gas stream (ω) can be calculated in kg water per kg of dry air using the following equations (Buonanno et al., 1994).

$$\omega = \frac{\left[h_0 - \left(c_{pw} - c_{pv}\right)T_{wb}\right]\omega_s - c_{pa}\left(T_{db} - T_{wb}\right)}{h_0 + c_{pv}T_{db} - c_{pw}T_{wb}} \quad [2\text{-}1]$$

$$c_{pa} = 1.0044 - 2.18264\times10^{-6}T_{db} + 6.19428\times10^{-7}T_{db}^2 \quad [2\text{-}2]$$

$$c_{pv} = 1.845 - 5.80838\times10^{-2}T_{db} + 3.47902\times10^{-5}T_{db}^2 - 1.66303\times10^{-7}T_{db}^3 + 6.61315\times10^{-10}T_{db}^4 \quad [2\text{-}3]$$

$$c_{pw} = 4.21754 - 1.54336\times10^{-3}T_{db} + 1.48244\times10^{-5}T_{db}^2 \quad [2\text{-}4]$$

$$\omega_s = \frac{M_w}{M_a}\frac{p_{ws}\left(T_{db}\right)}{P - p_{ws}\left(T_{db}\right)} \quad [2\text{-}5]$$

Where c_{pw}, c_{pv}, and c_{pa} are the specific heat capacities of liquid water, water vapour, and air in $Jg^{-1}K^{-1}$ respectively. The latent heat of vaporization (h_0) is 2500.8 Jg^{-1}. The saturated

humidity ratio (ω_s) is calculated from the molecular weights of air and water (M_w and M_a), the absolute pressure (P) and the saturation vapour pressure (p_{ws}) as calculated by Equation 2-5.

Experiments indicated that the wet-bulb method was as accurate as condensing the outlets to complete the water balance. However this method was much more effective during experimentation since the humidity ratios in the gas stream could be calculated in real time.

It was important to test membrane materials in a flow regime where the transport of water would be limited by diffusion through the membrane, and not limited by the boundary layer effects in the flow field. These boundary layer effects were minimized by insuring that gas flow velocities were over the membrane surfaces were greater than 0.5 m/s (Gibson et al., 2000). In doing so it was insured that the membrane was the rate limiting step in water transport in the test module, and that membrane materials could be compared against one another.

2.2 Air Permeation Testing

The wet and dry air permeation rates across the humidifier membrane were important to consider when selecting an appropriate membrane. Further details can be found in section 3.3.2. In order to examine the air permeation rate across membranes of interest, an air permeation module was created. In this apparatus a membrane sample is sealed between two plates as shown in Figure 2-10.

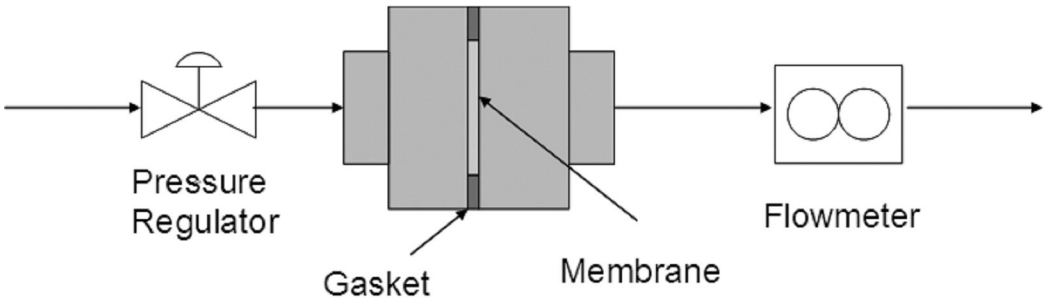

Figure 2-10: Air permeation testing apparatus.

The air pressure supplied to the upstream in controlled by an 8601D Compressed Gas Regulator from Brooks Instrument with a range of 0 to 100 kPag. Air flow is forced

through the membrane from the pressurized side to the atmospheric side where the flow rate is measured using a digital flow meter, model FVL-1606A from Omega. The digital flow meter has a range of 0.025 to 6.4 LPM. For lower flow rates a rotameter with a range of 0 to 50 CCM from Dwyer model RMA-151 was used. From the output of the flow meter, the dry gas crossover rate of the membrane could be measured at a given differential pressure in units of volume per time. The active membrane area in the module was 5.0 cm^2. By altering the supply pressure a pressure-flow curve could be created for a given membrane, in which the slope of the linear region divided by the membrane area provided the dry air permeation rate of the membrane. To determine the wet air permeation rate, a similar test was completed on the membrane. However, for the wet permeation test the membrane was soaked in de-ionized water for one hour prior to testing.

2.3 Mechanical Strength Testing

As described in section 4.3.3 a membrane material with relatively high mechanical strength will be required in order to insure that the membrane can withstand constant or intermittent increases in pressure.

The mechanical strength of a membrane material is tested by applying a constant axial strain to the sample and measuring the resultant stress to maintain this strain on the sample. The stress is defined as (Riley et al., 2002):

$$\sigma_{avg} = \frac{F}{A} \qquad [2\text{-}6]$$

Where F is the force applied to the material, A is the cross-sectional area of the material transverse to the axial force, and σ_{avg} is the average normal stress on the sample in units of force per area. The strain applied to the sample is calculated by (Riley et al., 2002):

$$\varepsilon = \left(\frac{l_i - l_0}{l_0} \right) \times 100 \qquad [2\text{-}7]$$

In which l_0 is the initial measured length of the sample and l_i is the current length of elongated sample. The strain, ε is the percent elongation.

Membrane samples were cut to a prescribed length of 2.5 cm and a width of 0.5 cm, the precise thickness, width, and length of each membrane sample was later determined using calipers. The samples were then placed on a Rheometric Scientific Minimat tensile test apparatus, where a constant axial strain was applied to the sample as a rate of 1 mm/min, as shown in Figure 2-11.

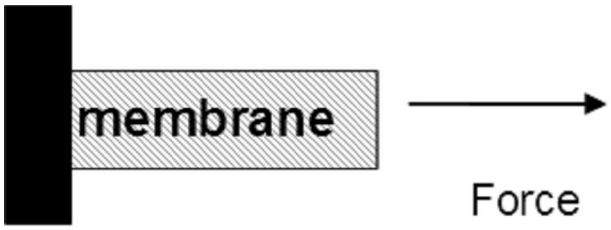

Figure 2-11: Stress-strain test on membrane material.

As a constant strain was applied, the stress was recorded and a stress-strain curve was created. The constant strain was typically applied for 3 to 5 minutes.

During the initial application of strain to the polymer membrane, it tends to react in an elastic manner. In this region a linear trend on the stress-strain curve prevails, as seen in Figure 2-12. A software package was used to find an appropriate tangent to the elastic region of the stress-strain curve. In this region, where stress and strain are linearly proportional, the Young's Modulus is the proportionality constant *E*, described as (Riley et al., 2002):

$$E = \frac{\sigma}{\varepsilon} \qquad [2\text{-}8]$$

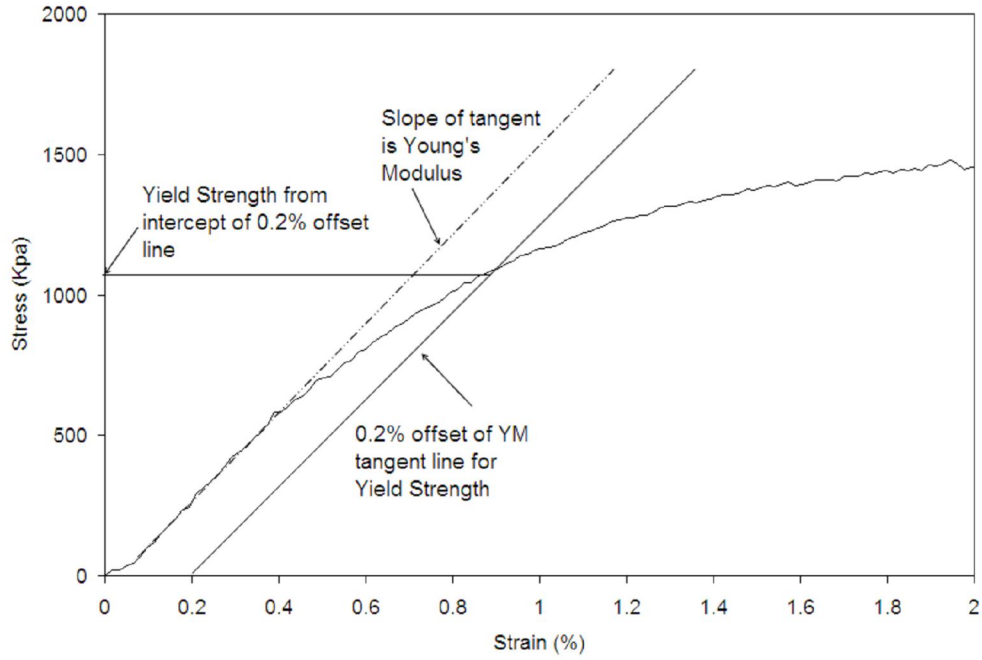

Figure 2-12: Stress-strain curve for a polymer membrane demonstrating Young's Modulus and Yield Strength.

The Young's Modulus was used as a metric to compare the mechanical strength of various membrane materials. Also of interest was the Yield Strength of the material, which was determined using the provided software package, but typically is taken as the stress point at which the 0.2% offset of the tangent line of the Young's Modulus meets the stress-strain curve, as shown in Figure 2-12. The Yield Strength is typically described as the point at which the deformation of the material becomes non-elastic such that the material is permanently deformed (Riley et al., 2002). The Minimat mechanical test apparatus could also be configured to test the membrane materials at elevated temperatures. Membrane materials which had been saturated in de-ionized water for 1 hour were also tested in this apparatus.

2.4 Scanning Electron Microscopy and Energy Dispersive X-ray Spectroscopy

Scanning electron microscopy (SEM) is a powerful method for analyzing materials at high levels of magnification. When studying polymer materials it allows the study of the surface characteristics, morphology, and defects. It may be particularly useful for comparing polymer membrane materials at the beginning and end of life, to assist in

failure modes analysis. Energy dispersive X-ray spectroscopy (EDS) can be used to study the atomic composition of the surface of materials, and may give insight into changes and contamination which have occurred on membrane surfaces.

The principle apparatus of the SEM is an electron gun, which emits electrons in a controlled fashion towards a sample. These electrons interact with the sample in and these interactions can be measured, allowing information to be gathered about the surface morphology of the material, as well as the surface composition of the material. The details of SEM function and operation are well documented in the literature (Bozzola and Russell, 1992).

Membrane samples of interest were cut to the desired size using a scalpel blade. The samples were then mounted to an aluminum stub using double sided conductive carbon tape. Membrane cross-sections were created by freeze-fracturing, by submerging the membrane sample in liquid nitrogen and then cracking it. This ensured a clean cross-section for analysis. This fractured sample was adhered to an aluminum bolt, which in turn was attached to an aluminum stub. The mounting of membrane samples for surface analysis can be seen in Figure 2-13.

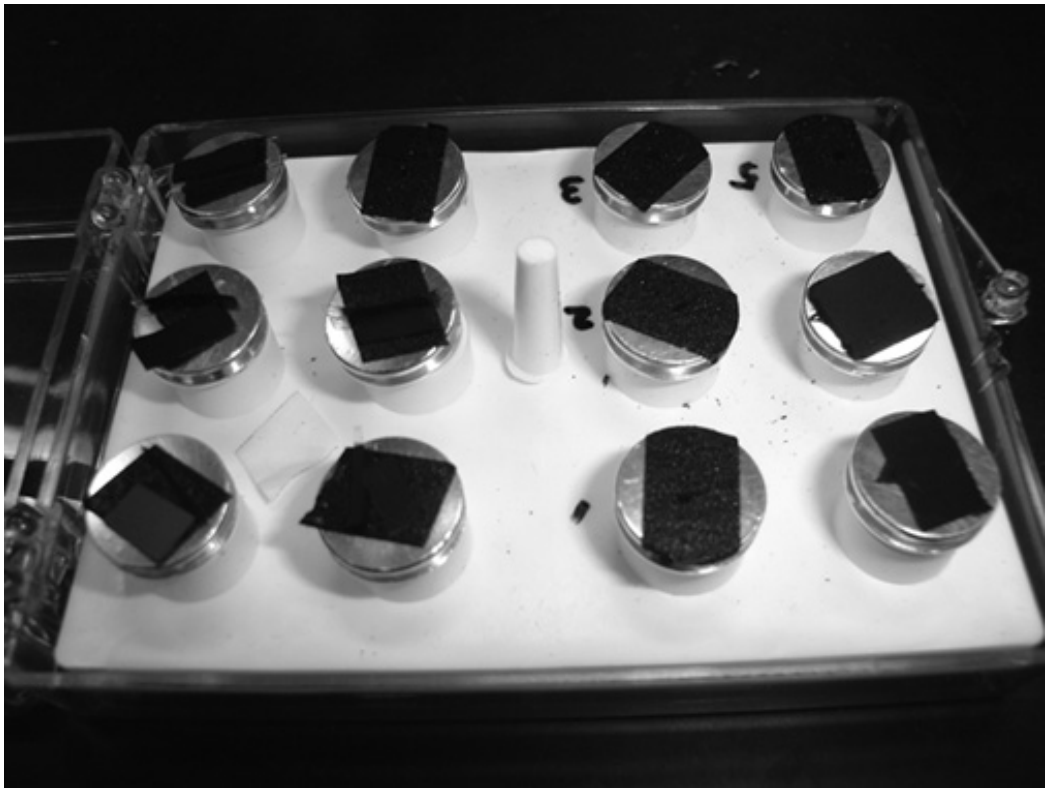

Figure 2-13: Samples mounted on stubs prepared for SEM analysis.

Prior to testing, the stubs with samples were placed in a vacuum oven for 24 hours at 80^{o}C. This insured that the samples were dry and oil free. Once the samples were mounted and dried, they were sputter-coated with gold under vacuum.

Coated samples were placed in the microscopy chamber and placed under vacuum. Typically the electron gun voltage was kept at 10 keV, and samples were studied from 100 to 50000 X magnification. EDS analysis of average surfaces and surface sections was generally completed at either 250 or 5000X magnification.

2.5 Accelerated Aging

A possible failure mechanism of the membrane material in the humidifier is oxidative degradation. Polymer oxidation may occur over extended periods of operation at increased temperatures. This may lead to membrane degradation, cracking, and overall humidifier failure. Since oxidation is a prolonged process, accelerated testing is desirable.

The Perox 80 test has been proposed as method to test polymer membranes for resistance to oxidation (Battery Council, 2002). The Perox 80 test analyzes the weigh loss and tensile strength loss of a material due to accelerated oxidation. The weight loss and tensile losses are calculated by equations 2-9 and 2-10 (Battery Council, 2002):

$$\%\ oxidative\ \ weight\ loss = \left(\frac{W_i - W_f}{W_i}\right)\times 100 \qquad [2\text{-}9]$$

Where W_i refers to the initial mass of the sample and W_f is the final mass of the sample.

$$\%\ tensile\ retention = \left(\frac{E_i - E_f}{E_i}\right)\times 100 \qquad [2\text{-}10]$$

Where E_i is the baseline or control tensile strength of the membrane sample, and E_f is the measure tensile strength of the sample following oxidation.

In this test 10 by 25 mm membrane samples were cut and weighed on a microbalance. Initial tensile tests were completed as described in Section 2.3 on 5 samples of the new membrane to determine baseline tensile modulus and yield strength of the samples. A

solution of 10% peroxide, 30% sulphuric acid (H_2SO_4), and 60% de-ionized water by weight was created, and transferred to vials containing 15 mL of the solution. The samples were placed in the vials, and the vials were placed into a water bath at 80^{o}C. Samples were removed at various increments and washed thoroughly in de-ionized water. After washing the samples were dried in an oven set at 80^{o}C for 24 hours. After drying the samples were are reweighed and then tested for mechanical strength.

2.6 Axisymmetric Drop Shape Analysis

Axisymmetric Drop Shape Analysis (ADSA) involves placing a sessile drop on the surface of a membrane and analyzing the drops interaction with the membrane surface. The contact angle of the drop with the surface is analyzed to study the extent to which a surface is hydrophobic or hydrophilic. ADSA experiments were completed using a VCA (Video Contact Angle) system from AST Products, Inc. Sessile drops were manually placed on the membrane surface. Experiments were completed at room temperature. The contact angle, width, height, and volume of the sessile drops were analyzed using the VCA software accompanying the equipment. A sample drop with contact angle is shown in Figure 2-14.

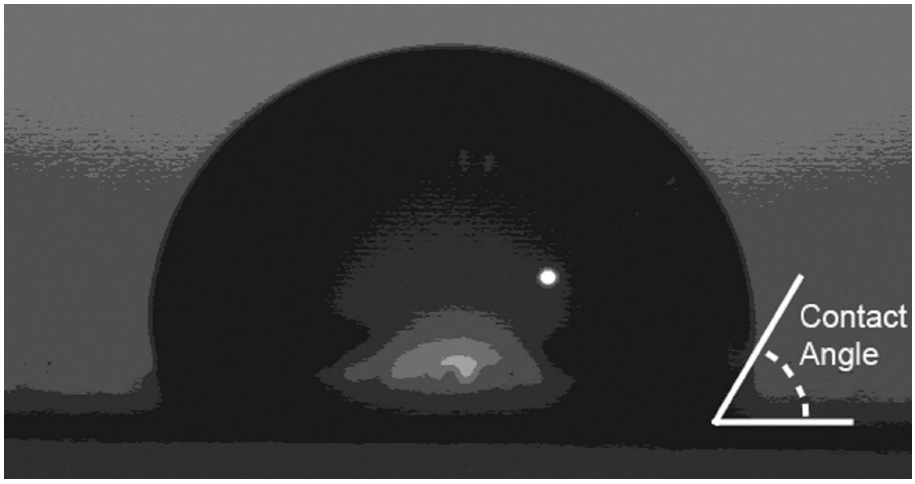

Figure 2-14: Sessile drop on membrane surface.

Sessile drops placed on hydrophilic surfaces will have large contact angles, while more hydrophobic surfaces will lead to lower contact angles. To study the interaction of the drop with the membrane surface, sequences of images were recorded over time. By observing the change in the contract angle of a drop placed on a membrane surface over

time the rate absorption of water into the membrane could be determined.

Ideally the sessile drop experiments should be completed in a sealed environmental chamber, in which the air is saturated with water. This would eliminate the affects of evaporation on the sessile drop. Such a chamber was not available for the experiments. To account for the rate of evaporation from the drop surface, a baseline experiment was completed on a Teflon surface which was impermeable to water. This experiment was completed in triplicate and the average rate of evaporation was calculated.

The calculations for absorptive flux can be found in Appendix A. The absorptive flux was a useful parameter for measuring the rate that a membrane used in the humidifier would become wet. Rapid absorption would be beneficial for membranes which may have high dry air permeation rates, but low wet air permeation rates, a high adsorption rate would ensure that the humidifier would not operated in the dry state for any significant period of time. Also a high adsorption rate may be indicative of high water permeation rates in a membrane.

The surface tension of various membranes was calculated from the initial contact angle of the material. This can indicate the wettability of the surface. The surface tension over time was also calculated for the membranes, although this may be of limited significance since the effect of evaporation on the contact angle cannot be determined directly.

The surface tension of a polymer material can be determined by the method explained by in which the Young's equation (Long and Chen, 2001)

$$\gamma_{LV}\cos(\theta) = \gamma_{SV} - \gamma_{SL} \qquad [2\text{-}11]$$

Can be combined with a modified Berthelot's rule (Kwok et al., 1998):

$$\gamma_{SL} = \gamma_{LV} + \gamma_{SV} - 2\sqrt{\gamma_{SV}\gamma_{LV}}\,e^{-\beta(\gamma_{LV}-\gamma_{SV})^2} \qquad [2\text{-}12]$$

To give:

$$\cos(\theta) = -1 + 2\sqrt{\frac{\gamma_{SV}}{\gamma_{LV}}}e^{-\beta(\gamma_{LV}-\gamma_{SV})^2} \qquad [2\text{-}13]$$

In which β tends to be 0.0001247 for polymer surfaces and γ_{LV} for water is 72.7 mJ/m^2 (Long and Chen, 2001). From this information and the contact angle measured, the surface tension of the polymer (γ_{SV}) was determined as a fitting parameter.

Finally the surface tension of water on the membrane γ_{LS} can be calculated from 2-11. It will be desirable to minimize this value for the humidifier application, as a minimal resistance to water wetting the membrane would be desirable.

2.7 Durability Testing

In order to test membrane for lifetime and durability, specialized membrane testing stations were designed and developed. These stations allowed various membranes to operate in environments similar to those that the membrane would be subjected to under operation in a fuel cell system. Two operating conditions were identified under which durability testing was completed. These operating conditions are summarized in Table 2-1.

Table 2-1: Operating conditions for low and high temperature durability stations.

Operating Regime	Flow Rate (SLPM)	Dry Inlet Temperature (^{o}C)	Dry Inlet Relative Humidity (%)	Wet Inlet Temperature (^{o}C)	Wet Inlet Relative Humidity (%)
Low Temperature	4	25	0	60	0
High Temperature	4	95	0	95	0

A low temperature durability station (LTDS) was created to test membrane materials at the low temperature conditions, while a high temperature durability station (HTDS) was created to test materials at the high temperature conditions.

Prior to testing membranes on the stations the membrane materials were cut into 4.5 cm by 18 cm pieces and weighed on a micro balance. The membrane samples were then placed in test modules similar to though described in Section 2.1.2. Once sealed in the module an air permeation test similar to that described in Section 2.2 was completed while the membrane was in the module. A standard water permeation test as described in

Section 2.1.2 was then completed. After these baseline tests were completed, the modules were placed on the durability stations, and operated under the specified conditions for a set time. This time was generally 300 to 500 hours, after which the station was shut down, and the membrane was allowed to dry under constant air flow for 24 hours. The modules were then removed from the station and air and water permeation tests were completed. Failure in the membrane was set as a decrease in water permeation of greater than 20% or an increase in air permeation of greater than 20%. If the material passed the water and air permeation tests, then the module was returned to the station for another 300 to 500 hour period. Membranes were operated on the durability station until failure, at which time failure modes analysis could be completed.

2.7.1 Low Temperature Durability Station

A process flow diagram of the low temperature durability station (LTDS) is shown in Figure 2-15 and a photo of the station can be found in Figure 2-16.

The manifolds on the station were tested to ensure that an equal distribution of flow was provided to each module. The water to gas membrane humidifiers were DX-1.5 humidifiers supplied by DPoint Technologies. The gas stream entering the modules labeled ‘S3’ was set to 60^{o}C and 100% relative humidity by adjusting the temperature of the water bath and measuring the resulting ‘S3’ temperature and relative humidity entering the modules. The stream labeled ‘S1’ was at room temperature and 0% relative humidity. The flow rate to each module was 4 SLPM.

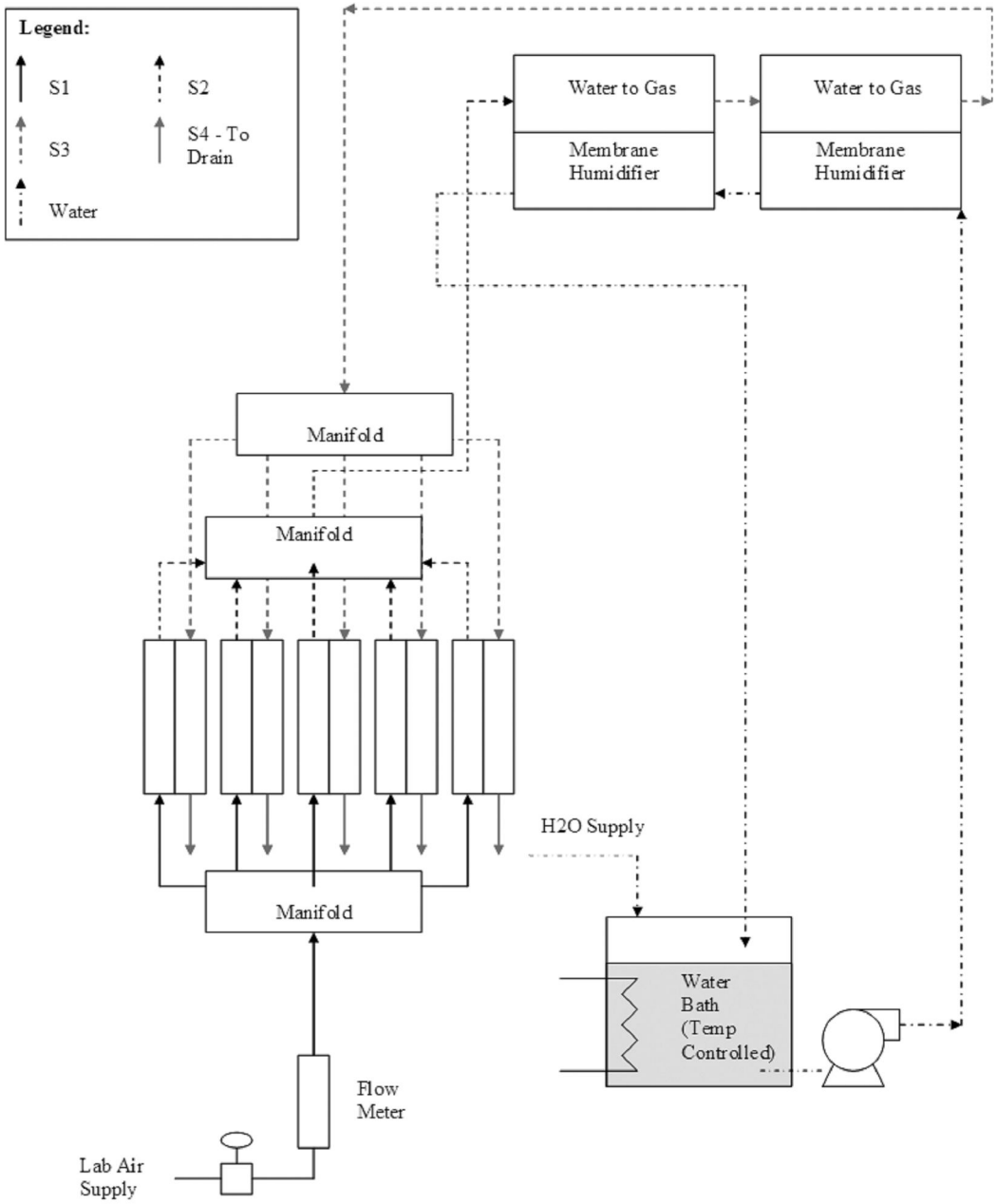

Figure 2-15: Process flow diagram of the low temperature durability station (LTDS).

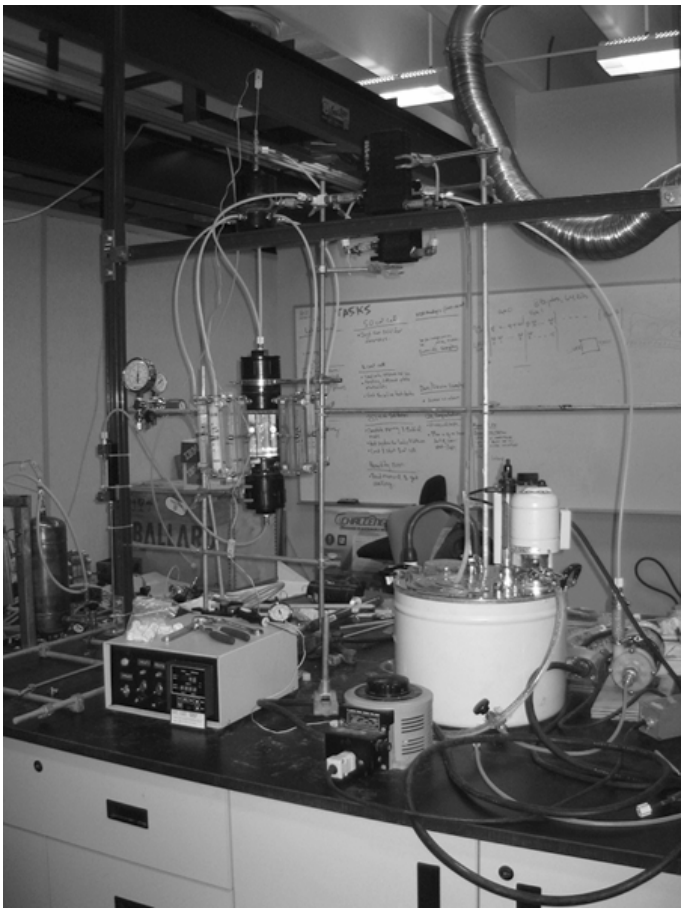

Figure 2-16: Photograph of the LTDS.

2.7.2 High Temperature Durability Station

A process flow diagram of the high temperature durability station (HTDS) is shown in Figure 2-17. A photo of the station can be found in Figure 2-18.

A temperature controlled laboratory oven ensured that the membrane modules were maintained at the desired temperature. A water to gas membrane humidifier, model DX-5 from DPoint Technologies was used to provide water saturated air at the set temperature. The temperature and humidity level of the gas stream 'S3' was controlled by adjusting the water bath temperature. The gas stream entering the modules labeled 'S3' was set to 85^{o}C and 100% relative humidity. The stream labeled 'S1' was at 80^{o}C and 0% relative humidity. The flow rate to each module was 4 SLPM.

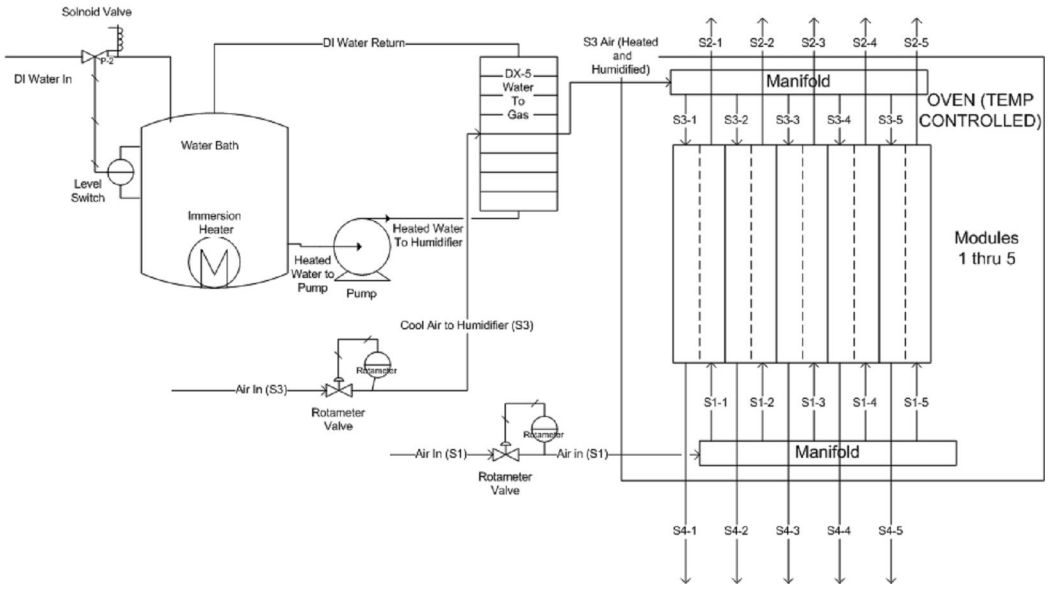

Figure 2-17: Process flow diagram of the high temperature durability station (HTDS).

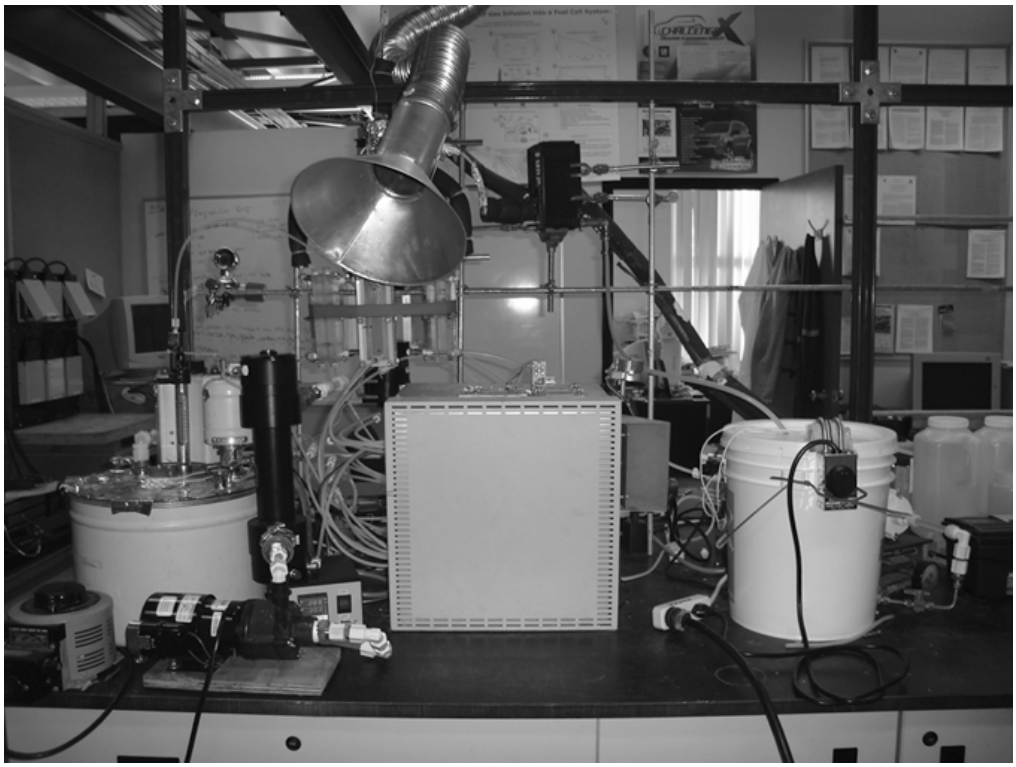

Figure 2-18: Photograph of the HTDS.

Chapter 3

3.0 Membranes for Gas to Gas Humidifiers

3.1 General Membrane Selection Procedure

The membrane is the most important component of the gas to gas humidifier. The membrane acts as a medium by which heat and moisture are transported from the hot, wet stream to the cool, dry stream. The membrane also acts as a barrier to gas permeation from one stream to the other. The failure of the membrane will lead to failure of the humidifier. In order to find appropriate membrane materials for the humidifier a selection procedure was created. This is outlined in Figure 3-1.

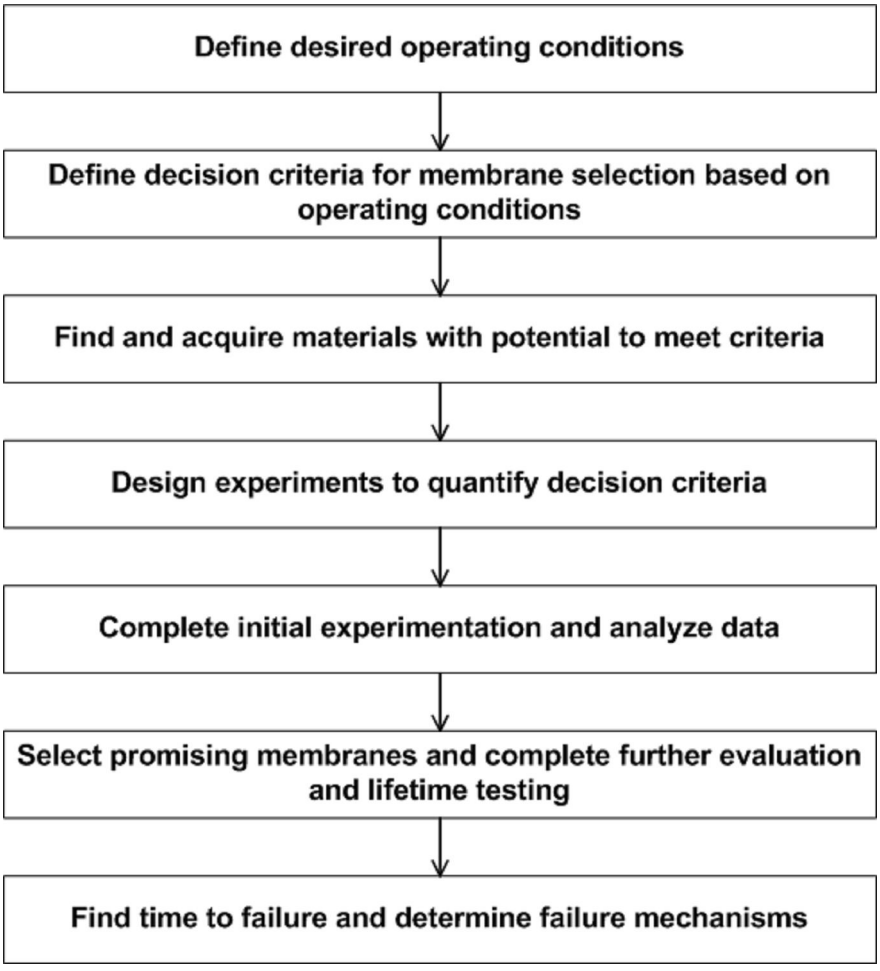

Figure 3-1: Membrane selection procedure.

3.2 Defining Operating Conditions

Two humidifier operational regimes were established. These conditions were based on the environment under which the fuel cell humidifier would be in service. Low temperature conditions were determined based on the standard PEM fuel cell environment, in which the fuel cell system would be used in back-up or residential power applications. High temperature conditions were based on the PEM fuel cell system under use in an automotive environment. The high and low temperature conditions are summarized in Table 3-1.

Table 3-1: Conditions of high and low temperature operational regimes.

Operational Regime	Low Temperature	High Temperature
Dry Inlet Temperature (^{o}C)	25	80 to 130
Dry Inlet Relative Humidity (%)	15	0
Dry Inlet Pressure (kPag)	< 20	80
Wet Inlet Temperature (^{o}C)	65	> 80
Wet Inlet Relative Humidity (%)	100	100
Wet Inlet Relative Pressure (kPag)	< 20	60
Operational Lifetime Requirements (h)	1500 to > 5000	> 5000

3.3 Membrane Selection Criteria

A vast array of polymer based membrane materials is currently available for gas and liquid separations. Different membranes have been designed with desirable permeation rates and selectivity for the systems they operate in which they operate. In screening and selecting appropriate membranes for a gas to gas humidifier, certain considerations must be made. Specifically the membrane must have the following characteristics:

- high liquid water and water vapour permeation rates
- low air permeation rate when the membrane is both in the wet and dry state
- high mechanical strength
- ease of handling

- a long operating lifetime
- appropriate temperature tolerance and
- preferably low cost

Membranes which are considered for a fuel cell gas to gas membrane based humidifier underwent go a rigorous screening process, through which candidate materials were selected. Materials which demonstrated the desirable characteristics were selected for further analysis. The following sections outline the selection criteria utilized in targeting desirable materials.

3.3.1 Water Permeation

The membrane must be highly permeable to water in the vapour or liquid form. If the membrane is incapable of transporting water from the wet stream to the dry stream in the humidifier at a sufficient rate, it will not be a good candidate material. Procedures for determining the water permeation rate of candidate material are summarized in experimental methods in Chapter 2.

In order to meet the outlined desired operating conditions, while maintaining a reasonable membrane active area in the humidifier, a minimum acceptable water flux was set. This value was based on operational considerations, and the performance of a baseline membrane material. The minimum water flux was set to be 14 $kg/m^2/h$ at a flow rate of 6 SLPM, in the standard water permeation testing apparatus, which is outlined in Section 2.1.2. Membranes which exhibited a water flux significantly less than this minimum value were rejected.

3.3.2 Air Permeation

Under general humidifier operating conditions, the membrane may be subjected to intermittent or constant differential pressures. In operation, the humidifier dry side inlet is upstream from the fuel cell while the humidifier wet side is downstream from the fuel cell. Flow through the fuel cell will be subjected to pressure losses due to forced flow through the flow-field channels. This leads to a pressure drop from the fuel cell inlet to the fuel cell outlet, which causes differential pressure across the membrane in the humidifier that acts against the direction of desirable water permeation. A highly porous membrane may lead

to the pressure gradient across the membrane driving convective flux of water in opposition to the chemical potential driven diffusion flux across the membrane. In this case, the pressure differential will be detrimental to the humidifier performance. Also pressure differentials in the humidifier may lead to reactant gases short circuiting through the porous membranes in the humidifier, leading to fuel cell performance losses. Evidently the permeability of gases through the membrane under wet and dry conditions will be an important consideration in choosing an appropriate humidifier membrane.

Most membranes tested for this application which pass gas when dry tend to 'wet out' when exposed to water. This means that water will sorb into the membrane and fill any pores present. The surface tension of the water in these pores then forms a barrier to convective gas permeation at pressures up to the bubble point pressure (Hoffman, 2003). For all but the largest pores, this pressure tends to be greater than most differential pressures that are observed in the humidifier environment. So generally when a porous membrane is wetted air permeation occurs largely based on gas diffusion through the water in the membrane pores. Based on this, the maximum wet air permeation rate of the membrane was set to less than 0.01 $cm^3\ min^{-1}\ cm^{-2}\ kPa^{-1}$.

The dry crossover rate of a polymer membrane will depend on the consistency of membrane, the membrane pore size, and the overall porosity. Since the membranes utilized tend to wet out in the humidifier environment, the dry crossover will only be a concern when the fuel cell system is initializing and the gas streams are still relatively dry. The maximum allowable dry air crossover rate was based on losing less than 5% of the flow to the fuel cell through the humidifier under an operating differential pressure, of 20 kPa. For a flow rate of 4 SLPM and a membrane area of 33.24 cm^2 this value was determined to be 3.0 $cm^3\ min^{-1}\ cm^{-2}\ kPa^{-1}$.

3.3.3 Mechanical Strength

When under some operating conditions the membrane may be exposed to constant differential pressures, or else intermittent increases in pressure. In a plate and frame type humidifier, the membrane is supported by ribs that run the length of the humidifier channel, as shown in Figure 3-2.

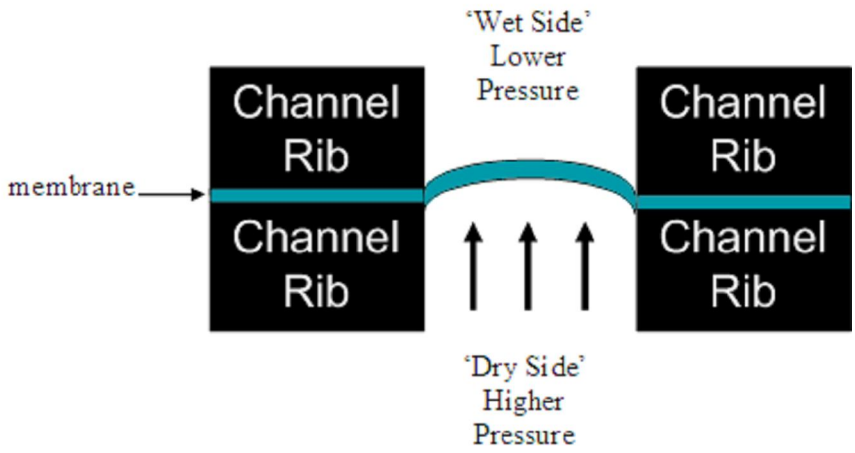

Figure 3-2: Cross-section of humidifier channel showing membrane creep under pressure.

When the membrane is exposed to pressure it is vital that the membrane does not stretch into the humidifier channel, which could potentially block air flow and cause greater increases in the differential pressure. It is also important that the membrane does not permanently deform into the channel due to either a rare pressure spike, or by creep caused by operating under constant differential pressures.

In order to ensure no deformation of the membrane under a pressure of 50 kPa, a channel with a width of 3 mm, a depth of 1 mm, and a membrane in the center was created in SolidWorks and tested for deformation using COSMOSXpress. A range of membrane elastic moduli were simulated under a pressure of 50 kPa and the maximum deflection was recorded. A sample simulation is shown in Figure 3-3 and a plot of membrane elastic modulus against deflection can be found in Figure 3-4. From Figure 3-4 it can be determined that an elastic modulus of greater than 75 MPa will ensure less than 10% deflection into the channel at 50 kPa, under this channel configuration. This value was increased by a safety factor of 1.5 in an attempt to account for the decreased tensile and yield strength of the membrane under hot and wet conditions. The specification for elastic modulus of the membrane was chosen to 122.5 be MPa.

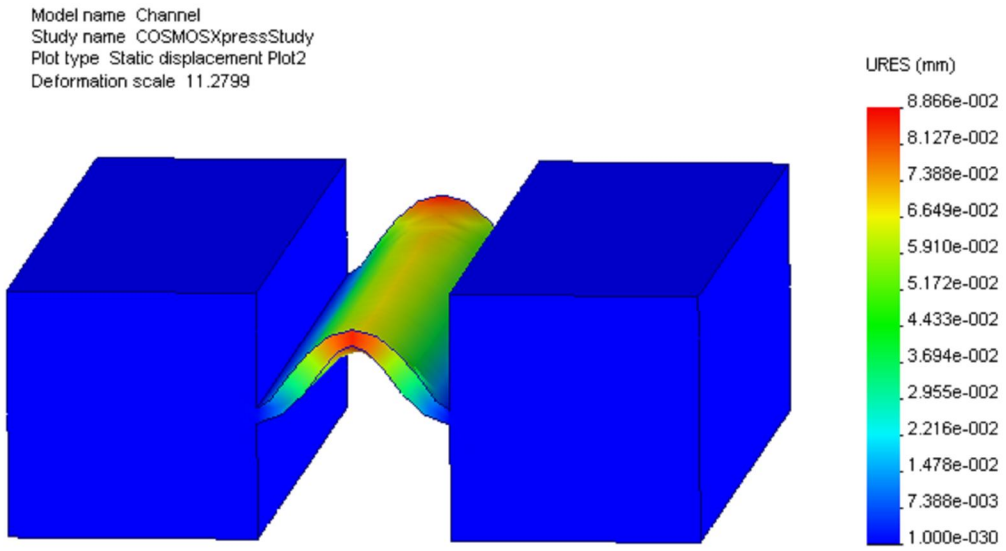

Figure 3-3: COSMOSXpress simulation of membrane deflection into the humidifier channel under 50 kPa of pressure, membrane elastic modulus of 75 MPa, deformation is exaggerated by a factor of 11.3.

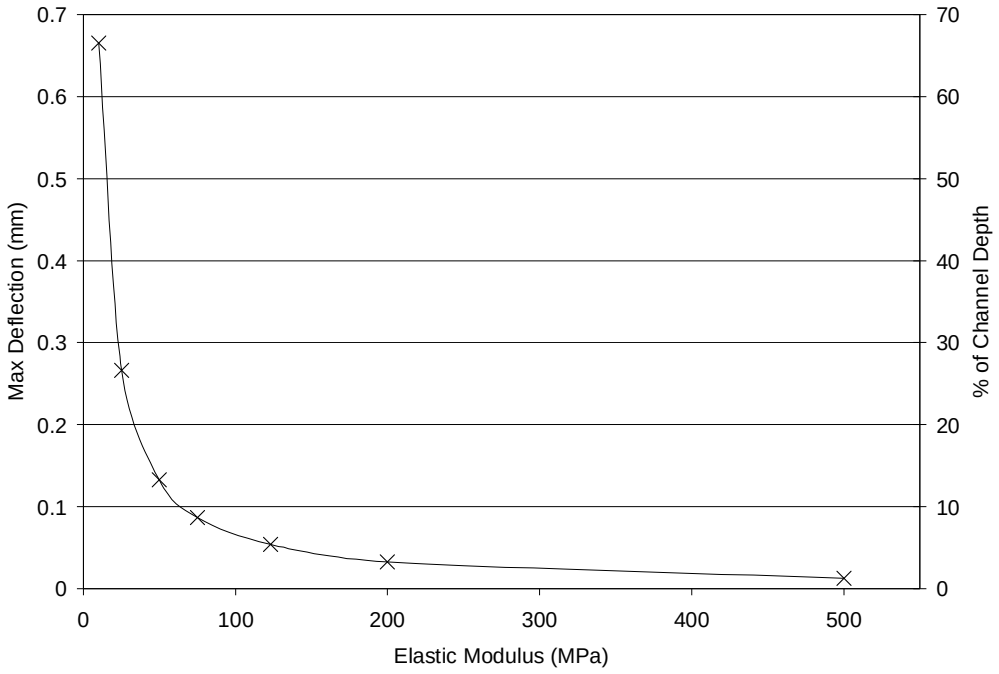

Figure 3-4: Membrane deflection at 50 kPa, as a function of elastic modulus, as simulated by COSMOSXpress.

To ensure this value was sufficient, a membrane with a similar modulus (value) was put into a single cell test jig with a channel width of 3 mm. The membrane was heated with

wet gas and pressurized to 35 kPa; minimal deformation was observed.

3.3.4 Handling and Dimensional Stability

The membrane must be robust enough to withstand moderate handling during the assembly of the humidifier. Building plate and frame humidifiers will require that the membrane be attached to humidifier plates, which are stacked together to generate the humidifier stack. The frames may also be insert molded over the membrane, in which case the membrane must be suitable for this process. Namely the membrane material should compatible with the polymer used to mold the frame. As well the membrane must be capable of tolerating the temperatures and stresses necessitated by the insert molding process. Finally many membrane materials, particularly ionomers will undergo swelling and dimensional changes in the presence of water. This could pose a problem if the humidifier is assembled with membranes in the dry state, as the membrane will deform inside the humidifier when it is put into operation.

Alternative humidifier assembly processes, such as pleating and potting, may help mitigate some issues presented by certain membrane materials. However, the material must be robust enough for moderate handling and have sufficient dimensional stability as not to compromise the humidifier's integrity when in the presence of water.

The quantification of these criteria is difficult. Membranes which presented significant handling issues during the standard test procedures were flagged as possible problem materials if further humidifier development with the material were desirable.

3.3.5 Lifetime

The operational lifetime requirements for the humidifier membrane at the desired conditions are presented in Table 3-1. Meeting these requirements is of great importance for humidifier design. Continual operation of membrane materials at elevated temperature, high humidity, increased pressure, and constant flow may lead to failure of the membrane. Failure mechanisms will be dependent on the operating conditions, and the composition of the membrane material. Membranes tested in situ were required to meet a minimum 1500 hours of operation. Membranes were operated in situ until failure was achieved. Failure was defined as a decrease in water flux of greater than 20% from the beginning of life

(BOL) value. An increase in air permeation rate of greater than 25% from the BOL value also indicated failure. Other failures included the cracking, fouling, or excessive deformation of the membrane material.

3.3.6 Overall Testing Procedure

The requirements outlined in the above sections were incorporated into a testing procedure, which is presented in Figure 3-5.

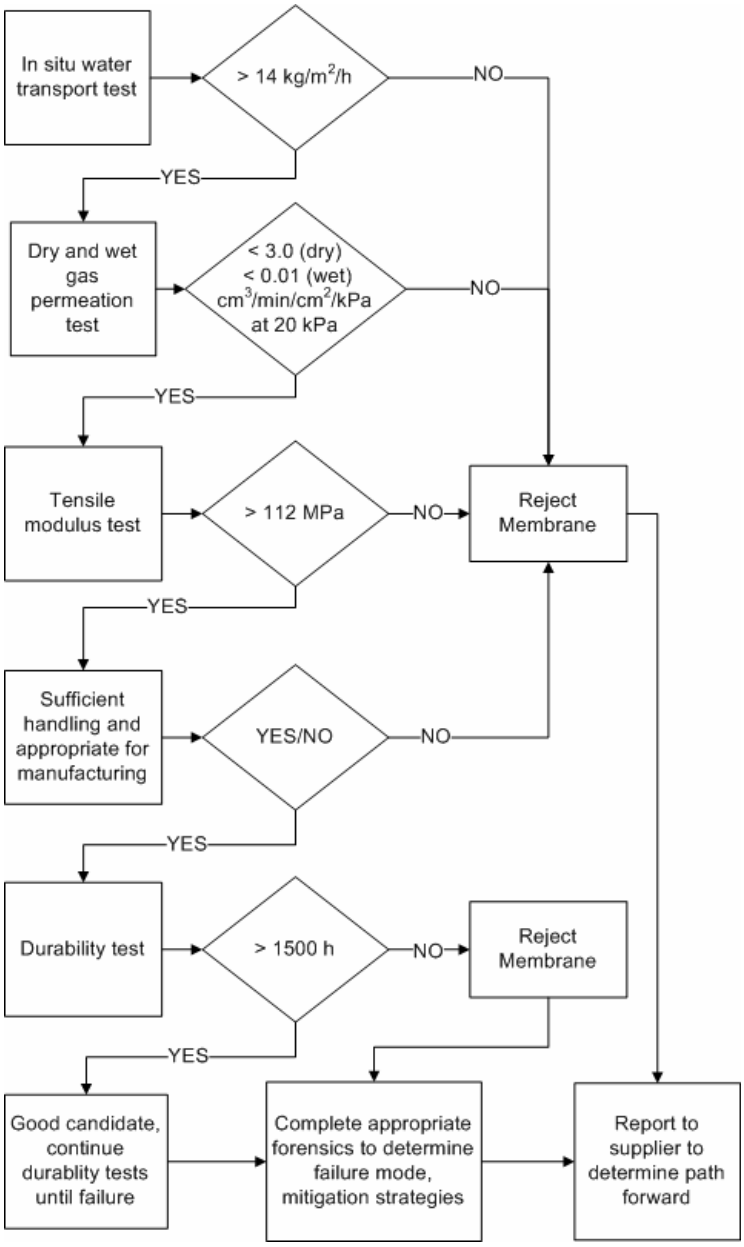

Figure 3-5: Membrane testing procedure.

3.4 Membranes Materials

3.4.1 Industries

In the past thirty years the polymer based membrane industry has grown dramatically. Processes in which synthetic membranes play a prominent role have become increasingly common and feasible (Scott and Hughes, 1996). Industries utilizing synthetic membrane materials are can be classified as follows (Keiran, 2000):

- Reverse Osmosis;
- Nanofiltration;
- Ultrafiltration;
- Microfiltration;
- Gas Separations;
- Pervaporation;
- Ion Exchange and Electrodialysis; and
- Battery Separator Applications.

3.4.1.1 Reverse Osmosis

The reverse osmosis process generally functions to remove dissolved salts from water. Solutes, such as salts and macromolecules are separated from the solvent (water) through a semi-permeable membrane. The membrane is permeable to the solvent but not the solute. In normal osmosis, the solvent would pass through the membrane from a region of high solvent concentration to a region of low concentration. This process is entirely driven by the chemical potential gradient across the membrane. In reverse osmosis, pressure is applied to the solvent-solute solution to overcome the osmotic pressure, forcing the solvent through the membrane against the chemical potential gradient (Scott and Hughes, 1996). Membranes for reverse osmosis are made from polymers such as cellulose acetate, polyamides, and polysulphones (Baker, 2004). Reverse osmosis membranes have pore sizes in the 1 to 10 Å range.

3.4.1.2 Nanofiltration

In this application membrane are typically used to separate multivalent ions from solutions, nanofiltration operates in a similar fashion to reverse osmosis (Scott and

Hughes, 1996). Nanofiltration membranes are semi-permeable but have larger pore sizes than reverse osmosis membranes, typically in the 5 to 100 Å range. This allows the passage of water and small monovalent ions such as sodium, but causes the rejection of larger and highly charged ions, sugars, and organic matter. Pressure is applied to the solution on one side of the membrane forcing species small enough in size and charge through the pores of the membrane. Nanofiltration membranes are made from polymers such as polysulphone and polyamide (Scott and Hughes, 1996).

3.4.1.3 Ultrafiltration

Ultrafiltration is also a pressure-driven process, similar reverse osmosis but with membranes having larger pore sizes than nanofiltration. Ultrafiltration membranes have pore sizes in the 100 to 1000 Å range. Most solvents, ions, proteins, and molecules with low molecular weighs will be passed through these membranes, including multivalent ions (Baker, 2004). The membranes exist as a polymer skin on top of a porous substrate, as shown in FIG (Baker, page 229). Polymers used include polysulphone, polyethersulphone, polyacrylonitrile, polyimide, and polyamide (Scott and Hughes, 1996).

3.4.1.4 Microfiltration

Microfiltration is another pressure driven process, with membranes having pore sizes larger than ultrafiltration membranes. The pore size range for microfiltration membranes is between 1000 and 100000 Å. The membranes tend to exist as thin films consisting of a wide range of polymer materials as well as ceramics, metals, and glasses (Scott and Hughes, 1996). Microfiltration membranes pass solvents, ions, larger molecules, and bacteria while filtering particulate matter.

3.4.1.5 Gas Separations

Membrane based gas separation is completed using both porous and dense membrane materials. The mechanisms for separation are quite different between these types of polymer, as shown in Figure 3-6. Separation is based on the size of the gas molecules and the solubility of the gas in the membrane.

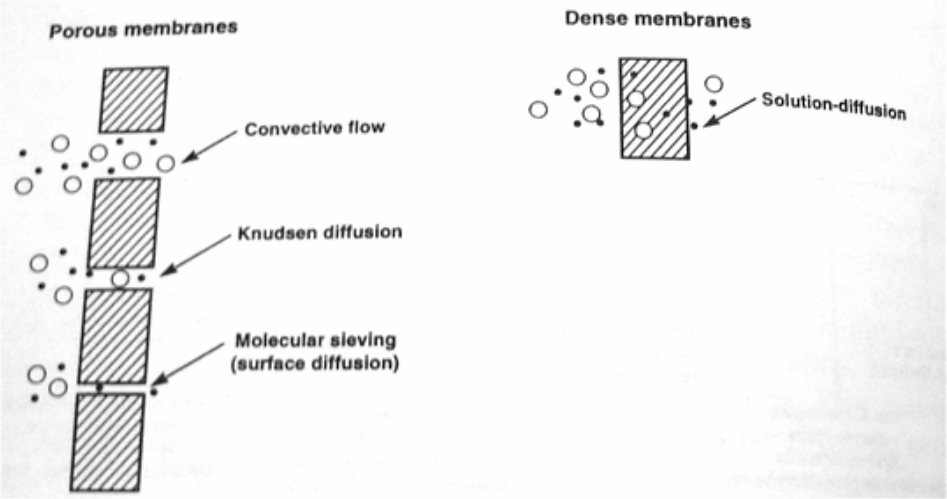

Figure 3-6: Comparison of transport in porous and dense membranes (Baker, 2004).

In membranes with large pore sizes under pressure, no separation is possible as all gas molecules will be transported through the membrane at an equal rate by convective flow. However, in membranes with smaller pore sizes, Knudsen diffusion dominates permeation and gas separations can occur based on the size of the pores and the molecular weight of the gas molecules (Bitter, 1991).

Use of porous membrane in commercial gas separations is rather limited, and gas separations are generally achieved through the use dense polymer membranes. In dense polymers, the solution-diffusion mechanism dominates transport through the membrane. In this mechanism, gases adsorb on the membrane surface on the high pressure or high concentration side of the membrane. The gases then diffuse through the dense polymer structure to the other side of the membrane where desorption occurs. Generally it is the diffusion step that is rate limiting in this process (Scott and Hughes, 1996). Smaller gases tend to have higher diffusion rates through the dense polymer matrix, allowing separation to occur. The permeation rate for a gas will also be affected by the solubility of different gases in the polymer.

3.4.1.6 Pervaporation

In pervaporation processes, a liquid mixture is present on one side of the membrane while a vacuum is applied to the other side of the membrane. Preferential sorption occurs on the liquid side of the membrane, followed by diffusion of the permeant through the membrane to the vacuum side where desorption of permeant occurs in the vapour phase (Scott and

Hughes, 1996). Hydrophobic membranes can be used to separate organics from water, and hydrophilic membranes can be used to dehydrate organic solutions. Membranes for permeation tend to be laminates of dense polymer films on a porous backing layer.

3.4.1.7 Electrodialysis and Fuel Cells

These processes use ion exchange membranes, which selectively allow the passage of either positively or negatively charged ions (Scott and Hughes, 1996). An electric potential is created across the membrane causing permeable ions to move from one side of the membrane to other. Electrodialysis is typically used to remove salts from water, separating the cations and anions from water using different membranes. PEM fuel cells utilize an ion exchange membrane which selectively transports hydrogen protons (cations) which have be isolated from hydrogen gas. Details about this process were covered in Chapter 1. Ion exchange membranes are made from various polymer materials such as polytetrafluoroethylene to which ion exchange groups such as sulphonic and carboxylic acid have been grafted.

3.4.1.8 Battery Separator Applications

Lead acid, lithium ion, and nickel metal hydride batteries utilize polymer based separator materials between the anode and cathode to prevent short circuiting, while at the same time allowing the passage of ionic species within the battery. This is accomplished though porous non-conductors (Bohnstedt, 1996). For lead acid batteries these are porous membrane materials that tend to consist of inorganic materials such as silica held together by polymers such as ultra high molecular weight polyethylene (UHMWPE) (Bohnstedt, 2001). For lithium ion and nickel metal hydride applications, the separator is typically a microporous olefin polymer based membrane (Venugopal et al., 1999; Kritzer, 2004).

3.4.2 Membrane Classification

3.4.2.1 Porous Membranes

Membranes with large pores will pass gas by convection, namely Poiseuille flow, and no separation will occur. This occurs when the mean pore size is much greater than the mean free path length (λ) of the gas of interest. The mean free path length of a gas can be

calculated by equation 3-1 (Scott and Hughes, 1996).

$$\lambda = \frac{RT}{\sqrt{2}\pi\sigma^2 p_i} \qquad [3\text{-}1]$$

Where σ is the collision diameter of the gas, and p_i is the partial pressure of the permeating gas molecule.

However, when the mean pore size is much smaller than the mean free path length for the gas, then gas molecules will be transported through the membrane by Knudsen diffusion and separation is possible (Baker, 2004). This tends to occur when the pore size smaller than about 1000 Å. In Knudsen diffusion, the rate of transport through the pores is inversely proportional to the square root of the molecular weight of the gas (Baker, 2004). This allows smaller molecules to permeate through the membrane at much greater rates than larger molecules, and gas separation can occur with high levels of selectivity. Selectivity (α) is defined as, the ratio of the permeability (P) of two gases, *i* and *j* through the membrane:

$$\alpha_{ij} = \frac{\mathrm{P}_i}{\mathrm{P}_j} \qquad [3\text{-}2]$$

For membranes with very small pore sizes, in the range of 5 to 20 Å, a sieving mechanism will dominate the flow of species through the membrane (Baker, 2004). This behavior tends to occur with zeolite based membrane material and involves a combination of surface diffusion within the pores, as well as diffusion within the gas phase (Scott and Hughes, 1996).

3.4.2.2 Dense Membranes

Dense or tight polymer membranes are essentially non-porous materials in which permeants must adsorb to the membrane surface and then diffuse through the membrane under the driving force of a chemical potential gradient (Bitter, 1991). This process is compared visually to transport in porous membranes in Figure 3-7.

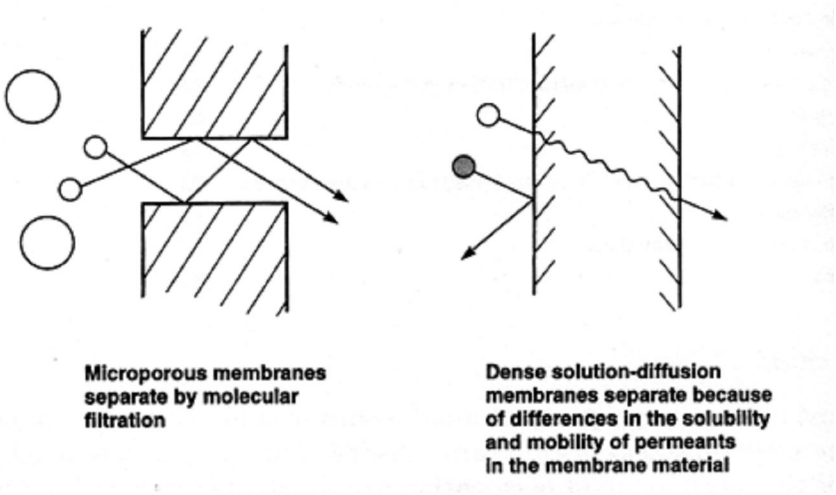

Figure 3-7: Comparison of transport in porous and solution-diffusion type membranes (Baker, 2004).

The permeation rate of a species through the membrane (*P*) is a product of the diffusion coefficient of the species through the membrane (*D*) and the sorption coefficient of the species in the membrane (*K*):

$$P = DK \qquad [3\text{-}3]$$

Selectivity in this type of membrane will be based on the differences of solubility and diffusion rates of the species in the membrane. The solution diffusion model describes transport in these types of membrane and is illustrated in Figure 3-8.

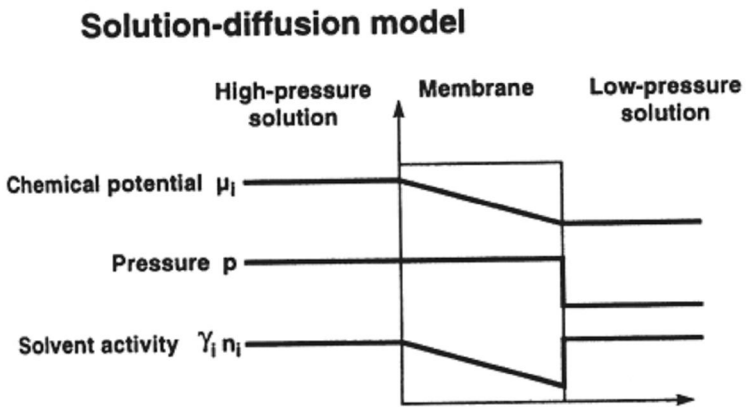

Figure 3-8: Cross-sectional profile of solution-diffusion process (Baker, 2004).

3.4.2.3 Isotropic and Anisotropic Membranes

Membranes can be classified as isotropic, meaning that they are the same consistency throughout. For porous materials, this infers that the material, the pore sizes and porosity are the same from one side of the membrane to the other. Similarly, nonporous isotropic dense membranes have a constant physical structure from top to bottom. Ionomers and electrically charged membranes will demonstrate no variation in charge and physical nature from side to side.

Membranes which are classified as anisotropic demonstrate changes through the cross-section of the membrane in a directional orientation. The rate of permeation through dense polymers will be inversely proportional to the thickness of the membrane, so it is desirable to make these membranes as thin as possible. However, making thinner dense membrane compromises mechanical strength and integrity. To resolve this issue, membrane manufacturers will make composite membranes with a very thin layer of the dense polymer on a porous substrate. Microporous membranes may also be created with cross-sections through which the pore size and porosity changes. Isotropic and anisotropic membranes are compared in Figure 3-9.

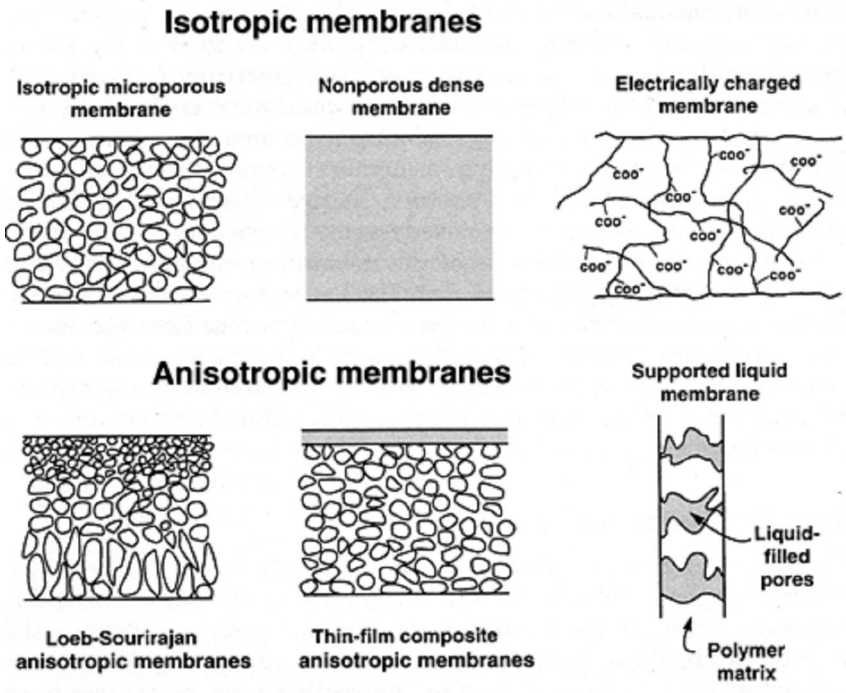

Figure 3-9: Comparison of isotropic and anisotropic membranes (Baker, 2004).

3.5 Summary of Membranes Materials Acquired and Tested

Below is a summary of the membrane materials used in this work. The actual commercial source of each membrane is confidential and so the membranes are identified with their test numbers below.

3.5.1 Membrane-01

This material is used as a battery separator; it has a thickness of 770 microns. The membrane is made by extrusion of polyvinyl chloride with a high content of hydrophilic silica additives. This yields a membrane that is fairly porous but capable of transporting water. The membrane is flat on one side and has ribs along the other side.

3.5.2 Membrane-02

The membrane is a microporous ultra high molecular weight polyethylene (UHMWPE) based battery separator, which is created using a membrane extrusion process. This membrane is 75 microns thick, with a pore volume of 50%. The membrane contains titanium dioxide (TiO_2) filler as well as a wetting agent such as dodecylphenoxy polyethoxy ethanol. The separator material is permanently wettable and has demonstrated improved battery life in various types of alkaline batteries.

3.5.3 Membrane-03

This membrane is an extruded microporous polypropylene based battery separator material. It has been coated with a wetting agent and was designed for aqueous electrolyte battery systems. The membrane has a thickness of 25 microns and a porosity of 37%.

3.5.4 Membrane-04

This membrane is similar to Membrane-03 with a porosity of 55%.

3.5.5 Membrane-05

This membrane is a UHMWPE based membrane containing a silica filler material. The polymer and inorganic filler are extruded with plasticizer oil and then calendared to form a sheet. The membrane is then stretched to produce a desired porosity, and the plasticizer oil

is removed using an appropriate solvent. This membrane has a thickness of 45 microns. It is designed for use as a battery separator in lithium ion batteries.

3.5.6 Membrane-06

This membrane is similar in consistency to Membrane-05 but is 180 microns in thickness.

3.5.7 Membrane-07

This membrane is similar in consistency to Membrane-05 but is 200 microns in thickness.

3.5.8 Membrane-08

Is a standard battery separator material extruded and calendared from a mixture of UHMWPE, silica, and plasticizer. This membrane is typically used as a separator material in lead acid batteries. The silica to polyethylene ratio of the material is 2.6 to 1. The membrane contains 10 to 12% residual plasticizer.

3.5.9 Membrane-09

This membrane material was designed for use in lithium ion batteries. The membrane consists of a non-woven polyethylene terephthalate (PET) containing a mixture of silica (SiO_2) and alumina (Al_2O_3) inorganic fillers. The membrane has a nominal thickness of 25 microns and a porosity of greater than 40%. The membrane is known to have excellent wettability and high temperature stability up to 210^{o}C.

3.5.10 Membrane-10

The membrane is a laminate material consisting of sulphonated styrene, polyethylene, and polypropylene based block co-polymer coated onto a microporous polyethylene support layer, the material may contain inorganic fillers as well. The material is typically used in energy recovery ventilation systems.

3.5.11 Membrane-11

The membrane is a UHMWPE material. The membrane is highly porous with a hydrophilic after treatment.

3.5.12 Membrane-12

This membrane is created using a similar material as that in Membrane-11 as a base material. The membrane consists of UHWWPE to which hydrophilic groups have been graphed in order to make the membrane hydrophilic.

3.5.13 Membrane-13

The membrane is an ionomer material produced using a perfluorosulfonic polytetrafluoroethylene copolymer. The material is inherently permeable to water, while being highly impermeable to gases. The thickness of this material is 25.4 microns.

3.5.14 Membrane-14

This membrane is the same material as Membrane-13 but has a thickness of 50.8 microns.

3.5.15 Membrane-15

This membrane is a standard battery separator material. The membrane is extruded as a blend of UHMWPE, silica, and plasticizer oil. The silica to polyethylene ratio is 2.5 to 1; the membrane contains 15% residual process oil. The membrane is 180 microns in thickness.

3.5.16 Membrane-16

The membrane is the same material as Membrane-15 with all of the process oil removed using a solvent.

3.5.17 Membrane-17

The membrane is similar to Membrane-16 with a silica to polyethylene ratio of 2.2 to 1. 2.2.

3.5.18 Membrane-18

The membrane is similar to Membrane-15 with a silica to polyethylene ratio of 3.01 to 1. The membrane contains 13% residual plasticizer oil. The membrane has ribs which are

0.25 mm thick and 0.18 mm in height, with spaces 0.7 mm apart running the length of the membrane, the membrane is 0.18 mm thick between the ribs.

3.5.19 Membrane-19

The membrane is the same material as Membrane-18 with 0% residual plasticizer.

3.5.20 Membrane-20

This membrane is made of the same material as Membrane-16 with 20% oxidation resistant coating agent.

3.5.21 Membrane-21

Membrane 21 is similar to Membrane-15, except that it contains unique process oil, ‘Oil A’.

3.5.22 Membrane-22

Membrane 22 is similar to Membrane-15, except that it contains unique process oil, ‘Oil B’.

3.5.23 Membrane-23

Membrane 23 is similar to Membrane-15, except that it contains unique process oil, ‘Oil C’.

3.5.24 Membrane-24

Membrane 24 is similar to Membrane-15, except that it contains unique process oil, ‘Oil D’.

3.5.25 Membrane-25

The membrane has a porous structure, is based on UHMWPE, and contains no inorganic filler material. The membrane thickness is 10 microns.

3.5.26 Membrane-26

The membrane has a porous structure, is based on UHMWPE, and contains 20% unspecified inorganic filler material. The membrane thickness is 10 microns.

3.5.27 Membrane-27

The membrane has a porous structure and is based on UHMWPE, and contains an unspecified inorganic filler material. The membrane has a porosity of 67.5% and a thickness of 17.7 microns.

3.5.28 Membrane-28

This membrane is similar to Membrane-27, with a porosity of 63.5% and a thickness of 15.1 microns.

3.5.29 Membrane-29

This membrane is laminate, consisting of proton exchange membrane perflourosulfonic acid polymer material on a porous polyethylene backbone.

3.5.30 Membrane-30

The membrane is a 20 micron thick nanoporous hydrophilic film. It is an ion exchange membrane, further details regarding this membrane were not disclosed.

3.5.31 Membrane-31

This membrane is a similar material to Membrane-30 with a thickness of 22 microns.

3.5.32 Membrane-32

This membrane is a similar material to Membrane-30 with a thickness of 20 microns. The alterations to this membrane are confidential, and were not revealed by the supplier.

3.5.33 Membrane-33

This membrane is a similar material to Membrane-30 with a thickness of 20 microns. The

alterations to this membrane are confidential, and were not revealed by the supplier.

3.5.34 Membrane-34

This membrane is a perfluorosulfonic acid polymer based material used as a proton exchange membrane.

3.5.35 Membrane-35

This membrane consists of an ionomeric polymer, sulphonated polyether ether ketone (s-PEEK) laminated to a porous substrate.

3.5.36 Membrane-36

This material consists of porous polyethylene filled with a perfluorinated sulphonic acid polymer.

3.5.37 Membrane-37

This a porous polypropylene based membrane.

3.5.38 Membrane-38

This membrane is an anion exchange membrane material reinforced on a polyether ether ketone (PEEK) backbone.

3.5.39 Membrane-39

This membrane is a homogenous membrane created with sulphonated polyether ether ketone (s-PEEK) polymer.

3.5.40 Membrane-40

This is an expanded polytetrafluoroethylene material used as a proton exchange membrane material. The thickness of this material is 10 microns.

3.5.41 Membrane-41

This membrane is similar to Membrane-40 but with a thickness of 18 microns.

3.5.42 Membrane-42

This material is standard battery separator material based on polyethylene based material with a silica based additive. The polyethylene to silica ratio is 2.5 to 1 and the residual plasticizer content is 13%. The membrane has a nominal thickness of 250 microns.

3.5.43 Membrane-43

This material is a polyethylene and silica based material used in electrochemical double layer capacitor (EDLC) applications. The membrane has a thickness of 110 microns, a silica to polyethylene ratio of 0.9 to 1, and a porosity of 55%.

3.5.44 Membrane-44

This material is similar to Membrane-43 with a silica to polyethylene ratio of 0.6 to 1, a thickness of 110 microns, and a porosity of 40%.

3.5.45 Membrane-45

This material is similar to Membrane-43 with a silica to polyethylene ratio of 0.7 to 1, a thickness of 85 microns, and a porosity of 50%.

3.5.46 Membrane-46

This membrane is a nylon based homogenous polymer membrane made with nylon 6, 6 polymer. The membrane is inherently hydrophilic, and is generally used as a transfer material in protein and DNA blot tests.

3.5.47 Membrane-47

The membrane is a polyester urethane polymer material which has a hydrophilic additive grafted to the base polymer.

3.5.48 Membrane-48

The membrane is a sulphonated polyetheretherketone (s-PEEK) material with a silica additive. The membrane contained 13% silica by weight and was 20 microns in thickness.

3.5.49 Membrane-49

The membrane is similar to Membrane-48 with a silica content of 13% and a thickness of 30 microns.

3.5.50 Membrane-50

The membrane is similar to Membrane-48 with unknown silica content and a thickness of 20 micron.

3.5.51 Membrane-51

The membrane is similar to Membrane-48 with a silica content of 17% and a thickness of 20 micron.

3.5.52 Membrane-52

The membrane is similar to Membrane-48 with a silica content of 25% and a thickness of 20 micron.

3.5.53 Membrane-53

The membrane is similar to Membrane-48 with a silica content of 30% and a thickness of 20 microns.

3.5.54 Membrane-54

The membrane is similar to Membrane-48 with an alternative type of silica and s-PEEK. The membrane has a thickness of 20 microns.

3.5.55 Membrane-55

The membrane is a homogeneous ion exchange membrane based on a copolymer of

tetrafluoroethylene and sulfonyl fluoride vinyl ether.

3.5.56 Membrane-56

The membrane is a fluoropolymer based material with a rough fabric surface. The membrane has a thickness of 510 microns.

3.5.57 Membrane-57

Membrane is similar to Membrane-56 with a thickness of 110 microns.

3.5.58 Membrane-58

The membrane is a fluoropolymer based material with a smooth surface. The membrane has a thickness of 110 microns.

3.5.59 Membrane-59

The membrane is similar to Membrane-58 with a thickness of 270 microns.

3.5.60 Membrane-60

The membrane was a polyvinyl alcohol based laminate membrane with an unknown backbone material. The membrane is typically used in pervaporation systems.

3.5.61 Membrane-61

This membrane was a porous paper type membrane that is typically used in energy recovery ventilator (ERV) systems.

Chapter 4

4.0 Design Methodology for Plate and Frame Humidifiers

This section outlines the creation of gas to gas plate and frame humidifiers for fuel cell systems. The architecture of these humidifiers is described, followed by some background on this type of humidifier. A series of experiments was completed in which the performance of these humidifiers under various geometrical considerations was evaluated. Humidifiers for these experiments were created using rapid prototyping methods; also the performance of similar commercial humidifiers was evaluated. Equations for humidifier design are evaluated, and a humidifier design procedure based on these equations and the humidifier packaging requirements is proposed. Portions of this Chapter have been submitted to the Journal of Engineering Design.

4.1 Gas to Gas Planar Humidifiers

Although membrane humidifiers have been developed, conventional designs are modeled after other well known devices such as planar, plate-and-frame heat exchangers. In the simplest implementation, a series of rigid plates similar to those shown in Figure 4-1 are separated by a membrane and aligned one on top of another to form a stack. The membrane is not permeable to gases, but it allows heat and water transport via micro- and macro-pores, hydrophilic additives, or by virtue of hydrophilic properties of the membrane material.

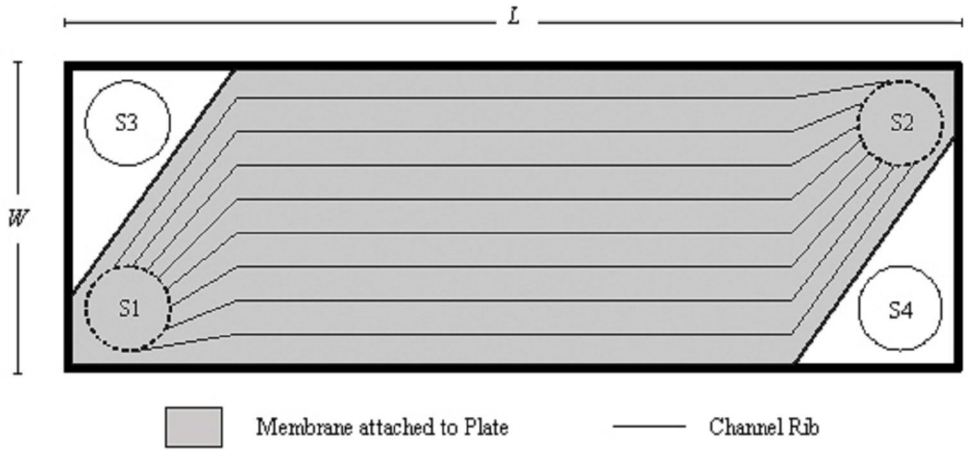

Figure 4-1: Single humidifier plate.

This topology defines flow channels with two membrane sides (wet and dry) and two sides delimited by the walls of the separating channel ribs as shown in Figure 4-2. The channel cross-sections (e.g. trapezoidal or square) are usually constant.

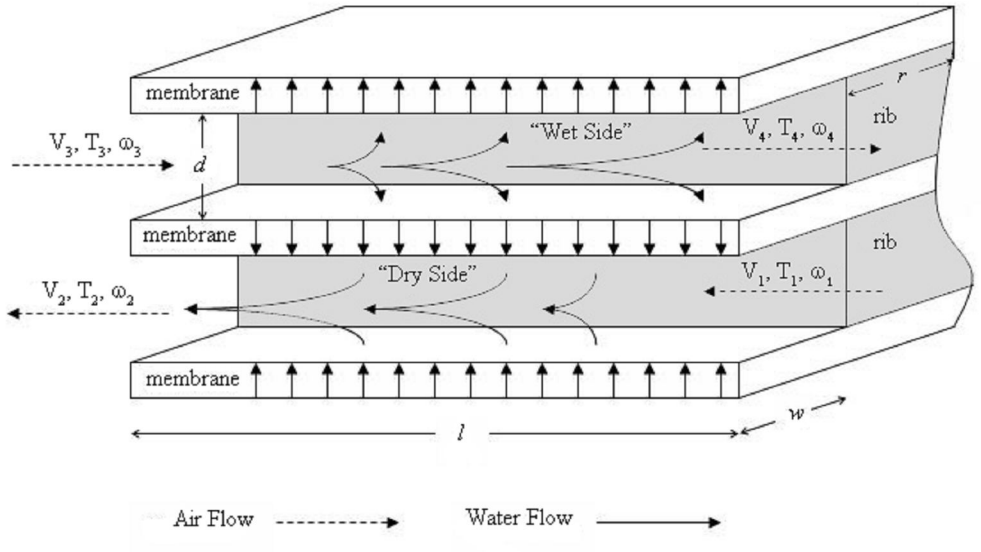

Figure 4-2: Schematic of transport in the channel of the heat and moisture exchanger.

The humidifier is comprised of plates similar to the one shown in Figure 4-1 which have flow inlet and outlet ports, and flow channels placed on top of the membranes. Many of these plates are combined together to produce a humidifier stack which has two set of inlets and outlets, one set for the cool dry stream, which is humidified in the unit before entering the fuel cell, and one set for the hot wet stream which is taken from a stream exiting the fuel cell stack. The overall flows to the humidifier are shown in Figure 4-3.

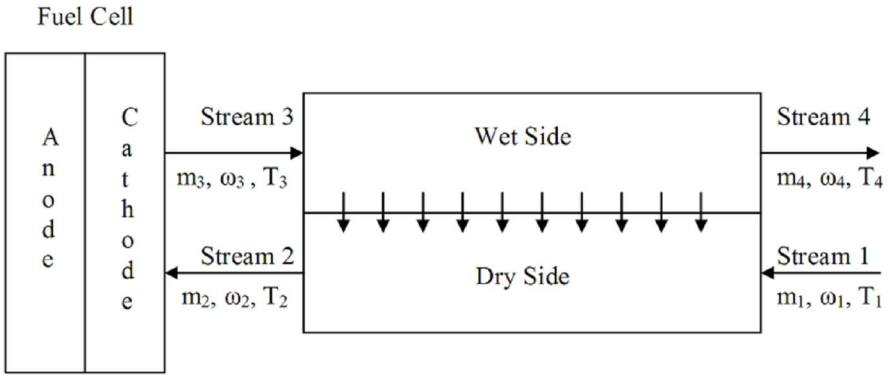

Figure 4-3: General schematic for operation of humidifier.

The hot wet stream entering the humidifier from the outlet of the cathode of the fuel cell

will not have exactly the same volumetric flow rate as that which enters the humidifier on the cool dry side, since oxygen is consumed and water is generated within the fuel cell. In the humidifier, hot and humidified excess gases exiting the fuel cell flow along one side of the membrane while cool, dry reactants flow into the fuel cell along the other side of the membrane. The vapour pressure and temperature differences across the membrane act as the driving forces for water and heat flux. Numerous patents describe this type of humidifier (Barton et al., 2001; Voss et al., 2002; Mossman, 2005).

4.2 Background for Design Process

In contrast to flows in circular tubes and parallel plates, the analysis of fluid flow in rectangular, square, and trapezoidal ducts requires two-dimensional analysis. There are no generalized solutions for the velocity, temperature, and concentration boundary layers along the channels. Moreover, if heat and mass transfer are included in the problem formulations, the approximations to these profiles require sophisticated numerical methods that are computationally demanding. Often flows in the humidifier unit will contain saturated reactant streams as well as condensed or condensing water, this two phase flow further complicates computations. As a result, the optimization of new humidifier topologies has relied on a balance between empirical design experiments, and simplified, predictive models that incorporate these results.

4.2.1 General Considerations

The design of planar gas to gas humidifiers involves optimizing the channel geometry and selecting the appropriate membrane materials. These factors must maximize water and heat transfer while simultaneously complying with practical design constraints such as minimal pressure drop, minimal volume, and low cost. The performance of the humidifier can be described in terms of the water transported from the wet stream to the dry stream, or similarly the output dew point temperature of the dry stream. Desirable performance occurs when the water transport rate is maximized or, conversely, when the dew point of the exiting dry stream approaches that of the incoming wet stream. In this work the performance was described by a water recovery ratio expressed as a percentage,

$$WRR = \frac{\omega_2 - \omega_1}{\omega_3} \times 100 \qquad [4\text{-}1]$$

In which ω is the humidity ratio in the gas,

$$\omega = \frac{M_w}{M_a} \cdot \frac{P_w}{P - P_w} \qquad [4\text{-}2]$$

These parameters are used to provide a simple comparison metric of the performance of various humidifiers.

The general schematic for transport in the exchanger can be found in Figure 4-3. Where ω_2 refers to the humidity ratio at the dry stream outlet (stream 2), ω_1 the humidity ratio at the dry stream inlet (stream 1), and ω_3 the humidity ratio at the wet stream inlet (stream 3). The water recovery ratio compares the amount of water that has been transferred to the dry stream in the humidifier to the amount of water that was provided to the humidifier in the wet stream. The gas entering at stream 1 is generally ambient and has little water content, and in the experiments completed for this work the air supply was pre-dried, so ω_1 was zero. In this work, wet gas entering at stream 3 was saturated with water to 55°C, 65°C, or 75°C. Consequently, the range of experimental values for ω_3 was between 0.11 and 0.39. In fuel cell systems, stream 3 will be exiting the fuel cell as exhaust. This gas stream will likely be saturated with water at the fuel cell operating temperature and will often contain some condensed water droplets. As the dry, low temperature air in stream 1 passes through the humidifier to point 2, it will gain moisture content and heat; ω_2 will indicate how much moisture the humidifier has transferred.

4.2.2 Development of the Dimensionless Parameter

It is desirable to have a design equation by which proper humidifier design can be ensured. Full humidifier membrane hydration (at steady state) is assumed since the fuel cell exhaust generally contains some liquid water and further condensation will occur in the humidifier, also the membrane used is hydrophilic. Laminar flow is assumed since the Reynolds number (Re) for all experimental flows presented here was smaller than 500. Using these assumptions, the performance of a heat and moisture exchanger can be described by defining a ratio of residence to diffusion time within the humidifier channels (Voss et al., 2002). As described in US Patent 6,416,895, the optimal performance regime of the exchanger can be achieved by ensuring that the residence time of a parcel of gas passing through the humidifier channels is greater than the diffusion time of water from the

membrane surface into the channels.

4.2.2.1 Residence Time

The patent considers the residence time of water molecules in the flow channel, and the time required for the molecules to diffuse (through air) over the depth of the channel. A channel is defined by dimensions *w*, *l*, and *d* as shown in Figure 4-2. The residence time in the channel can be calculated from knowledge of this geometry and the flow rate of gas to the humidifier.

$$\tau = \frac{mnLwd}{2Q} \qquad [4\text{-}3]$$

In equation 4-3, *n* is the number of channels per plate and *Q* is the volumetric flow rate to the humidifier. The number of plates in the humidifier, *m*, is used since the plates must be stacked to create the humidifier, as the plates are stacked, one plate will create a set of 'dry side' channels and the next will create a set of 'wet side' channels. So for a humidifier of eight plates, there will be four sets of 'dry channels' and four sets of 'wet channels'. The full flow, *Q* will pass through only half of the total number of plates per pass, so the equation must be divided by two.

4.2.2.2 The Diffusion Time

The diffusion time for a hypothetical water molecule in the chamber has been calculated in the aforementioned patents as a ratio involving the channel depth and D_{WA}, the diffusion coefficient of water in air at the average temperature across the humidifier channel (Barton et al., 2001; Voss et al., 2002; Mossman, 2005).

$$\tau_D = \frac{d^2}{D_{WA}} \qquad [4\text{-}4]$$

Equation 4-4 is derived from the solution for one dimensional transient diffusion in a semi-infinite medium. Beginning with Fick's Second Law of diffusion, in this case for water in air;

$$\frac{\partial c}{\partial t} = D_{WA}\frac{\partial^2 c}{\partial y^2} \qquad [4\text{-}5]$$

In this equation, *c* is the concentration of water, D_{WA} is the diffusion coefficient of water in air, *t* is time, and *y* is the position into the channel from the membrane surface. This equation is integrated from time zero to time *t* and from the membrane surface a distance of *y* into the channel, giving the following equaiton (Incropera and DeWitt, 2002).

$$\frac{c(y,t)-c(y,0)}{c(0,0)-c(y,0)} = erfc\left(\frac{y}{\sqrt{4D_{WA}t}}\right) \qquad [4\text{-}6]$$

The 'dry side' humidifier channel in Figure 4-2 is bounded by water saturated membrane surfaces on the top and bottom, and has a channel depth, *d*. Since water is diffusing from these two opposing surfaces into the channel, it will be of interest to know the diffusion time from the membrane surface in the center of the channel. With two surfaces contributing the air in the channel will be approaching the surface concentration at this point. Naturally this is a gross over-simplification of the phenomenon occurring in the channel, however it acts as a decent measure for basic humidifier design, as demonstrated in the following sections.

Applying boundary conditions of:

$$c(y,t) = \frac{1}{2}c_{surface} \qquad c(y,0) = 0 \qquad y = d \qquad [4\text{-}7]$$

Equation 4-6 reduces to;

$$0.5 = erfc\left(\frac{d}{\sqrt{4D_{WA}t}}\right) \qquad [4\text{-}8]$$

The complementary error function can be approximated to equal 0.5 at erfc(0.5) (Edwards et al., 1979);

$$\frac{d}{\sqrt{4D_{WA}t}} = 0.5 \qquad [4\text{-}9]$$

Solving equation 4-9 for time, *t* leads to equation 4-4, where $t = \tau_D$.

4.2.2.3 The 'R-Value'

The authors of the aforementioned patents have described empirical correlations between the maximum water flux across and the humidifier geometry as a dimensionless parameter, *R*, defined as the ratio of residence time to channel diffusion time:

$$R = \frac{\tau}{\tau_D} = \frac{mnlwD_{WA}}{2Qd} \qquad [4\text{-}10]$$

According to the previous studies, the best humidifier performance was obtained for R-values between 0.75 and 3. Despite the serious limitations in this simplified model, this parameter (R) can be an effective indicator of overall humidifier efficiency. In this study the usefulness of this parameter was examined for humidifier plates of different channel depths, and at varying operating temperatures and flow rates. Recommendations for a humidifier design procedure will then be presented utilizing the R-value.

4.3 Experimental

4.3.1 Prototype Humidifiers

A rapid prototyping machine was used to create three sets of eight humidifier plates with varying channel geometries, these plates were similar to the sample drawing of a plate shown in Figure 4-1. Half of the eight plates are mirrored, so when stacked four plates will comprise the 'wet side' of the humidifier, and four plates will comprise the 'dry side' of the humidifier. The parameter changed between each of these sets of plates was the channel depth, while length and width were held constant. Three humidifiers were assembled from these plate sets, the plate geometries are listed as humidifiers A, B, and C in Table 4-1.

The humidifier plate sets were created using a Stratasys Fused Deposition Modeling (FDM) Titan rapid prototyping machine. The humidifier plates were designed in using SolidWorks 2005 computer aided design (CAD) software. The CAD files were then pre-processed using the Insight software provided by Stratasys. This ensured that the extrusion paths for rapid prototyping were optimized. The Insight files were the loaded to the Stratasys FDM Titan rapid prototyping machine for prototyping. Each plate set was created with ABS plastic. FDM created the humidifier plate sets by depositing ABS in

layers following the extrusion path created using the Insight software.

For further comparison, two commercial gas to gas membrane humidification units from DPoint Technologies were obtained and tested. As well, a single membrane testing module was used for comparison. The dimensions of these units are listed as humidifiers D, E, and F in Table 4-1.

Table 4-1: Geometries for various humidifiers tested.

Humidifier	Number of Plates, *m*	Number of Wet and Dry Sides	Number of Channels per Plate, *n*	Channel Width, *w* (mm)	Channel Depth, *d* (mm)	Channel Length, *l* (mm)
A	8	4	20	3.0	1.0	255
B	8	4	20	3.0	1.4	255
C	8	4	20	3.0	2.0	255
D	2	1	7	3.0	1.0	160
E	50	25	20	3.0	1.6	255
F	50	25	7	3.0	1.1	125

4.3.2 Humidifier Testing Procedures

The humidifier stacks were assembled, and sealed to ensure no external or crossover leaks were present. A test stand with the appropriate control of air stream temperature, humidity, and flow was utilized to test the performance of the humidifier stacks. Air was supplied on one side of the plates completely dry and at room temperature, at a given set of flow rates, at position 1 in Figure 4-3. Simultaneously; air that had been heated and saturated to 100% relative humidity at 55, 65, and 75^{o}C was supplied on the side of the plates at the same set of flow rates at position 3 in Figure 4-3. At position 2 in Figure 4-3, the dry bulb and wet bulb temperatures were measured using thermocouples. From these values the mass balance over the humidifier was used to determine the overall water and heat transport performance of the humidifiers.

The test station provided air to the humidifier at position 1 pre-dried at a controlled flow rate, and ambient temperature. Air supplied at position 3 was passed through a bubbler

humidifier consisting of a sparger in a sealed water column to heat and saturate the gas stream to the desired temperature. A heated line from the bubbler to the prototype humidifier maintained the gas stream at the desired temperature. The test station employed data acquisition software which tracked the flow rates and temperatures of the gas streams entering and exiting the prototype humidifiers. Humidifiers were run at given flows and temperatures until steady state operation was achieved, at this point data was recorded in 15 second intervals for ten minutes at steady state. Temperature data under steady state operation was averaged over the operating time for data analysis.

4.4 Results and Discussion

4.4.1 Residence Time

From equation 4-3 it can be seen that decreasing the gas flow to the humidifier will increase the residence time of the gas in the humidifier, this decreases the velocity of gas passing over the membrane in the channels. Increasing the residence time of gas in the humidifier will lead to greater time for moisture and heat to transfer to the dry stream. This increased transport time will lead to increased performance as indicated by the water recovery ratio experimentally. The effect of residence time on the water recovery ratio is shown in Figure 4-4.

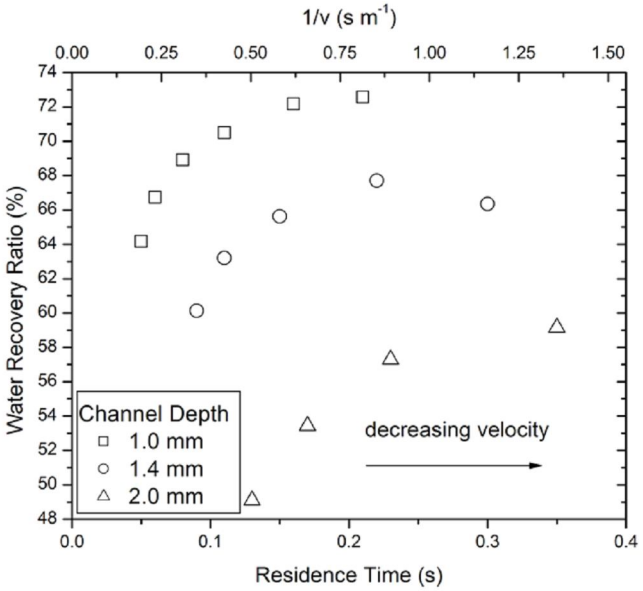

Figure 4-4: Humidifier performance as a function of residence time, values for three plate sets with different channel depths (1.0, 1.4, and 2.0 mm), at stream 3 temperature and

dew point of 75°C, flow rates from 10 to 60 SLPM.

It can be seen that increasing the residence time by decreasing the supply gas flow has a great effect on the water recovery ratio at low residence times. However, as the flow is further decreased, the positive effect of increasing residence time diminishes and little increase in water recovery is gained by greater increases in residence time. In designing the humidifier it will be desirable to have a higher residence time, so the velocity in the humidifier channels should be low, and the channel length should be long. However increasing the residence time in the humidifier demonstrates diminishing returns past a certain point. This means that it is important to design the humidifier so that the channels are long enough that a sufficiently large residence time will be achieved at the rated flow, but not so long that optimal overall design, size and material usage is compromised.

4.4.2 Diffusion Time

From equation 4-4 it is predicted that increasing the channel depth in the humidifier will increase the diffusion time of water from the membrane surface into the center of the humidifier channel. Three different humidifiers were made with plates having channel depths, *d* of 1.0, 1.4, and 2.0 mm to determine if the diffusion time does in fact affect humidifier performance. Increases in diffusion time will lead to a decrease in humidifier performance; this is shown in Figure 4-5.

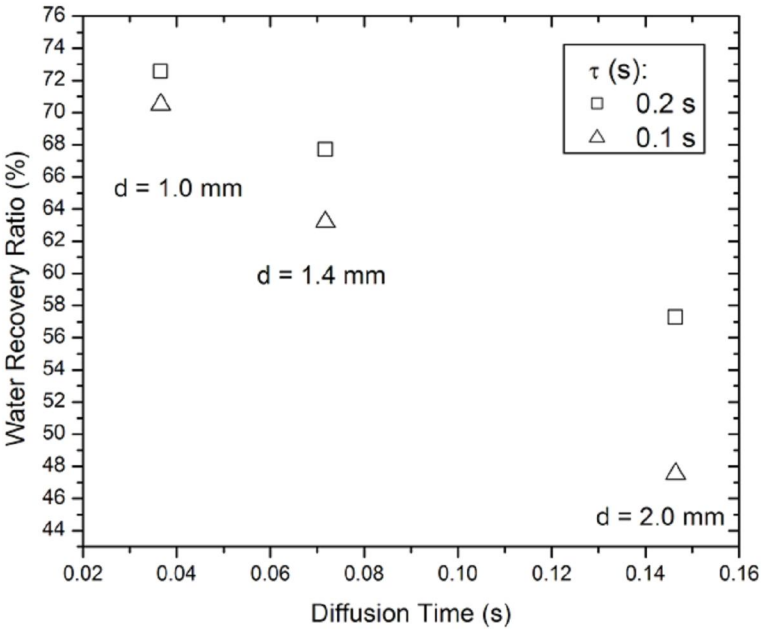

Figure 4-5: : Humidifier performance as a function of diffusion time, values for three plate sets of differing channel depths (1.0, 1.4, and 2.0 mm) at residence times of 0.1 and 0.2s, at stream 3 temperature and dew point of 75°C.

The velocities and residence times were calculated for each of the three sets of plates at different flow rates. If the channel depth had no effect on the humidifier performance then it would be expected that the three humidifiers of different channel depths would perform similarly at the same residence times. It can be seen in Figure 4-5 that this is not the case. At the same residence times the humidifiers made with plates with smaller channel depths performed much better than those with larger channel depths. These results are similar to those reported for heat exchange in fully developed laminar flow under forced convection in rectangular ducts. Such as the case for a heat exchanger in which the channel side walls are considered adiabatic while heat is transferred from the top and bottom channel walls. This case presented by Shah and London found that decreasing the aspect ratio of duct width over duct height led to a decreased Nusselt number, this would indicate decreased heat transfer for deeper channels (Shah and London, 1978). Results show the diffusion time value proposed in equation 4-4 may be a good metric for performance in a planar gas to gas humidifier. Since, increasing the diffusion time by increasing the channel depth leads to a decrease in overall humidifier performance, the channel depth in the humidifier

design should be minimized. However, smaller channel depths will lead to increased pressure drops across the humidifier unit, this must be considered in an appropriate design.

The velocity and depth data is summarized in a surface plot in Figure 4-6, for experiments completed at 65°C. Evidently decreasing depth has a strong positive effect on performance, and decreasing velocity also has a positive effect on performance.

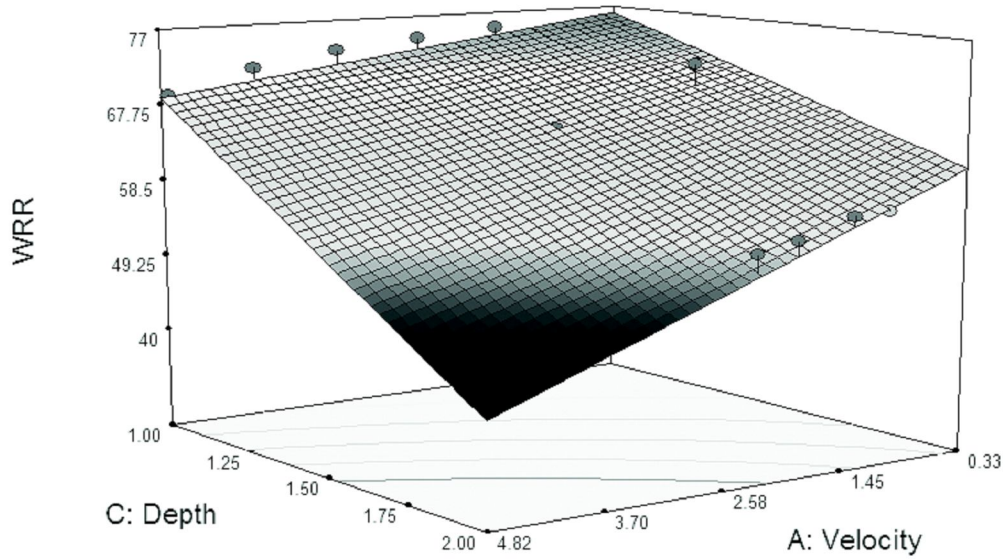

Figure 4-6: Response surface for tests completed at 65°C, showing the combined effects of velocity (m/s) and channel depth (mm) on WRR (%).

4.4.3 The 'R-Value' Parameter

The residence time and the diffusion time have differing effects on humidifier performance. Increased residence times will have a positive effect on the humidifier performance within a limited operation range. Whereas increased diffusion times in the humidifier channel will have a negative effect on the humidifier performance. Individually, the residence time and diffusion time do not offer a single parameter by which to quantify humidifier performance. The R-value parameter presented in equation 4-10 attempts to combine both of these effects into a dimensionless number that can be used for humidifier design. The water recovery ratio for each experiment was plotted

against the calculated dimensionless R number in Figure 4-7.

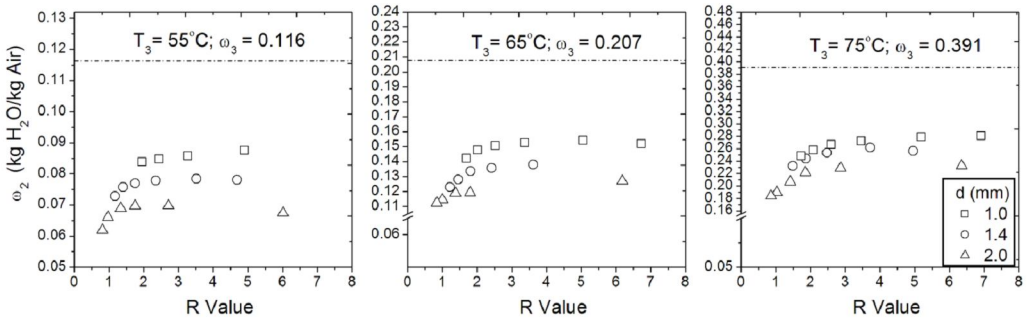

Figure 4-7: Stream 2, dry outlet humidity ratios for experiments at different R-values with three plate sets (1.0, 1.4, and 2.0 mm) at three wet inlet stream 3 dew point temperatures (55, 65, and 75°C) and various flow rates (10 to 60 SLPM).

It can be seen that the performance of the humidifier indicated by, ω_2 drops rapidly for R-values below 2.0 for any design or operating conditions. However humidifier performance tends not to increase significantly at R-values greater than 4.0. It can be noted from Figure 4-7 that increasing the wet inlet dew point temperature at stream 3 from 55°C to 75°C increases the water content in the dry outlet, stream 2. This is due to the increased heat and moisture provided to the humidifier by increasing the stream 3 temperature and dew point, which increases the driving force for water transport across the membrane. It can be seen that a well designed humidifier should have an R-value in the range of 2 to 4 to ensure that good humidifier performance will be achieved. Optimally a value of 3 should be targeted for good performance. Various humidifiers produced by DPoint Technologies with different geometries have been tested and found to show optimal performance in this range as well, the geometries of all the humidifiers created are summarized in Table 4-1 and their performance plotted against their R-values can be found in Figure 4-8.

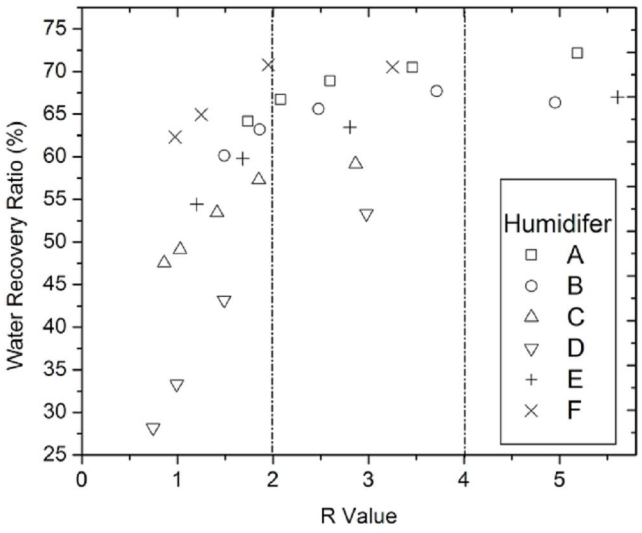

Figure 4-8: Water recovery ratios for various humidifiers (see Table 4-1) as a function of the R-value at stream 3 dew point temperature of 65^{o}C.

4.5 Gas to Gas Membrane Plate and Frame Humidifier Design Procedure

The following sections present a procedure for humidifier design based on the empirical results and the equation presented. This procedure follows the assumption that minimal packaging is desired for the humidifier to fit into the balance of plant of the fuel cell system. Minimal packaging is achieved, while ensuring good humidifier performance will be attained. This based on the humidifier channel, and external geometries, and various design considerations. A sample design is presented in the section as well.

4.5.1 Background for the Design Procedure

For a plate and frame humidifier with the basic volume dimensions as shown in Figure 4-9, and channel dimensions in Figure 4-2, the overall humidifier channel design procedure follows a series of design equations as summarized in and described below.

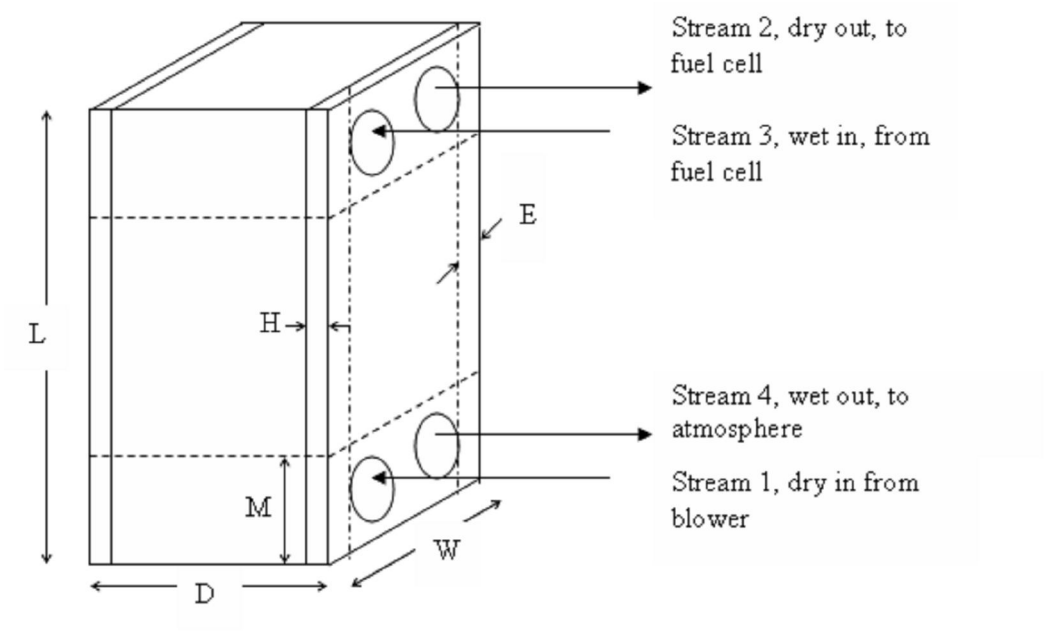

Figure 4-9: External humidifier geometry.

The humidifier should be designed according to the requirements and constraints defined by the fuel cell system. Requirements will be based on the nominal flow rate to the fuel cell, the fuel cell operating temperature, and the required input water content. The nominal flow rate to the humidifier is calculated from P_e, the rated power of the fuel cell, V_c, the rated cell voltage of individual cells in the fuel cell stack at the given operating conditions, and λ, the required air stoichiometry provided to the fuel cell (Larminie and Dicks, 2003).

$$m_{air} = \lambda \frac{P_e}{4FV_c} \frac{M_a}{x_{O_2}} \qquad [4\text{-}11]$$

This value is converted to volumetric flow, Q by dividing it by the average gas density in the channels; this value is used in equation 4-10 to design the humidifier. If less than saturated reactant conditions are required at fuel cell inlet (stream 2), then the rated flow can be decreased proportionally to the relative humidity required.

As shown in Figure 4-5 it is desirable to minimize the channel depth in the humidifier, however manufacturing restraints may prevent the creation of a humidifier with very shallow channels. Also, a decrease the channel depth will lead to an increase in the pressure drop across the humidifier and increased pressure drops will lead to increased parasitic power requirements for air supply blowers in the fuel cell system. Also the

exhaust air exiting the fuel cell and entering the wet side of the humidifier often contains condensed or condensing water, so it is important to ensure that the channel depth is not so small that channel blockage may occur due to water droplets which adhere to the channel surface. For this analysis, the minimal channel depth will be set at 1 mm.

The channel width for the humidifier is constrained by the differential pressure across the humidifier membrane, the membrane tensile strength, and creep resistance of the membrane. Increasing the channel width will increase the residence time, the membrane area, and overall humidifier performance as well as decrease the overall humidifier size. This means larger channel widths are desirable. However in the presence of increased or constant differential pressures the membrane may stretch or creep into the humidifier channel if the channel width is too large. This means that it is important to understand the membrane material properties when choosing the humidifier channel width. For this sample analysis, the maximum channel width will be set to 3 mm. The remaining variables, *l* the humidifier length, *n* the number of channels per plate, and *m* the number plates in the humidifier will depend on the packaging requirements for the humidifier in the fuel cell system. These values must be solved by an iterative approach in which packaging restraints, *L*, *W*, and *D* are met while the R-value is kept within the desired range of 2.0 to 4.0. The humidifier external geometry is outlined in Figure 4-9.

The external humidifier width, *W*, will be related to *n* the number of channels per humidifier plate, *w* the channel width, and *r* the spacer rib thickness. The spacer rib thickness will have to be sufficient to ensure that the ribs can easily line up when the humidifier plates are stacked during assembly, for this analysis the *R-value* will be set to 2.0 mm. The channel width (*w*) and the rib thickness (*r*) values are set by the aforementioned mechanical requirements, this means the external humidifier width, *W* will be governed by the number of channels chosen for each humidifier plate. If an external width is imposed on the humidifier design by the packaging requirements, then the maximum number of channels per plate will be set by,

$$n_{\max} = \frac{W_{\max} - 2E + r}{w + r} \qquad [4\text{-}12]$$

In which *E* is the required space for the outer sealing edges of the humidifier, as shown in Figure 4-9. It is important to note that the choice of overall humidifier thickness and

number of channels per plate may also depend on the manifolding and inlet and outlet header design for the humidifier

The external humidifier length, L will be a function of l, the humidifier channel length and may also be constrained by the packaging requirements for the humidifier. It will also be important to ensure that the humidifier length is sufficiently large enough to ensure a good residence time for the gases in the humidifier channel. The maximum humidifier channel length will be set by,

$$l_{\max} = L_{\max} - 2M \qquad [4\text{-}13]$$

In which M is the required space for the humidifier inlet and outlet manifolds.

Finally the external humidifier depth, D will be a function of d the channel depth, and δ the membrane thickness. The humidifier depth, D may be constrained by packaging requirements. The maximum number of humidifier plates, m_{max} will be set by,

$$m_{\max} = \frac{D_{\max} - 2H}{d + \delta} \qquad [4\text{-}14]$$

In which H is the required space on either end of the humidifier stack for the endplate as well as the inlet and outlet ports.

Another thing to consider in the humidifier design is that increasing the velocity of the gas in the channel to higher values, as seen in Figure 4-4, will rapidly decrease the performance of the humidifier. Keeping the velocity in the channel below 2 m s^{-1}, ensures that performance will be sufficient for most designs. Velocity in the channel can be calculated by:

$$v = \frac{2Q}{mnwd} \qquad [4\text{-}15]$$

Using the values for m_{max}, and n_{max} in equation 4-15 the minimum channel velocity, v_{min} can be calculated. If the minimum velocity is less than 1 m s^{-1} then the humidifier design can likely undergo further optimization, and if the minimum velocity is greater than 2 m s^{-1} then the flow may be too large and the packaging volume may be too small for the humidifier requirements. A target velocity of 1.5 m s^{-1} will be used in this design

procedure.

Equations 4-10 through 4-15 are used together to solve for the humidifier geometry based on the required flow and packaging requirements for the humidifier. Often the packaging requirement for the humidifier in the fuel cell system will cause the humidifier to be constrained in at least one of the variables *W*, *L*, or *D*. With or without packaging requirements imposed on the humidifier design, it will be desirable to minimize the overall humidifier volume. The volume will be a product of the final external depth, width, and length of the humidifier (*D*, *W*, and *L*) which can be solved by rearranging equations 4-12, 4-13, and 4-14:

$$V = DWL \qquad [4\text{-}16]$$

Since the combined channel width, *w* and rib thickness, *r* are generally larger than the combined channel depth, *d* and membrane thickness, δ the overall volume, *V* will be kept to a minimum by using the maximum number of plates and the minimum number of channels in order to achieve the R-value and velocity values imposed on equations 4-10 and 4-15. This means that in equation 4-16, D will be maximized and W and L will be minimized. However, increased values of *m*, means more humidifier plates are used in the stack, meaning longer assembly times, and an increased likelihood of assembly error, which may lead to leaks and humidifier failure. It may be prudent to consider this in the design and set an upper limit on the number of plates per stack in a feasible range. Also when designing the humidifier plates, it would be beneficial to make plates that can be used for a large number of different humidifiers so that manufacturing costs can be minimized. With one type of plate design set, humidifiers for fuel cells of many different rated powers can be created by changing the number of plates in the humidifier, *m*.

4.5.2 Using the Design Procedure, an Example

The humidifier design procedure is demonstrated in the following paragraphs, the selected variables are summarized in Table 4-2 and the overall procedure is summarized in Figure 4-10.

Table 4-2: Parameters used in the sample humidifier design presented.

Parameter	Unit	Design Note	Value for Example
P_e	W	Nominal power for fuel cell	3000
V_c	V	Nominal cell voltage for fuel cell	0.7
λ	-	Stoichiometry coefficient for fuel cell	2.0
Q	$m^3\ s^{-1}$	Calculated required flow to humidifier	2.4×10^{-3}
W	m	Packaging width for humidifier, constraint	0.140
L	m	Packaging length for humidifier, constraint	0.300
D	m	Packaging depth for humidifier, constraint	0.125
d	m	Channel depth, want to minimum allowable	0.001
w	m	Channel width, want maximum allowable	0.003
r	m	Channel rib width, want minimum allowable	0.002
E	m	Required space for sealing surface on edges of humidifier	0.005
M	m	Required space for manifolds on top and bottom of humidifier stack	0.025
H	m	Required space for endplates on humidifier stack	0.025
δ	m	Membrane thickness	2×10^{-4}
n_{max}	-	Maximum number of humidifier channels per plate, output from Eq. 4-12	26
l_{max}	m	Maximum length of humidifier channel, output from Eq. 4-13	0.25
m_{max}	m	Maximum number of humidifier plates, output from Eq. 4-14	62
R_{max}	-	Output from Eq. 4-10, with max values	8.4
v_{min}	$m\ s^{-1}$	Output from Eq. 4-15, with max values	0.96
V_{max}	L	Maximum packaging volume	5.25
R		Set as target value	3.0
v	$m\ s^{-1}$	Set as target value	1.5
m	-	Value for volume minimizing procedure	62
n	-	Value output from Eq. 4-15 with target v	17
l	m	Value output from Eq. 4-10 with target R	0.140
V	L	Volume, minimized while keeping v and R in desired ranges	2.20

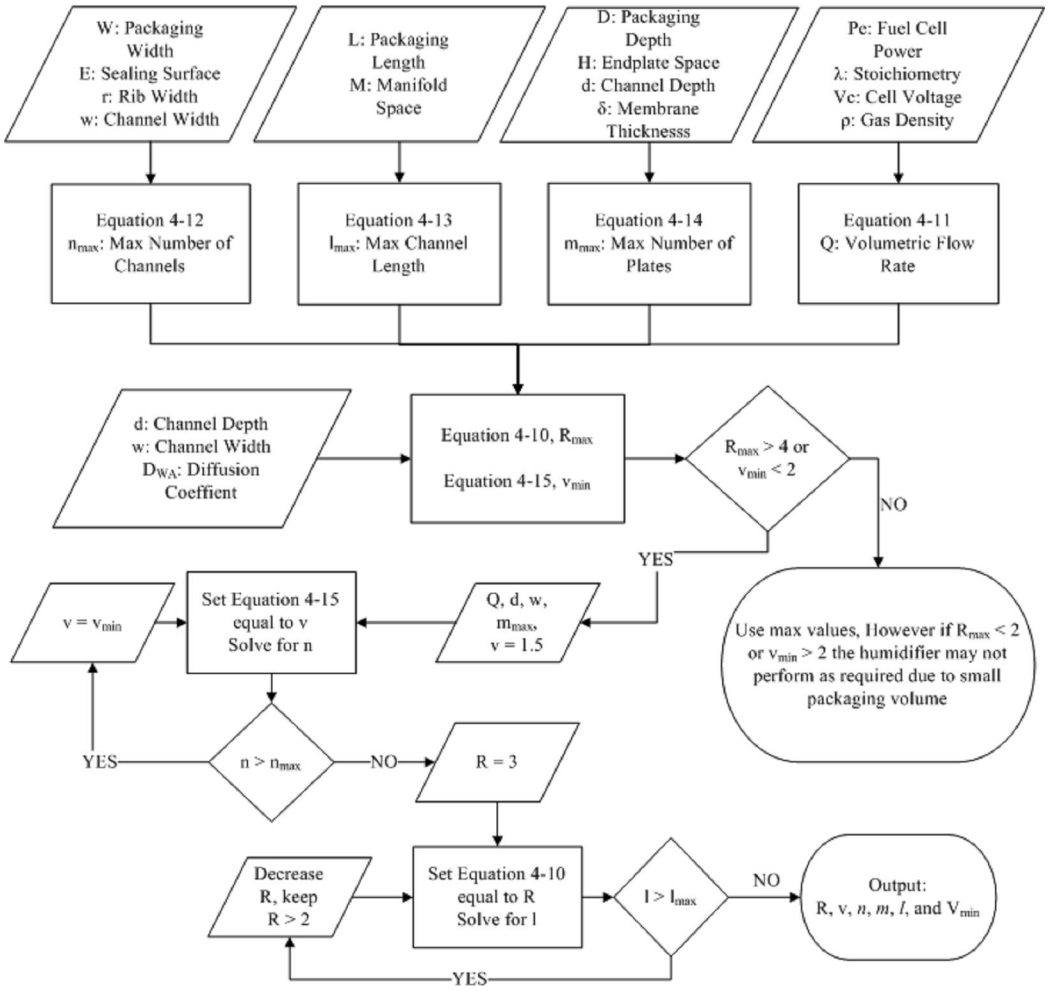

Figure 4-10: Flowchart for humidifier design procedure.

For this analysis, P_e the rated power for the fuel cell will be 3 kW, λ the air stoichiometry will be 2.0, and V_c the individual cell voltage will be 0.7 V. Using equation 4-11 the required mass flow to the humidifier is calculated to be 3.0×10^{-3} kg s^{-1} and Q the standard volumetric flow is 2.4×10^{-3} m^3 s^{-1}. The channel depth is set to an assumed minimum of 1.0 mm, and the channel width at its maximum for the selected membrane mechanical properties at 3.0 mm, and the channel rib thickness was set to 2.0 mm. The required edge thickness of the plates, E is set to 5 mm. The required space for the endplate on the humidifier stack, H is set to 25 mm and the required space for the inlet and outlet manifolds, M is set to 30mm. The membrane thickness, δ is 0.2 mm. The external humidifier length, width, and depth constraints for packaging will be assumed to be W_{max} = 140mm, L_{max} = 300mm, D_{max} = 125mm, giving a maximum packaging volume, V_{max} =

5.3 L.

Substituting the given values into equations 4-12, 4-13, and 4-14; n_{max} the maximum number of channels, l_{max} the maximum channel length, and m_{max} the maximum number of plates are calculated. For this example these values are 26 channels, a 250 mm channel length, and 62 plates respectively. These values are then entered into Eq. 4-10 and 4-15 to determine R_{max} and v_{min} for the humidifier at the maximum allowable humidifier size. If R_{max} is below 2 or v_{min} is greater than 2 m s^{-1} then the size constraints are too small to design an optimized humidifier for the rated flow under the given packaging requirements. If R_{max} is greater than 4 then the humidifier can be made smaller and can be optimized. In this case the R_{max} value is 8.3 and v_{min} is 0.96 so the humidifier can be made smaller than the maximum volume. The humidifier number of channels (n), the length of the channels (l), and the number of plates (m) can be decreased to find a combination of the three that outputs an R-value between 2 and 4, with a target of 3 in this design procedure. There will be multiple combinations of these values at which R will be 3.0. So as an added constraint the channel gas velocity will be kept between 1.0 and 2.0 m s^{-1} and the gas velocity target for this procedure will be 1.5 m s^{-1}. This leads to a volume minimizing procedure, which will ensure good humidifier performance.

Generally, the increasing the number of plates allows for the greatest increase in performance with the least increase in volume. Accordingly, the volume minimizing procedure uses the maximum number of plates, m_{max} to minimize the stack volume, and a target value of 1.5 m s^{-1} is set for the channel velocity, v to ensure good performance. This value is input into equation 4-15 and the required number of channels, n is solved. If n is greater than n_{max} at this velocity, then the velocity is increased to v_{min} and n_{max} is used in the design. The values are then input into equation 4-10, which is set to the target value of 3.0, and the channel length is solved. If the channel length required is greater than l_{max} then the R-value may be adjusted between 2.0 and 4.0 to achieve the necessary length. At this point all the humidifier dimensions are solved for the given packaging constraints and the overall volume should be minimized while still ensuring good humidifier performance.

The final design in the example had a channel length, l of 140 mm, each humidifier plate had 17 channels (n), and there were 62 plates in the humidifier (m). At these set points R was 3.0, and v was 1.5 m s^{-1}, so it will be known that the designed humidifier will perform

well. The final humidifier volume was 2.2 L.

It is important to point out that there are limitations to this approach. The overall design equations used for the R-values calculated are not rigorous, and do not account the actual amount of water transported in the humidifier unit. As well, the procedure depends on empirical observations of the optimal velocity and R-value performance ranges for humidifiers based on relatively straight channels. Nonetheless, the presented R-value approach has shown to provide a good basis for humidifier design as shown in Figure 4-8. Also, the assumptions made may not be valid for a broad range of pressure and relative humidity conditions, and may be dependent on the membrane material used for the humidifier. Appropriate membrane selection will also be of great importance to the humidifier design (and is the subject of ongoing work); the R-value approach presented here only considers the geometrical considerations involved in the humidifier design. Unusual humidifier channel geometry and manifolding may limit the accuracy of this approach.

4.6 Conclusions

Prototype humidifiers were created to determine the validity of the R-value as a dimensionless parameter for humidifier design. The R-value is a combination of the residence time and the diffusion time of water molecules in the humidifier channels. Increasing the residence time of water molecules in the humidifier channels was found to increase the humidifier performance. However greater increases in the residence time past a certain point tend to demonstrate diminishing returns in humidifier performance. Increasing the diffusion time of water from the surface of the membrane into the channel leads to a decrease in the overall humidifier performance. Combining these effects, the optimal R-value range for good planar gas to gas membrane humidifier design was found to be between 2.0 and 4.0, in which the optimal value is near 3.0 Future works should focus on developing parameters for humidifier design based on a more fundamental analysis. As well design approaches using various types of membrane materials should be considered. The ideal R-value volume minimizing design algorithm was presented demonstrating a humidifier design procedure based on geometrical constraints for packaging the humidifier in the fuel cell system. This procedure can be used as a starting point for humidifier design.

Chapter 5

5.0 Membrane Evaluation Results and Discussion

5.1 Water Permeation Testing

5.1.1 Static Water Vapour Permeation Testing

Static water permeation tests were completed as described in Section 2.1.1. These tests were completed as an initial test of some membrane materials. However, evidence from these tests indicated that dynamic water permeation testing would provide a better metric by which to compare membrane materials for this application. Accordingly, static permeation testing was discontinued.

5.1.1.1 Results

Some initial results of static water permeation testing are presented in Figure 5-1.

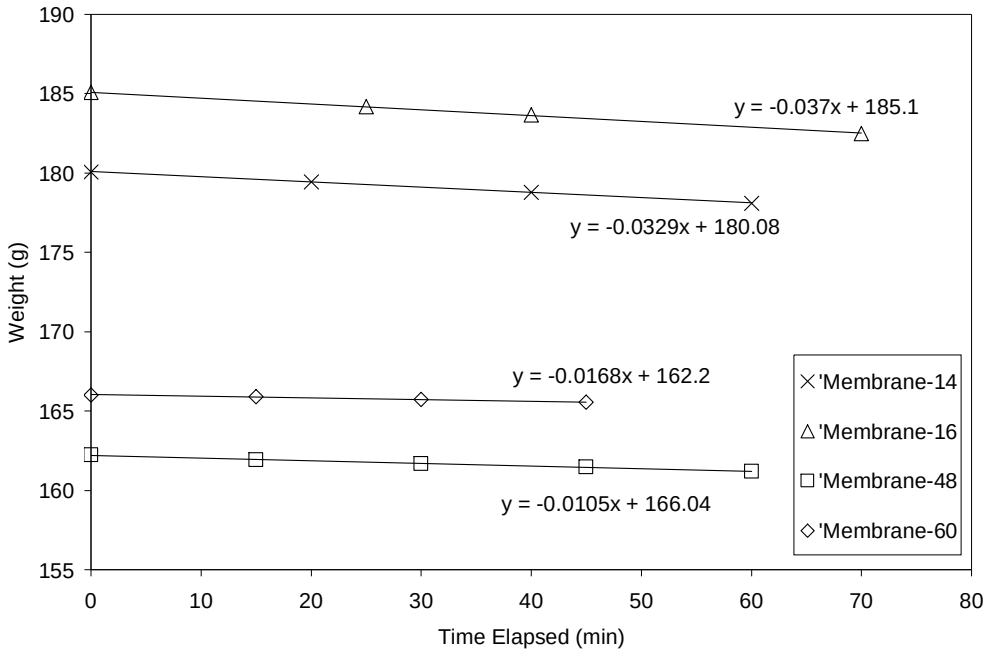

Figure 5-1: Static water permeation tests for four membranes at 80^{o}C.

The static cup tests for the data presented in Figure 5-1 were completed in an oven at

80°C. The linear regression of the data was completed, and the slope of the line for each data series was calculated. Evidently the linear fit was strong for all tests, with R^2 value exceeding 99%. The slope generated from each test was indicative of the water permeation rate of the membrane for that experiment.

Similar experiments were completed at room temperature conditions for some membrane materials. The results of these experiments are presented in Figure 5-2. The data fit the linear regression well, with R^2 values exceeding 99%.

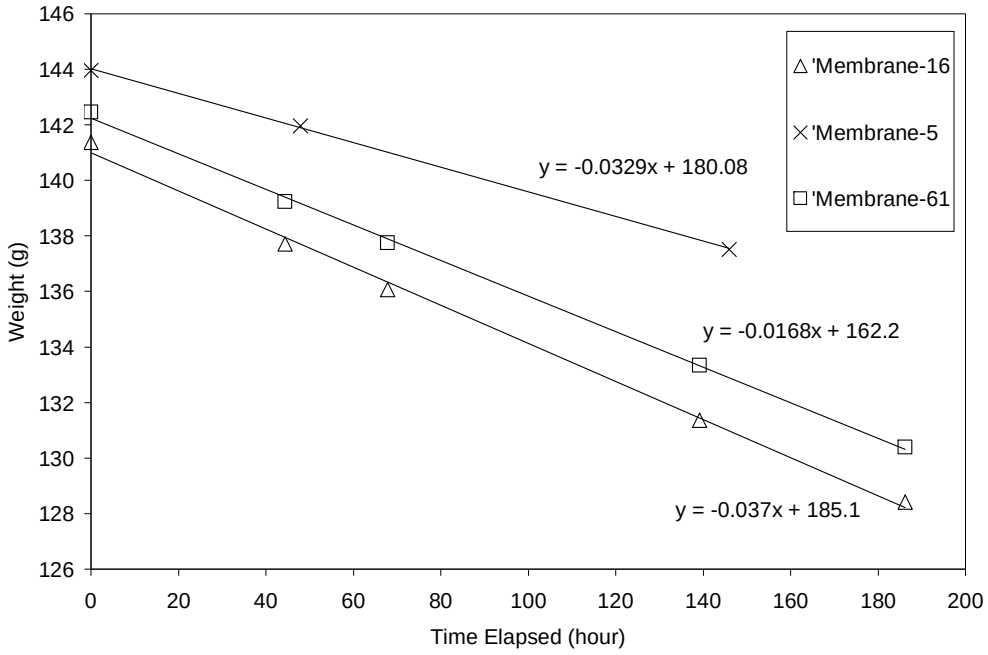

Figure 5-2: Static water permeation tests for four membranes at 22°C.

A summary of the static water permeation experiments can be found in Table 5-1.

Table 5-1: Static water permeation test results from various membrane tests.

Membrane	Trials	External Temperature (^oC)	Average Water Flow ($g\ h^{-1}$)	Average Water Flux ($kg\ h^{-1}\ m^{-2}$)	Average Water Permeation ($g\ h^{-1}\ m^{-2}\ kPa^{-1}$)
14	2	80	1.702	20.80	440.0 ± 98.6
16	2	80	2.141	26.17	553.6 ± 28.1
48	2	80	1.055	12.90	272.9 ± 17.4
60	2	80	0.672	8.21	173.8 ± 16.1
16	2	22	0.061	1.22	623.6 ± 113.0
5	1	22	0.053	1.06	543.0
61	1	22	0.054	1.09	556.2

For comparison, dynamic tests for three of the membranes shown in Figure 5-1 are presented in Figure 5-3.

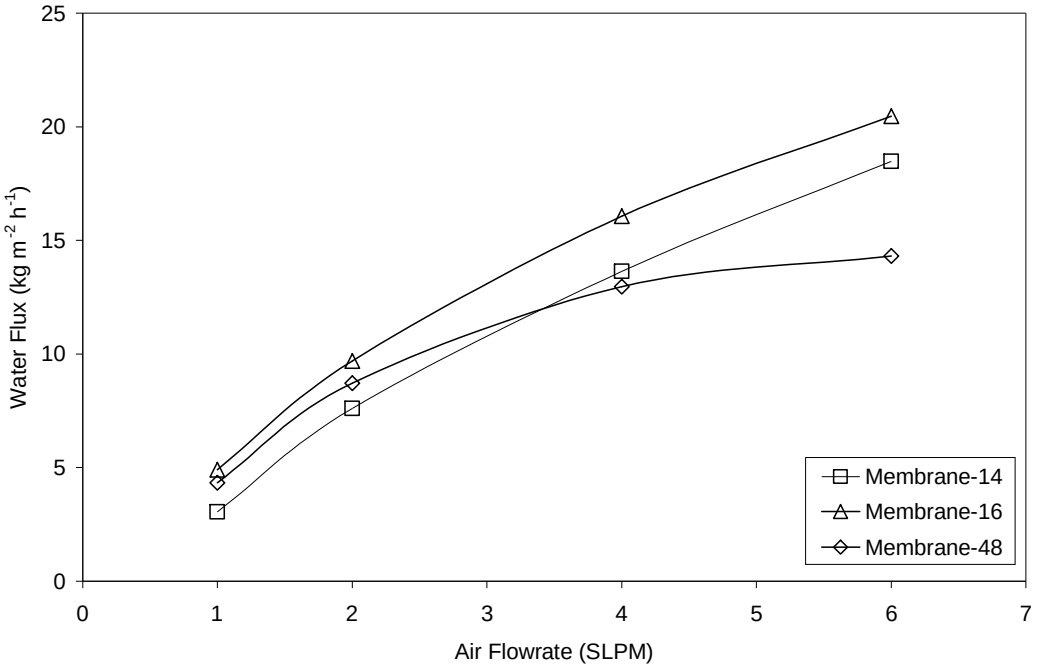

Figure 5-3: Dynamic water permeation tests for three membranes, Stream 3 inlet: 80^{o}C and 100% RH, Stream 1 inlet: 22^{o}C, 0% RH.

5.1.1.2 Discussion

From the data presented it is evident that the static water permeation test provides decent resolution for comparing membrane materials. However, as demonstrated by the standard deviations shown in for some of the samples in Table 5-1, there may be an issue with the repeatability of the tests. The static results for Membranes 14, 16, and 48 in Figure 5-3 with the results presented in Table 5-1 can be compared to show that the ranking of the membranes would be the same in dynamic test at the high end flow rate and the static tests. However, the dynamic results vary for different membrane materials at different flow rates.

Evidently, the static water permeation method allows various membranes to be compared. However, in the fuel cell humidifier, the membrane will be in contact with a flowing saturated stream of air at elevated temperatures. This leads to two problems with this water vapour transmission test. Firstly, the test does not take the convective effects of the flowing stream into consideration. Secondly, the test has to be completed at increased temperatures in order to obtain data that would be relevant to the application. However, increasing the temperature of the water will greatly increase the vapour pressure, and effective pressure on the water side of the membrane. This may lead to porous membranes demonstrating an undesirable positive bias in the test. One other issue with this test is that the gas stream in the humidifier will contain condensing droplets of water which will come into contact with the surface of the membrane. The contact of liquid water with the membrane surface will alter the method of water transport in certain membranes. These affects will not be observed in the water vapour transmission test.

From the various problems presented with the static test, and the desire to find membranes which will operate effectively in the humidifier the decision was made to use dynamic testing the quantify the water permeation of membrane materials.

5.1.2 Dynamic Water Permeation Testing

The experimental method for completing dynamic water permeation testing is presented in Section 2.1.2. Water permeation tests were the first test completed on all membranes when following the membrane selection flow chart in Figure 3-5. Membranes will water transport rates below 14 $kg/m^2/h$ were rejected, and generally no further tests were

completed on these materials. Completing the water permeation test on a membrane resulted in a plot of flow rate against water flux through the membrane. The flow rate can also be compared to the outlet dew point of stream 2, the gas stream that has been heated and humidified in the experiment. Sample results from permeation tests are shown in Figure 5-4.

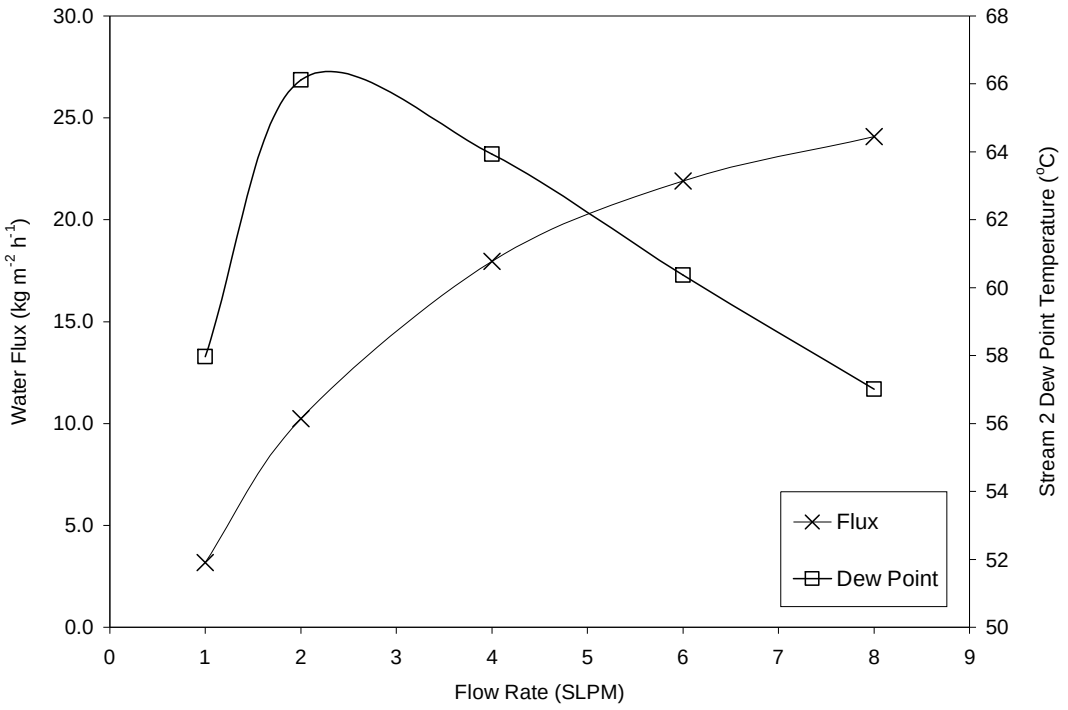

Figure 5-4: Water permeation test for Membrane 16 at S1: 23°C, 0% RH; and S3: 75°C, 100% RH, membrane area = 33.24 cm^2

The water flux refers to the amount of water being transported through the membrane from the hot and wet gas (Stream 3) to the cool dry gas (Stream 1). This value is recorded at the dry side exhaust (Stream 2) where the gas stream would be entering the humidifier. It is desirable achieve the greatest water content available in Stream 2. Similarly, maintaining a high dew point temperature at Stream 2 is required. Figure 5-4 demonstrates that although increasing the flow increases the water flux, it does so at the expense of the dry stream outlet dew point above 2 SLPM in the water permeation test module. This is part of the optimization problem that was discussed in Chapter 5, that there is an optimal flow range for the channel geometry. As the flow increases, the amount of water available to transport to the gas stream becomes membrane limited. This causes the dew point to decrease at higher flow rates, even though the actual amount of water transported

increases. Normalizing by the velocity of the gas in the channel as shown in Figure 5-5, demonstrates a similar trend as the dew point graph. From an efficiency stand point, it is best to present the data in this manner. However, for comparing the transport of different membranes in the same module, it is easiest to use the water flux against flow rate convention.

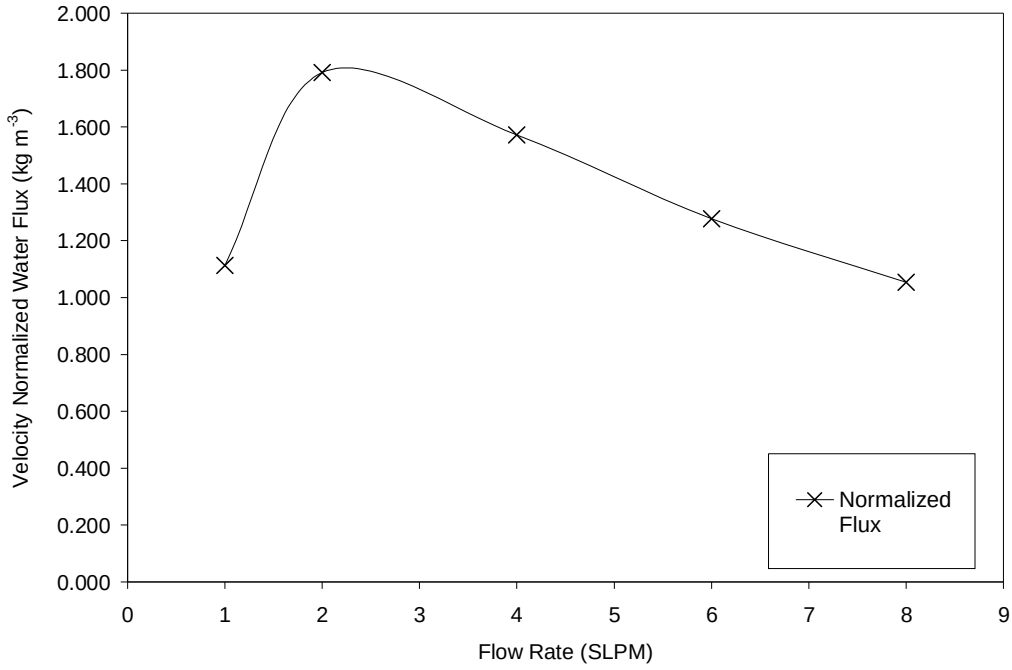

Figure 5-5: Velocity normalized flux of water through membrane 16, in the water permeation test module S1: 23°C, 0% RH; and S3: 75°C, 100% RH, membrane area = 33.24 cm^2

In addition, better resolution between membranes occurs at flow rate above 2 SLPM in the test module, as shown in Figure 5-6. Comparing membranes at an increased flow rate allows greater certainty in stating differences between membranes; this also ensures that the module is operating in the membrane limited flux regime. Membranes were tested from 1 to 8 SLPM, but were generally compared at 4 or 6 SLPM. For membrane selection, the minimum acceptable flux was set as 14 $kg/m^2/h$ at 6 SLPM at stream 1 conditions of 23°C and 0% RH, and stream 3 conditions of 75°C and 100% RH, as tested in the standard water permeation test module. The overall results for all membranes tested are summarized in Figure 5-7. The water permeation narrowed the selection of membranes by nearly 30%, from 62 down to 45 membranes.

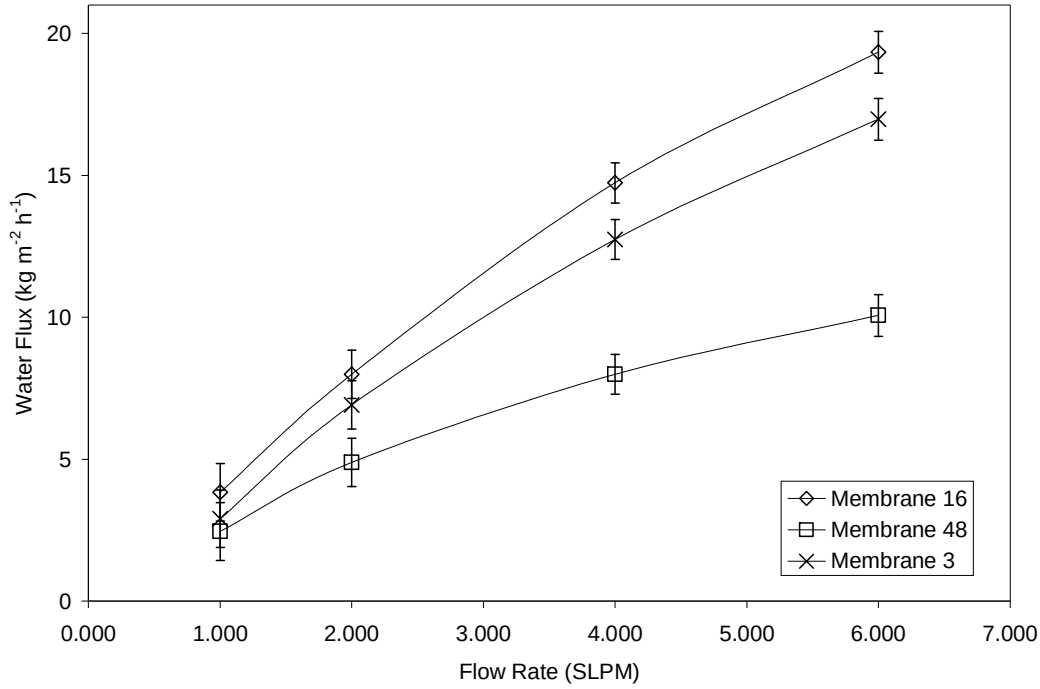

Figure 5-6: Comparison of three membranes, demonstrating the increase in resolution at higher flow rates in water permeation module, at conditions S1: 23°C, 0% RH; and S3: 75°C, 100% RH, membrane area = 33.24 cm^2.

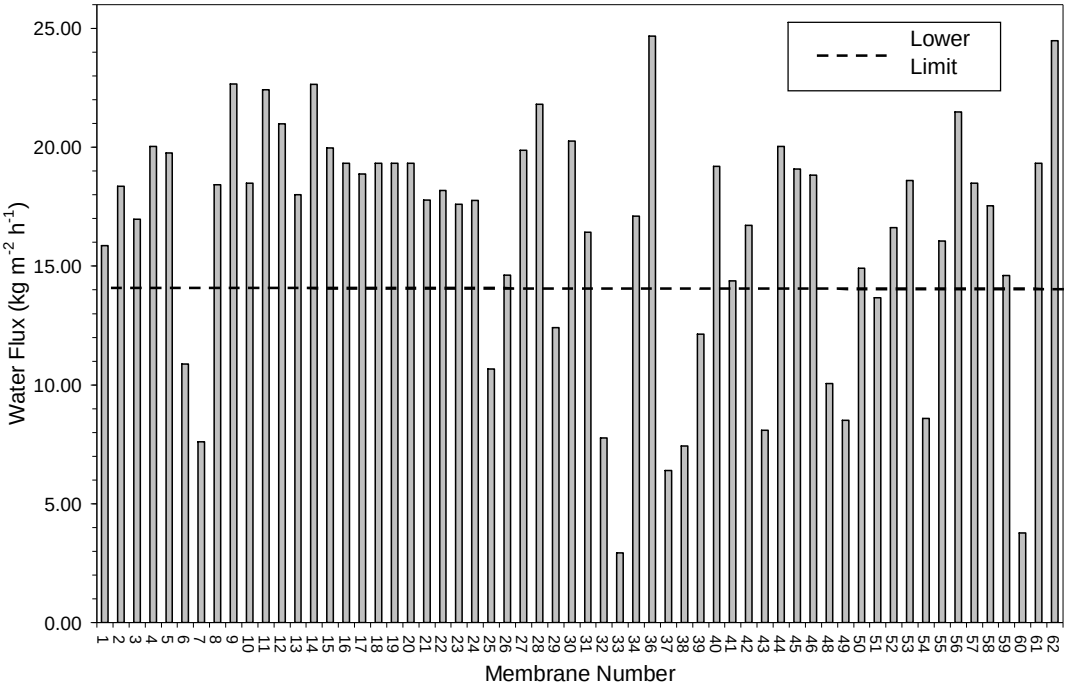

Figure 5-7: Membrane water flux values at 6 SLPM in water permeation module at conditions S1: 23°C, 0% RH; and S3: 75°C, 100% RH, membrane area = 33.24 cm^2.

5.2 Air Permeation Testing

Membranes which passed the water transport test, we then tested for dry and wet air crossover. Sample permeation curves are shown in Figure 5-8. The plots show a linear tend which is expected for porous materials, increasing the air pressure applied will increase the flow through the membrane. Membranes were tested both in the dry and wet state. When wet, the pores in hydrophilic porous materials will be filled with water, this will act as a barrier to convective gas crossover, as demonstrated by membrane 16 in Figure 5-9. The membrane when wet demonstrates no gas crossover at the pressures to which it was subjected. Membranes with larger pore sizes have lower bubble points, and will begin to allow the passage of gas in the wet state at lower pressures. This phenomena is demonstrated by membrane 5 in Figure 5-9, where in the dry state the crossover is higher than in the wet state, but at 10 kPa water is forced from some of the larger pores leading to gas crossover. Smaller pores are still filled and the surface tension of water in these pores resists the flow of gas through the membrane, causing the wet permeation rate to be lower than in the dry state.

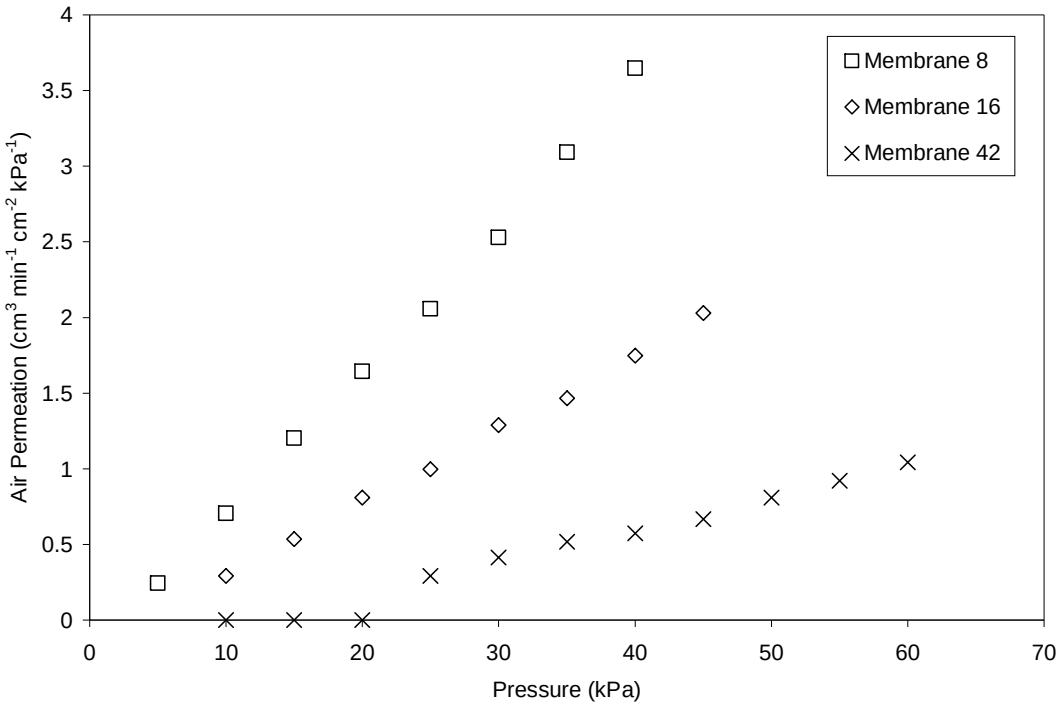

Figure 5-8: Air permeation plots for three membranes.

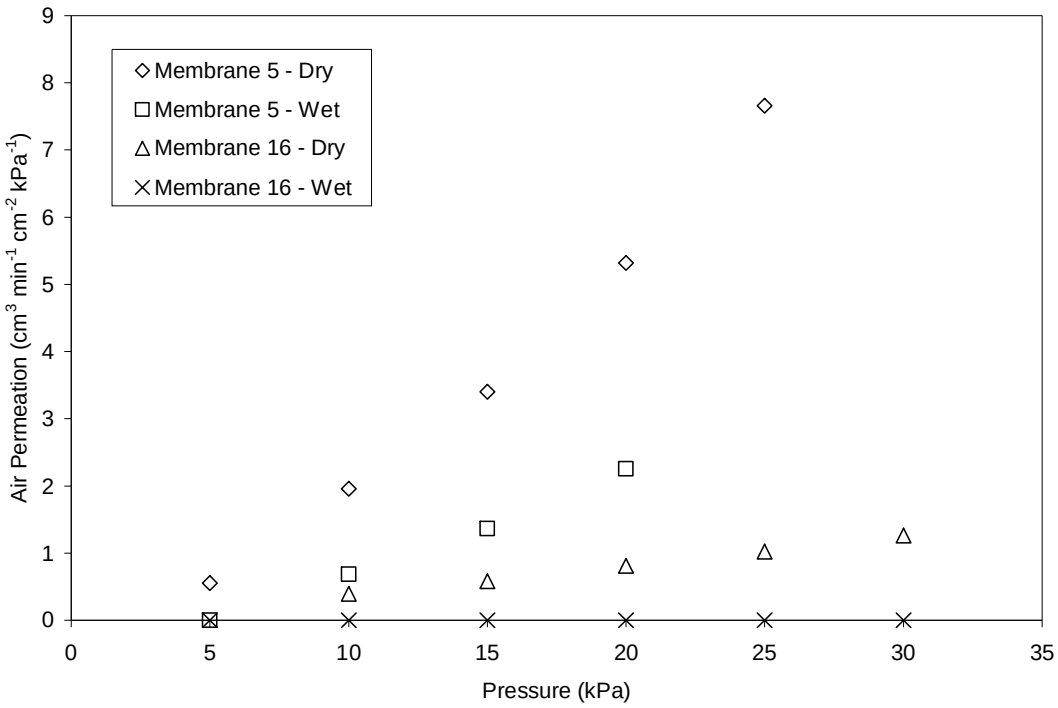

Figure 5-9: Wet and dry air permeation for two membranes.

The membranes which passed the water transport test were tested for wet and dry air permeation and values were recorded at 21 kPa differential pressure. The dry air crossover results are shown in Figure 5-10. Membranes that demonstrated dry air permeation rates greater than 3 cm^3 min^{-1} cm^{-2} kPa^{-1} at 21 kPa were rejected. Membranes that demonstrated any wet permeation were also rejected. This test eliminated 14 out of the 45 remaining membranes. Membranes which passed the water transport and air permeation tests were considered for durability testing.

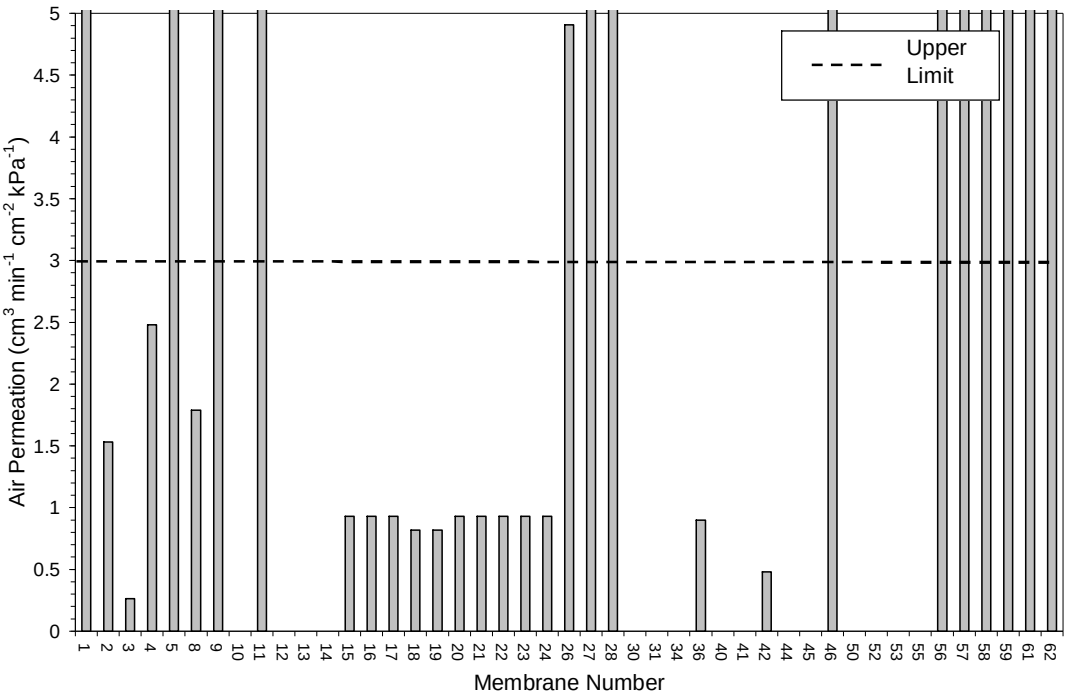

Figure 5-10: Dry air permeation for membranes at 21 kPa, module area = 5 cm^2.

5.3 Mechanical Strength Testing

Initially tests of the elastic modulus and yield strength were completed on al materials. However, this test was not completed on all materials, as most membranes which were mechanically weak could be eliminated by testing burst pressure in the air permeation test. Membranes which did not burst at 50 kPa differential pressure were of sufficient strength for use in the humidifier.

Membranes of interest were tested using a Minimat™ materials tester. The elastic modulus and yield strength were analyzed to compare different membranes, as well as the effects of temperature, moisture, and age on the materials. Some specific tests of interest are summarized in the following sections.

5.3.1 Statistical Methods

From experience completing tensile tests on membrane materials, it is known that sample standard deviations are rather large in these types of experiments. In order to compare the mean tensile strength of two membrane materials, hypothesis testing using a student t-test

was completed as described in standard statistical textbooks (Montgomery, 2005). The null hypothesis chosen was the true mean tensile moduli of two given materials were equal at 90, 95, and 99% significance levels. The alternate hypothesis was that the true mean tensile moduli of the two materials were statistically different at 90, 95, and 99% significance levels. A rejection of the null hypothesis indicated that one membrane has a tensile modulus which is statistically greater than the other at a given significance level. Accepting the null hypothesis indicates that the two membranes do not demonstrate statistically significant differences in tensile modulus at a given significance level. The hypothesis test is outlined in Equation 5-1.

$$H_0 : \bar{\mu}_{membrane1} - \bar{\mu}_{membrane2} = 0 \qquad H_1 : \bar{\mu}_{membrane1} - \bar{\mu}_{membrane2} \neq 0 \qquad [5\text{-}1]$$

The hypothesis was tested by finding the mean tensile strength and standard deviation of each membrane from equations and 5-2 and 5-3.

$$\bar{x}_{membrane} = \frac{1}{n}\sum_{i=1}^{n} x_i = \frac{1}{n}\left(x_1 + \cdots + x_n\right) \qquad [5\text{-}2]$$

$$s_{membrane} = \sqrt{\frac{1}{n-1}\sum_{i=1}^{n}\left(x_i - \bar{x}\right)^2} \qquad [5\text{-}3]$$

The difference in the sample means (M_d) and the estimated standard error of the difference in means (s_{Md}) are calculated using equations 5-4 and 5-5 respectively.

$$M_d = \bar{x}_{membrane1} - \bar{x}_{membrane2} \qquad [5\text{-}4]$$

$$s_{Md} = \sqrt{\frac{2MSE}{n}} \qquad [5\text{-}5]$$

In which n is the sample size, in this case it was five and mean squared error (MSE) is calculated using equation 5-6.

$$MSE = \frac{s^2_{membrane1} + s^2_{membrane2}}{2} \qquad [5\text{-}6]$$

The t-test is completed by using equation 5-7.

$$t_{obs} = \frac{M_d - (\bar{\mu}_{membrane1} - \bar{\mu}_{membrane2})}{s_{Md}} \quad [5\text{-}7]$$

In which the difference in true means was set by the hypothesis to equal zero. Once the observed t-value was determined it was compared to the critical t-value (t_{crit}) which was found from a t-table. The critical t-value was determined using the degrees of freedom for the MSE (equation 5-8) and the desired significance level; 0.01, 0.05, or 0.1, corresponding to 99, 95, and 90% confidence levels.

$$df = n_{membrane1} - 1 + n_{membrane2} - 1 \quad [5\text{-}8]$$

If t_{crit} is less than t_{obs} then it is known that the hypothesis is rejected at the chosen significance level and that the true mean tensile strengths of the membrane samples are significantly different. Alternatively, if the value for t_{obs} is less than the value for t_{crit} then the true mean tensile strengths of the two membranes are not different at the chosen level of significance. A similar test was completed for the yield strength of the materials.

5.3.2 Membranes 16 and 19

Membranes 16 and 19 were composed of similar materials, precipitated silica and UHMWPE. However membrane 16 had a silica to polyethylene (PE) ratio of 2.51, while membrane 19 had a silica to PE ratio of 3.01. Also membrane 19 had rib running the length of the material. It was of to determine if these ribs contribute to the mechanical strength of material in the channel when the membrane ribs are perpendicular to the channel flow field. The direction of force applied to the membrane is shown in Figure 5-11.

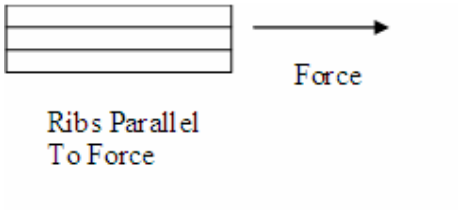

Figure 5-11: Ribbed membrane orientation in experiments.

This will be the direction of pressure forces exerted on the membrane in the humidifier. Cross-sections of the two materials are shown in Figure 5-12.

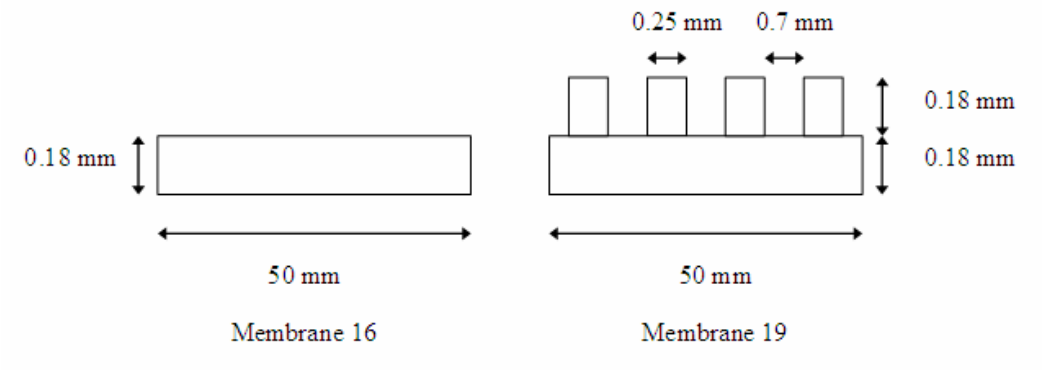

Figure 5-12: Cross sections flat and ribbed membranes, ribs are not to scale, number of rib is not to scale.

Since the extra area provided by the ribs was not accounted for in the calculation of the modulus and yield, any increase in mechanical strength will be due to the contribution of the ribs, or else the excess silica content. However it would be expected that increased silica or in other words, decreased polymer content would lead to a weaker membrane. Since the membrane with the ribs contains less polymer by weight, then any increase observed will be due to the additional rib structure. Five samples were measured for each membrane, the results are summarized in Table 5-2.

Table 5-2: Comparison of results for flat and ribbed silica/UHMWPE materials.

Value	Elastic Modulus (MPa)	Standard Deviation	Yield Strength (kPa)	Standard Deviation
Membrane 16 – Flat	279.7	51.7	3474.4	296.0
Membrane 19 - Ribbed	419.7	22.1	4244.0	145.0

Table 5-3: Statistical analysis comparing the means for yield and modulus of flat and ribbed membranes.

Value	Membrane 16 compared to Membrane 19
Difference in Modulus (%)	-33.3
Difference in Yield (%)	-18.1
Modulus t-test 99%	reject null hypothesis
Yield t-test 99%	reject null hypothesis

The results of the statistical analysis of the data are summarized in Table 5-3. The results indicate a difference in the mean elastic moduli and yield strengths of the ribbed and flat membranes at a 99% significance level. This is a strong result and the ribs contribute to a 33.3% increase in the elastic modulus of the membrane, and an 18.1% increase in the yield strength of the membrane. For higher pressure applications the ribbed membrane should be preferred over the flat sheet membrane.

5.3.3 Membranes 8 and 16

Membranes 8 and 16 are similar flat sheet UHMWPE and silica based membranes from two different companies. The compositions of the membranes are similar, except that the specifics of the processing methods, and base materials used are unknown. In order to test if the membranes have comparable mechanical properties mechanical tests were completed. The results of tests on these materials are summarized in Table 5-4. The results of the statistical analysis of the materials are shown in Table 5-5.

Table 5-4: Comparison of results for two similar flat sheet silica/UHMWPE materials.

Membrane	Elastic Modulus (MPa)	Standard Deviation	Yield Strength (kPa)	Standard Deviation
Membrane 8	216.7	36.1	2924.2	43.6
Membrane 16	279.7	51.7	3474.4	296.0

Table 5-5: Statistical analysis comparing the means for yield and modulus similar flat silica/PE materials.

Value	Membrane 16 compared to Membrane 19
Difference in Modulus (%)	29.1%
Difference in Yield (%)	18.1%
Modulus t-test 99%	accept null hypothesis
Modulus t-test 95%	accept null hypothesis
Modulus t-test 90%	reject null hypothesis
Yield t-test 99%	reject null hypothesis

The results indicate no difference in the mean elastic moduli between the materials at the

99% and 95% significance levels; however a difference is statistically significant at the 90% level. The mean yield strength of the materials is different at a 99% level of significance. These results indicate that membrane 16 has a yield strength 18.1% greater than membrane 8, and that membrane 16 may have a 29.1% greater modulus of elasticity than membrane 8. This means that caution should be taken in exchanging one material for the other in the humidifier, particularly when the humidifier will be operating with increased differential pressures across the membrane.

5.3.4 Temperature and Humidity Effect on Membrane 16

Mechanical tests on membrane 16 were completed at room temperature and 75°C, when the membrane was dry and saturated with water. The results of tests comparing the materials are summarized in Table 5-6.

Table 5-6: Comparison of mechanical tests on membrane 16 in dry and wet state, at room temperature and 75°C.

Compare	Difference in Elastic Modulus (%)	Difference in Yield Strength (%)	Confidence Level for difference in modulus means (%)	Confidence Level for difference in yield means (%)
Room temperature dry and wet	-42.3	-26.8	99	99
75°C dry and wet	-36.3	-57.5	90	99
Room temperature and 75°C dry	-43.4	-64.6	99	99
Room temperature and 75°C wet	-37.6	-79.5	95	99

The results indicate that the membrane demonstrates a decreased elastic modulus and yield strength when in the wet state. The results also indicate the modulus and yield show an inverse relationship to temperature. These results are expected, as it has been shown that increasing the temperature and moisture content of polymer materials will decrease the yield strength and elastic modulus of polymer materials (Burchill, 1989; Bartolotta et al., 1993). This is due to relaxation in the polymer chains, causing greater mobility, and lower elasticity and strength. The tensile strength of the material decreases by as much as 80% between dry, room temperature conditions, and hot, wet conditions. This results will be important to consider when selecting a membrane for a humidifier which will be operating

at elevated temperature and moisture content.

5.4 Axisymmetric Drop Shape Analysis

5.4.1 Background

Axisymmetric drop shape analysis (ADSA) was used to study the time dependent behavior of water on the surface of various membranes. By studying the time-dependant contact angles on these surfaces it was hoped that two goals could be achieved:

- To find if ADSA was a good method by which various membranes could be easily qualified for their potential as a water transport membrane in the humidifier.
- To gain an understanding of the rate of permeation of water for various membrane surfaces this could be related to the performance of the humidifier.

Five membranes were studied using this technique, they each had unique properties and are summarized in Table 5-7.

Table 5-7: Membranes studied using ADSA.

Membrane Number	Description of Membrane
16	Polyethylene membrane with hydrophilic silica additive, silica to polyethylene ratio: 2.5:1
48	Sulphonated polyetheretherketone (s-PEEK)
4	Polypropylene membrane with a hydrophilic additive
58	Porous fluoropolymer based membrane
46	Nylon intrinsically hydrophilic membrane

5.4.2 Time-Dependant Contact Angles, Drop Volumes, and Drop Radii Results

Table 5-8 summarizes the initial contact angles of the various membranes, the surface tension of the membrane, the rate of surface tension decrease as water permeates into the membrane, the rate of contact angle decrease, rate of drop volume decrease, and rate of drop radii change. Decreases in contact angle, surface tension, volume, and radii

were essentially linear with time. The initial surface liquid-solid surface tensions (γ_{LS}) of the membranes indicated the wettability of the membranes. Having lower γ_{LS} or conversely, a high solid-vapour surface tension (γ_{SV}) should mean the membrane is membrane is more wettable.

Table 5-8: Summary of ADSA Testing Results.

Membrane #	Initial Contact Angle (deg)	Initial Surface Tension of γ_{LS} / γ_{SV} (mJ m^{-2})	Rate of Surface Tension Change, γ_{LS} (mJ m^{-2} min^{-1})	Rate of Contact Angle Decrease (deg min^{-1})	Rate of Drop Volume Decrease (uL min^{-1})	Rate of Drop Radii Change (mm min^{-1})
16	101	36.1 / 22.5	-2.26	3.59	0.361	-0.0018
48	69	15.9 / 42.6	-0.78	1.79	0.216	-0.0007
4	92	30.1 / 28.2	-2.80	4.81	0.415	0.0151
58	122	48.8 / 10.8	-0.51	0.88	0.200	-0.0099
46	54	8.4 / 51.6	-158.8	626	74.5	1.154

Table 5-9 summarizes the evaporation corrected average absorptive fluxes for each of the five membranes as calculated as described in Appendix A.

Table 5-9: Average Evaporation Corrected Absorptive Fluxes and Net Absorption for the Five Membranes

Membrane #	Average Absorptive Flux (g min^{-1} cm^{-2})	Total Absorbed Weight (g)
16	0.01723	0.0128
48	0	0
4	0.0167	0.0107
58	0	0
46	4.0724	0.0299

5.4.3 Effectiveness of Using ADSA for Membrane Qualification

The results of ADSA testing varied greatly. The ability of ADSA to study water-membrane surface interaction was largely dependent on the type of membrane under study. As it can be seen in Table 5-8 and Table 5-9 the rates of change for membrane 46 were very high. Also from Table 5-9 it can be seen that the evaporation corrected

absorptive flux for membranes 48 and 58 was zero. This meant that evaporation accounted for all water lost from the drops in these experiments, and no water permeated into these membranes.

Comparing these results to the in humidifier performance of these membranes shown in Figure 5-13, it can be seen that all these membranes performed rather well in the humidifier. This was not the case in the ADSA measurements, thus it could be concluded that ADSA is not a good method for quickly qualifying membranes for the application.

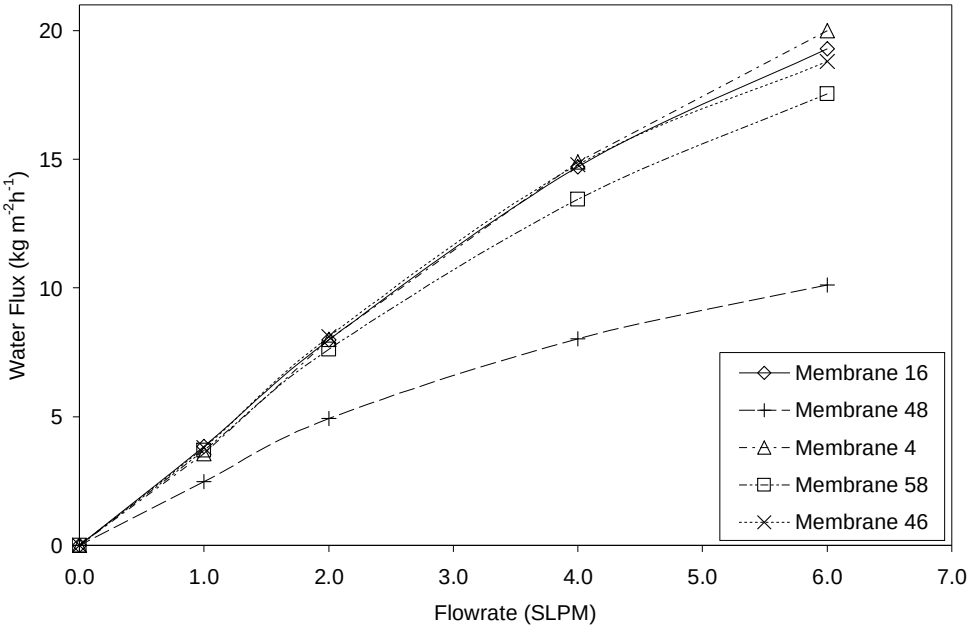

Figure 5-13: In humidifier performance for membranes tested.

5.4.4 Membrane Specific ADSA Considerations

Considering Table 5-8 and Table 5-9, it can be observed that membranes 16, 4 and 46 performed well using ADSA. On the other hand, results for membranes 48 and 58 showed poor results using ADSA. However the ADSA maybe still be useful in understanding the different transport phenomena which are occurring in the membrane. Analysis of each individual membrane follows.

5.4.4.1 Membrane 16

Membrane 16 was made of a blend of silica and polyethylene, in a ratio of 2.51:1. Polyethylene is rather impermeable to water, however the silica absorbs water quite well, which make this membrane attractive for the humidifier application.

It can be seen in Figure 5-14, that the absorptive flux decreases from the initial value and then levels off over time. This is due to the membrane under the drop becoming saturated with water, so the activity of water in the membrane approaches that of drop and the driving force for permeation decreases.

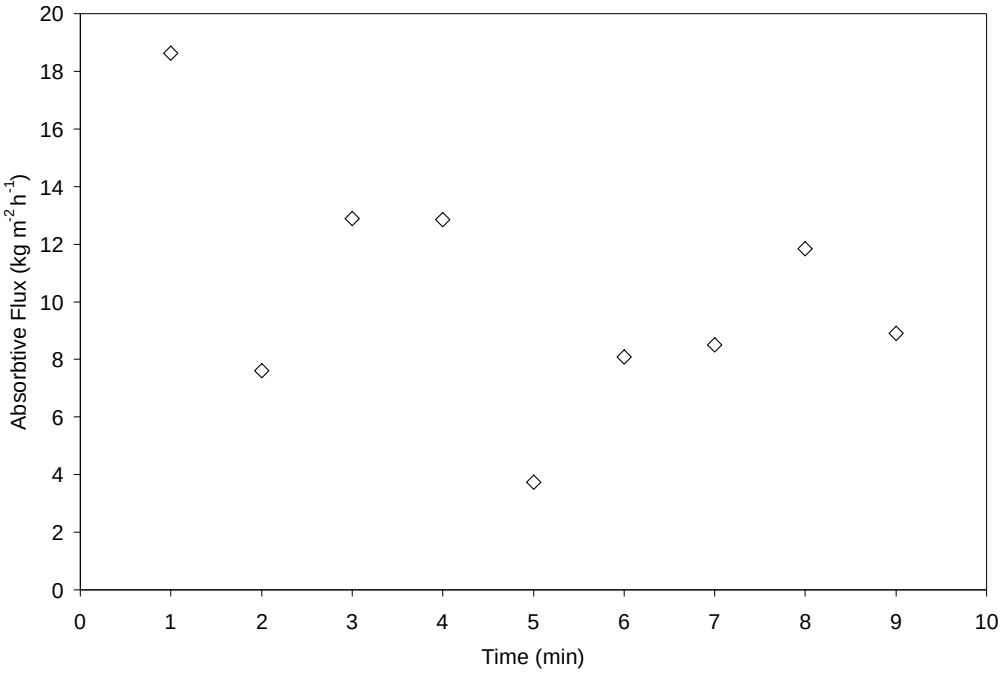

Figure 5-14: Absorptive flux in membrane 16 over time.

As observed in Figure 5-15, the surface tension of membrane 16 with liquid water decreases with time, and the surface tension of membrane with air increases with time. As the water enters the membranes the wettability of the membrane decreases due to saturation of the membrane.

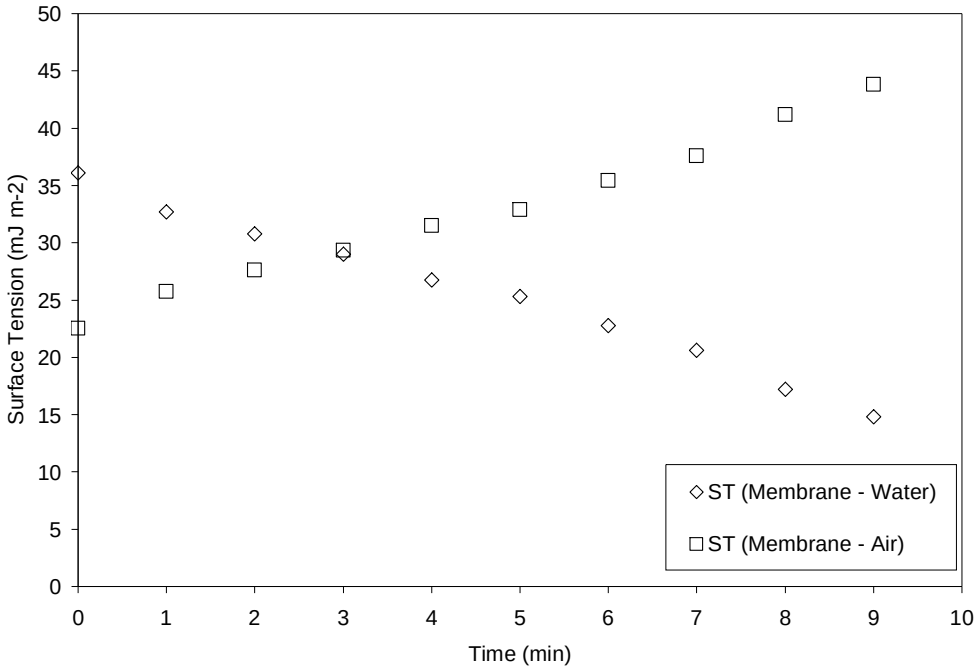

Figure 5-15: Change in surface tensions at the membrane – water interface over time.

The average absorptive flux in the membrane from Figure 5-14 was 10.2 kg/m^2/h. The flux obtained for membrane 16 at similar conditions in the static water permeation tests presented in 5.1.1.1 was 1.2 kg/m^2/h. Since the rate of absorption of water into this membrane is much more rapid that the overall permeation through the membrane, it can be deduced that rate limiting step for water transport through this membrane will be diffusion of water through the membrane rather than the absorption or desorption steps.

5.4.4.2 Membrane 48

The study of membrane 48 using ADSA was problematic. This membrane was a sulphonated polymer which absorbs water well but changes morphology upon water sorption. This led to the membrane changing shape over time, as shown in Figure 5-16, which made measurement of the ADSA images very inaccurate.

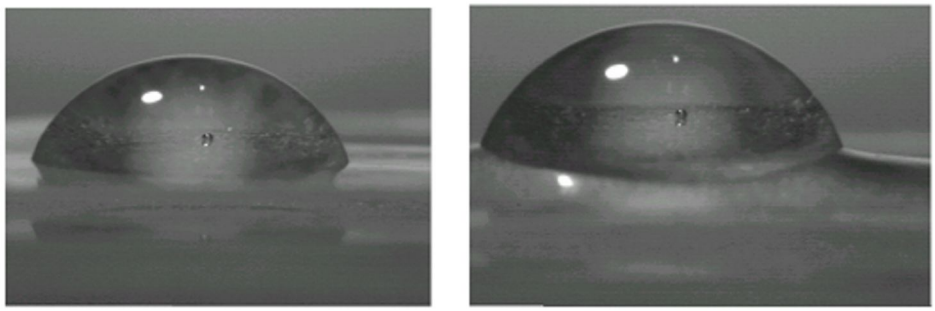

Figure 5-16: Change of membrane 48 shape over time, shown to alter the ability of the camera to gain time dependent information.

The membrane had a rather low initial contact angle, and one of the highest initial S-V surface free energy as seen in Table 5-8, which should mean that the membrane should be easily wet. However the absorptive flux of this membrane was measured to be zero. This is explained by the large errors in measuring the geometry of the membrane and drop due to the changing morphology of the membrane. Evidently studying sulphonated polymers or polymers which have low dimensional stability in the presence of water using ADSA requires specialized equipment to stretch the membrane to ensure that these membranes do not warp as they absorbs water.

5.4.4.3 Membrane 4

Membrane 4 was a polypropylene based membrane with a hydrophilic additive. It showed similar results to membrane 1, as shown in Figure 5-17. As it can be seen in Figure 5-17, within the first three of minutes the rate of flux decreases to nearly zero. For this reason, the average rate of absorptive flux for this membrane was only calculated over the first 4 minutes. However, membrane 4 still had a lower average absorptive flux than membrane 16, and from Table 5-8, it can be seen that this membrane had an increasing radius over time. Membrane 4 was quite thin, being 25 microns compared to the 180 micron thickness of membrane 16. This meant that there was less volume of membrane below the drop into which water could permeate before spreading laterally over the surface of the membrane, causing the radius to increase with time. This indicates a further issue with using the ADSA test to study membrane materials.

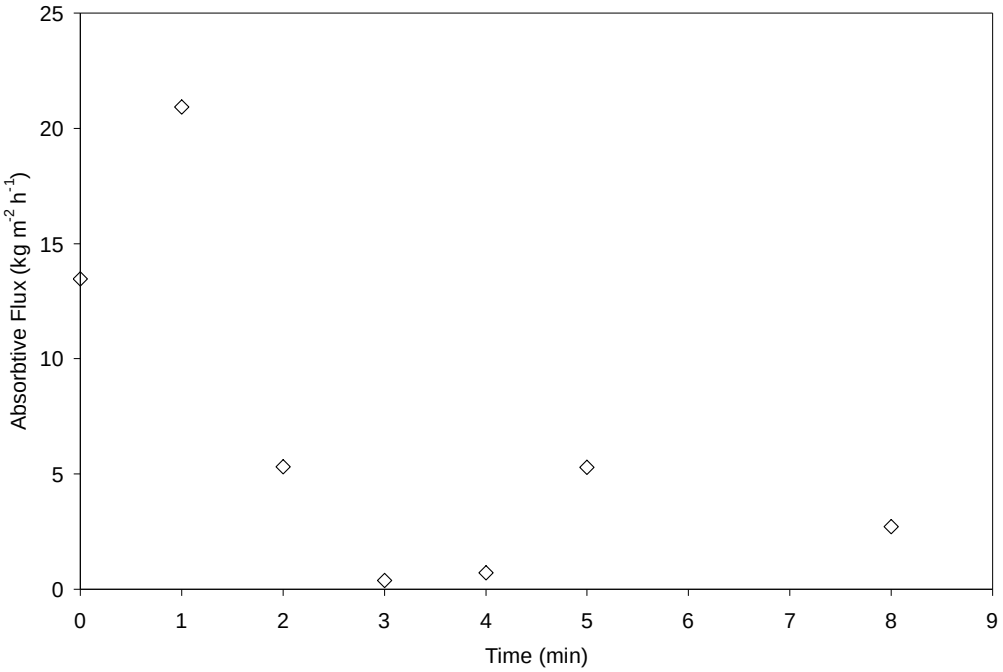

Figure 5-17: Absorptive flux in membrane 4 over time.

5.4.4.4 Membrane 58

Membrane 58 was a porous membrane based on fluoropolymer. It showed no adsorptive flux, and due to its high L-S surface tension, and lower S-V surface tension it was the least wettable of the membranes tested. This was likely due to the hydrophilic nature of fluoropolymer material of the membrane. For the liquid water to enter the membrane, the pressure force induced by the droplet would have to overcome the high surface energy of water on the membrane, so that water would to enter the membrane pores. Evidently this did not occur. However as shown Figure 5-13, this membrane still performs well in the humidifier. During humidifier operation the membrane is in contact with water vapour, more so than liquid water. Water in the vapour form penetrates the pores of the hydrophilic membrane with greater ease than liquid water, so better performance in the presence of water vapour would be expected. However, this would also mean that gases, such as air could pass through the membrane as well, if the vapour does not condense and fill the pores. This would be an undesirable result.

5.4.4.5 Membrane 46

Membrane 46 demonstrated the most rapid absorption of water of the five membranes studied. The average lifetime of a droplet on the membrane surface was less than 5 seconds as seen in Figure 5-18, as opposed to greater than 10 minutes with other membranes. The L-S surface tension of the membrane was low, and the L-V surface tension of the membrane was high, so the membrane had very high wettability.

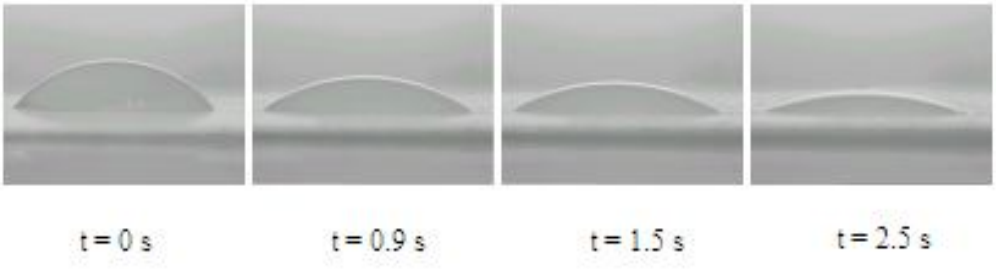

Figure 5-18: Sessile drops on membrane 46 with time.

Water permeated into the membrane rapidly, but the overall performance of the membrane was no greater than membranes in which the absorptive flux was lower, as seen in Figure 5-13. This would indicate that the transport through this membrane is not limited by the rate of absorption or permeation, but rather one of the other process steps. This may be the rate of evaporation of water into the humidifier channel, which is not a property of the membrane, but rather a property of the process conditions and the geometry of the test module. From the experiments completed, it is believed that this membrane would be the best candidate for the humidifier.

5.4.5 Conclusions for ADSA Testing

It was determined that although ADSA is a useful method of determining surface tensions for the membranes, it was difficult to qualify membrane performance from the ADSA method. Different types of membranes responded differently to the ADSA experiments, which made comparison between membranes difficult. Membranes which had hydrophilic additives or were inherently hydrophilic responded well to the ADSA tests, and absorptive fluxes were obtained for these membranes. Membranes which have low dimensional

stability in the presence of water are not appropriate for this type of testing.

For some hydrophilic membranes, insight the rate determining step in the humidifier process can be obtained. Through ADSA surface tension and relative wettability of all membranes can be obtained.

5.5 Accelerated Aging

One of the failure mechanisms suspected for polyethylene based membrane materials was the oxidation of the polymer chain. This would lead to the membrane cracking, losing mechanical stability, increased air permeation, and the possible loss of hydrophilic additives. Tests were completed to simulate this aging process.

5.5.1 Oxidation of Polyethylene

5.5.1.1 Effects of Process Conditions on Polyethylene

Polyethylene is known to oxidize in the presence of air, oxygen, chemical oxidants, and ultraviolet light (sunlight). Increased temperatures have been shown to increase the rate of oxidation exponentially as shown in Figure 5-19.

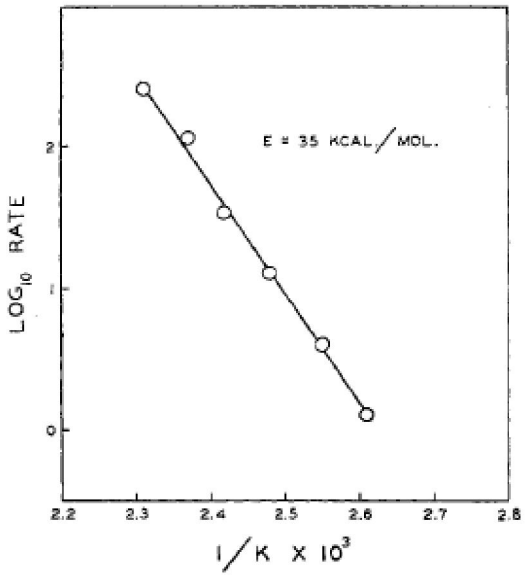

Figure 5-19: Rate of polyethylene oxidation with temperature (Wilson, 1955).

Figure 5-19 demonstrates that as temperature increases from right to left between 160°C

and 110^{o}C a two fold increase in the magnitude of the oxidation reaction occurs.

The presence of metals has been reported to initiate polyethylene oxidation as well (Baum, 1959).

5.5.1.2 Mechanism of Oxidation

Oxidation of polyethylene occurs by a free radical mechanism(Bolland and Gee, 1946). The mechanism follows the form presented by Daly and Yin in reactions 1 through 8 where * indicates a free radical (Daly and Yin, 1998):

Initiation:	Formation of R* (ie. RH → R* + H*)	[1]
Propagation:	$R^* + O_2 \rightarrow RO_2^*$	[2]
	$RO_2^* + RH \rightarrow ROOH + R^*$	[3]
	$ROOH \rightarrow RO_2^* + OH^*$	[4]
	$ROOH + 2RH \rightarrow 2R^* + ROH + H_2O$	[5]
Bimolecular:	$R^* + R^* \rightarrow R_2$	[6]
Termination:	$RO_2^* + R^* \rightarrow$ products (ketone + 2R*)	[7]
	$RO_2^* + RO_2^* \rightarrow$ products	[8]

5.5.1.2.1 Initiation, Reaction 1

The formation of the alkyl radical may occur by many occur by direct air oxidation of weaknesses in the polyethylene chain, through reaction 3, or through reaction 5. The initiation reaction 1 begins from the presence of heat, radiation, or various processing conditions.

5.5.1.2.2 Propagation, Reactions 2 through 5

These reactions are where much of the oxidation occurs. Reactions involving 'RH' indicate that the polymer chain is under attack by the free radicals. Tertiary hydrogens (found at the end of the polymer chain, CH_3) are most susceptible to oxidation in reaction 2, followed by secondary hydrogen ($-CH_2-$), followed by primary hydrogen (-CH-) (Cullis et al., 1947). This occurs since the O_2 reactions occur at the surface and in the top layers of

the polymer where O_2 is mobile. Thermodynamically reactions of oxygen with tertiary hydrogens are more favourable than with secondary hydrogens. However reactions 3 and 4 will occur at various locations with the polymer chain on secondary hydrogens. Secondary hydrogens are found in greater proportions at sites in the relatively fixed polymer matrix. As more radicals are developed over time reactions rates increase and permeate into the polymer matrix (Daly and Yin, 1998).

5.5.1.2.3 Termination, Reactions 6, 7, and 8

These reactions lead to the formation of oxidative degradation products such as ketones and aldehydes. These reactions may also develop further free radicals in the polymer matrix. Simulations indicate that reaction 7 is more predominant than reaction 8 (Daly and Yin, 1998).

5.5.1.3 Preventative Measures

Antioxidants may be added to the polymer to prevent free radical reactions from propagating. These antioxidants react much more rapidly with free radicals than the polymer chain so oxidation rates in the polymer can be minimized. These are often added to the surface of the polymer as oxidation generally begins at the polymer surface and than propagates into the polymer matrix. These antioxidants may also be added during processing to prevent initiation during processing and subsequently oxidation after processing. Popular antioxidants to add to polyethylene are aromatic amines and phenols.

Higher molecular weight polymers will resist the effects of oxidation better than low molecular weight polymers as more reactions must occur to reduce the high molecular weight polymer to a lower average molecular weight.

Reducing exposure of the polymer to oxidizing conditions such as sunlight, high temperatures, and oxidative reactants will increase the life of the polymer.

5.5.2 PEROX Accelerated Oxidation Test

The methods of this test are summarized in Section 2.5. This test was completed to compare the oxidative resistance of various membrane materials. Two membranes were tested, membrane 20 and membrane 16. These membranes were UHMWPE and silica

based membranes, and were identical except for the addition of an antioxidant coating to membrane 20. The antioxidant coating acts as a sacrificial oxidant, degrading in place of the polyethylene in the membrane which would cause membrane failure over time.

The percent weight loss for the two membranes are summarized in Figure 5-20. The rate of weight loss from the two membranes is shown in Figure 5-21. Membrane 20 demonstrates a large weight loss, 15.8% in the first 3 hours of the PEROX test; this is followed by a gradual increase in weight loss. Consequently the initial rate of weight loss is rapid for Membrane 20, after which the rate slows. Membrane 16 demonstrates a rather constant rate of weight loss. The large initial rate of loss in membrane 20 is likely due to the loss of the surface antioxidant coating which has been added to the membrane. After this much of the surface coating is oxidized in the first few hours, oxidation of the coating within the membrane pores in likely occurring along with some polyethylene oxidation at a slower rate. The oxidation occurring in membrane 16 is completely of the polyethylene in the membrane.

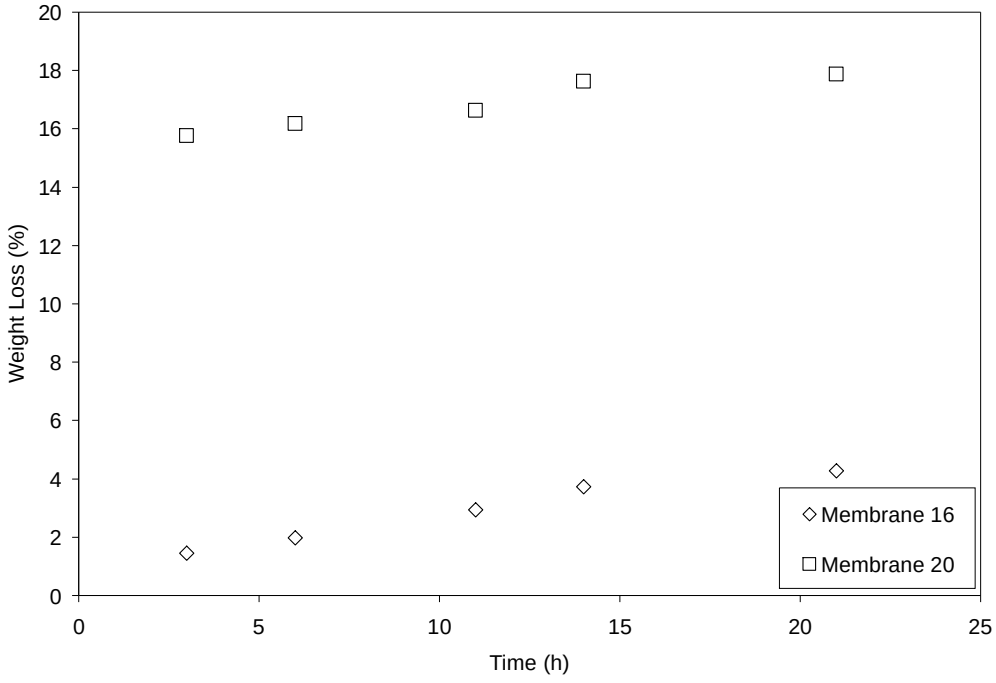

Figure 5-20: Percent weight loss in polyethylene and silica membranes with (20) and without antioxidant (16) in PEROX test.

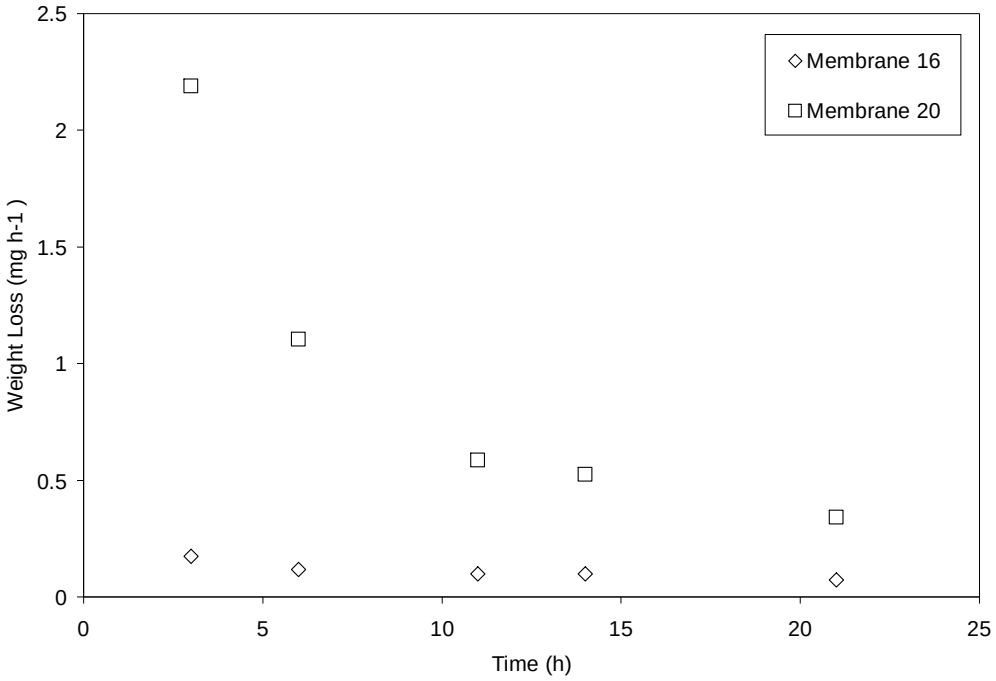

Figure 5-21: Rate of weight loss in polyethylene and silica membranes with (20) and without antioxidant (16) in PEROX test.

In order to quantify the effect of the oxidation on the membranes, mechanical tests were completed on the materials before and after the PEROX tests. The results are compared in Figure 5-22. The normal membrane without antioxidant coating, membrane 16, experiences a 13.7% decrease in elastic modulus during the PEROX test, indicating polyethylene oxidation. Conversely the membrane with antioxidant coating only demonstrates a 2.4% decrease in elastic modulus, indicating very little polyethylene oxidation. The antioxidant coating certainly helps protect the membrane from polymer oxidation, and may help extend the life of these membranes.

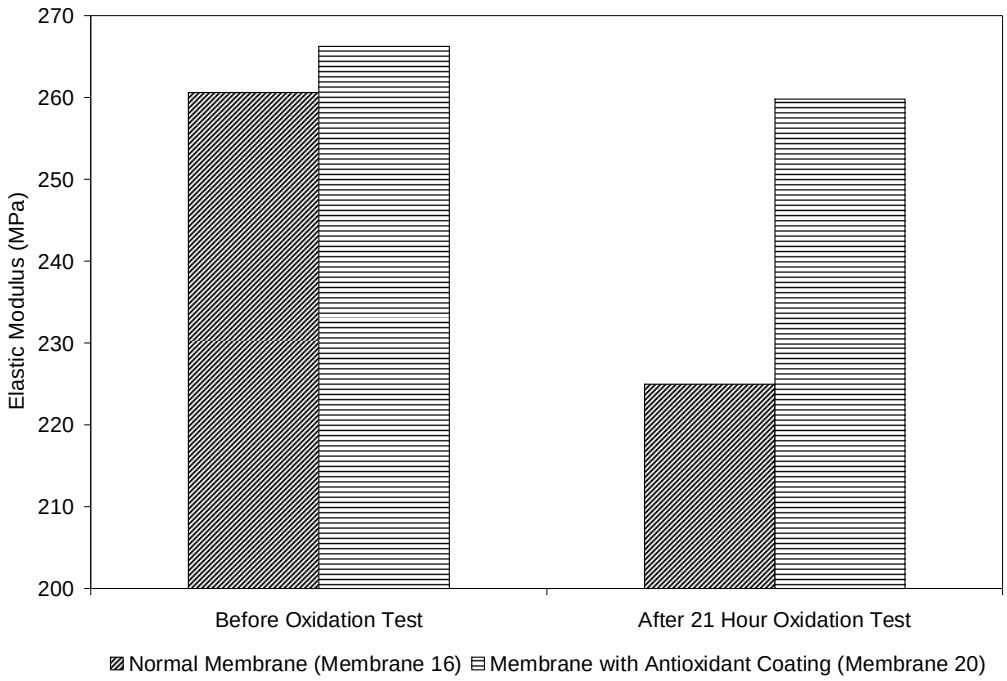

Figure 5-22: Average elastic modulus of membranes with and without antioxidant coating before and after PEROX test.

5.6 Analysis of Silica Content of s-PEEK Membranes

Membranes 48 through 54 were based on sulphonated polyetheretherketone (s-PEEK) with a silica additive. The polymer s-PEEK has been modified to act as an ion exchange membrane, so the membrane will imbibe water. PEEK is a high performance polymer, offering chemical stability, high temperature tolerance, and high mechanical strength. Silica has been added to the membrane to help absorb water and keep the membrane hydrated. Many of these membranes tested had the same properties and thickness, with the exception of the silica content in the membrane. This allowed for a study of the effect of the weight percentage of silica in the membrane on the membrane water transport performance. A summary of the membranes used in this test can be found in Table 5-10.

Table 5-10: Summary of s-PEEK/silica membranes tested.

Membrane #	Weight % Silica
48	13
51	17
52	25
53	30

The water performance of these membranes is presented in Figure 5-23.

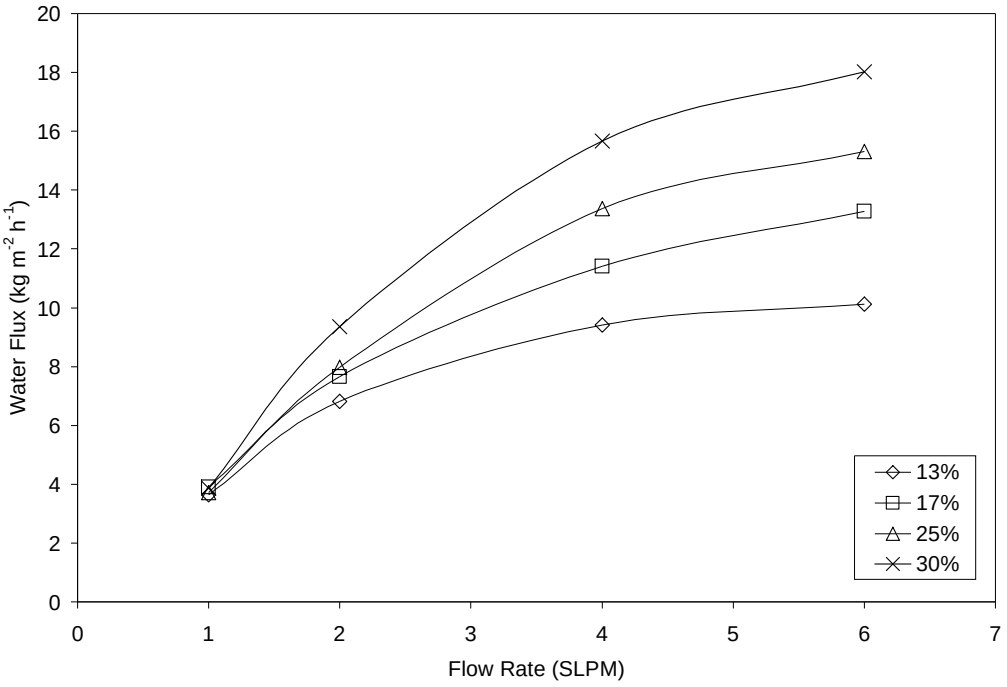

Figure 5-23: Water transport performance of s-PEEK/silica membranes with different silica content.

Evidently the silica content has a positive effect on the water transport performance; this is likely due to the increased capacity for water absorption and retention provided by the silica additive. A surface contour comparing the effects of silica and flow rate on the water flux can be found in Figure 5-24. This plot helps visualize the positive effect of the silica, particularly at higher flows.

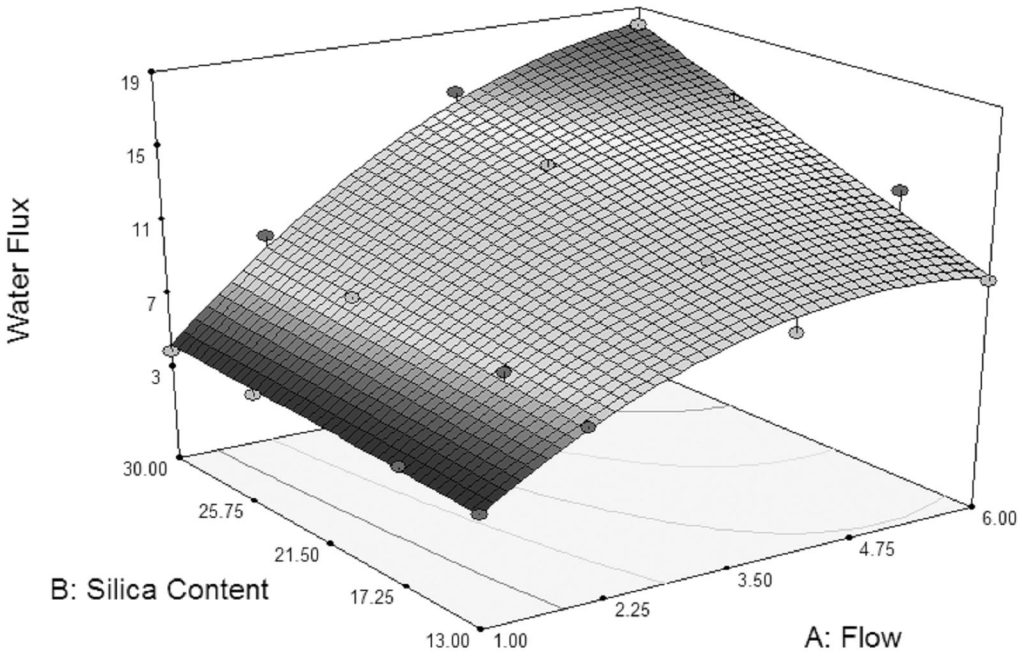

Figure 5-24: Surface contour plot of the effects of silica % and flow on the water flux of the s-PEEK/silica membranes.

5.7 Summary of Results

The results of the tests completed on the membranes were tracked. Membranes which passed the water transport, air permeation, and mechanical strength tests, and demonstrated satisfactory handling were then tested for durability. These results are summarized in the following chapter. Figure 5-25 shows the tracking sheet for all of the membranes. Some membranes failed the dry air permeation test, but demonstrated rapid wetting, and had zero wet air permeation. These membranes were numbers 5, 46 and 62; they were also selected for durability testing.

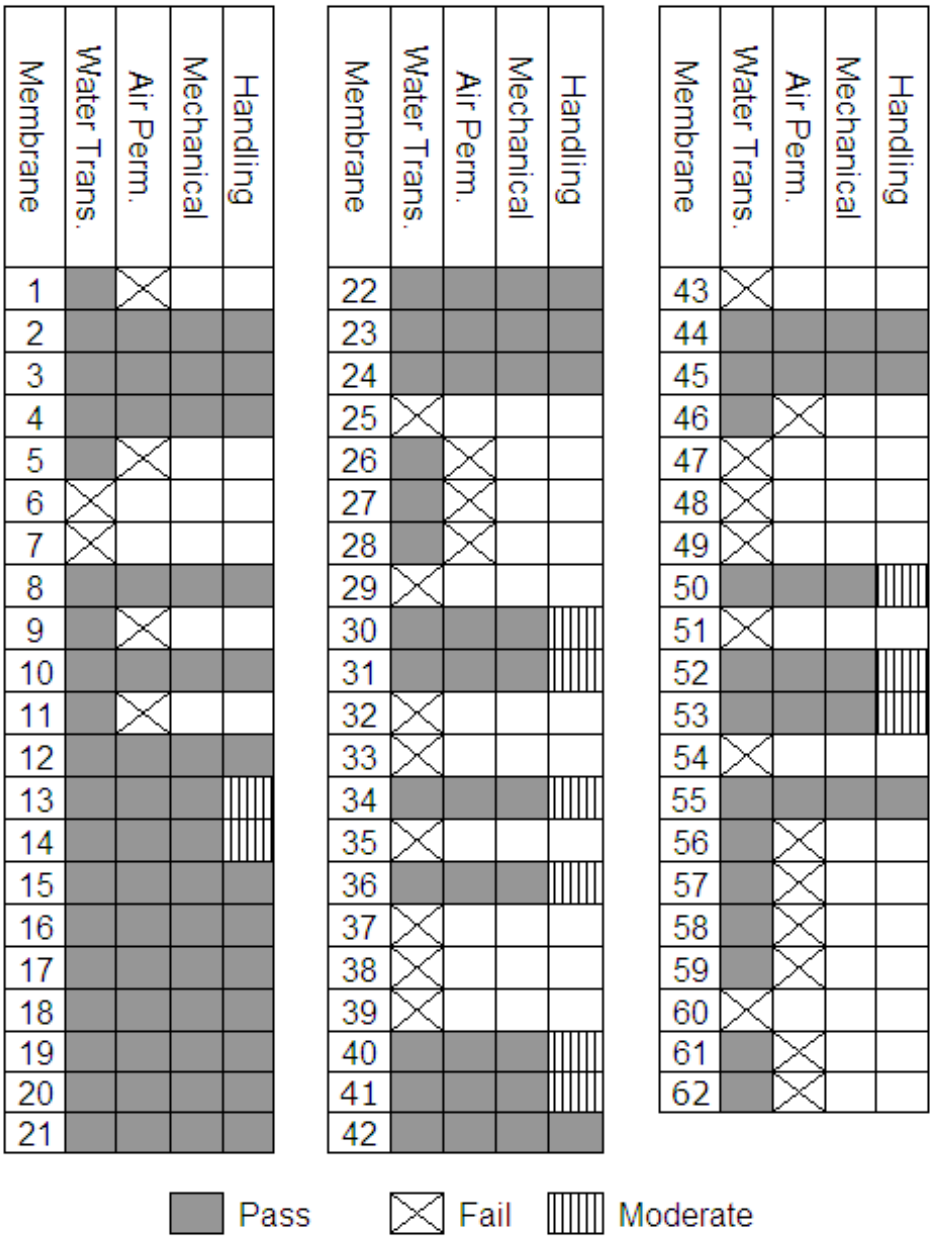

Figure 5-25: Membrane testing results chart.

Chapter 6

6.0 Membrane Durability Testing and Failure Analysis

The results of durability testing for membranes which qualified for additional examination are presented in this section. Results are presented for membrane lifetimes which were tested on the low temperature durability station (LTDS). On the LTDS, membranes were subjected to stream conditions of 23^{o}C and 0% relative humidity (RH) and stream 3 conditions of 65^{o}C and 100% RH. Durability testing was also completed on the high temperature durability station (HTDS), with stream 1 at 85^{o}C and 0% RH and stream 3 at 85^{o}C and 85% RH.

The membranes were tested for water transport at stream 1 conditions of 23^{o}C and 0% RH and stream 3 conditions of 75^{o}C and 100% RH, unless otherwise noted at the beginning of life (BOL). The air crossover at 21 kPa in the test module was also measured a BOL. Intermittently, the membranes were tested for water transport and air transport after extended periods of operation. Decreases of greater than 20% in the water transport rate of the membrane, or increases of air crossover of greater than 25% constituted the failure of the membrane. Membranes which experienced failure were analyzed at the end of life (EOL) and failure mechanisms and mitigation strategies are proposed if appropriate.

6.1 Membrane 2

Membrane 2 was a microporous ultra high molecular weight polyethylene (UHMWPE) based battery separator, which is created using a membrane extrusion process. This membrane is 75 microns thick, with a pore volume of 50%. The membrane contains titanium dioxide (TiO_2) filler as well as wetting agent such as dodecylphenoxy polyethoxy ethanol. The separator material is permanently wettable, and has demonstrated improved battery life in various types of alkaline batteries.

6.1.1 Low Temperature Durability Testing

The membrane was tested on the LTDS but demonstrated failure after 730 hours, this failure is shown in Figure 6-1. At 730 hours, the water transport for this membrane had

decreased by 45% at 6 SLPM; this constituted a lifetime failure of the membrane.

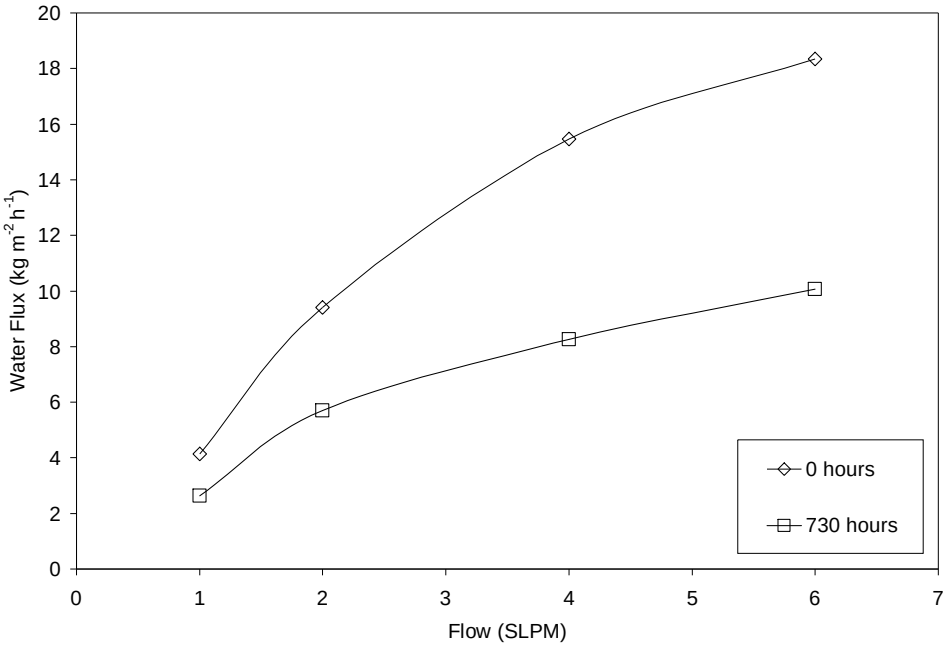

Figure 6-1: Water transport tests results for Membrane 2 on LTDS at BOL and after 730 hours of operation.

6.1.1.1 Failure Analysis

Due to the nature of the membrane, namely that it contained a wetting agent which was added to the material to increase wettability; it was proposed that the wetting agent had leached from the material during operation. This led to a decreased ability for the membrane to absorb water, and thus transport was affected. The membrane was not designed to operate in a system in which the membrane was in constant contact with flowing gases and water, but rather in a more static battery environment. The mobility of the additive was greatly increased due to the dynamic nature of the humidifier environment. The leaching of this wetting agent could be detrimental to the fuel cell environment, which is upstream from the dry side of the humidifier. Since leaching has likely occurred, this membrane was rejected as a candidate material for a fuel cell humidifier, as the leaching not only reduced performance, but may also contaminate the fuel cell stack itself.

6.1.2 High Temperature Durability Testing

The BOL water transport performance for membrane 2 at 6 SLPM was 20.9 kg/m^2/h and the dry air crossover rate was measured to be 0.524 LPM at 21 kPa. On the HTDS, the membrane showed decreasing performance in the first 400 hours of operation, this is shown in Figure 6-2. At this time the dry air crossover rate of the membrane was 0.583 LPM, which did represent a significant increase. However after 705 hour of operation on the HTDS, the membrane was found to have a very high air crossover rate. Upon inspection, it was found that the membrane had cracked sometime between 400 and 705 hours of operation on the HTDS.

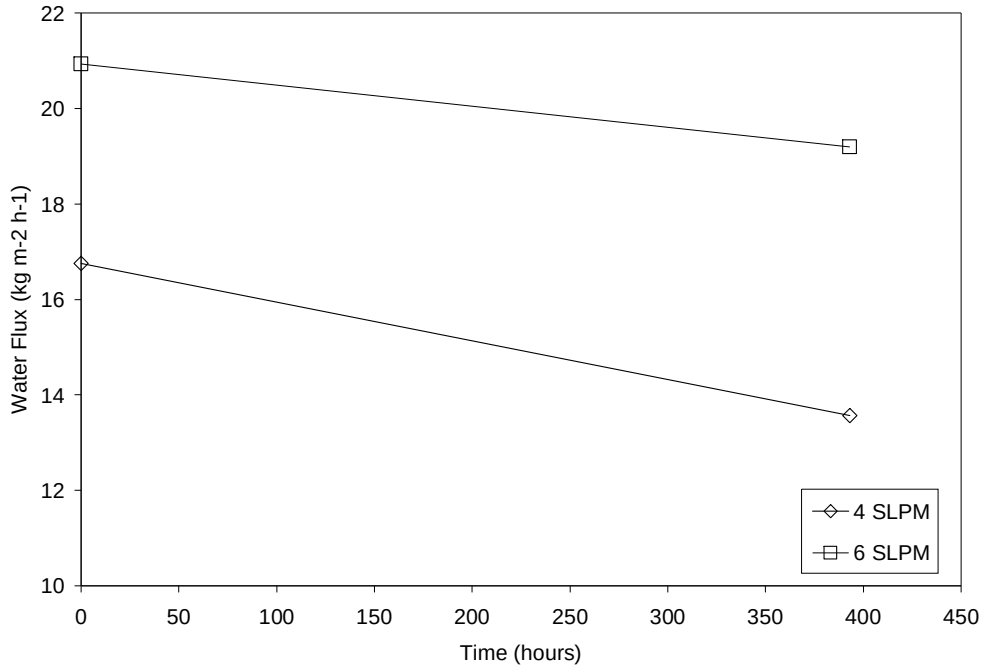

Figure 6-2: Water transport performance decrease at 4 and 6 SLPM in membrane 2 on HTDS over time.

6.1.2.1 Failure Analysis

The decrease in performance in membrane 2 between 0 and 400 hours was likely due to the loss of hydrophilic additives, as explained in section 6.1.1.1.

The cracked membrane is shown in Figure 6-3, this cracking was occurred along one of the channels of the test module. At increased temperatures and under the presence of

moisture, the membrane may be weakened mechanically, leading to failure during operation. This will be particularly true when differential pressures and compression forces are applied to the membrane material, as in the humidifier assembly itself. The environmental stress cracking observed here was likely due the embrittlement of the polyethylene base material. This may have occurred due to oxidation of the polymer chain, which has been reported to be accelerated at increased temperatures and when polyethylene based materials are under stress (Needham et al., 2006).

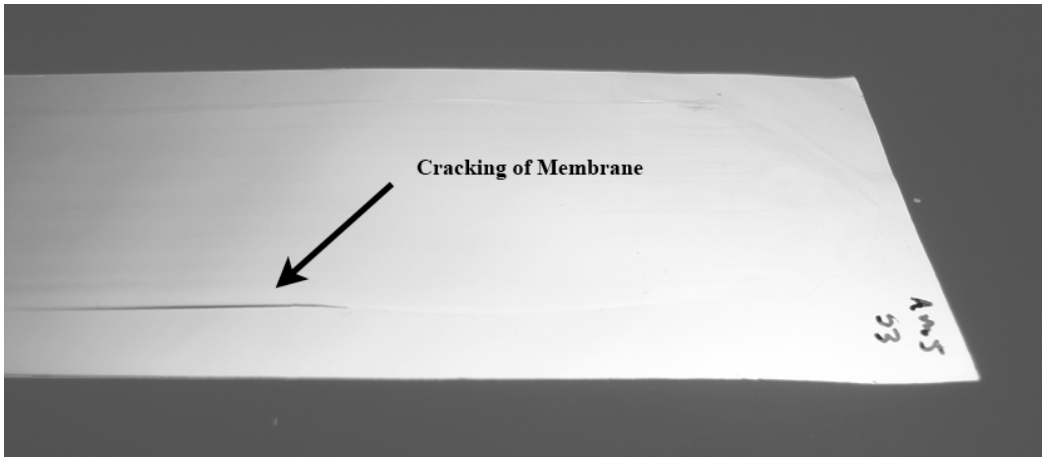

Figure 6-3: Membrane 2 after 700 hours on the HTDS, cracking in material.

Regardless, this membrane was rejected as a potential candidate material for a gas to gas humidifier, as a failure of this nature would not be acceptable during operation.

6.2 Membranes 3 and 4

Membranes 3 and 4 were extruded microporous polypropylene based battery separator materials. They were coated with a wetting agent and were designed for aqueous electrolyte battery systems. Membrane 3 had a thickness of 25 microns, and a porosity of 37%, and membrane 4 had a porosity of 55%.

Since these membranes were of the same composition, only membrane 4 was tested on the LTDS.

6.2.1 Low Temperature Durability Testing

Membrane 4 demonstrated a BOL water flux of 20.0 kg/m^2/h and an air crossover rate of 1.5 LPM at 21 kPa. However after 300 hours on the LTDS the membrane had already

demonstrated a significant decrease in water flux, as shown in Figure 6-4. This decrease was even more evident at 550 hours of operation, at this point the membrane water flux had decreased by 41% at 6 SLPM. This value exceeded the acceptable failure criteria of a 20% decrease in water transport.

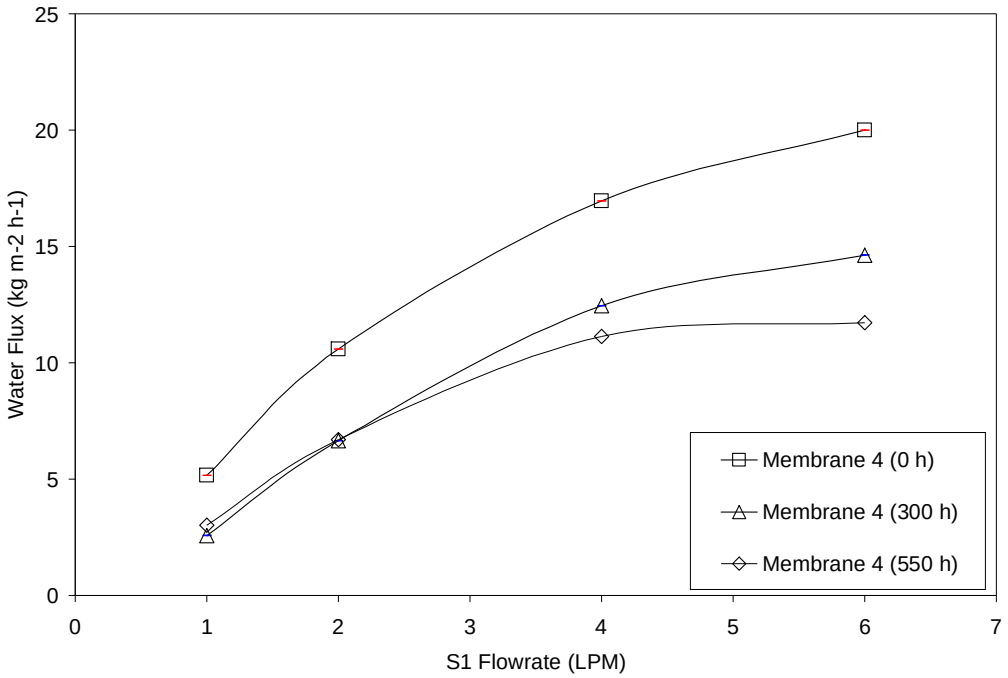

Figure 6-4: Water transport tests results for Membrane 4 on LTDS at BOL and up to 550 hours of operation.

6.2.1.1 Failure Analysis

Similar to membrane 2, this membrane contained a topical surface wetting agent, which is believed to have been lost from the surface of the membrane during operation. The membrane was rejected as a candidate material; similarly membrane 3 was also rejected since the material was also coated with this wetting agent.

6.3 Membrane 5

The membrane is a UHMWPE based membrane containing a silica filler material. The polymer and inorganic filler are extruded with plasticizer oil, and then calendared to form a sheet. The membrane is then stretched to produce a desired porosity, and the plasticizer oil is removed using an appropriate solvent. This membrane has a thickness of 45 microns.

It is designed for use as a battery separator in lithium ion batteries. This membrane failed the air permeation test, however it was still of interest to consider the lifetime of this material since the manufacturer was capable of making this material with a smaller porosity, which would lead to a lower air permeation rate in the material.

6.3.1 High Temperature Durability Testing

The membrane was tested on the HTDS for 412 hours, at which time cracking of the material was observed.

6.3.1.1 Failure Analysis

Since this membrane was a polyethylene based material, environmental stress cracking as summarized in section 6.1.2.1 was likely the cause of this membranes failure.

6.4 Membrane 8

This membrane was a standard battery separator material extruded and calendared from a mixture of UHMWPE, silica, and plasticizer. This membrane is typically used as a separator material in lead acid batteries. The silica to polyethylene ratio of the material is 2.6 to 1; the membrane contains 10 to 12% residual plasticizer.

The membrane was very similar in composition to membranes 15 and 16, except that membrane 8 was obtained from a different supplier, which may have affected the performance characteristics of the material. However, the degradation mechanisms should be similar for both types of membrane, and details of the failure mechanisms are explained in detail in sections 6.7 and 6.8 below. The plasticizer was removed by washing the membrane in hexane prior to use in accordance with findings from membrane 15 in section 6.7.

6.4.1 Low Temperature Durability Testing

Membrane 8 was tested on the LTDS, and showed slow degradation over time; this is shown in Figure 6-5. The water transport performance loss over 3000 hours was 15.5% at 6 SLPM. The air crossover for the membrane also decreased over time, as shown in Figure 6-6, this represents a 13% decrease in air crossover over 3000 hours.

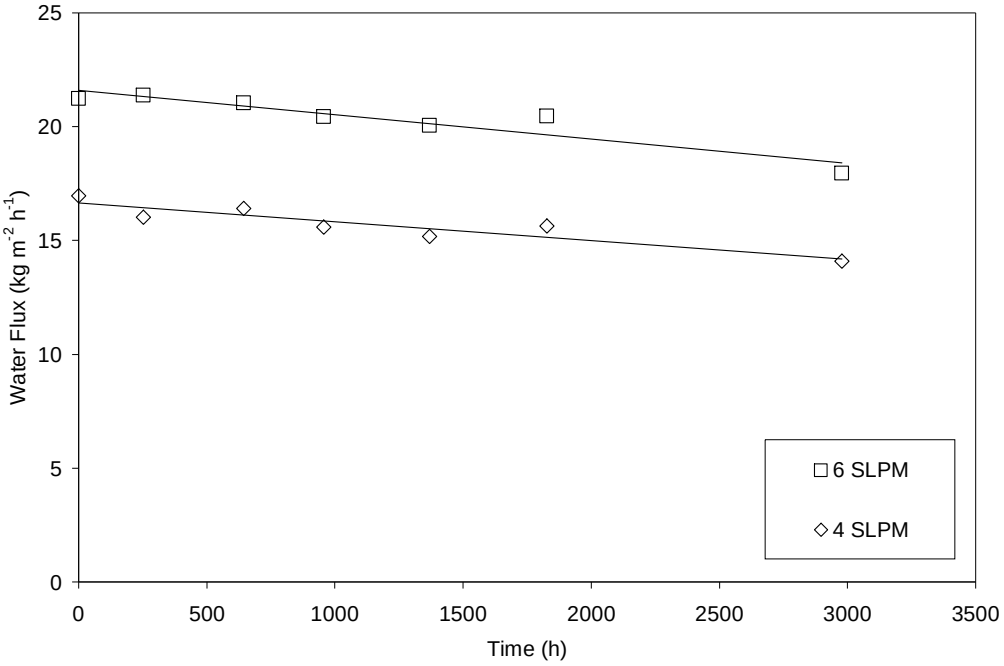

Figure 6-5: Water transport performance decrease at 4 and 6 SLPM in membrane 8 on LTDS over time.

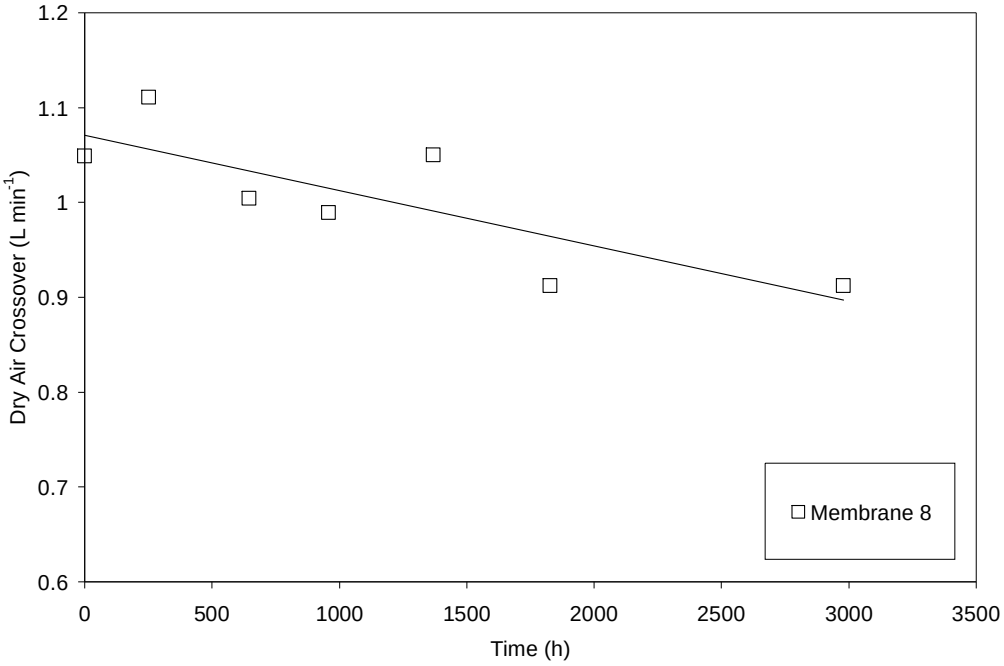

Figure 6-6: Dry air crossover in test module for membrane 8 over time while under operation on the LTDS.

6.4.1.1 Failure Analysis

The degradation in water transport performance, and decrease in air permeation observed in this membrane are explained in detail in section 6.7. This change was related to the changes in silica on the surface of the membrane.

6.5 Membrane 10

The membrane was a laminate material consisting of sulphonated styrene, polyethylene, and polypropylene based block co-polymer coated onto a microporous polyethylene support layer, the material may contain inorganic fillers as well. The material is typically used in energy recovery ventilation systems, and was designed for operation at low temperatures (less that 40^{o}C).

6.5.1 Low Temperature Durability Testing

Membrane 10 was operated for 558 hours on the LTDS, the performance did not decrease over this time, and air crossover did not increase. However, the membrane became significantly deformed over this operating time, which can be observed in Figure 6-7.

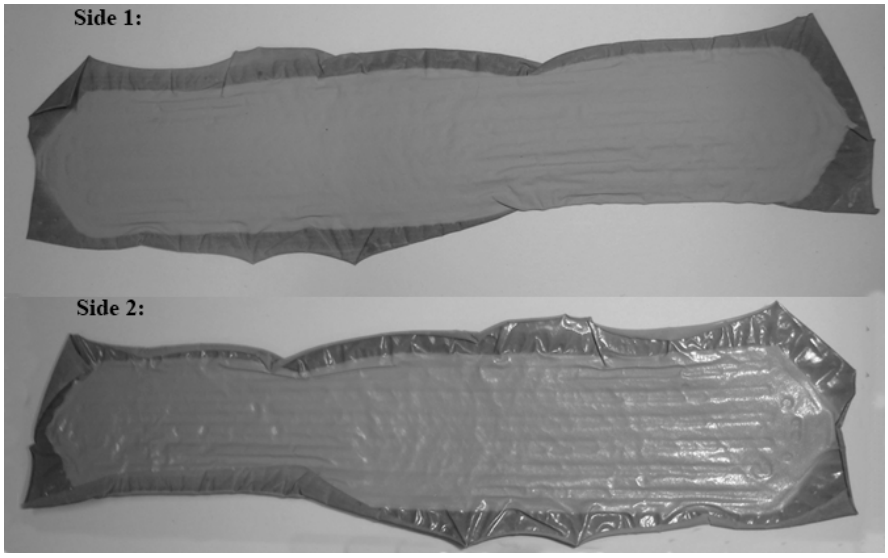

Figure 6-7: Deformation of membrane 10 after 558 hours of testing on LTDS.

6.5.1.1 Failure Analysis

Although this membrane did not fail in terms of performance, the observed deformation would be detrimental in the humidifier environment. The deformation of the membrane is related to the membrane being a laminate two materials. Failure has occurred due to the different dimensional stabilities of the two materials. When operating in an environment of increased temperature and humidity, one of the two laminated materials changes more than the other material. This leads to observed shriveling of the membrane. This warping of the membrane would affect pressure drop and flow in the humidifier channels. Also this deformation may lead to leaks in the humidifier over time. Accordingly the membrane was rejected for use as a humidifier membrane.

6.6 Membrane 12

Membrane 12 consists of UHMWPE to which hydrophilic groups have been graphed in order to make the membrane hydrophilic.

6.6.1 Low Temperature Durability Testing

The membrane was tested on the LTDS and demonstrated failure after 400 hours of operation due to decrease in water transport, as shown in Figure 6-8. This decrease represented a 20% decrease in water transport, which classified as failure of the membrane.

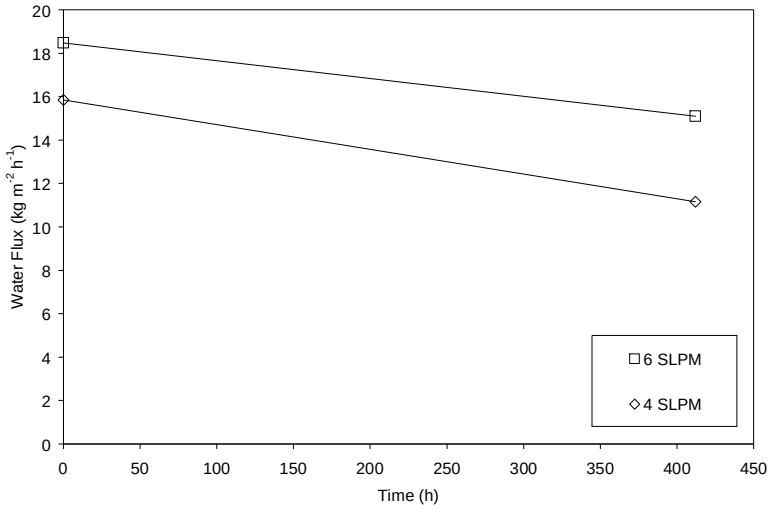

Figure 6-8: Water transport performance decrease at 4 and 6 SLPM in membrane 12 on LTDS over time.

6.6.1.1 Failure Analysis

The membrane was being tested simultaneously on the HTDS where it experienced similar failures. EOL failure analysis is presented in the following section.

6.6.2 High Temperature Durability Testing

Two samples of membrane 12 were tested on the HTDS. Both samples demonstrated decreasing trends in water transfer performance over time; this is presented in Figure 6-9. Sample 1 decreased in water transport by 32% by 724 hours, and sample 2 showed a similar 32% decrease by 1146 hours. No significant change in air crossover was observed during these operating periods.

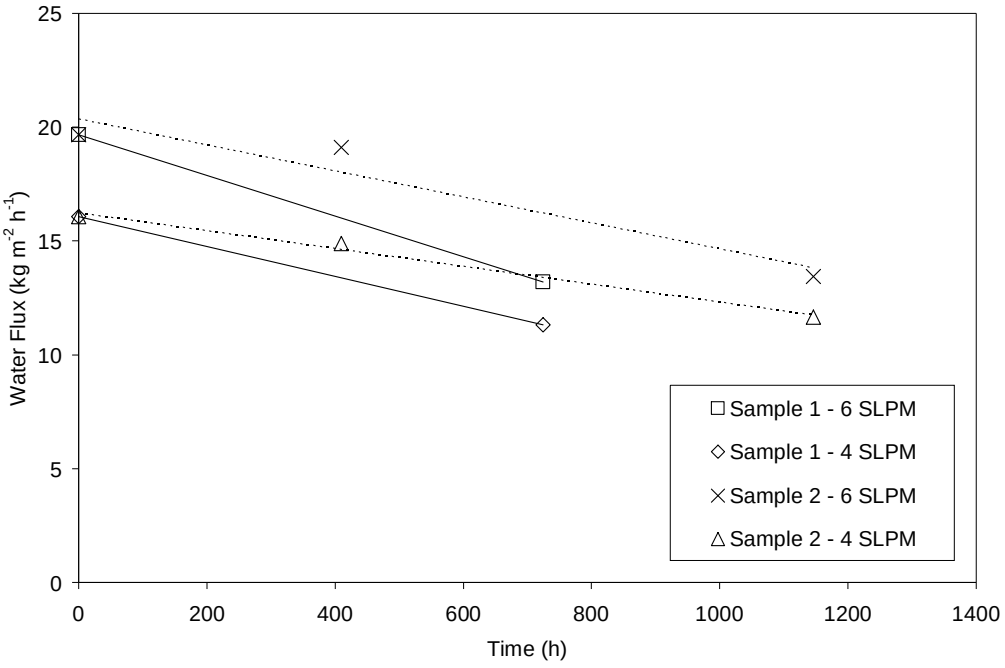

Figure 6-9: Water transport performance decrease at 4 and 6 SLPM in membrane 12 on HTDS over time.

6.6.2.1 Failure Analysis

Water transport performance dropped rapidly for this membrane on both the LTDS, and the HTDS. Evidently some degradation mechanism is occurring in the membrane under operation in the humidifier environment, causing a loss in water transport performance. The new and used membranes were analyzed using SEM techniques, in order to observe

any changes in the surface morphology of the membrane. A portion from the within the flow channel in the durability test module of the failed membrane was analyzed from both the dry and wet operating sides of the membrane.

Comparing the new and used samples at 1000x magnification, it appears that the new membrane (Figure 6-10) has a much smoother surface overall than the used membrane (Figure 6-11). The used membrane surface appears to have polymer fibers which are much better defined than the new membrane; this may be related to loss of the graphed hydrophilic groups from the surface of the polymer.

The new and used membranes are also compared at 20000x magnification in Figure 6-12 and Figure 6-13 respectively. The new membrane demonstrates a smoother surface overall in comparison to the used membrane surface. Polymer fibers on the surface of the used membranes have experienced some cracking and overall the surface appears to have a lower density of polymer webbing.

The membrane surfaces were analyzed using energy dispersive X-ray spectroscopy (EDS) at 250x magnification. The EDS results indicated a slight change between the new and used atomic carbon and oxygen percentages on the membrane surfaces. The new material surface consisted of 96.36% carbon and 3.64% oxygen, while the used membrane surface was 96.84% carbon and 3.16% oxygen. It was difficult to draw any overall conclusions from this data, since change was quite small. Also the composition of the hydrophilic groups which had been graphed to the polyethylene was proprietary and confidential. However, UHMWPE should not contain any oxygen, so the atomic oxygen observed in the EDS analysis must come from the hydrophilic additive. Since there is a decrease in atomic oxygen content on the used membrane surface it is possible that some of the graphed hydrophilic groups have been selectively lost. This would account for the large loss in the water transport rate observed in the used materials. Less hydrophilic groups on the membrane surface would mean a greater proportion of hydrophobic polyethylene and consequently the membrane would have a decreased ability to absorb and transport water.

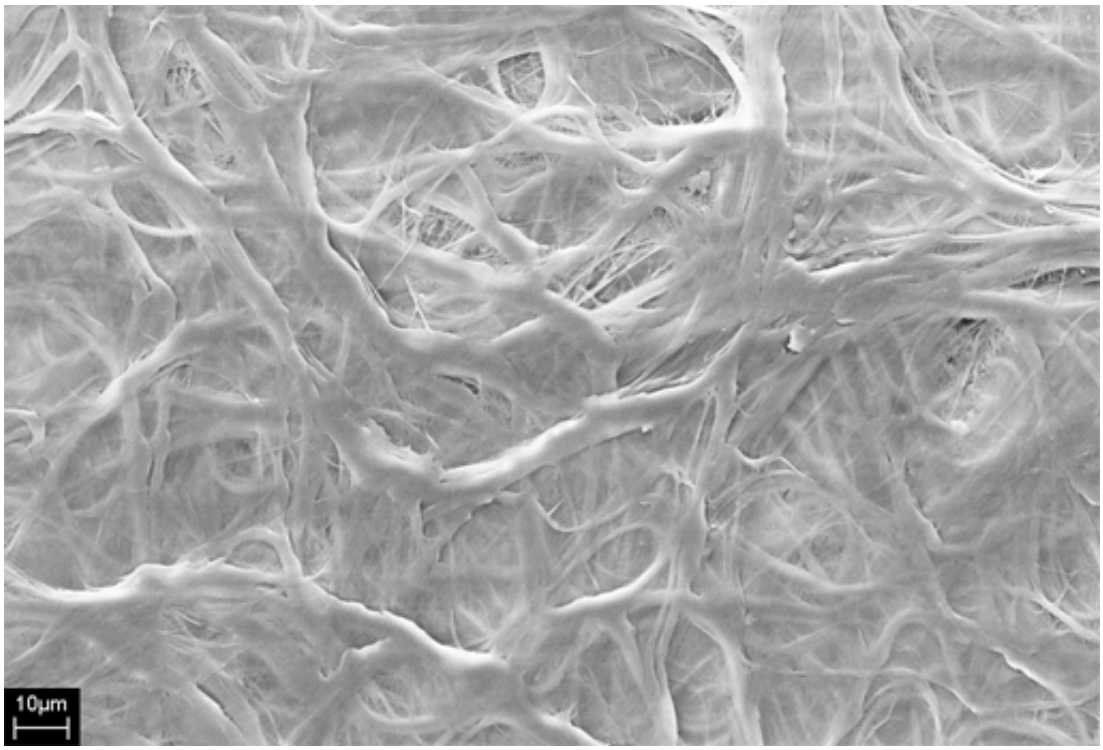

Figure 6-10: Membrane 12, new at 1000x magnification under SEM.

Figure 6-11: Membrane 12 at 1000x magnification after 1146 hours of operation on HTDS under SEM.

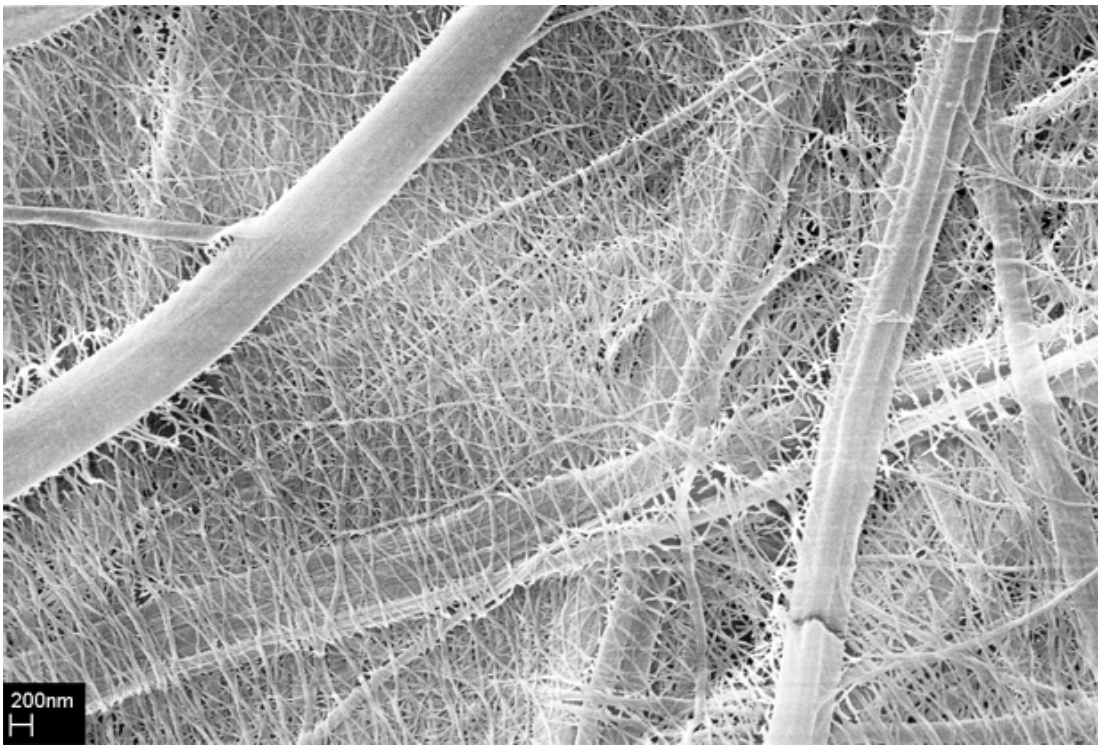

Figure 6-12: Membrane 12, new at 20000x magnification under SEM.

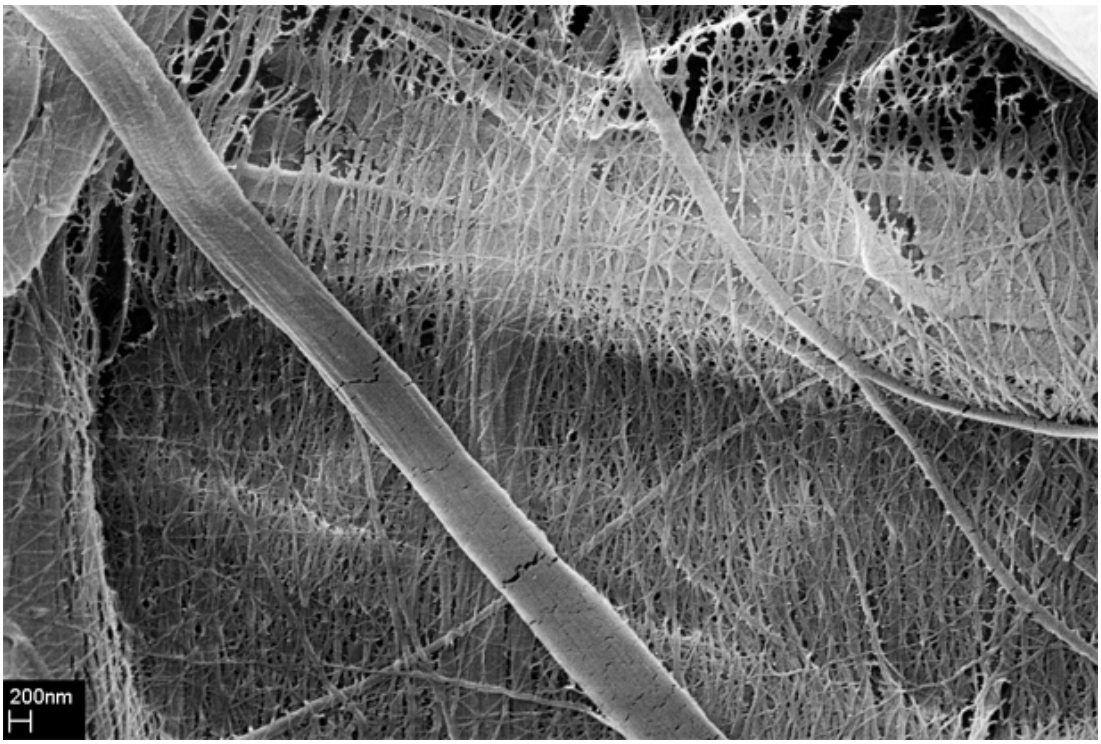

Figure 6-13: Membrane 12 at 20000x magnification after 1146 hours of operation on HTDS under SEM.

6.7 Membrane 15

Membrane 15 was a standard battery separator material consisting of silica and UHMWPE in a 2.51 to 1 ratio, the membrane contained 15% by weight residual processing oil.

6.7.1 Low Temperature Durability Testing

The membrane demonstrated a rapid decrease in performance, occurring over the first 20 hours of operation, this performance degradation is shown in Figure 6-14. The water transport performance decreased by 28% in less than 15 hours of operation.

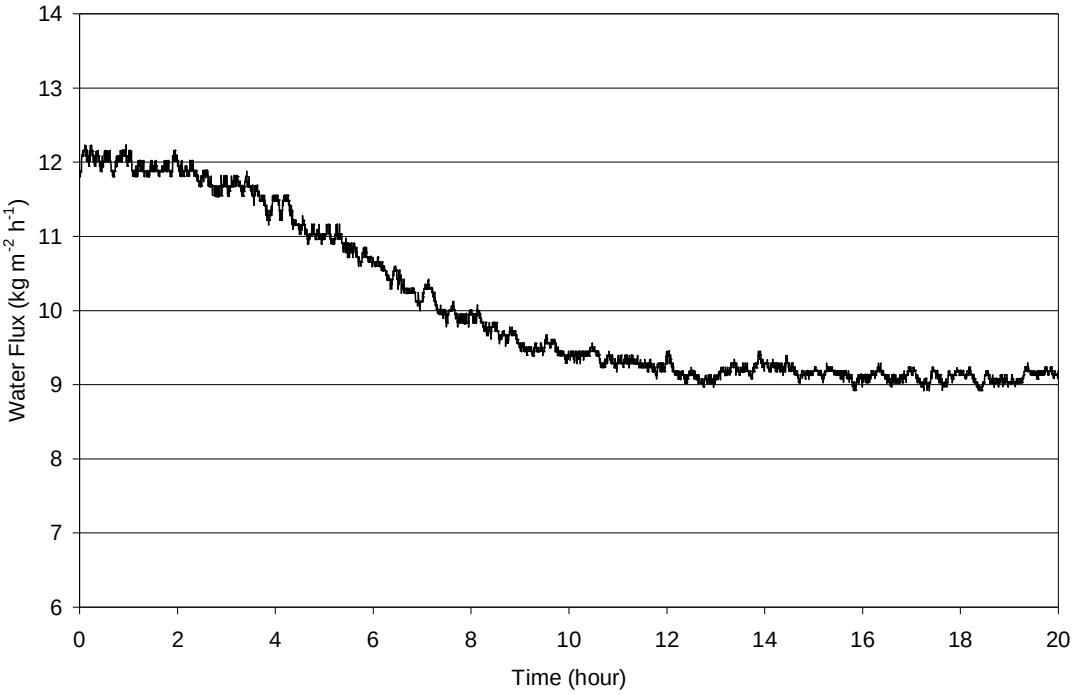

Figure 6-14: Membrane 15 water transport performance at 4 SLPM, from BOL to 20 hours, operating at stream 1 temperature of 23°C and 0% RH and stream 3 temperature of 75°C and 100% RH.

6.7.1.1 Failure Analysis

New and failed samples of membrane 15 were analyzed under SEM. Comparing the new and used membrane at 10000x in Figure 6-15 and Figure 6-16 respectively; it would seem that the silica particles on the surface of the used membrane are larger than those on the surface of the new membrane. I would appear that the plasticizer oil has become mobile and may be coating the silica particles of the membrane, which would act as a barrier to water transport in the membrane.

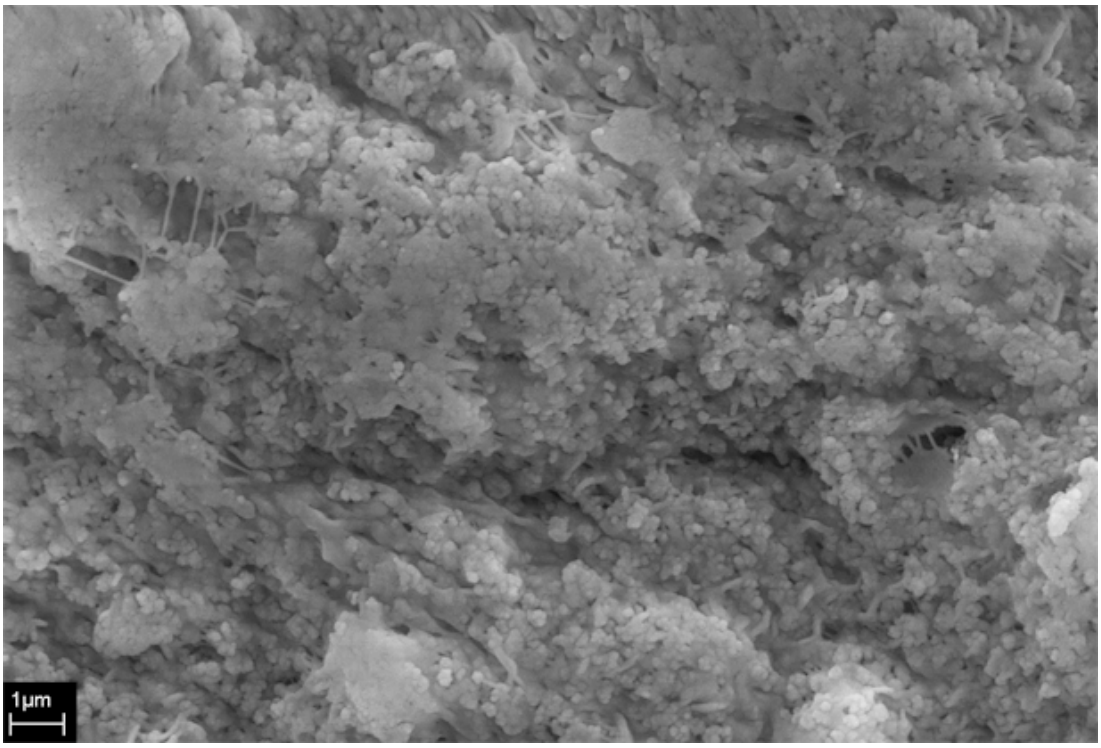

Figure 6-15: Membrane 15, new under SEM at 10000x magnification.

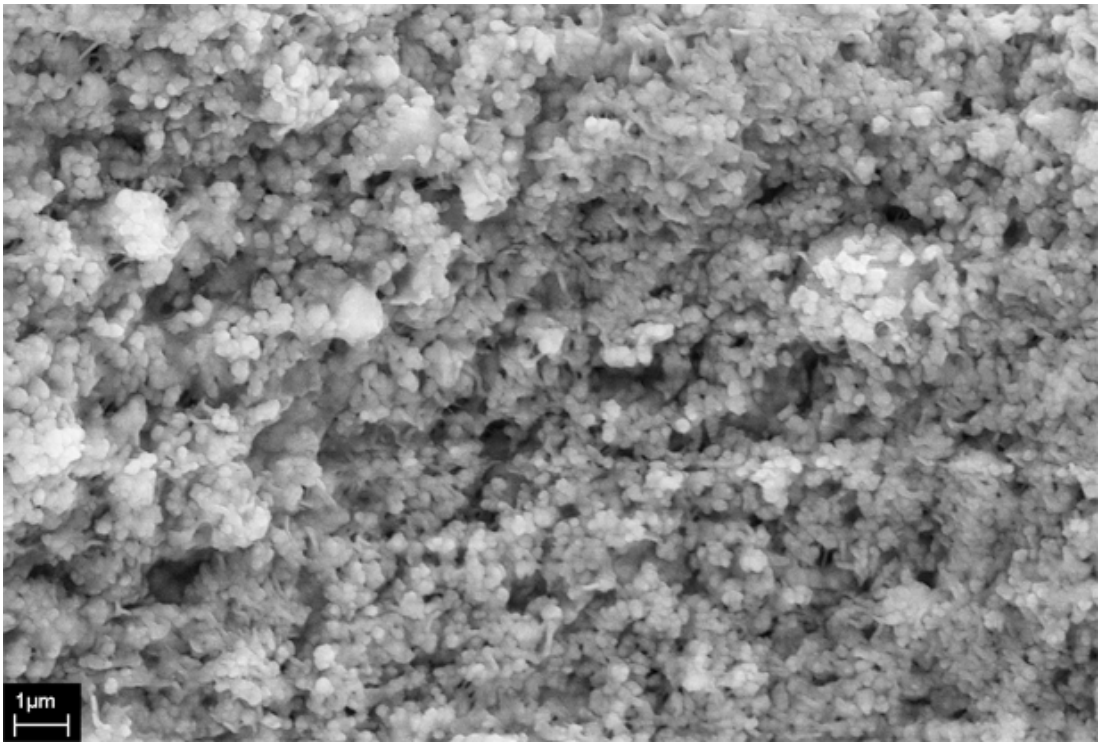

Figure 6-16: Membrane 15 after 20 hours of operation, under SEM at 10000x magnification, on the dry side of the membrane.

In order to confirm that the plasticizer was causing the loss in water transport performance, the failed membrane was washed in hexane, and then tested for water transport performance once again, the results are shown in Figure 6-17. After the failed membrane is washed with hexane, removing the plasticizer oil, the performance returns to its original performance level.

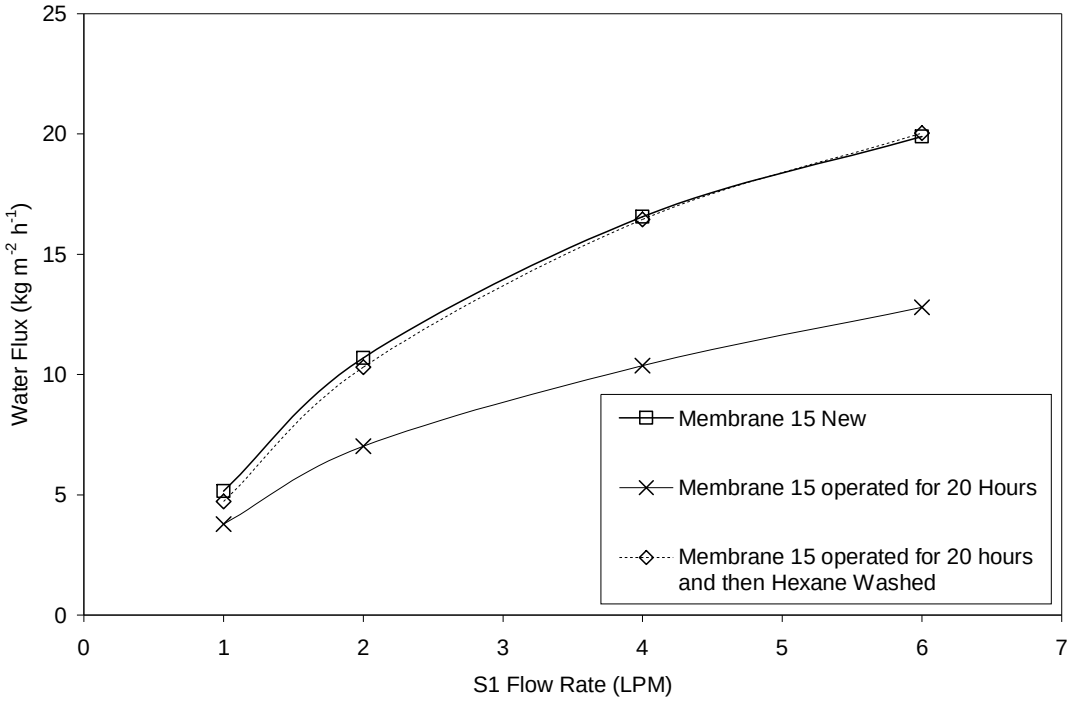

Figure 6-17: Membrane 15 at BOL, 20 hours of operation, and then after being washed with hexane, operating at stream 1 temperature of 23°C and 0% RH, and stream 3 temperature of 75°C and 100% RH.

It is observed that removing the plasticizer from the membrane using hexane leads to a return to the higher level of water transport performance. In order to use this membrane, the plasticizer must be removed prior to use.

6.8 Membrane 16

This membrane was the same as membrane 15, except that all of the plasticizer oil in the membrane had been removed. The membrane consisted of silica and UHMWPE in a ratio of 2.51 to 1.

6.8.1 Low Temperature Durability Testing

Two samples of the membrane were tested on the LTDS, the water transport results over time are shown in Figure 6-18. Air crossover rates were recorded for the second sample, and are presented over time in Figure 6-19.

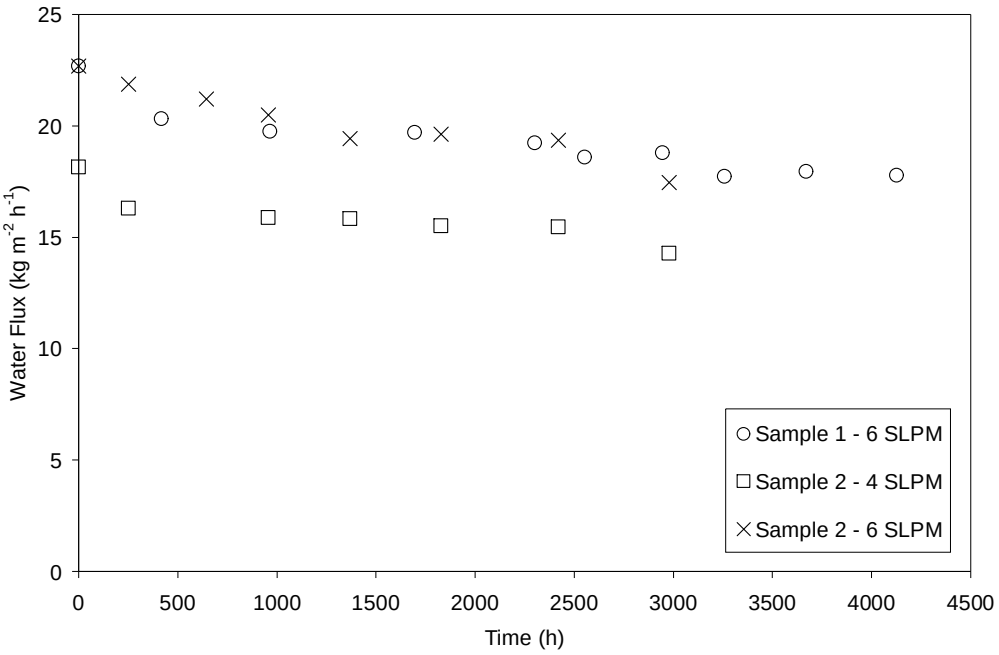

Figure 6-18: Water transport performance for two samples of membrane 16 over time during operation on the LTDS.

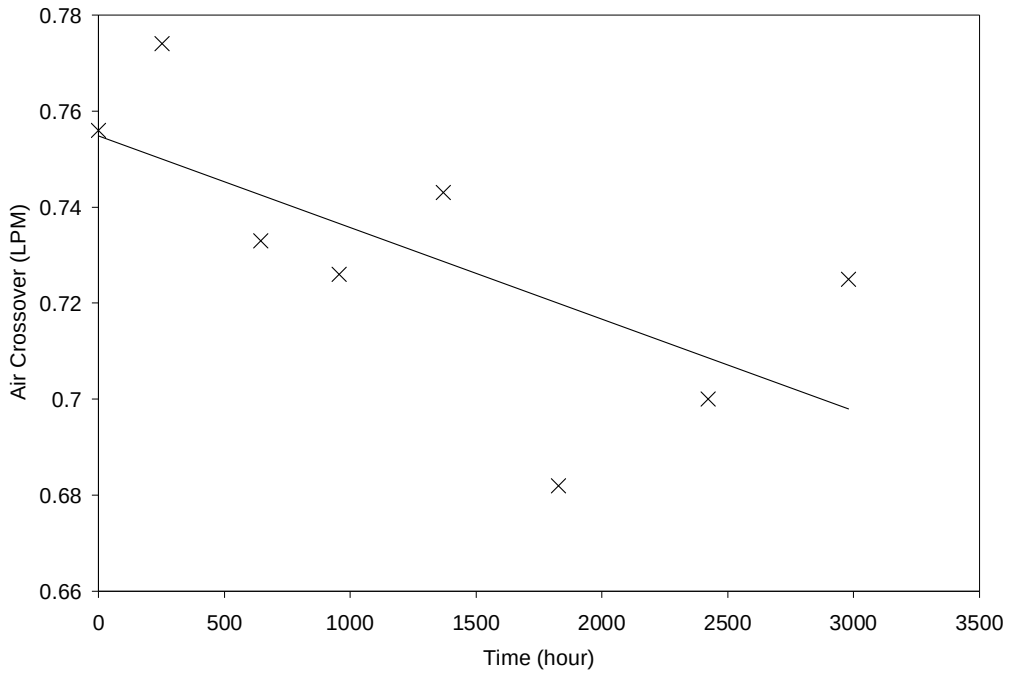

Figure 6-19: Air crossover at 21 kPa for membrane 16 over time during operation on LTDS.

It can be seen that there is a slow decay in water transport performance over time demonstrated by both samples. Both samples showed a decrease in water transport performance of 27% by 3000 hours of operation. As well, there is an overall decreasing trend in the air crossover rate of the membrane over time.

6.8.1.1 Failure Analysis

The decrease in water transport performance was believed to be related to changes in membrane surface over time. The surface silica content, which allows water transport to occur in the membrane, was thought to be changing during the operating life of the membrane. The membrane was analyzed at the beginning of life and at the end of life under SEM and EDS to compare the change in the surfaces of the membranes over time. Observing the BOL membrane in Figure 6-20 it can be seen that the surface is covered with hydrophilic silica held together by a UHMWPE.

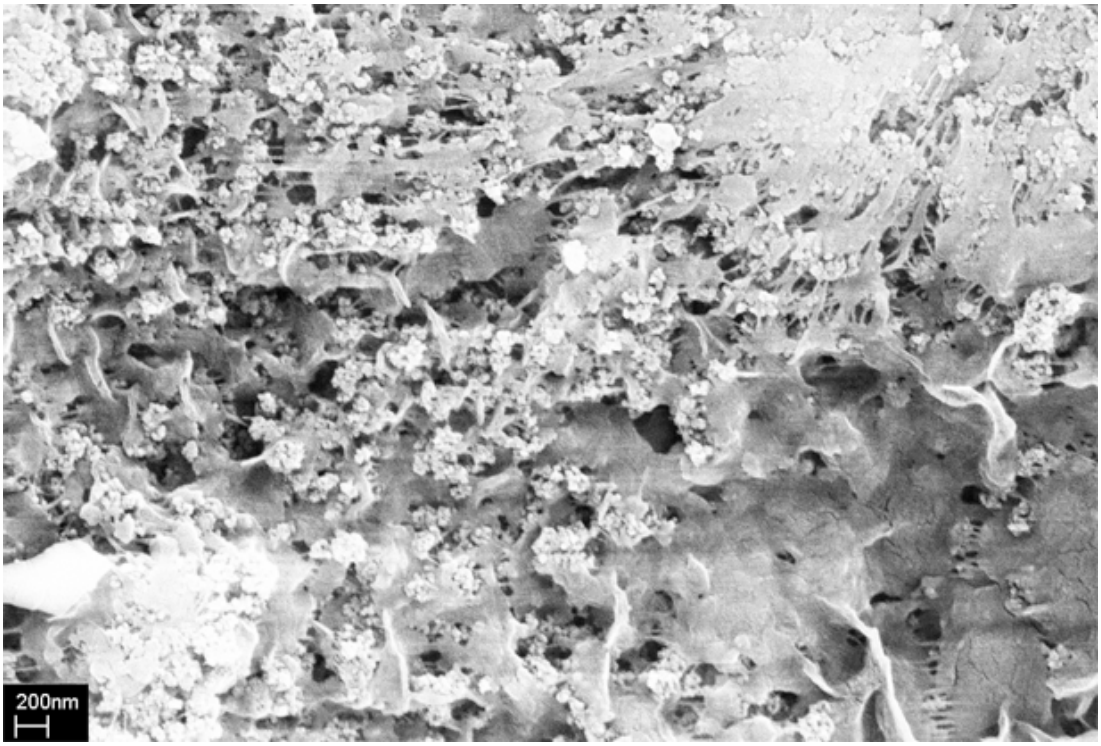

Figure 6-20: Membrane 16 at BOL under SEM at 30000x magnification.

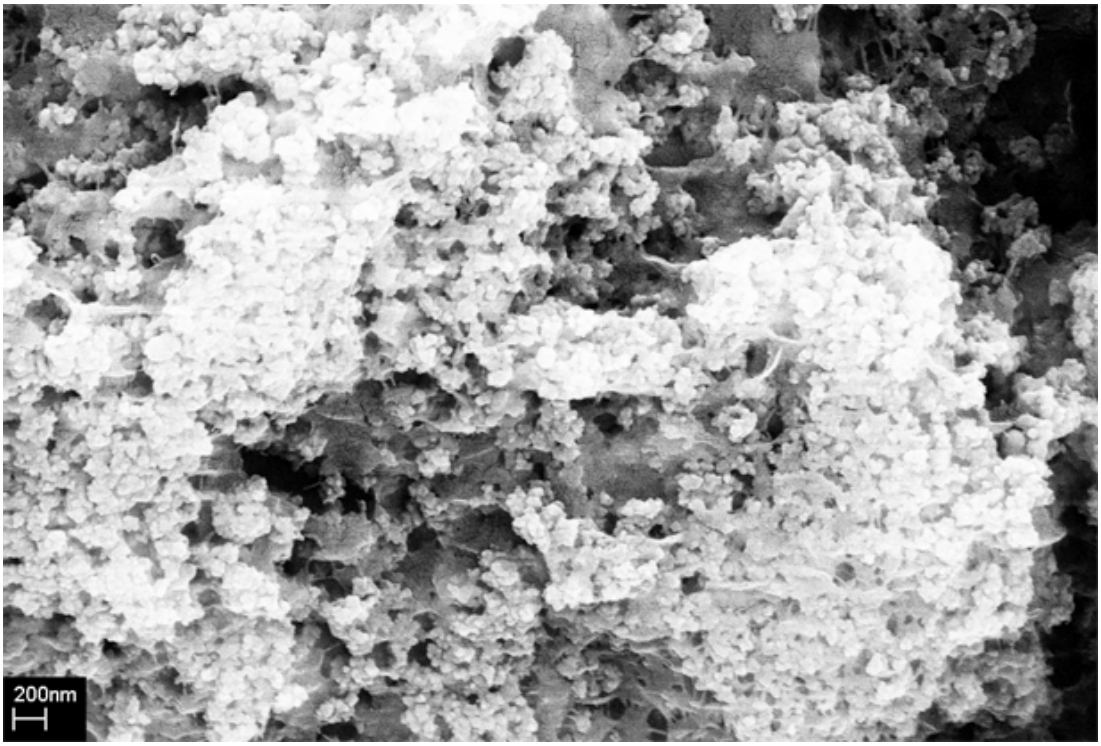

Figure 6-21: Dry side of membrane 16 at EOL under SEM at 30000x magnification.

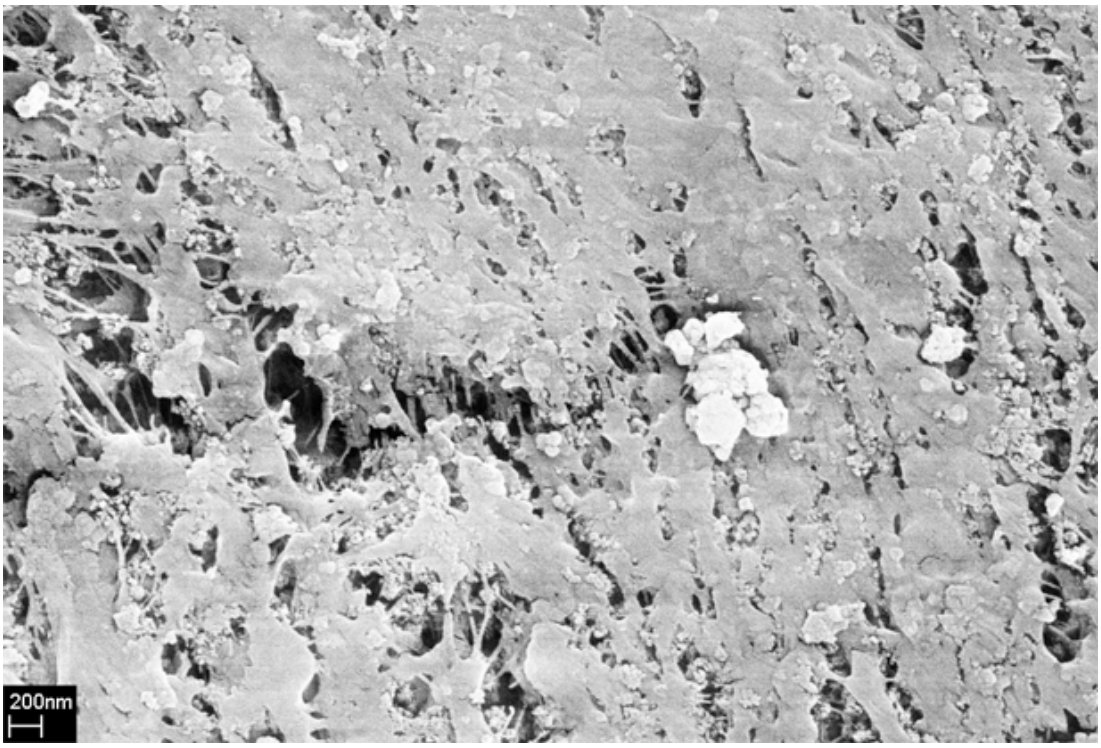

Figure 6-22: Wet side of membrane 16 at EOL under SEM at 30000x magnification.

Similar to the BOL membrane, the dry side surface of the EOL membrane in Figure 6-21 is largely covered in silica. Comparing this to the wet side of the EOL membrane in Figure 6-22 it can be seen that the wet side of the membrane has very little silica on its surface. Rather, the surface is largely polyethylene, with very little silica. With little remaining hydrophilic silica on the wet side of the membrane, less water would be absorbed into the membrane, and thus water transport would decrease. This explains the observed decrease in water transport performance of the membrane over time.

It is still unclear why the two surfaces of the EOL membrane are so different. Water transport in the membrane travels from the wet side of the membrane to the dry side. If the polymer becomes mobile under these hot and wet conditions and it will travel through the membrane in the direction of water transport. Also, the polymer may become mobile and travel with the wet stream, which is passing over the wet side of the membrane, leading to the polymer coating the surface silica on the wet side. Alternatively, the silica may be removed by the hot wet stream passing over the membrane.

EDS data were obtained for the BOL and EOL membranes on the wet and dry sides. This data is presented in Table 6-1. The silicon content on the wet side has certainly decreased,

while the carbon content has increased. This confirms what has been observed in the SEM images, that silica has been lost from the wet side of the EOL membrane.

Table 6-1: EDS results for Membrane 16 at BOL and EOL.

Membrane	Side	Average Atomic %		
		Carbon	Oxygen	Silicon
Membrane 16 BOL	N/A	50.3	34.9	14.9
Membrane 16 EOL	Dry	36.9	45.2	17.8
Membrane 16 EOL	Wet	66.3	25.2	8.5

The cross-section of the EOL membrane was also observed under SEM, as shown in Figure 6-23. EDS data was recorded across the cross-section of the membrane at locations designated by boxes in Figure 6-24.

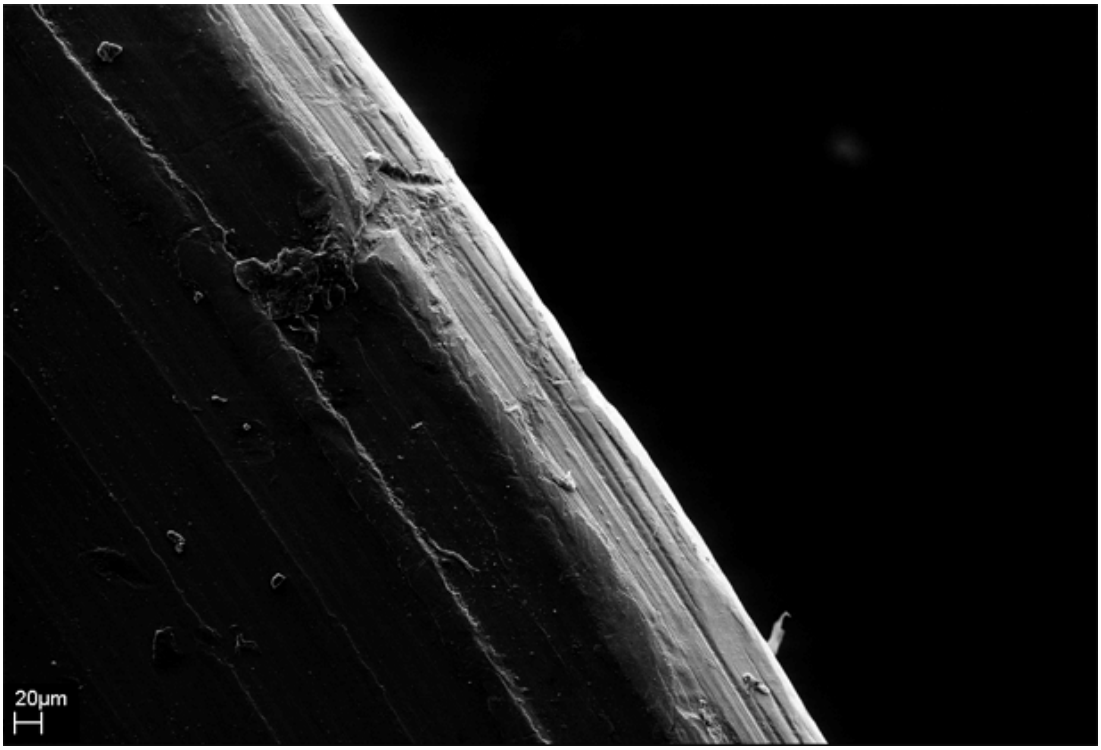

Figure 6-23: Cross-section of membrane 16 at EOL at 250x magnification.

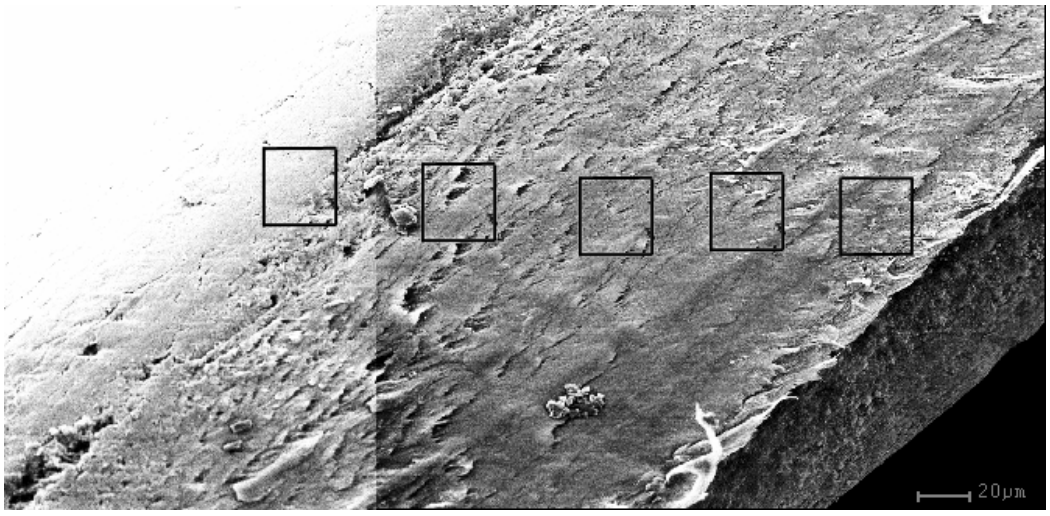

Figure 6-24: Cross-section of membrane 16 at EOL, at 1000x magnification, the boxes indicate the location of EDS scans.

The atomic carbon and silicon content across the membrane cross-section were analyzed by EDS. These results were compiled and plotted as a percent distance across the membrane as shown in Figure 6-25. The ratio of atomic carbon to silicon across the membrane cross-section is plotted in Figure 6-26.

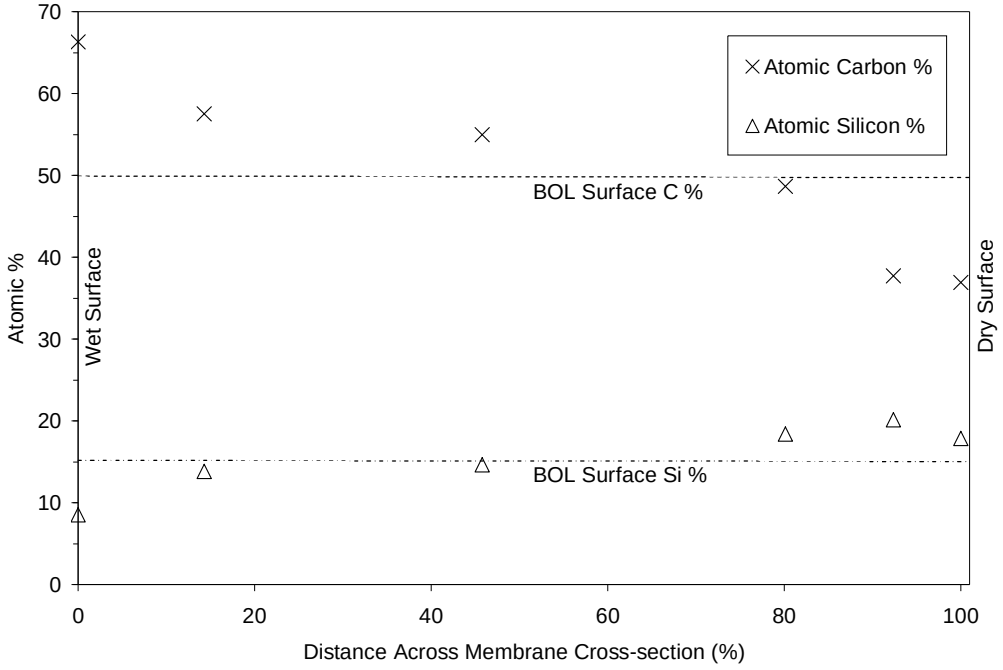

Figure 6-25: Atomic percentages of carbon and silicon through a cross-section of membrane 16 at the EOL.

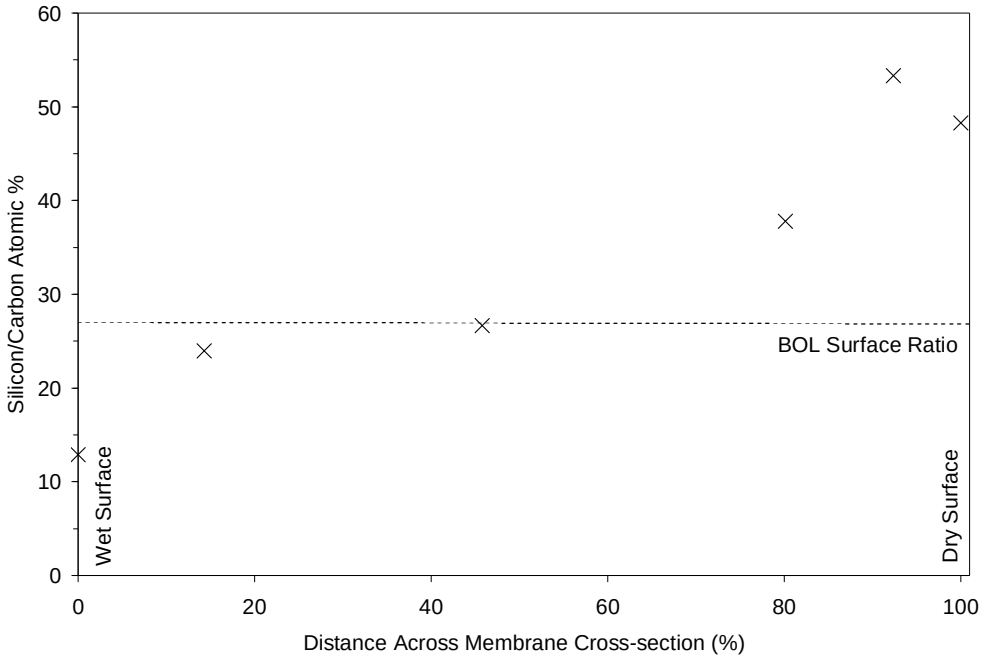

Figure 6-26: Ratio of silicon to carbon through a cross-section of membrane 16 at EOL.

Figure 6-25 and Figure 6-26 show a trend of decreasing silica content from the dry to the wet surface, and increasing carbon content from the dry to the wet surface.

If the polymer has become mobile within the membrane under operation, then it would move from wet surface to the dry surface along the direction of water transport. However, if this were the case then the carbon content would be increased on the dry side rather than on the wet side, which has not occurred. However if the polymer becomes partially mobile and begins to travel within the membrane from the wet side to the dry side but accumulates part way through the membrane, it will form a barrier the water transport. With the polymer moving away from the wet surface, the silica will no longer have the polymer matrix to support it, and will be easily removed by the wet gas flowing across the membrane surface. This causes the loss of silica observed on the wet surface. This phenomena is summarized in Figure 6-27.

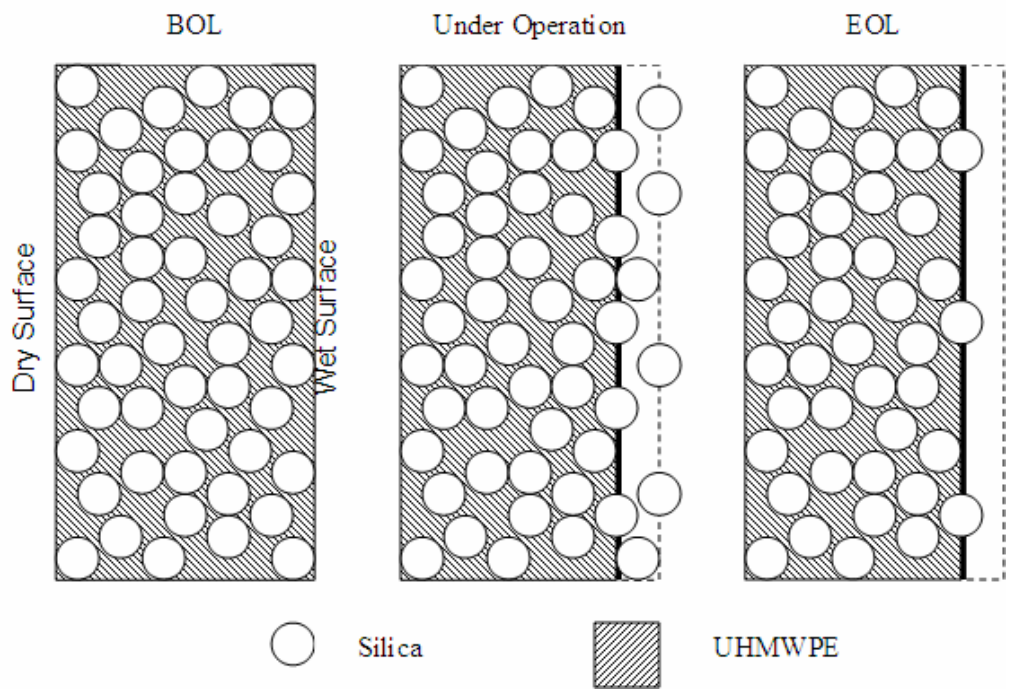

Figure 6-27: Movement of polyethylene in the membrane 16 under operation leading to loss of silica on the wet side of the membrane.

A sample of material was collected from the effluent from a humidifier created with membrane 16. This material was a black power when dried. The material was observed under SEM and its composition was analyzed using EDS. The results indicated that 22% of this material was silica (SiO_2), which would indicate that silica is indeed being lost from the membrane during operation.

The EOL membrane has a layer of polymer on its wet surface, the silica has been lost from this surface due to the movement of the polymer matrix, and water transport rates have decreased. This would also explain why the gas crossover rate has decreased over time as observed in Figure 6-19, the polymer layer has formed a barrier and the pore structure of the polymer in this layer in lost, and gas has limited access to the porous silica content of the membrane. The membrane was flipped over and tested with the used dry side (with no loss in silica) acting as the wet side, however no improvement in water transport was observed. This would indicate that the polymer barrier has formed on the used wet surface, and the decrease in performance was perminant.

A mitigation strategy in which the polymer to silica ratio is altered was proposed. Decreasing the polymer content may extend the time before the polymer migrates enough

to form a barrier to water transport. Alternatively membranes with greater polymer content may allow the polymer matrix to maintain intact under operation. This would prevent the polymer from becoming mobile, preventing a barrier to forming. However, large increases in polymer content might decrease the initial water transport performance of the membrane. Membranes with various silica and to polymer ratios are under development by the supplier.

6.8.2 High Temperature Durability Testing

Membrane 16 was tested on the HTDS, however it demonstrated cracking before 300 hours. The cracking of membrane 16 experienced on the HTDS is shown in Figure 6-28.

Figure 6-28: Cracking of membrane 16 after 300 hours of operation on HTDS.

6.8.2.1 Failure Analysis

Membranes operating on the HTDS are subjected to hotter and dryer conditions than those membranes operated on the LTDS. Under these conditions, environmental stress cracking may be caused by oxidation of the polymer material. This led to embrittlement of the membrane and the cracking observed in Figure 6-28 occurred. BOL and EOL membrane samples were tested for mechanical strength. The time to breakage, or elongation would be a good indication of whether polyethylene oxidation had occurred. Stress-strain curves for membrane 16 at BOL and EOL on the HTDS is shown in Figure 6-29. The EOL membrane, being much more brittle breaks at less than 4% strain, while the new membrane does not break beyond 6% strain. This indicates that polymer oxidation has occurred in the EOL membrane, leading to the weakening of the membrane, cracking, and failure.

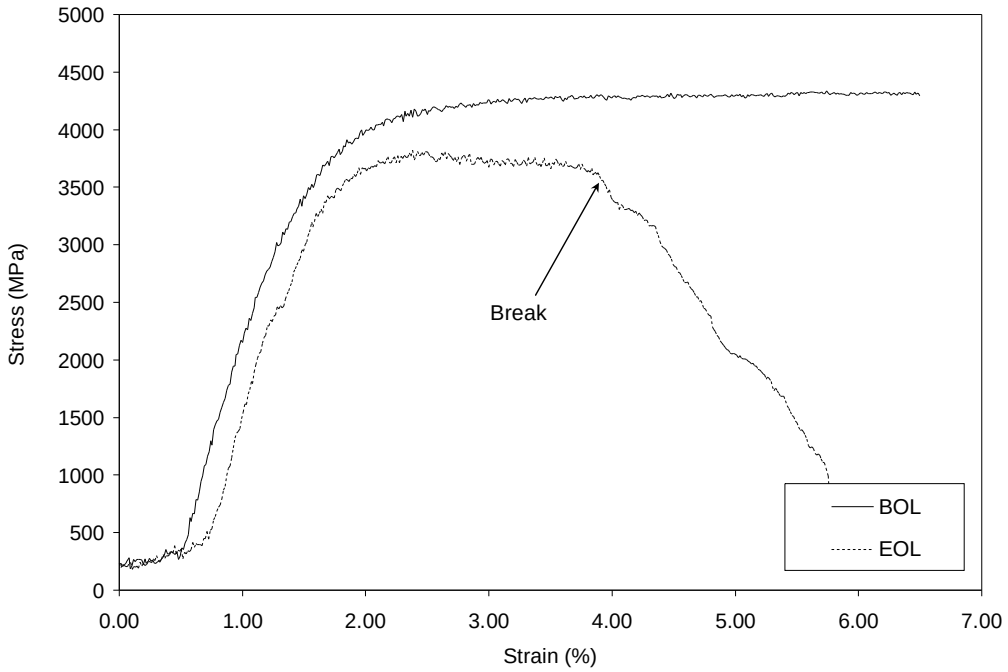

Figure 6-29: Membrane 16 tensile testing for BOL and EOL material from the HTDS.

6.9 Membrane 20

Membrane 20 consisted of silica and UHMWPE in a ratio of 2.51 to 1, with 20% by weight antioxidant coating. This material was the same as membrane 16; accept for the addition of antioxidant. Experiments summarized in section 5.5 indicated that the antioxidant coating helped prevent degradation of the polyethylene chain, and so it was hoped that membrane 20 would have a longer performance lifetime than membrane 16.

6.9.1 Low Temperature Durability Testing

Membrane 20 was operated on the LTDS; however after less than 20 hours of operation the membrane demonstrated a significant decrease in performance, as shown in Figure 6-30. The wet bulb temperature at stream 2 is directly related to the water transport in the humidifier module, decreasing wet bulb temperature over time indicates a decrease in water transport performance over time. The decrease is very rapid indicating a significant loss of water transport over a short period.

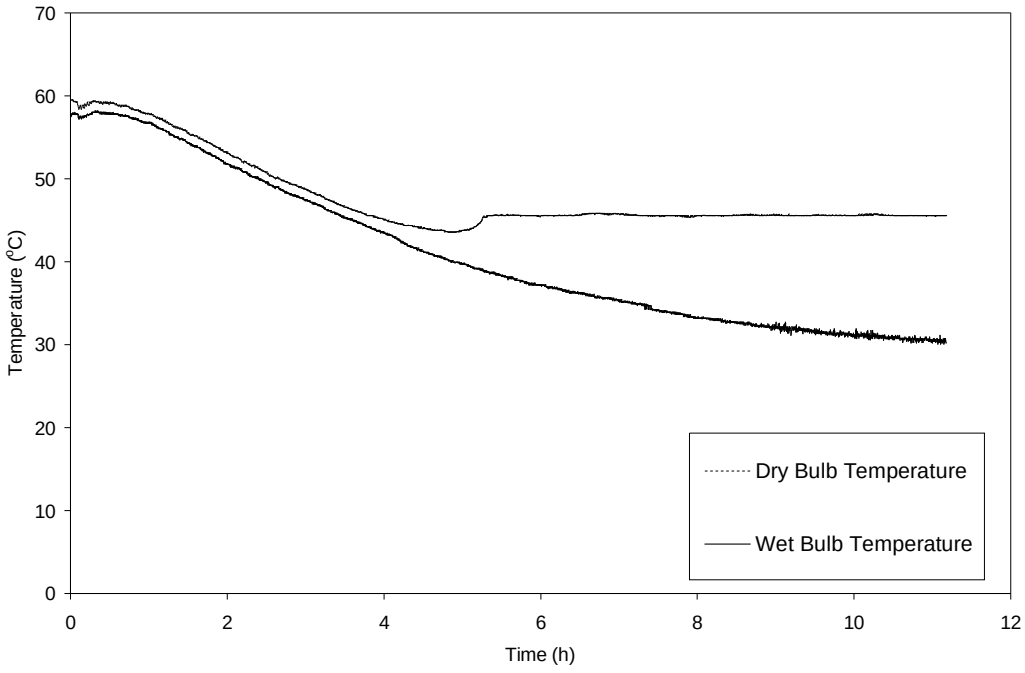

Figure 6-30: Stream 2 wet and dry bulb temperature for membrane 20 from BOL to 11 hours of operation.

6.9.1.1 Failure Analysis

Membrane 16 was essentially the same membrane as membrane 20, except that membrane 20 had an antioxidant coating. Since membrane 16 did not demonstrate this large decrease in performance over the first 10 hours of operation, it was believed that the antioxidant coating was related to the failure of the membrane. Membrane 20 was analyzed under SEM at BOL and after failure, the results can be observed in Figure 6-31 through Figure 6-33.

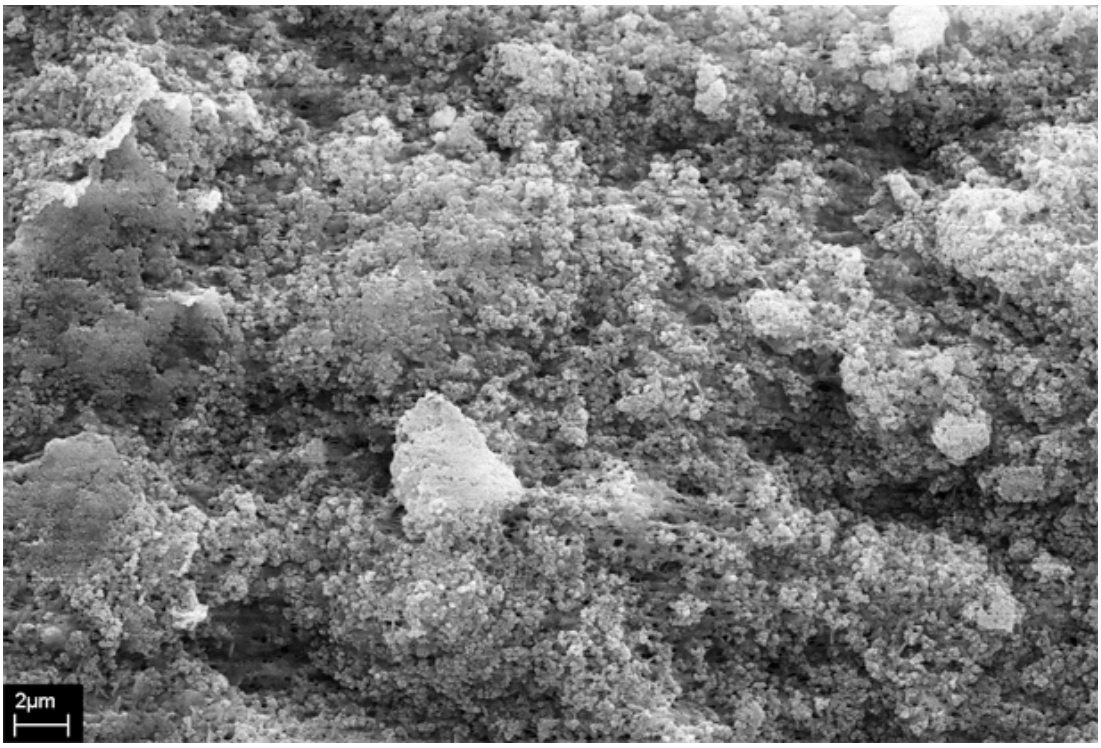

Figure 6-31: Membrane 20 under SEM at 5000x magnification at BOL.

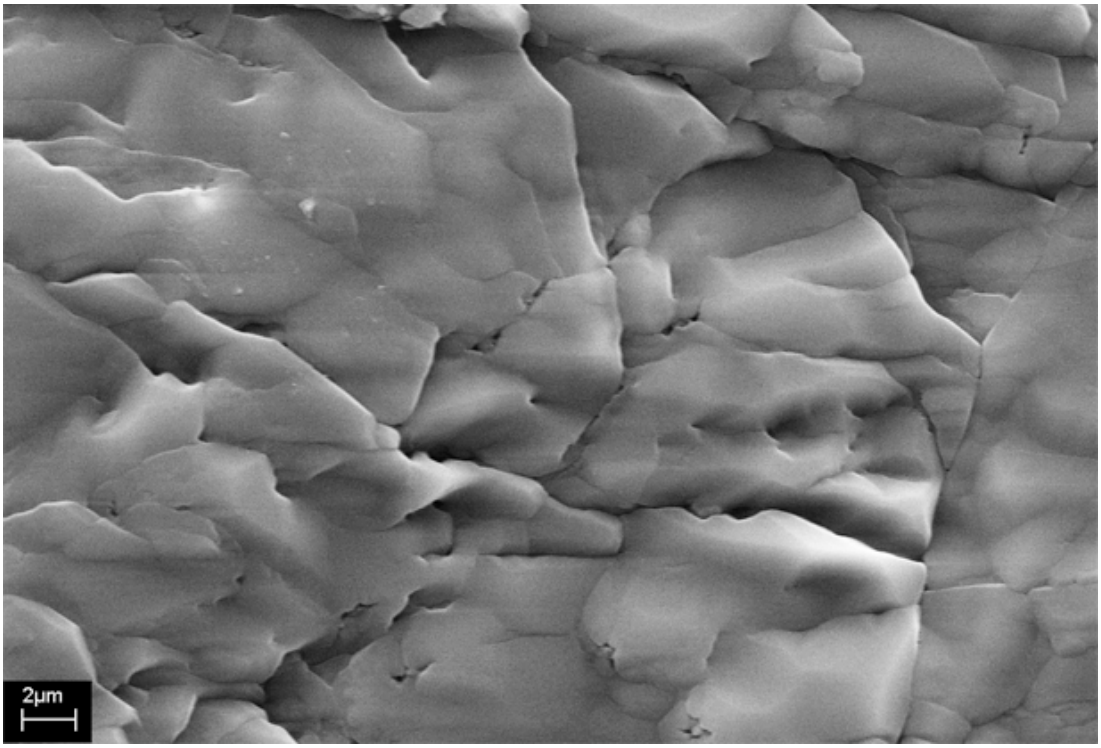

Figure 6-32: Dry side of membrane 20 after 20 hours of operation, under SEM at 5000x magnification.

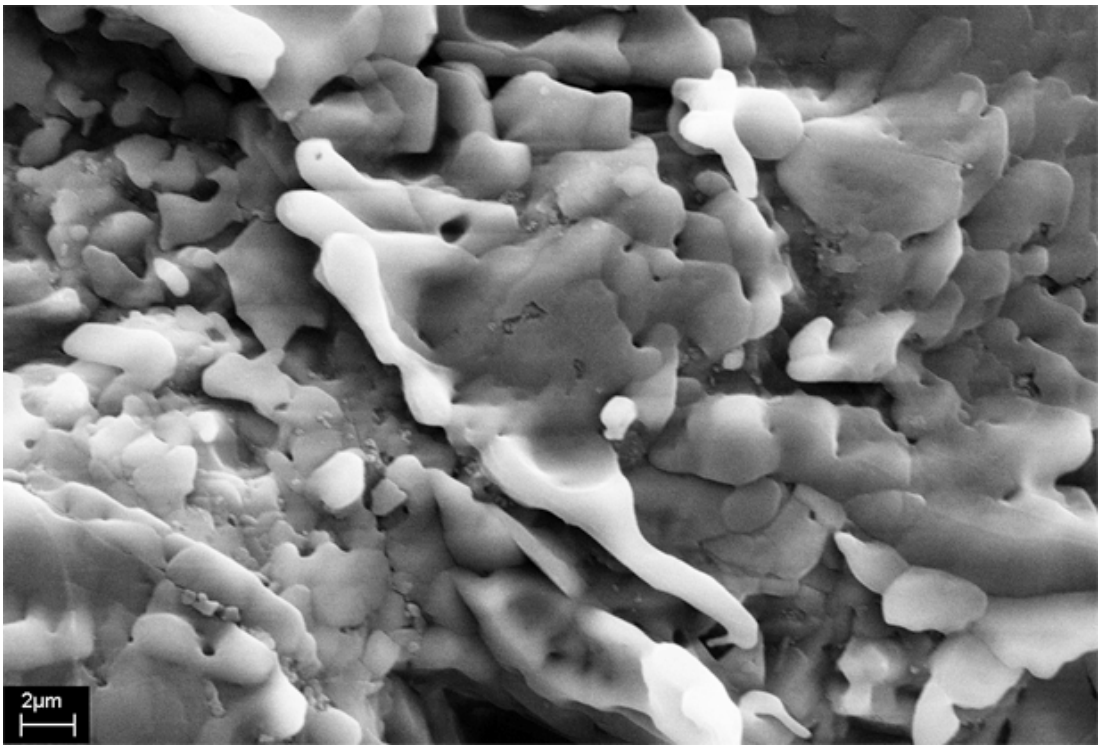

Figure 6-33: Wet side of membrane 20 after 20 hours of operation, under SEM at 5000x magnification.

From the SEM images it is obvious that there has been a large change in the morphology of the membrane surface from BOL to after 20 hours of operation on both the wet and dry sides of the membrane. In the used samples it appears that scale-like fouling has covered the membrane surface, this was not present on the new membrane surface. It is believed that the scaling effect observed on the surface of the used membrane in Figure 6-32 and Figure 6-33 was caused by the antioxidant coating which has been added to the membrane. Observing the membrane surface from a lower magnification in Figure 6-34 it can be seen that this coating is covering large portions of the membrane surface, with some patches of silica still present. This interface is shown in detail in Figure 6-35 and Figure 6-36.

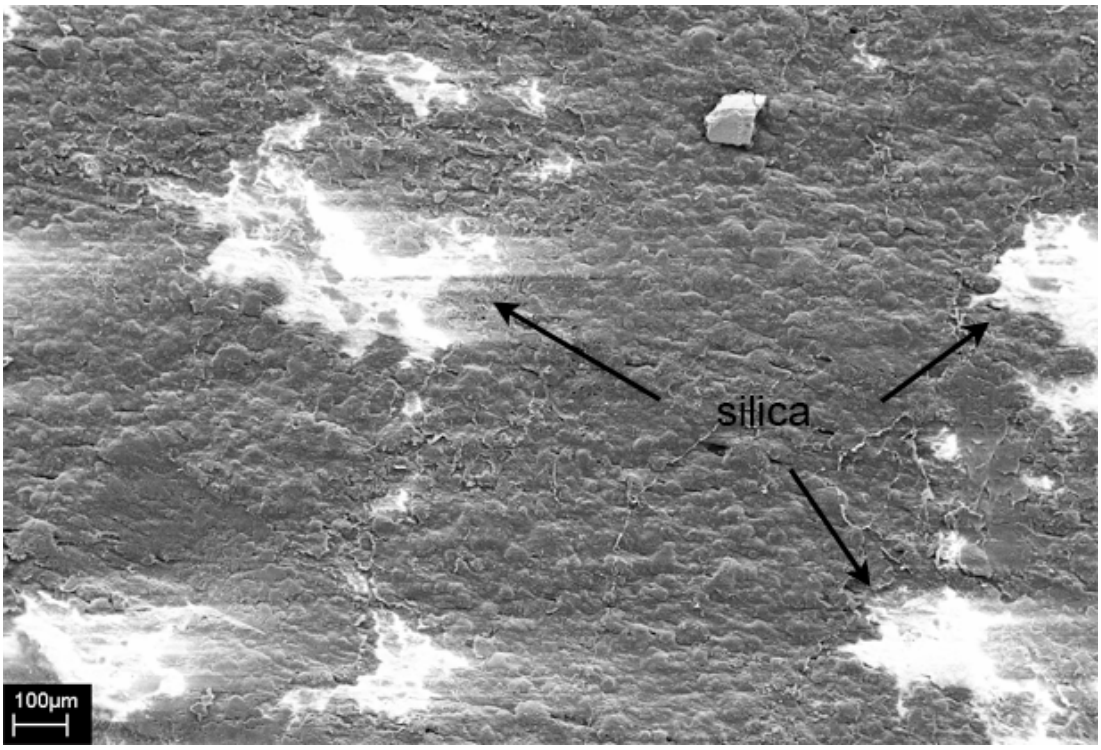

Figure 6-34: Membrane 20 after 20 hours of operation, at 100x magnification, surface is largely coated, with some areas of exposed silica.

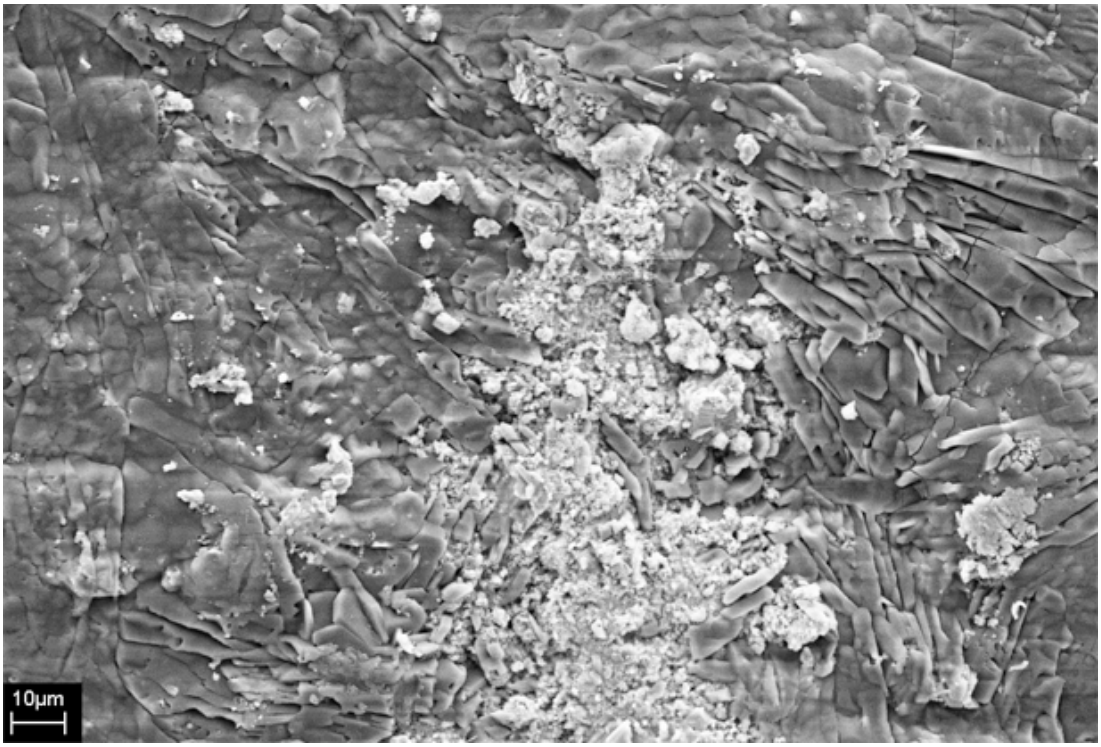

Figure 6-35: Membrane 20 after 20 hours of operation, at 1000x magnification showing interface between the silica and the fouling covering the membrane.

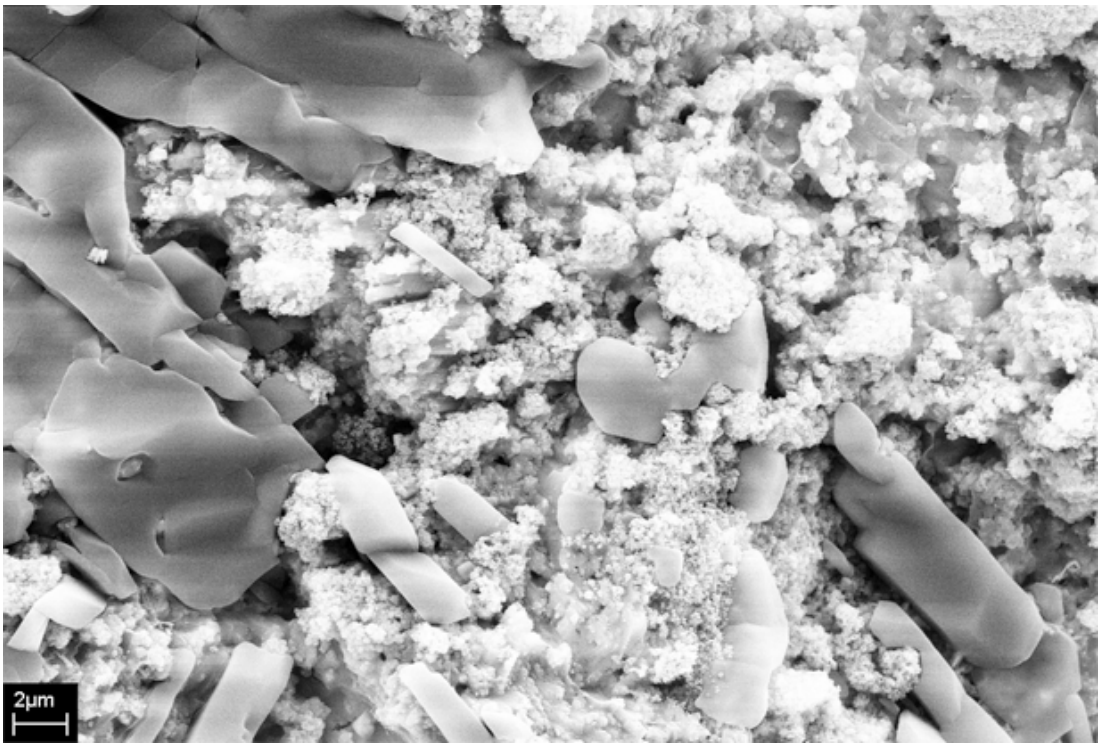

Figure 6-36: Membrane 20 after 20 hours of operation, at 5000x magnification showing interface between the silica and the fouling covering the membrane.

The failure mechanism appears to be that the antioxidant coating has caused fouling, forming a barrier on the surface of the membrane, which is blocking a large portion of the silica sites from contact with the gas streams passing over the membrane. This would cause a decrease in the membranes ability to adsorb and transport water from one side of the membrane to the other, leading to the decrease in water transport observed in Figure 6-30. Evidently the antioxidant coating is detrimental to the long term operation of the membrane, and should not be used.

6.10 Membranes 21 to 24

Membranes 21 to 24 were the same composition as membrane 15; they had a silica to polyethylene content of 2.5 to 1, and contained 15% plasticizer content. However each membrane, 21 through 24 contained a different plasticizer oil. These oils were labels A through D. The membranes were tested to see if the rapid performance degradation failure observed with membrane 15 could be mitigated by using a different type of plasticizer.

6.10.1 Low Temperature Durability Testing

The membranes were tested for water permeation performance at zero hours, and then placed on the durability station of 15 hours of operation. The results for each membrane as displayed in Figure 6-37 through Figure 6-40.

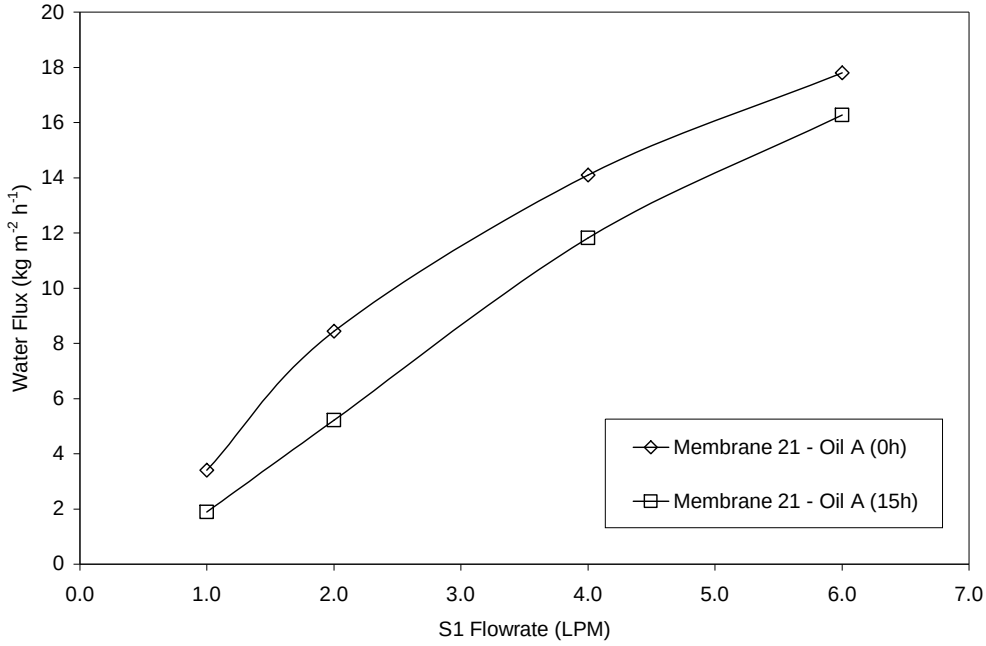

Figure 6-37: Water transfer performance of membrane 21, containing 'Oil A' at BOL and after 15 hours of operation.

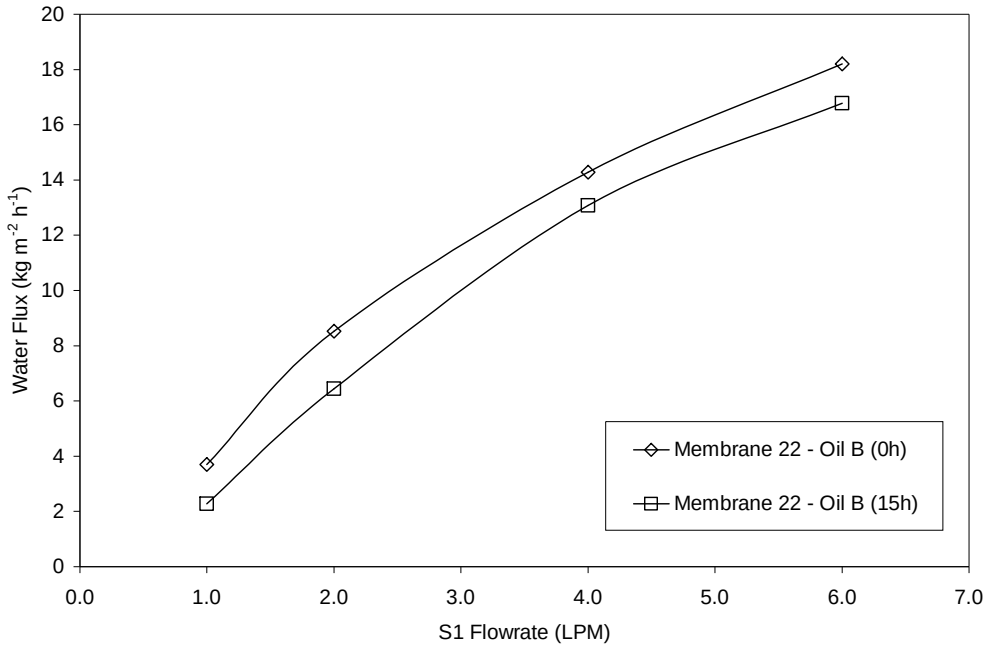

Figure 6-38: Water transfer performance of membrane 22, containing 'Oil B' at BOL and after 15 hours of operation.

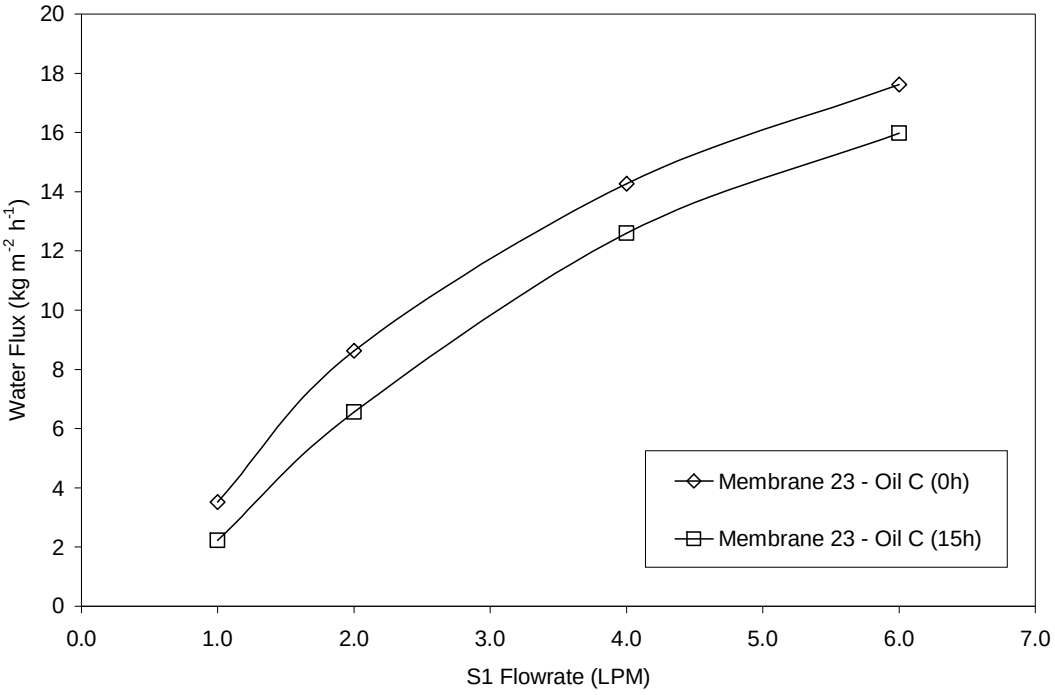

Figure 6-39: Water transfer performance of membrane 23, containing 'Oil C' at BOL and after 15 hours of operation.

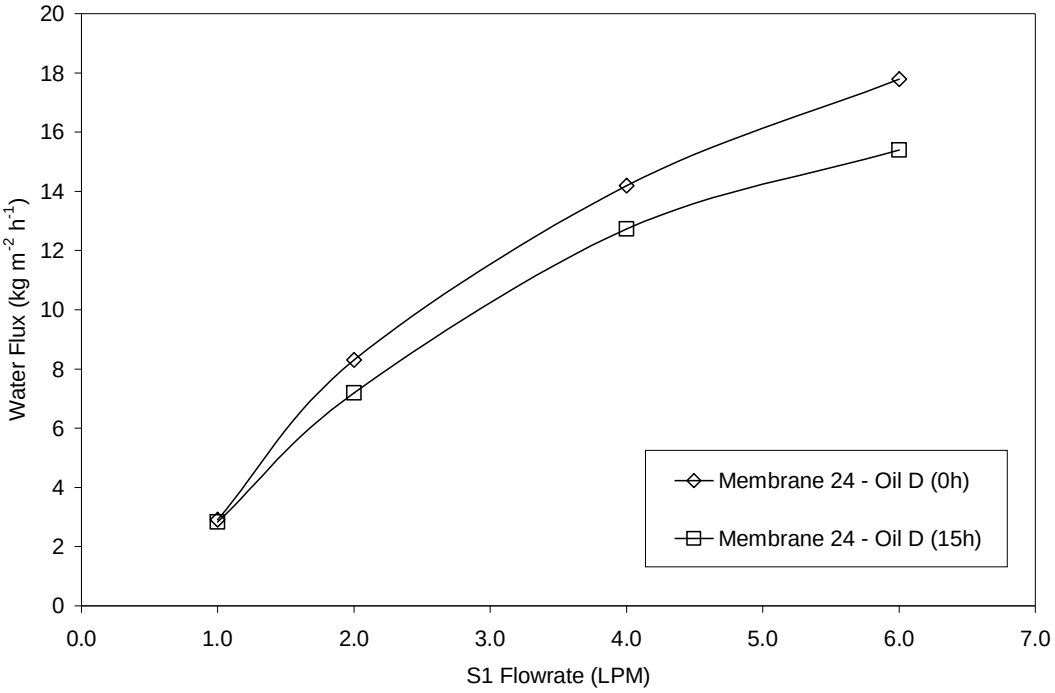

Figure 6-40: Water transfer performance of membrane 24, containing 'Oil D' at BOL and after 15 hours of operation.

All membranes demonstrated a drop in performance over time, the water transfer performance decreases are summarized in Table 6-2.

Table 6-2: Performance decrease in membranes with different plasticizer oil types over 15 hours of LTDS.

Membrane	Oil	Percent Decrease in Performance from BOL at 15 hours (%)
Membrane 21	Oil A	8.5
Membrane 22	Oil B	7.8
Membrane 23	Oil C	9.4
Membrane 24	Oil D	13.4

All membranes with plasticizer content demonstrated a decrease in performance in the first 15 hours. This would indicate that the failure mechanism caused by the plasticizer oil in membrane 15 occurs in all polyethylene and silica membranes containing substantial amounts of residual plasticizer oil. In order to mitigate this problem, these types of membranes were thoroughly washed in hexane before use in any subsequent testing.

6.11 Membrane 32

This membrane was sulphonated PEEK membrane on a porous polyethylene backbone material. The laminate material would offer the transport, selectivity, and temperature tolerance of the s-PEEK material, while the support layer would offer increased mechanical strength.

6.11.1 Low Temperature Durability Testing

Membrane 32, demonstrated good initial water transport performance, however before the transport test could be completed, the membrane demonstrated a decrease in performance.

6.11.1.1 Failure Analysis

After removing the membrane from the test module it was evident that the s-PEEK layer had detached from the porous substrate, as observed in Figure 6-41.

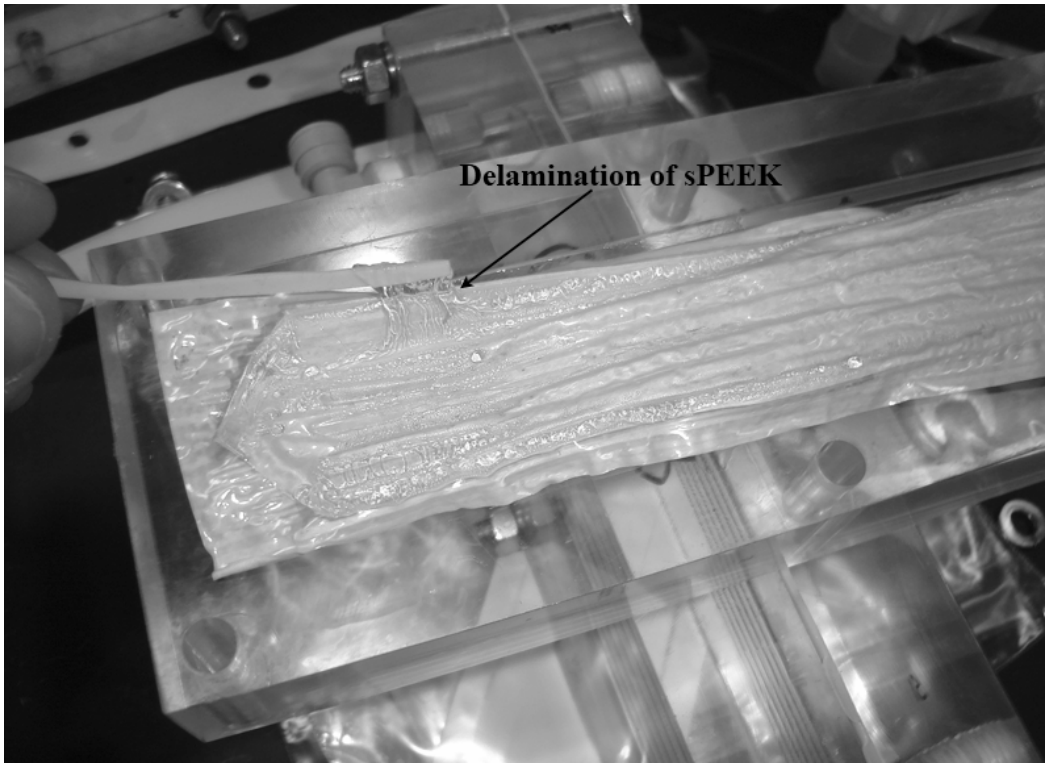

Figure 6-41: Delaminating of s-PEEK from porous substrate in membrane 31, after 1 hour of operation at stream 3 temperature of 75^{o}C, 100% RH.

This material obviously could not be used in a fuel cell humidifier. Further development of a material which will not delaminate is underway at the supplier.

6.12 Membrane 40

The membrane consisted of expanded PTFE material, and acts as an ion exchange membrane. The membrane expands to some extent in the presence of water.

6.12.1 Low Temperature Durability Testing

The membrane was tested for 1000 hours, and demonstrated failure in performance over time, as shown in Figure 6-42.

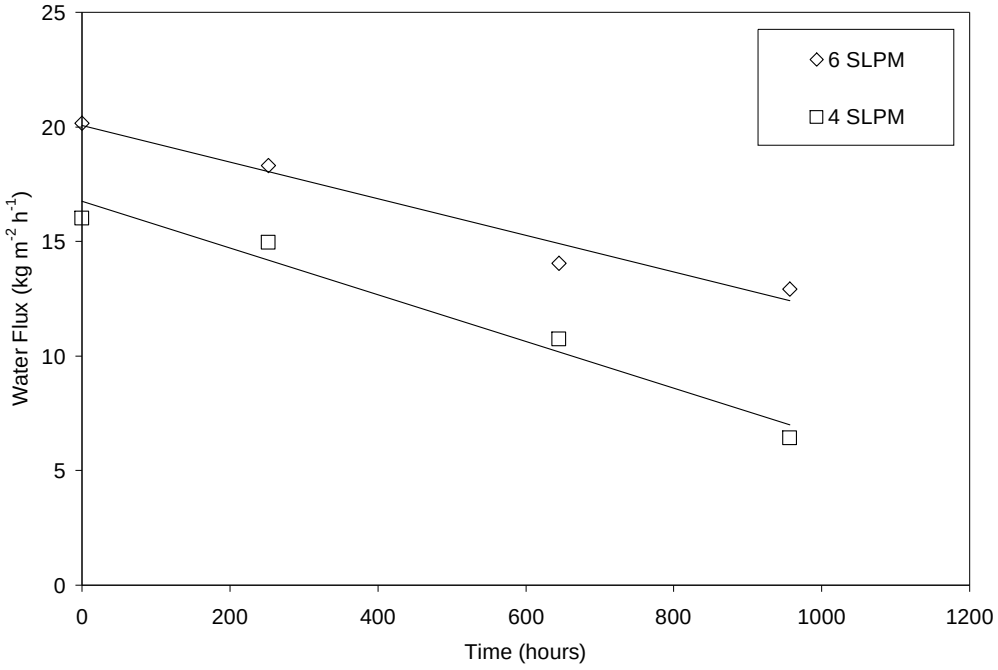

Figure 6-42: Degradation in water transport performance for membrane 40 over time on the LTDS.

6.12.1.1 Failure Analysis

New and used samples of the membrane were analyzed under SEM as shown in Figure 6-43 and Figure 6-44. The BOL membrane appears to have a rather smooth surface, while

the membrane which was operated on the LTDS for 1000 hours demonstrates at mottled surface. It seems as though the membrane has either absorbed foreign material, or else the membrane is swelling and 'bubbling' and separation is occurring within the membrane layers.

EDS studies on the membrane at BOL and after 1000 hours indicated similar atomic distributions of carbon, oxygen, and fluorine in the membrane before and after operation. However the membrane which had been operated for 1000 hours contained approximately 1.06 atomic percentage of aluminum. There is a possibility that some aluminum ion contamination has entered the membrane from fittings on the LTDS system which may account for some of the failure observed in the performance. However, for the observed spotting in the EOL membrane covers much of the membrane surface, for this to be caused entirely by aluminum ion contamination the atomic percentage of aluminum would have to be much greater than 1%. It is reasonable to believe that the performance loss in the membrane is related to phenomena in addition to aluminum contamination. This may include separation of the polymer layers in within the membrane, causing a disconnection between one side of the membrane and the other, leading to decreased water transport. Further testing of this material is recommended.

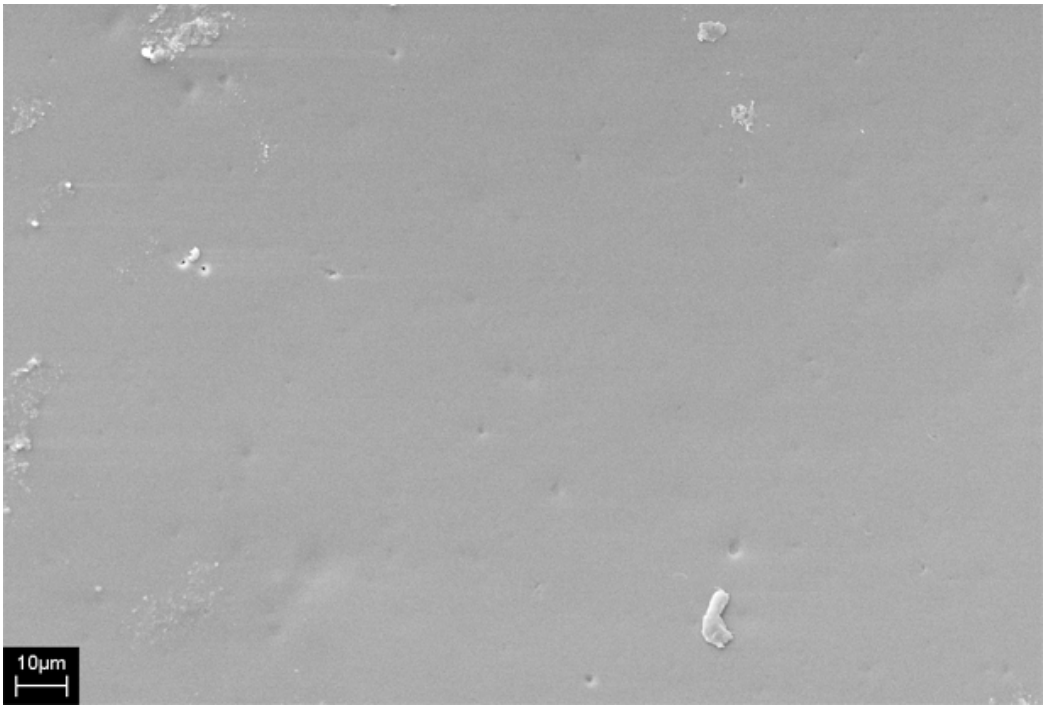

Figure 6-43: Membrane 40 at BOL, under SEM at 1000x magnification.

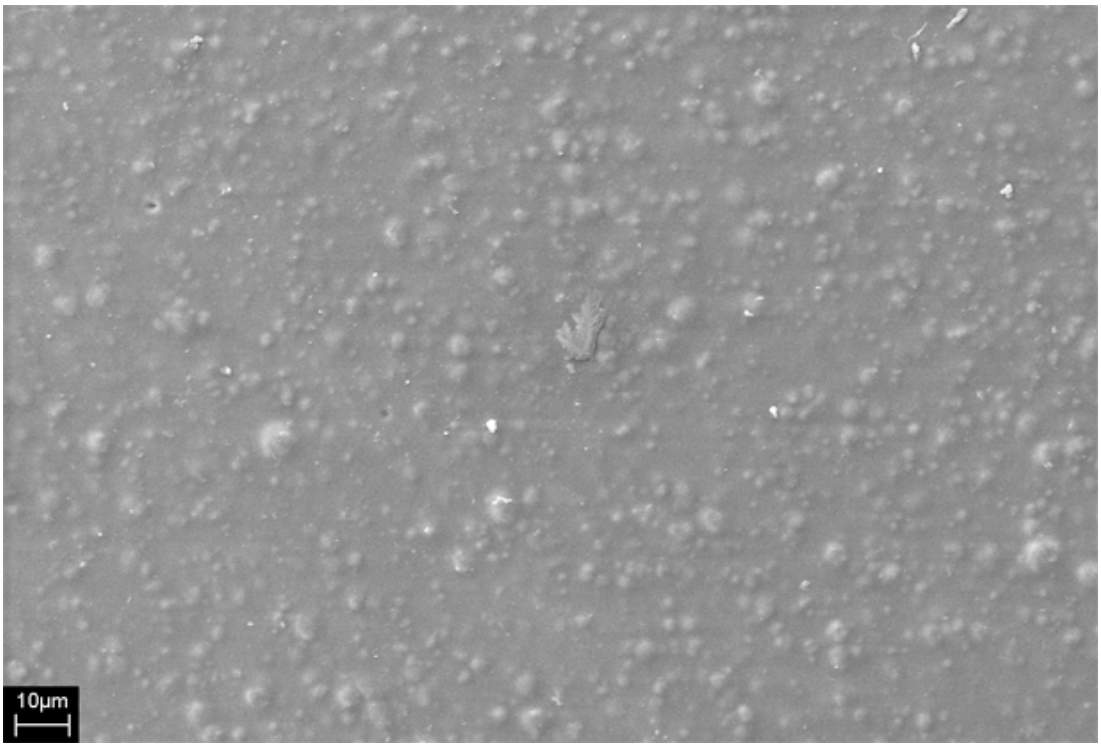

Figure 6-44: Membrane 40 after 1000 hours of operation (EOL) under SEM at 1000x magnification.

6.13 Membrane 43

Membrane 43 was a UHMWPE membrane with a silica additive combined in a ratio of 1 to 0.9.

6.13.1 Low Temperature Durability Testing

The membrane was tested on the LTDS for 3000 hours, as shown in Figure 6-45. The membrane has demonstrated a 22% decrease in performance at 6 SLPM over 3000 hours.

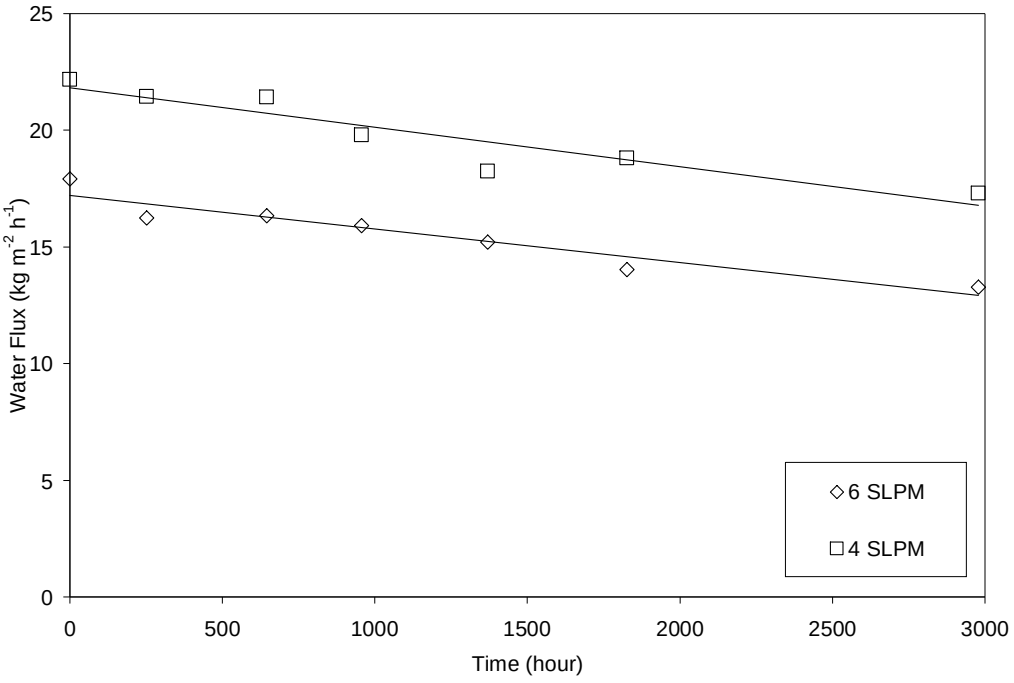

Figure 6-45: Water transport performance of membrane 43 over time on the LTDS.

6.13.1.1 Failure Analysis

The decrease in performance observed is due to the mobility of the polymer under operation. This failure was summarized in Section 6.8.1.1. The silica to polymer ratio was quite low in this membrane (1 to 0.9). This would indicate that increasing the polymer content in the membrane does not prevent the failure mechanism associated with polymer migration.

6.14 Membrane 45

Membrane 45 was similar to membrane 43; it contained UHMWPE and silica in a ratio of 1.0 to 0.7, and has a thickness of 85 microns.

6.14.1 High Temperature Durability Testing

The membrane was tested on the HTDS, however after 400 hours the membrane has cracked, as shown in Figure 6-46.

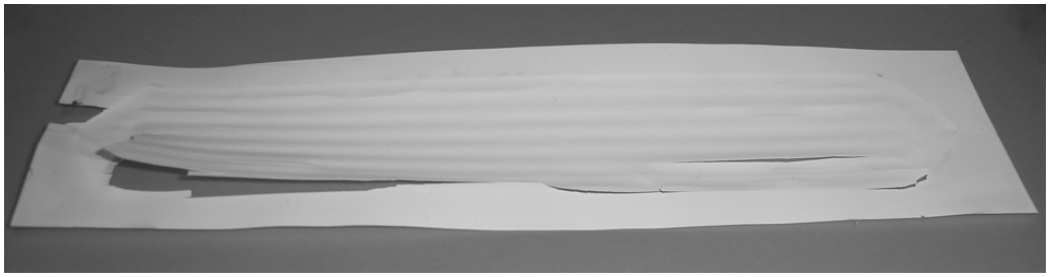

Figure 6-46: Failure due to cracking of membrane 45 on HTDS (sample is 28cm long).

6.14.1.1 Failure Analysis

The cracking phenomena observed is due to environmental oxidation cracking due to the increased temperatures the membrane is subjected to on the HTDS. This membrane will not be appropriate for high temperature operation.

6.15 Membrane 46

Membrane 46 was a nylon based membrane material. It was inherently hydrophilic so it provided excellent water transport. However, it demonstrated high air crossover when dry. Even so, the membrane was tested for durability since it had demonstrated very rapid wetting, and near zero air crossover when wet.

6.15.1 Low Temperature Durability Testing

Membrane 46 demonstrated no significant loss in water transport over 2000 hours of testing, this is shown in Figure 6-47.

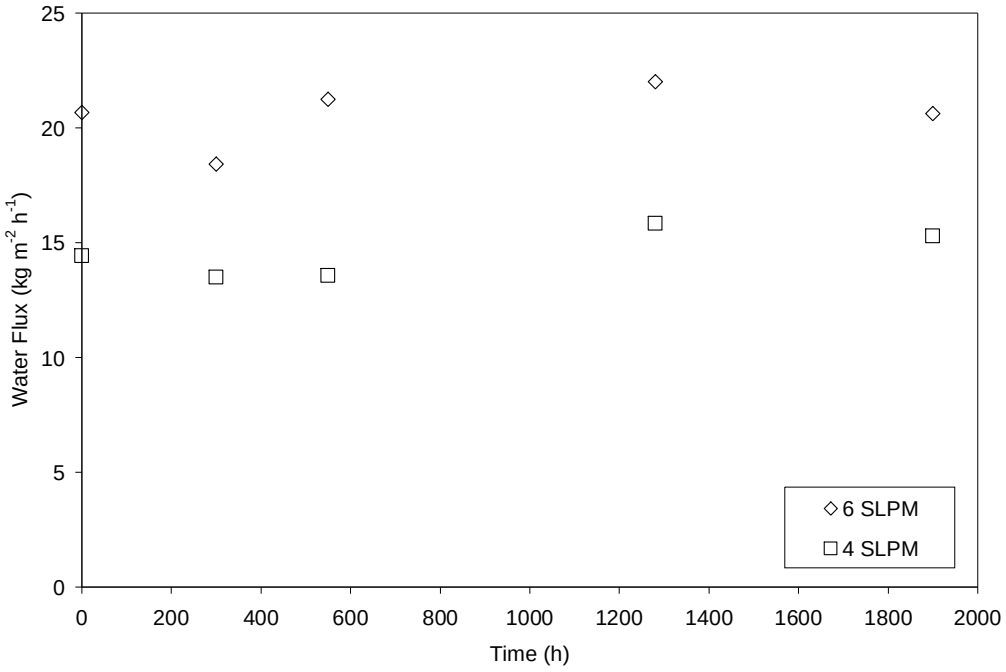

Figure 6-47: Results for membrane 46 on LTDS over 2000 hours.

However the wet crossover increased slightly in this material over this operational period. Further inspection of the used membrane indicated that there was a change in the membrane surface. A photograph of the used membrane surface can be observed in Figure 6-48.

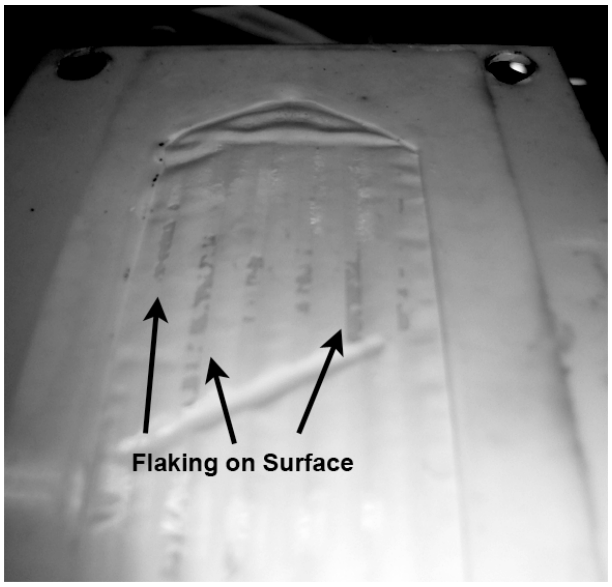

Figure 6-48: Surface of membrane 46 after 2000 hours of operation on the LTDS, flaking of surface can be observed.

It can be seen that the surface of membrane demonstrates a 'flaking' phenomena, in which parts of the polymer have detached from the surface under operation. This would account for the increased wet air crossover of the material over time.

This membrane is a candidate material for use in fuel cell humidifier where high dry air crossover is not an issue. However, further durability testing is recommended to determine if the observed 'flaking' on the surface is an isolated event.

6.16 Membranes 50 through 54

These membranes consisted of s-PEEK with varying quantities of silica additive. Sulphonated PEEK undergoes expansion upon absorbing water.

6.16.1 Low Temperature Durability Testing

Various samples of these membranes were tested for durability on the LTDS; membrane 50 for example demonstrated no significant decrease in water transport performance after 300 hours of operation, as shown in Figure 6-49.

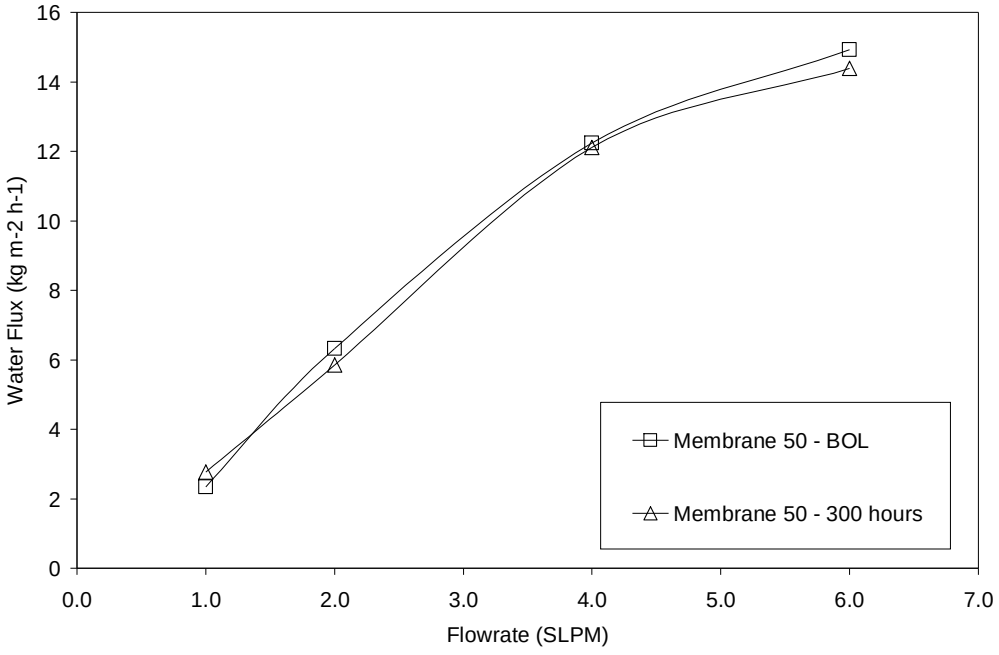

Figure 6-49: Water transport performance for membrane 50 at BOL and 300 hours of operation on the LTDS.

However, after 500 hours of operation, small tears were found in the membrane material, as shown in Figure 6-50.

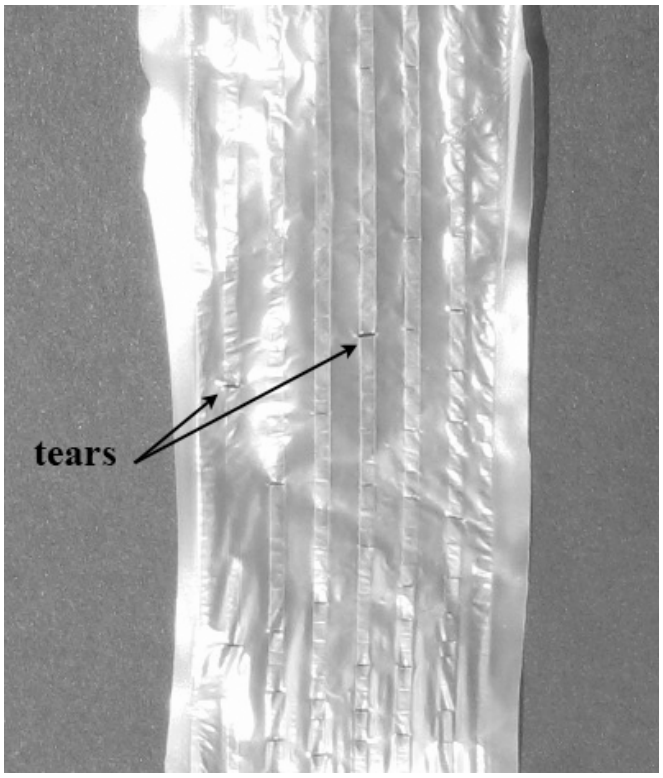

Figure 6-50: Membrane 50 after 500 hours of operation on the LTDS.

This tearing was observed in membranes 49, 51, 53, and 54 as well, these failures occurred before 700 hours of operation.

6.16.1.1 Failure Analysis

The tearing observed occurred at compression points on the membrane along where the flow field channels contacted the membranes. The s-PEEK of which the membranes consisted has the tendency to swell and expand when in contact with water. Under operation the membrane will be expanding and contracting depending on the local concentration of water in the membrane. This would lead to mechanical stresses in the membrane, particularly at points of compression, which over time would lead to the failure of the membrane, due to tearing. This has been observed in the membrane material tested. In order to mitigate this problem the membrane would have to be manufactured with a greater thickness, or else from a more robust material. Alternatively the humidifier assembly would have to account for the dimensional instability of the membrane under

wet conditions.

6.17 Membrane 55

This membrane was a homogeneous ion exchange membrane based on a copolymer of tetrafluoroethylene and sulfonyl fluoride vinyl ether. The membrane absorbs water when it comes in contact with liquid and vapour. The membrane is rather thick compared to similar ion exchange membranes offering it increased mechanical strength under wet conditions.

6.17.1 High Temperature Durability Testing

The membrane performed well over 1000 hours of operation of the HTDS, as shown in Figure 6-51.

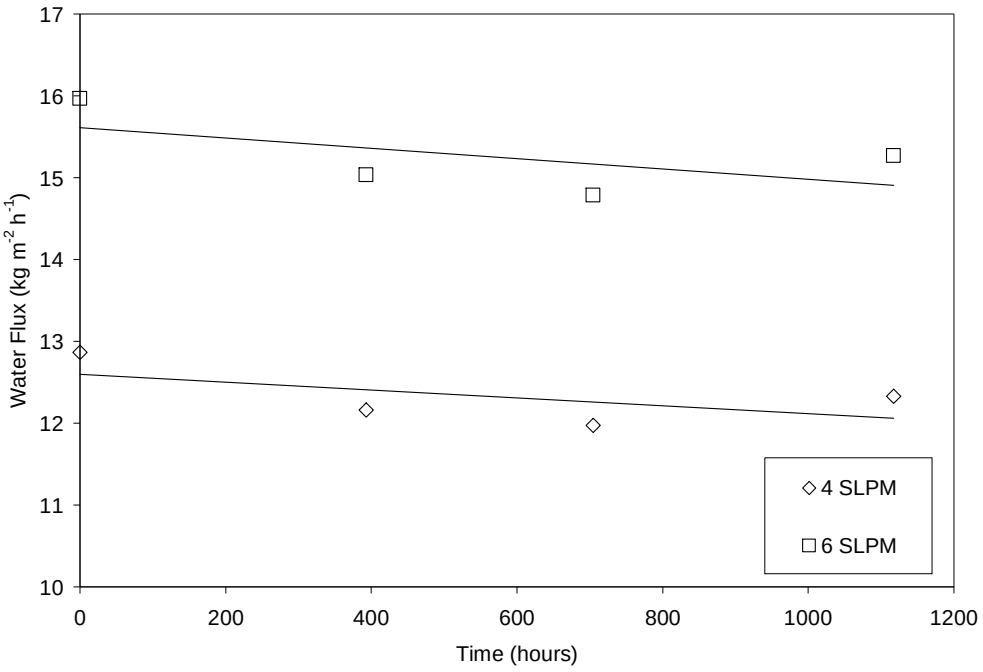

Figure 6-51: Performance of Membrane 55 after 1100 hours of operation on HTDS.

Although the membrane did not demonstrate failure, it had a water transfer performance which was considerably lower than other membranes tested; this was likely due its increased thickness. Also the high cost of the membrane would prohibit it from being considered for humidifier manufacture. Under these concerns, it was decided that the

membrane should be rejected, and no further testing was completed.

6.18 Summary of Durability Results

A summary of the membranes tested on the LTDS and HTDS is shown in Table 6-3 and Table 6-4 respectively, below.

Table 6-3: Summary of membranes tested on the LTDS with failures, failure mechanisms and recommendations.

Membrane	LTDS (hours to failure)	Failure	Failure Mechanism	Mitigation Strategy or Recommendation
2	730	Decrease in water transport	Loss of wetting agent	Membrane is not appropriate due to leaching of wetting agent
4	550	Decrease in water transport	Loss of wetting agent	Membrane is not appropriate due to leaching of wetting agent
8	3000+	Decrease in water transport	Loss of hydrophilic silica additive on wet side of membrane	Membrane is appropriate for low temperature operation for short lifetimes (<2000 hours)
10	558	Deformation of the membrane	Changes in the dimensional stability of the laminated materials.	Membrane is not appropriate for the humidifier in the current embodiment, may be considered for alternative humidifier designs
12	400	Decrease in water transport	Loss of hydrophilic groups graphed to the base polymer	Membrane is not appropriate for humidifier application

15	20	Decrease in water transport	Plasticizer oil interaction with membrane surface blocking water transport	Hexane washing restores performance, membranes should be washed in appropriate solvent prior to usage
16	1500 to 2500	Decrease in water transport	Mobility of polymer, leads to loss of silica, and loss of porous structure of the membrane, forming a barrier to water transport	Membrane is appropriate for lower temperature operation for limited lifetimes (<2000 hours) Membranes with altered silica to polymer ratios may allow increased lifetimes.
20	20	Decrease in water transport	Anti-oxidant additive forms 'skin' over membrane surfaces, creating a barrier to water transport	Anti-oxidant coating does not extend operational lifetime due to negative surface interactions
21 – 24	20	Decrease in water transport	Plasticizer oils interact with membrane surface blocking water transport	Four different oils, demonstrate no benefit over standard oil, all must be removed from the membrane via solvent washing prior to usage
32	2	Deformation of membrane	s-PEEK laminate layer detached from substrate	Membrane is not appropriate for humidifier applications, if a stable laminate membrane can be developed, the membrane may become a candidate material

40	1000	Decrease in water transport	Contamination, or else deformation of material, leading to 'bubbling' in polymer, causing lower water transport	Further testing of membrane is recommended, however the current results indicate the membrane will not be appropriate for the application
43	3000	Decrease in water transport	Mobility of polymer forming barrier to water transport	Membrane is appropriate for low temperature operation for limited lifetimes (< 2000 hours)
46	2000	Increase in wet air permeation	Detachment of polymer from surface	Membrane may be a candidate material, further testing is recommended
50 – 54	300 and 700	Increase in air permeation	Tearing of membrane due to expansion and contraction of polymer under operation	Membranes are not appropriate for humidifier application in the current form, increased mechanical and dimensional stability are required

Table 6-4: Summary of membranes tested on the HTDS with failures, failure mechanisms and recommendations

Membrane	HTDS (hours to failure)	Failure	Failure Mechanism	Mitigation Strategy or Recommendation
2	400 – 700	Increased air permeation	Oxidative cracking	Membrane is not appropriate due to failure on LTDS and cracking on HTDS
5	412	Increased air permeation	Oxidative cracking	Membrane is not appropriate for HT operation due to cracking

12	724 and 1146	Decrease in water transport	Loss of hydrophilic groups graphed to the base polymer	Membrane is not appropriate for humidifier application
16	300	Increase in air permeation	Oxidative cracking of polymer	Membrane is not appropriate for high temperature operation
45	400	Increase in air permeation	Oxidative cracking of polymer	Membrane is not appropriate for high temperature operation
55	1000+	No failure	N/A	Membrane expense would prohibit commercialization

Many membranes tested exhibited failure on the low and high temperature durability stations. Membrane which are based on polymers and inorganic additives such as silica may be appropriate for lower temperature operation, where lifetimes greater than 2000 hours are not required. These membranes include membranes 8, 16, and 43. Also membrane 46, based on Nylon 6,6 is a candidate material for low and high temperature operation, where initial dry crossover of air is not an issue.

Further testing is recommended for some membranes for which durability testing was not completed. These membranes are dense membranes made with specialized polymers such as membranes 31, 32, and 41. Membrane 40 may be appropriate for both high and low temperature operation, however more testing would be required to confirm this. Some membrane materials show promise for the application if additional development yields materials which can prevent the observed failures. These membranes include membranes 12, 32, 40, and 50 through 54. Membrane 55 would be an appropriate material for the application if the cost of material is decreased by an order of magnitude. Further sourcing of membrane materials is recommended, particularly for high temperature operation. The development of a membrane tailored to the fuel cell humidifier application would be desirable.

Chapter 7

7.0 Conclusions and Recommendations

PEMFC technology requires some method of humidification of the reactant streams in order to ensure that the PFSA based membrane electrode assembly maintains conductivity. Humidification not only ensures high performance, but durability of the fuel cell can also be maintained. External humidification utilizing gas to gas membrane based planar humidifiers is one method of humidifying fuel cell reactant gases, and holds the promise as a low cost component for fuel cell systems. This type of humidification also offers the benefit of recycling heat and moisture from the fuel cell exhaust, by returning it to the reactants entering the fuel cell thus reducing the need for carrying a water source.

This work addressed design issue associated with planar membrane humidifier design. Specifically, this word addressed two key areas associated with membrane based fuel cell humidifiers:

- humidifier channel and plate design; and,
- humidifier membrane selection.

7.1.1 Humidifier Channel and Plate Design

A procedure for humidifier channel design was proposed based on prototype humidifier testing. Humidifiers were created using a rapid prototyping technique. These humidifiers were tested at different operating conditions in order to validate design equations. The design equation involved optimization based on a dimensionless parameter which described the ratio of gas residence time, and water diffusion time from the membrane surface. It was determined that the optimal range for this ratio was between 2 and 4, in order to ensure efficient humidifier performance. The design also considered designing a humidifier on limited volume constraints in which the humidifier would have to fit into the fuel cell system. The methodology offered a good starting point for humidifier design.

7.1.2 Humidifier Membrane Selection

The most important part of this type of humidifier is the membrane which is used. This

membrane must have the following characteristics:

- high liquid water and water vapour permeation rates;
- low air permeation rate when the membrane is both in the wet and dry state;
- high mechanical strength;
- ease of handling;
- a long operating lifetime;
- high temperature tolerance; and
- low cost.

Based on these requirements, specific criteria targets where developed as summarized in Table 7-1 below, and a membrane selection procedure was developed. This procedure was used to screen 60 different membrane samples as candidates for fuel cell humidifiers through a series of experimental test procedures detailed below in Table 7.2. Membranes which passed the initial screening tests were tested on high temperature and low temperature durability stations in order to determine the operating lifetimes of these membranes at fuel cell conditions. Membranes which failed were analyzed in order to determine their fail modes, and mitigation strategies where appropriate.

Table 7-1: Summary of criteria for membrane materials.

Criteria	Target
Water transport in test module	14 kg m^{-2} h^{-1} at S1: 6 SLPM, 25^{o}C, 0% RH S3: 6 SLPM, 75^{o}C, 100% RH
Air permeation	< 3.0 cm^3 min^{-1} cm^{-2} kPa^{-1} at 20 kPa (dry) < 0.01 cm^3 min^{-1} cm^{-2} kPa^{-1} at 20 kPa (wet)
Tensile Modulus	> 112 MPa
Handling and Dimensional Stability	Sufficient for desired operating conditions and assembly techniques
Lifetime	> 1500 hours at under operating conditions

Table 7-2: Summary of experimental procedures used to screen membrane materials for fuel cell humidifiers.

Membrane Property	Test(s)
Water Permeation	Static Vapour Cup Test (rejected)
	Axisymmetric Drop Shape Analysis (rejected)
	Dynamic Water Permeation Test – In standard test module with membrane area of 33.24 cm^2, stream 1 conditions: flow variable, 25^oC, 0% RH, stream 3 conditions: flow variable, 75^oC, 100% RH
Air Permeation	Air Permeation Test – In standard test module, dead-ended, values recorded at 21 kPa.
Mechanical Strength	Stress-Strain Test – On Minimat materials test equipment
Durability	Low Temperature Durability Station – Stream 1 conditions: 4 SLPM, 25^oC, 0% RH; Stream 3 conditions: 4 SLPM, 60^oC, 100% RH
	High Temperature Durability Station - Stream 1 conditions: 4 SLPM, 80^oC, 0% RH; Stream 3 conditions: 4 SLPM, 85^oC, 100% RH

Based on the testing conducted the following membrane characteristics were not desirable in a humidifier membrane:

- low affinity for water or hydrophobicity;
- large pore sizes and high porosity;
- thin membranes with low mechanical strength;
- dimensionally instability when in contact with water; and
- low tolerance to increased temperature and humidity conditions.

In summary the following material characteristics were indicative of positive membrane performance:

- high affinity for water or hydrophilicity;
- dense membranes or small pore sizes;
- demonstrates high mechanical strength;

- has high temperature tolerance; and
- maintains dimensional stability under increased temperature and humidity conditions.

Currently the membranes recommended for use in lower temperature fuel cell systems (<65^{o}C) are membranes 16, 43, and 46. These membranes exhibited high water transport performance, rapid wetting, low air permeation, and near zero air permeation when wet. These membranes also demonstrated at least 2000 hours of continuous operation without failure on the LTDS.

For higher temperature operation, new membrane materials are required. Some materials such as membrane 31, 40, 54, and 55 may show promise for high temperature operation, if further development, cost reduction, and testing is completed. Membrane 46 may be appropriate for high temperature operation as well. However, membranes which can demonstrate longer lifetimes approaching 5000 hours of operation at high temperature conditions have not been found. For this to be achieved, sourcing or else custom development of membrane materials is required.

7.1.3 Recommendations for Future Studies

- Further sourcing and evaluation of long life materials for high temperature operation;
- Development of new membrane materials based on high performance polymers, such as polyethylene terephthalate (PET), polyimide PI, and polyetheretherketone (PEEK) with inorganic hydrophilic additives;
- Refinement the humidifier design equations to incorporate the coupled heat and mass transport effects occurring in the humidifier;
- Exploration of new humidifier geometries such as pleated designs and spiral wound membrane bundles; and
- Development of accelerated test procedures for testing fuel cell humidifiers

7.1.4 Final Recommendations

During this work a procedure for the design of a planar membrane fuel cell humidifier was developed, and allows for design of a humidifier to meet fuel cell system requirement as well as space and packaging needs.

Also through an experiment test screen program it was determined that membranes based on polyethylene and silica are promising candidates for low temperature operation, when life times less than 2000 hours are required. For longer lifetime and higher temperature operation, PFSA based ionomers are currently the best option even though they may be prohibited by their high cost. However, membranes based on nylon 6,6 and similar hydrophilic polymers may prove to be strong candidate materials if further developments can be made to lower their dry crossover rates. Also membranes based on s-PEEK may become a viable option for high temperature fuel cell humidifiers if their mechanical strength can be increased. Finally, membranes based on laminating a porous substrate with an ionomer material may provide membrane with desirable water transport, zero air transport, and sufficient mechanical strength.

8.0 References

ASTM-E96 (2005). Standard Test Methods for Water Vapor Transmission of Materials, ASTM International.

Baker, R. W., *Membrane technology and applications*. J. Wiley,Chichester, England ; New York, 2004.

Bartolotta, A., G. Di Marco, M. Lanza and G. Carini, Elastic behavior of polymers: Anharmonic and relaxational effects, *Physical Review B* **48**(14): 10137, (1993).

Barton, R. H., B. Wells and J. A. Ronne *Plate and frame fluid exchanging assembly with unitary plates and seals* #US6171374. 2001-01-09.

Battery Council, I., *BCI Battery Technical Manual*. Battery Council International,Chicago, Illinois, 2002.

Baum, B., The mechanism of polyethylene oxidation, *Journal of Applied Polymer Science* **2**(6): 281-288, (1959).

Bernardi, D. M. and M. W. Verbrugge, A Mathematical Model of the Solid-Polymer-Electrolyte Fuel Cell, *Journal of The Electrochemical Society* **139**(9): 2477-2491, (1992).

Besmann, T. M., J. W. Klett, J. J. J. Henry and E. Lara-Curzio, Carbon/Carbon Composite Bipolar Plate for Proton Exchange Membrane Fuel Cells, *Journal of The Electrochemical Society* **147**(11): 4083-4086, (2000).

Bird, R. B., W. E. Stewart and E. N. Lightfoot, *Transport phenomena*. J. Wiley,New York, 2007.

Bitter, J. G. A., *Transport mechanisms in membrane separation processes*. Plenum Press,New York, 1991.

Bohnstedt, W., Automotive lead/acid battery separators: a global overview, *Journal of Power Sources* **59**(1-2): 45-50, (1996).

Bohnstedt, W., Aspects of optimizing polyethylene separators, *Journal of Power Sources* **95**(1-2): 234-240, (2001).

Bolland, J. L. and G. Gee, Kinetic studies in the chemistry of rubber and related materials. III. Thermochemistry and mechanisms of olefin oxidation, *Transactions of the Faraday Society* **42**: 236-243, (1946).

Bozzola, J. J. and L. D. Russell, *Electron microscopy : principles and techniques for biologists*. Jones and Bartlett Publishers,Boston, 1992.

Buchi, F. N. and S. Srinivasan, Operating Proton Exchange Membrane Fuel Cells Without External Humidification of the Reactant Gases, *Journal of The Electrochemical Society* **144**(8): 2767-2772, (1997).

Buonanno, G., A. A. Carotenuto, L. Crovini and M. Dell'Isola, A comparison of ideal and real moist air models for calculating humidity ratio and relative humidity in the 213.15 to 473.15 K range and up to a pressure of 1 MPa, *International Journal of Thermophysics* **V15**(3): 483-504, (1994).

Burchill, P. J., Effect of absorbed water, temperature and strain rate on the yield strength of two methylmethacrylate-based plastics, *Journal of Materials Science* **24**(6): 1936-1940, (1989).

Chamberlin, C. E., P. A. Lehman, R. M. Reid and T. G. Herron Preliminary Results of the Schatz Fuel Cell Research Project, Proceedings of the 10th World Hydrogen Energy Conference, Florida, International Association for Hydrogen Energy, (1994).

Choi, K. H., D. J. Park, Y. W. Rho, Y. T. Kho and T. H. Lee, A study of the internal humidification of an integrated PEMFC stack, *Journal of Power Sources* **74**(1): 146-150, (1998).

Choi, K. H., D. H. Peck, C. S. Kim, D. R. Shin and T. H. Lee, Water transport in polymer membranes for PEMFC, *Journal of Power Sources* **86**(1-2): 197-201, (2000).

Cullis, C. F., C. N. Hinshelwood, M. F. R. Mulcahy and R. G. Partington, Labile molecules in the kinetics of hydrocarbon reactions, *Discussions of the Faraday Society* **2**(11): 111-132, (1947).

Daly, B. and J. Yin, Subsurface oxidation of polyethylene, *Journal of Biomedical Materials Research* **42**(4): 523-529, (1998).

Edwards, V. E. Denny and A. F. Mills, *Transfer processes : an introduction to diffusion, convection, and radiation*. Hemisphere Pub. Corp. ; Montreal : McGraw-Hill Book Co.,Washington, 1979.

EmpriseCorporation. "Humidicore Specifications." Retrieved January 2007, from http://www.humidicore.com/.

Escoubes, M. and M. Pineri (1982). Perfluorinated Ionomer Membranes. Washington, DC, American Chemical Society.

Fuller, T. F. and J. Newman, Experimental Determination of the Transport Number of Water in Nafion 117 Membrane, *Journal of The Electrochemical Society* **139**(5): 1332-1337, (1992).

Gavach, C., G. Pamboutzoglou, M. Nedyalkov and G. Pourcelly, AC impedance investigation of the kinetics of ion transport in Nafion(R) perfluorosulfonic membranes, *Journal of Membrane Science* **45**(1-2): 37-53, (1989).

Ge, S., X. Li and I. M. Hsing, Internally humidified polymer electrolyte fuel cells using water absorbing sponge, *Electrochimica Acta* **50**(9): 1909-1916, (2005).

Gibson, P., D. Rivin and C. Kendrick, Convection/diffusion test method for porous textiles *International Journal of Clothing Science and Technology* **12**(2): 96-113, (2000).

Gierke, T. D. and W. Y. Hsu (1982). Perfluorinated Ionomer Membranes. Washington, DC, American Chemical Society.

Glises, R., D. Hissel, F. Harel and M. C. Pera, New design of a PEM fuel cell air automatic climate control unit, *Journal of Power Sources* **150**: 78-85, (2005).

Grot, W. *Solutions of Fluorinated Polymers* #GB1286859. 1969/11/13/.

Hakenjos, A., H. Muenter, U. Wittstadt and C. Hebling, A PEM fuel cell for combined measurement of current and temperature distribution, and flow field flooding, *Journal of Power Sources* **131**(1-2): 213-216, (2004).

Hasegawa, T., T. Kondo and Y. Mitamura *Humidifier* #US2007/0007674A1. Jan. 11, 2007.

He, W., J. S. Yi and T. Nguyen, Two-phase flow model of the cathode of PEM fuel cells using interdigitated flow fields, *AIChE Journal* **46**(10): 2053-2064, (2000).

Hiroshi, S., K. Yoshio, S. Mikihiro and K. Toshikatsu *Humidifier* #JP2005098695. 2005-04-14.

Hoffman, E. J., *Membrane separations technology : single-stage, multistage, and differential permeation*. Gulf Professional Pub.,Amsterdam ; Boston ; London, 2003.

Incropera, F. P. and D. P. DeWitt, *Introduction to heat transfer*. Wiley,New York, 2002.

Kaufman, A. and P. Terry *Hydrogen Air Fuel Cell* #US5776625.

Keiran, L. (2000). The 2000 Guide to the Membrane Industry. Norwalk, Connecticut BCC, Business Communications Company, Inc.

Kim, J., S. M. Lee, S. Srinivasan and C. E. Chamberlin, Modeling of Proton Exchange Membrane Fuel Cell Performance with an Empirical Equation, *Journal of The Electrochemical Society* **142**(8): 2670-2674, (1995).

Kinoshita, K. "ELECTROCHEMICAL USES OF CARBON." Electrochemistry Encyclopedia Retrieved January 2007, from http://electrochem.cwru.edu/ed/encycl/art-c01-carbon.htm.

Kreuer, K. D., On the development of proton conducting polymer membranes for hydrogen and methanol fuel cells, *Journal of Membrane Science* **185**(1): 29-39, (2001).

Kreuer, K. D., S. J. Paddison, E. Spohr and M. Schuster, Transport in Proton Conductors for Fuel-Cell Applications: Simulations, Elementary Reactions, and Phenomenology, *Chemical Reviews* **104**(10): 4637-4678, (2004).

Kritzer, P., Separators for nickel metal hydride and nickel cadmium batteries designed to reduce self-discharge rates, *Journal of Power Sources* **137**(2): 317-321, (2004).

Kwak, S. H., T. H. Yang, C. S. Kim and K. H. Yoon, The effect of platinum loading in the

self-humidifying polymer electrolyte membrane on water uptake, *Journal of Power Sources* **118**(1-2): 200-204, (2003).

Kwok, D., C. Lam, A. Li, K. Zhu, R. Wu and A. Neumann, Low-rate dynamic contact angles on polystyrene and the determination of solid surface tensions, *Polymer Engineering & Science* **38**(10): 1675-1684, (1998).

Larminie, J. and A. Dicks, *Fuel Cell Systems Explained*. John Wiley & Sons Ltd.,Chichester, England, 2003.

Laurencelle, F., R. Chahine, J. Hamelin, K. Agbossou, M. Fournier, T. K. Bose and A. Laperrière, Characterization of a Ballard MK5-E Proton Exchange Membrane Fuel Cell Stack, *Fuel Cells* **1**(1): 66-71, (2001).

Lee, W. k., S. Shimpalee and J. W. V. Zee (2003). Verifying Predictions of Water and Current Distributions in a Serpentine Flow Field Polymer Electrolyte Membrane Fuel Cell, ECS. **150:** A341-A348.

Liu, F., B. Yi, D. Xing, J. Yu, Z. Hou and Y. Fu, Development of novel self-humidifying composite membranes for fuel cells, *Journal of Power Sources* **124**(1): 81-89, (2003).

Long, J. and P. Chen, Surface Characterization of Hydrosilylated Polypropylene: Contact Angle Measurement and Atomic Force Microscopy, *Langmuir* **17**(10): 2965-2972, (2001).

Masaharu, S., I. Tamio and H. Takahiro *Hollow Fiber Membrane Module and Humidifier of Fuel Cell* #JP2005034715. 2005-02-10.

Merida, W. Diagnosis of PEMFC Stack failures via Electrochemical Impedance Spectroscopy, Thesis in Mechanical Engineering, University of Victoria, Victoria, B.C., Canada (2002).

Montgomery, D. C., *Design and analysis of experiments*. John Wiley & Sons,Hoboken, NJ, 2005.

Mossman, A. *Membrane exchange humidifier* #US2005191530 2005-09-01.

Motupally, S., A. J. Becker and J. W. Weidner, Diffusion of Water in Nafion 115 Membranes, *Journal of The Electrochemical Society* **147**(9): 3171-3177, (2000).

Needham, A. D., J. W. N. Smith and E. M. G. Gallagher, The service life of polyethylene geomembrane barriers, *Engineering Geology* **85**(1-2): 82-90, (2006).

Nguyen, T. V. and R. E. White, A Water and Heat Management Model for Proton-Exchange-Membrane Fuel Cells, *Journal of The Electrochemical Society* **140**(8): 2178-2186, (1993).

PermapureInc. "Perma Pure Fuel Cell Website." Retrieved January, 2007, from http://www.permapure.com/FC/.

Qi, Z. and A. Kaufman, PEM fuel cell stacks operated under dry-reactant conditions,

Journal of Power Sources **109**(2): 469-476, (2002).

Rajalakshmi, N., P. Sridhar and K. S. Dhathathreyan, Identification and characterization of parameters for external humidification used in polymer electrolyte membrane fuel cells, *Journal of Power Sources* **109**(2): 452-457, (2002).

Reid, R. C., J. M. Prausnitz and B. E. Poling, *Properties of gases and liquids*. McGraw-Hill,New York ; Montreal, 1987.

Riley, W. F., L. D. Sturges, D. H. Morris, W. F. S. a. m. o. m. Riley and m. Statics and mechanics of, *Statics and mechanics of materials : an integrated approach*. J. Wiley,New York, 2002.

Santis, M., D. Schmid, M. Ruge, S. Freunberger and F. N. Büchi (2004). Modular Stack-Internal Air Humidification Concept-Verification in a 1 kW Stack. **4:** 214-218.

Scott, K. and R. Hughes, *Industrial membrane separation technology*. Blackie Academic & Professional,London, 1996.

Shah, R. K. and A. L. j. a. London, *Laminar flow forced convection in ducts : a source book for compact heat exchanger analytical data*. Academic Press,New York, 1978.

Smith, J. M., H. C. Van Ness and M. M. Abbott, *Introduction to Chemical Engineering Thermodynamics*. McGraw-Hill,New York, NY, 2001.

Springer, T. E., T. A. Zawodzinski and S. Gottesfeld, Polymer Electrolyte Fuel Cell Model, *Journal of The Electrochemical Society* **138**(8): 2334-2342, (1991).

Srinivasan, S., E. A. Ticianelli, C. R. Derouin and A. Redondo, Advances in solid polymer electrolyte fuel cell technology with low platinum loading electrodes, *Journal of Power Sources* **22**(3-4): 359-375, (1988).

Takahiro, S. *Gas Humidifier and Method for the Same* #JP2004028490. 2004-01-29.

Tanaka, S. *Hollow Fiber Membrane Humidifier* #JP2005158517. 2005-06-16.

Tanaka, S. and T. Inamura *Humidifier* #US2005/0110172 A1. May 26, 2005.

Thorat, B., A. Shevade, K. Bhilegaonkar, R. Aglawe, U. Parasu Veera, S. Thakre, A. Pandit, S. Sawant and J. Joshi, Effect of Sparger Design and Height to Diameter Ratio on Fractional Gas Hold-up in Bubble Columns, *Trans. IChemE* **76**(A7 Special issue: Particle Technology): 823-834, (1998).

Uchida, H., Y. Ueno, H. Hagihara and M. Watanabe, Self-Humidifying Electrolyte Membranes for Fuel Cells, *Journal of The Electrochemical Society* **150**(1): A57-A62, (2003).

Venugopal, G., J. Moore, J. Howard and S. Pendalwar, Characterization of microporous separators for lithium-ion batteries, *Journal of Power Sources* **77**(1): 34-41, (1999).

Voss, H., R. Barton, B. W. Wells, J. Ronne and H. A. Nigsch *Solid polymer fuel cell system and method for humidifying and adjusting the temperature of a reactant stream* #US6416895. 2002-07-09.

Watanabe, M., Y. Satoh and C. Shimura, Management of the Water Content in Polymer Electrolyte Membranes with Porous Fiber Wicks, *Journal of The Electrochemical Society* **140**(11): 3190-3193, (1993).

Watanabe, M., H. Uchida and M. Emori, Polymer Electrolyte Membranes Incorporated with Nanometer-Size Particles of Pt and/or Metal-Oxides: Experimental Analysis of the Self-Humidification and Suppression of Gas-Crossover in Fuel Cells, *J. Phys. Chem. B.* **102**(17): 3129-3137, (1998).

Watanabe, M., H. Uchida, Y. Seki, M. Emori and P. Stonehart, Self-Humidifying Polymer Electrolyte Membranes for Fuel Cells, *Journal of The Electrochemical Society* **143**(12): 3847-3852, (1996).

Williams, M. V., H. R. Kunz and J. M. Fenton, Operation of Nafion(R)-based PEM fuel cells with no external humidification: influence of operating conditions and gas diffusion layers, *Journal of Power Sources* **135**(1-2): 122-134, (2004).

Wilson, J. E., Oxygen Uptake of Polyethylene at Elevated Temperatures, *Industrial and Engineering Chemistry* **47**(10): 2201-2205, (1955).

Wood, D. L., J. S. Yi and T. V. Nguyen, Effect of direct liquid water injection and interdigitated flow field on the performance of proton exchange membrane fuel cells, *Electrochimica Acta* **43**(24): 3795-3809, (1998).

Yoon, Y. G., W. Y. Lee, T. H. Yang, G. G. Park and C. S. Kim, Current distribution in a single cell of PEMFC, *Journal of Power Sources* **118**(1-2): 193-199, (2003).

Zawodzinski, Jr., C. Derouin, S. Radzinski, R. J. Sherman, V. T. Smith, T. E. Springer and S. Gottesfeld, Water Uptake by and Transport Through Nafion 117 Membranes, *Journal of The Electrochemical Society* **140**(4): 1041-1047, (1993).

Zawodzinski, Jr., T. E. Springer, J. Davey, R. Jestel, C. Lopez, J. Valerio and S. Gottesfeld, A Comparative Study of Water Uptake By and Transport Through Ionomeric Fuel Cell Membranes, *Journal of The Electrochemical Society* **140**(7): 1981-1985, (1993).

Zawodzinski, T. A., T. E. Springer, F. Uribe and S. Gottesfeld, Characterization of polymer electrolytes for fuel cell applications, *Solid State Ionics* **60**(1-3): 199-211, (1993).

Appendix A

A.0 Calculation of Absorptive Flux for ADSA

The rate of evaporation from any droplet at constant ambient temperature and relative humidity should be a function of time and the surface area of the droplet. The surface area of the droplet was calculated assuming that the drop was a segment of a sphere. This assumes that the surface tension of the droplet, which would tend to make the drop spherical was much greater than the force of gravity on the droplet, which would tend to compress the droplet. The volume of the droplet under this assumption could be calculated using the following formula:

$$V_{cap} = \frac{1}{6}\pi h\left(3a^2 + h^2\right) \qquad \text{[A-1]}$$

In which 'a' is the base radius of the drop, and h is the height of the drop. This volume was compared the volume of the drop calculated computationally by the image analysis software, the percent error between the two calculations was no greater than 1.5%. Thus it was believed that the assumption of a spherical segment was valid.

The surface area of a spherical segment was then calculated using the following formula:

$$S_{cap} = 2\pi rh = \pi\left(a^2 + h^2\right) \qquad \text{[A-2]}$$

This value was then used to calculate the evaporative flux from the surface of the drop by the following equation:

$$J = \frac{\frac{dm_{H2O}}{dt}}{SA_{average}} = \frac{\frac{(mH2O_{t2} - mH2O_{t1})}{t_2 - t_1}}{SA_{average}} \qquad \text{[A-3]}$$

In which the evaporative flux in g $min^{-1}mm^{-2}$ was calculated by taking the change in mass over a given time period was divided by the average surface area over that time period. From these values average evaporative flux, $\overline{J}_{avg}$ was determined.

The average evaporative flux was then used to calculate the mass of water lost due

to evaporation from the droplets on the water transport membranes by the following equation:

$$dm_{evap} = \overline{J}_{avg} \cdot dt \cdot A_{avg} \qquad \text{[A-4]}$$

In which A_{avg} is the average surface area of the drop over the time period, dt. This value was then subtracted from the total water weight loss to give the absorbed weight of the time period:

$$dmH2O_{absorbed} = dmH2O_{total} - dmH2O_{evap} \qquad \text{[A-5]}$$

Finally this value was divided by the time period and the average water-membrane contact area (assumed circular) over that time period to give the absorptive flux:

$$J_{absorp} = \frac{dmH2O_{absorbed}}{dt \cdot \overline{A}_{W-M}} \qquad \text{[A-6]}$$

Appendix B

B.0 Calculated Membrane Parameters

B.1 Membrane Water Flux and Air Permeation Values

Table B-1: Summary of water flux and dry air permeation values for all membranes.

Membrane #	Water Flux (kg m^{-2} h^{-1})	Dry Air Permeation (cm^3 min^{-1} cm^{-2} kPa^{-1})
1	15.9	10.14
2	18.4	1.53
3	17.0	0.26
4	20.0	2.48
5	19.8	5.80
6	10.9	N/A
7	7.6	N/A
8	18.4	1.79
9	22.7	6.20
10	18.5	0.00
11	22.4	21.25
12	21.0	0.00
13	18.0	0.00
14	22.6	0.00
15	20.0	0.93
16	19.3	0.93
17	18.9	0.93
18	19.3	0.82
19	19.3	0.82
20	19.3	0.93
21	17.8	0.93
22	18.2	0.93
23	17.6	0.93
24	17.8	0.93
25	10.7	0.93
26	14.6	4.91
27	19.9	23.45

28	21.8	23.45
29	12.4	0.00
30	20.3	0.00
31	16.4	0.00
32	7.8	0.00
33	2.9	0.00
34	17.1	0.00
35	N/A	0.00
36	24.7	0.90
37	6.4	0.81
38	7.4	0.00
39	12.1	0.00
40	19.2	0.00
41	14.4	0.00
42	16.7	0.48
43	8.1	0.00
44	20.0	0.00
45	19.1	0.00
46	18.8	22.74
47	N/A	N/A
48	10.1	0.00
49	8.5	0.00
50	14.9	0.00
51	13.7	0.00
52	16.6	0.00
53	18.6	0.00
54	8.6	0.00
55	16.1	0.00
56	21.5	60.15
57	18.5	60.15
58	17.5	60.15
59	14.6	60.15
60	3.8	0.00
61	19.3	5.11

Appendix C

C.0 Sample Calculations

C.1 Water Flux Calculations

Data for water tested was completed using a Greenlight Power Technologies FCATS™ G-50 Fuel Cell Test Station. Stream 3 temperature and dew point were both set at 75°C for most experiments. The stream 1 temperature was near 25°C and 0% relative humidity for most experiments. The flow rates for streams 1 and 3 were then varied, and the resulting temperatures were recorded at the outlets of the test module. The data was recorded over time and then the stream 2 wet and dry bulb temperatures were plotted as shown in Figure C-1.

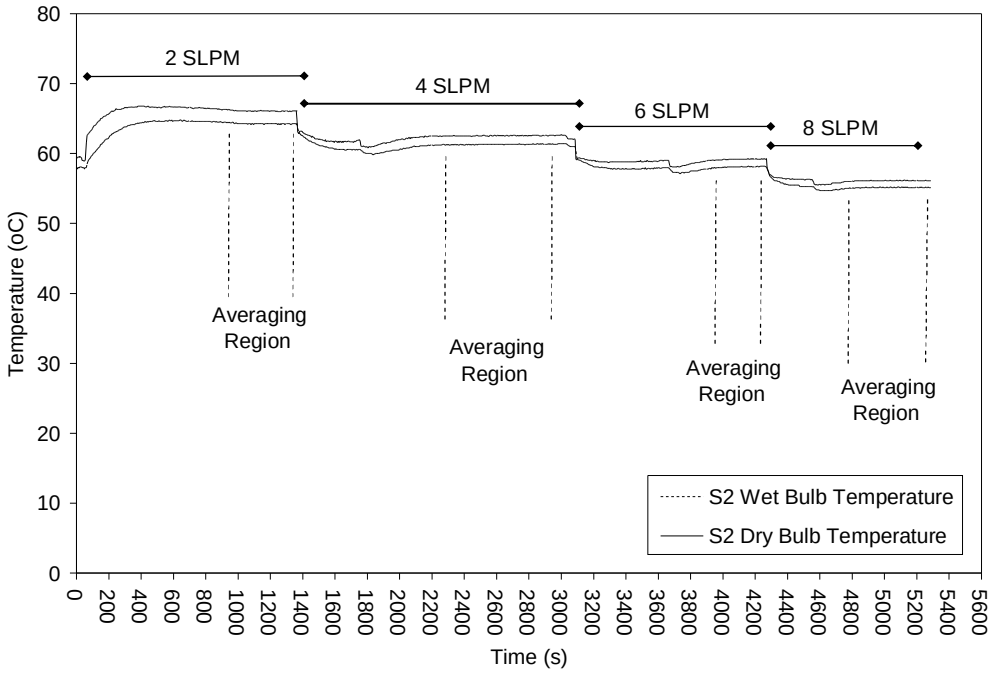

Figure C-1: Data for stream 2 wet and dry temperatures recorded for testing a membrane at different flow rates, with stream 3 at 75°C and 100% relative humidity and stream at 25°C and 0% relative humidity.

As shown in the figure above, there was some variation when changing between flow rates, or else due to fluctuations in the saturator temperature. In order to ensure

consistency, data was averaged only over steady state regions, as shown in Figure C-1. The averaged data is shown in Table C-1.

Table C-1: Averaged data for results shown in Figure C-1.

Flow Rate (SLPM)	T1 (^oC)	T2 Wet Bulb (^oC)	T2 Dry Bulb (^oC)	T3 (^oC)	T4 (^oC)
2	24.8	64.4	66.2	75.2	59.8
4	25.0	61.3	62.5	75.1	63.2
6	24.9	58.0	59.2	75.0	65.2
8	24.7	55.1	56.1	75.0	64.8

The wet bulb (T_{wb}) and dry bulb (T_{db}) temperatures were the data of interest, as they represented the amount of water transported through the membrane. The averaged values were used to calculate the humidity ratio of the gas at stream 2 using the standard psychrometric calculations outlined below.

$$e_s = 6.112 \exp\left(\frac{17.67 \cdot T_{db}}{T_{db} + 243.5}\right) \quad [C\text{-}1]$$

$$e_w = 6.112 \exp\left(\frac{17.67 \cdot T_{wb}}{T_{wb} + 243.5}\right) \quad [C\text{-}2]$$

$$E = e_w - (0.00066(1 + 0.00115T_{wb})(T_{db} - T_{wb})P) \quad [C\text{-}3]$$

$$\omega = 0.62197\frac{E}{P - E} \quad [C\text{-}4]$$

In these equations; e_s is the saturation vapour pressure at the dry bulb temperature, e_w is the saturation pressure at the wet bulb temperature, E is the Goff-Grach factor, P is the pressure in millibar and ω is the specific humidity of the air in grams of water per grams of air.

Assuming that the humidity ratio at stream 1 is zero, the mass balance indicates that all the water present at stream 2 is due to transport through the membrane. The flux can then be calculated using the following equation.

$$J_w = \frac{Q\rho_{air}\omega}{A_{mem}} \qquad [C\text{-}5]$$

In this equation, J_w is the flux of water in g cm^{-2} min^{-1}, Q is the volumetric flow rate at standard conditions in SLPM, ρ_{air} is the density of dry air at standard conditions (1.29 g L^{-1}), and A_{mem} is the area of membrane in the module (33.24 cm^2). This flux value is then converted to kg m^{-2} h^{-1} for better resolution. The calculated specific humidity and flux values for the presented data are summarized in Table C-2 below.

Table C-2: Specific humidity and water flux for sample data at different flow rates.

Flow Rate (SLPM)	ω (g water/g dry air)	Flux (kg m^{-2} h^{-1})
2	0.199	9.2
4	0.165	15.4
6	0.137	19.2
8	0.116	21.6

C.2 Air Permeation Calculations

In the standard air permeation test, membranes were tested in a test module with an active area of 4.9 cm^2. The pressure was increased on side of the membrane to 21 kPa, with the other side of the membrane open to the atmosphere. The flow rate of air through the membrane was measured on the atmospheric side of the membrane in SLPM. The permeation of air through the membrane was then calculated by the following equation.

$$\kappa = \frac{Q}{A\Delta P} \qquad [C\text{-}6]$$

In this equation; κ is the permeation rate in (L min^{-1} cm^{-2} kPa^{-1}), Q is the volumetric flow rate through the membrane in L min^{-1}, A is the active area in the test module (4.9 cm^2), and ΔP is the differential pressure across the membrane in kPa. This permeation value is then converted to cm^3 (STP) cm^{-2} min^{-1} kPa^{-1} for better resolution.

For example, a membrane was tested in the air permeation test module, and found to have

a crossover flow rate of 0.1 SLPM at 21 kPa. Inputting these values into the permeation equation and converting to the desired units, the air permeation for this membrane was calculated to be 0.97 cm^3 (STP) cm^{-2} min^{-1} kPa^{-1}.

Appendix D

D.0 Humidifier Phenomena

D.1 Orientation Effects

The water permeation test module was used with membrane 16 to test the effect of orientation on the humidifier performance. Five different arrangements were tested as shown in Figure D-1.

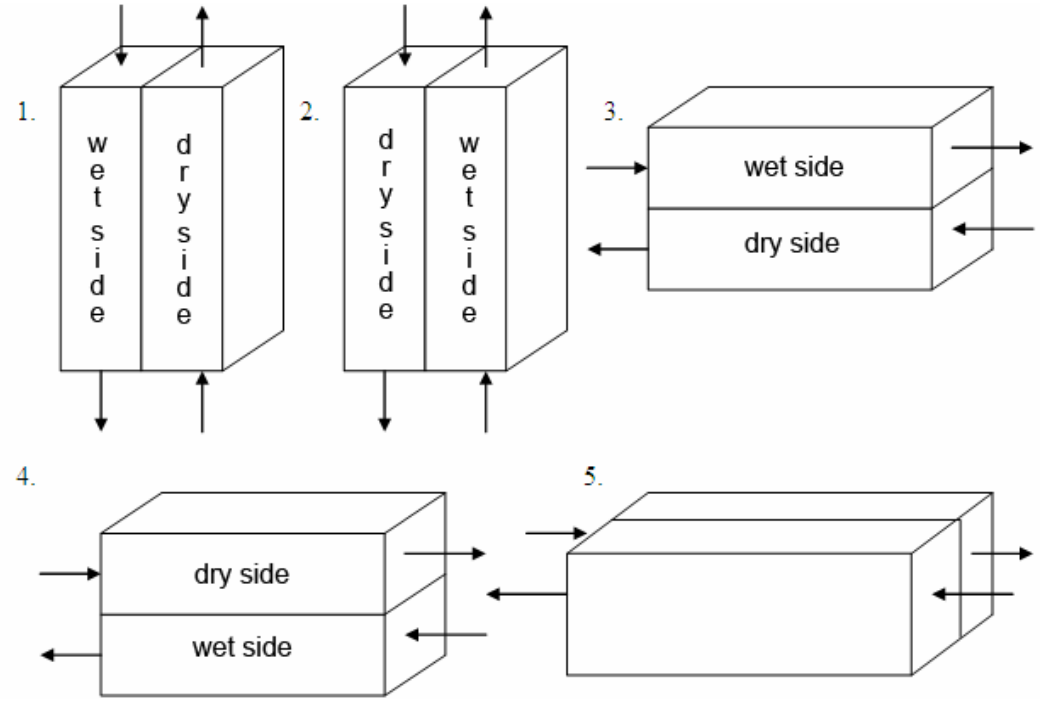

Figure D-1: Test module arrangements for orientation tests, 1)Vertical – Wet on Top; 2) Vertical – Dry on Top; 3) Horizontal – Wet on Top; 4) Horizontal – Dry on Top; 5) Horizontal – Membrane Vertical.

The performance under each of these arrangements is presented in Figure D-2. It can be observed that the humidifier orientation has little effect on the overall humidifier performance. However, operation in the vertical orientations caused some problems with condensed water interfering with the flow of gases through the humidifier channels. It is recommended that if the humidifier is to be operated vertically, design of the manifolds will be required to ensure that sufficient drainage of condensed water can be obtained. The vertical arrangement in which stream 3 is at the top of the humidifier (orientation 1) allows

easier removal of water, since the flow of the wet side of the humidifier will be moving with gravity in this case.

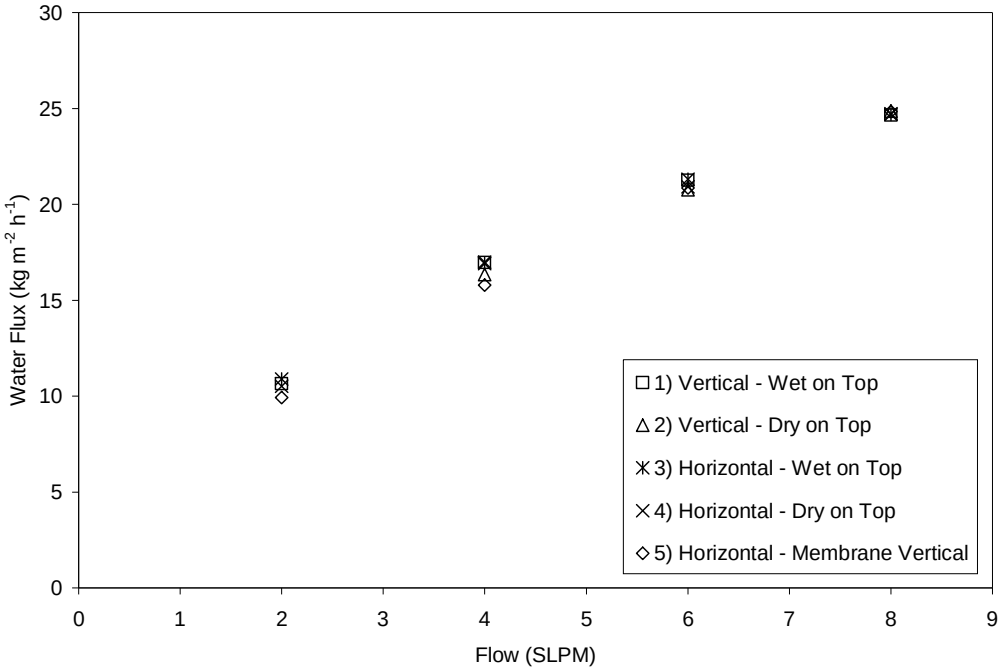

Figure D-2: Results for humidifier orientation tests.

For all further testing completed, the horizontal arrangement of the humidifier in which the membrane is vertical (orientation 5) was used. This ensured that no orientation bias would be observed in testing.

D.2 Flow Arrangement

The water permeation test module was used with membrane 16 to test the effect of flow arrangement. The tests were completed in co-flow and counter-flow modes. Co-flow refers to both the wet and the dry streams flowing in the same direction along the respective membrane surfaces. Counter-flow refers to the wet and dry stream flowing in opposite directions along the respective membrane surfaces. The results of these experiments can be found in Figure D-3.

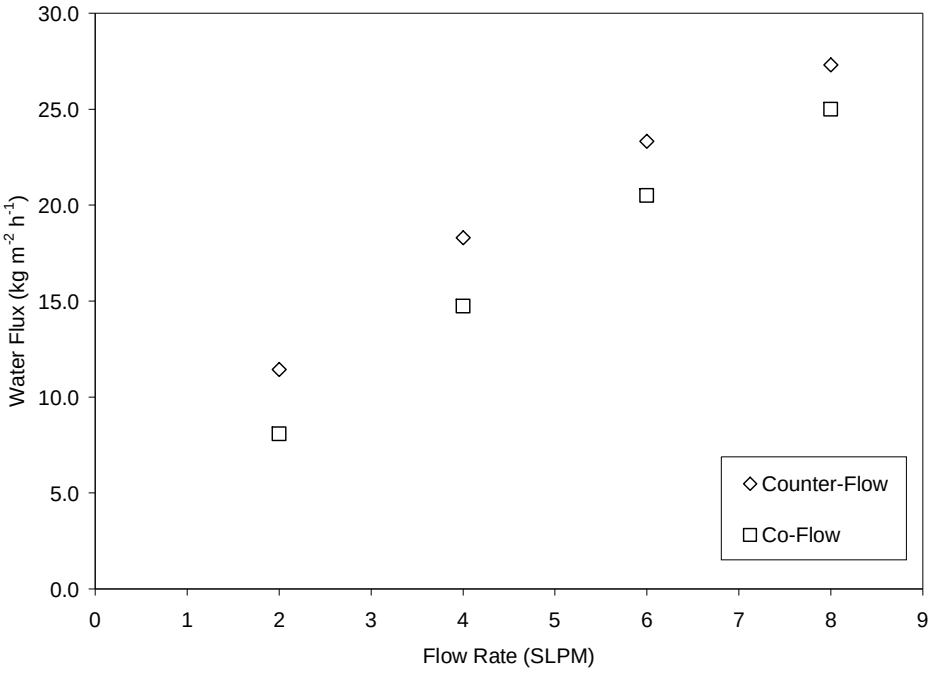

Figure D-3: Comparison of performance under co-flow and counter-flow arrangements.

Evidently the counter-flow arrangement provides significantly greater water transport performance. This is similar to heat exchangers, in which counter-flow arrangements also provide greater heat transport. It was recommended that the humidifier be operated in the counter-flow arrangement.

D.3 Temperature and Flow Effects

The water permeation test module was used with membrane 16, in order to study to effects of flow and the stream 3 temperature and dew point on the water transported through the membrane. The results are presented in Figure D-4. It is evident that increasing the dew point temperature of stream 3 leads to an increase in water flux through the membrane. This is due to higher dew point temperatures leading to increased water concentration in stream 3. The increase in water concentration on the wet side of the membrane means that there is a greater driving force for transport through the membrane, thus an increased flux. Increasing the flow increases the flux as well, but this demonstrates diminishing returns as the flow rate increases.

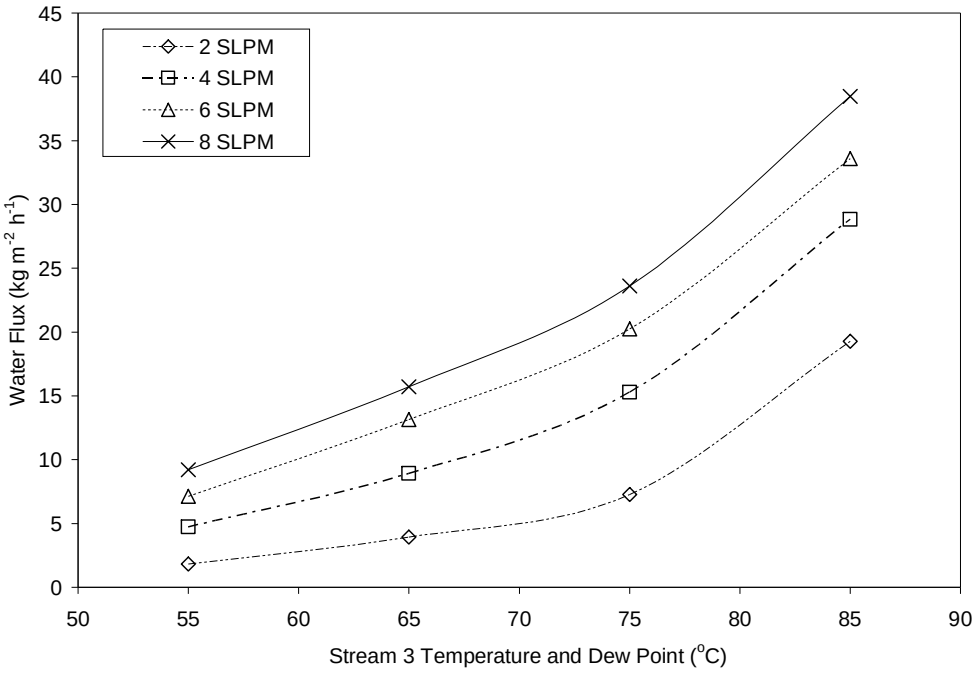

Figure D-4: Temperature and flow effects of humidifier test module.

D.4 Relative Humidity Effect

Membrane 16 was tested in the standard water permeation test module at a constant temperature of 75°C. The dew point, and thus the relative humidity on stream 3 was increased in increments, and the flux was recorded. This produced the curve shown in Figure D-5. This figure is similar to a sorption isotherm for the membrane. The membrane performs best at 100% relative humidity, but still performs rather well at a relative humidity of 80%. The membrane performance decreased to less than half its peak performance at 50% relative humiditiy.

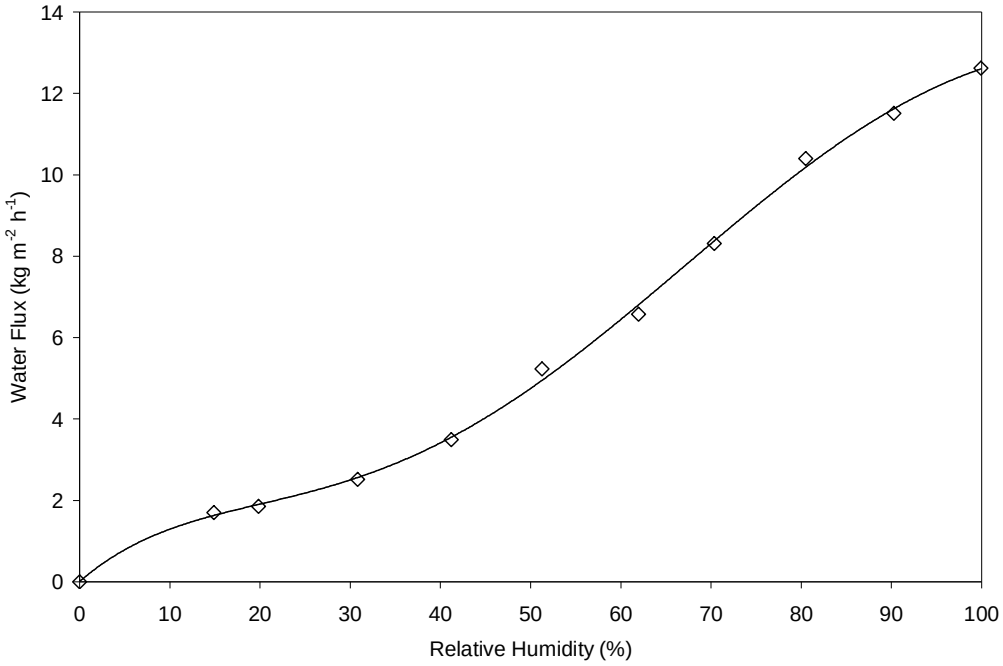

Figure D-5: Effect of relative humidity of stream 3 on water flux, stream 3 conditions: 75°C, 0 to 100% RH; stream 1: 75°C, 0% RH.

D.5 Membrane Thickness

Membrane 16 was tested in the water permeation test module as a single membrane. Two membrane were then stack together and tested. This increase in membrane thickness caused a decrease in water transport performance. It can be concluded that thinner membranes are likely to demonstrate better water transport performance. Thin membranes will be desirable given that they have sufficient mechanical strength properties.

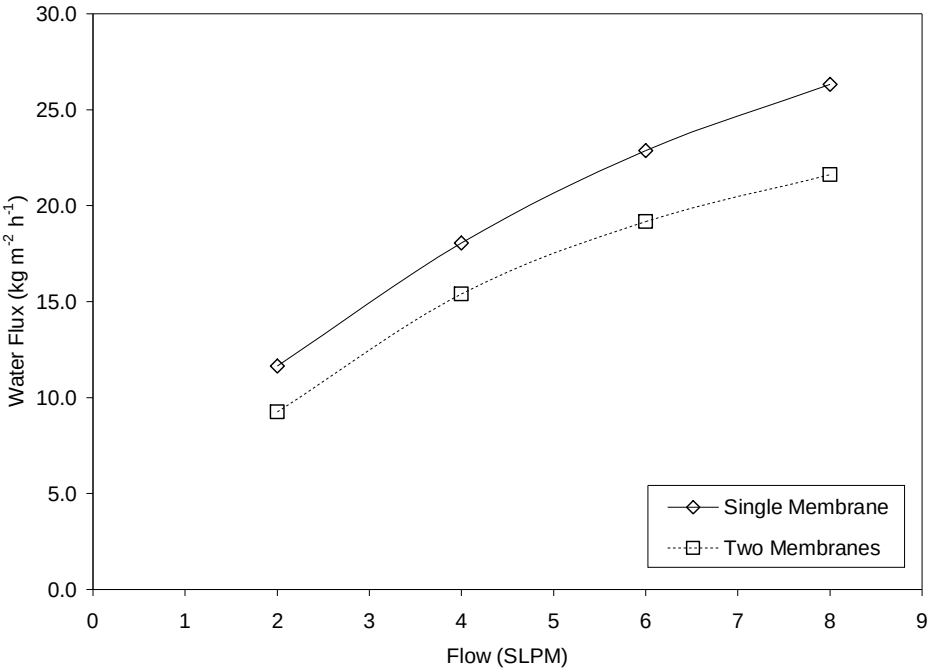

Figure D-6: Results for test with a single membrane and two membranes stacked together at stream 3 conditions: 75o, 100% RH; stream 1: 25oC, 0% RH.